Leveraging Cell Micropatterning Technology for Rapid Cell-Based Assessment of Chemical Toxicity and Population Variation in Toxicity Susceptibility

by

Le Phuong Ngo

B.A., Rutgers University (2011)

Submitted to the Department of Biological Engineering
in partial fulfillment of the requirements for the degree of

Doctor of Philosophy

at the

MASSACHUSETTS INSTITUTE OF TECHNOLOGY

January 2018 [February 2018]

Author . . . Signature redacted . . . . . .
Department of Biological Engineering
January 15, 2018

Certified by. Signature redacted . . .
Bevin P. Engelward and Leona D. Samson
Professors of Biological Engineering
Thesis Supervisors

Accepted by . . . . Signature redacted . . . . . .
Mark Bathe
Chair, Biological Engineering Graduate Committee

This doctoral thesis has been examined by a committee of the Department of Biological Engineering as follows:

Professor Peter C. Dedon
Committee Chair

Professor Bevin P. Engelward
Thesis Supervisor

Professor Leona D. Samson
Thesis Co-Advisor

Professor John M. Essigmann

Acknowledgements

First and foremost, I would like to convey my deepest appreciation to my two wonderful advisors and teachers, Professors Bevin P. Engelward and Leona D. Samson. I would like to thank both of them for their generosity and kindness that gave me the opportunity to become a member in their research groups. I also deeply appreciate the freedom to explore interesting questions and ideas with the benefit of their scientific insights and encouragement.

I would like to thank Bevin for her boundless creativity that made the journey an exciting adventure, enthusiasm that made tough problems fun to solve, and unwavering positivity that turned failures into valuable lessons.

I am deeply grateful to Leona for being my rock, whom I could always rely on for insightful perspectives and brilliant reasoning, for the most practical and honest advice, and most importantly, for unfaltering support even during the toughest of times.

I would like to thank my committee for guiding me through the past several years. I am in debt to Professor Pete Dedon as a committee chair as he always kept me focused and helped my progress stay on track. Besides being my committee chair, Pete also taught a class in drug development that I attended. His enthusiastic dedication to the pursuit of better medicine kept me inspired and excited about opportunities for clinical translation. Professor John Essigmann always had insightful perspectives that motivated me to think more deeply about my work, and his dedication to environmental health has always been a great source of inspiration.

For giving me the opportunity to become a member of a great community full of brilliant, collaborative, and caring individuals, I would like to thank the Department of Biological Engineering at MIT.

I would also like to convey my appreciation to the institute, which offers endless opportunities and almost limitless resources to chase any idea. I have had the privilege of working with people from so many different backgrounds at MIT, and it has always been a great experience. I am truly grateful to be part of this community.

The completion of this work would not have happened without the support of my amazing colleagues and friends in the two labs. Dr. Jing Ge was my mentor when I first joined, and I could not ask for a more helpful and positive friend and teacher. Dr. Marcus Parrish had been my late-night buddy until his own graduation, always able to cheer me up and keep me sane through the long days. Dr. Zac Nagel, Dr. Isaac Chaim, and Patrizia Mazzucato were a fantastic team of scientists, without whom my work with human lymphocytes would not have been possible. Dr. Mariacarmela Allocca, Christy Chao, Josh Corrigan, Dr. Jenny Kay, and Ian Tay were always willing to help and lend an ear whenever I needed support or advice. Kathy Reposa was incredible at keeping the lab running and taking care of everyone.

The animal study in this dissertation would have not been possible without the help from Dr. Supawadee Chawanthayatham, who generously gave her time to train me. I would also like to

thank Professor James R. Mitchell for providing me with the animals and Gustavo Satoru Kajitani for making it happen.

Many more colleagues, collaborators, friends, and mentors provided me with invaluable support throughout my time at MIT, and I am deeply grateful for having met and worked with these incredible people.

To my best friend, Chau Ong, and the best sisters in the world, Quynh and Khanh, I send my heartfelt thanks for your love and support during tough times and for your laughter and great cheers in good times.

I would like to dedicate this dissertation to my parents, who have devoted their whole lives for their children's education and futures. I have not met anyone more hard working, caring, and selfless. From the bottom of my heart, I want to thank *cha* and *mẹ* for making it possible for me to be here.

To Adrian, my mentor, best friend, and above all, my companion, I dedicate this thesis.

Leveraging Cell Micropatterning Technology for Rapid Cell-Based Assessment of Chemical Toxicity and Population Variation in Toxicity Susceptibility

by

Le Phuong Ngo

Submitted to the Department of Biological Engineering on
in partial fulfillment of the requirements for
the degree of
Doctor of Philosophy

Abstract

With the advent of combinatorial chemistry, the number of novel synthetic chemicals has skyrocketed over the past three decades, bringing about tremendous advances in medicine and material science. At the same time, the massive libraries of existing chemicals coupled with the unprecedented rate of new chemical generation presents a unique and costly challenge to toxicity testing in the 21st century. In recent years, the United States has seen large coordinated efforts across governmental agencies to shift from expensive and slow traditional *in vivo* tests to more affordable and higher throughput *in vitro* methods.

For each human cell, about 100,000 DNA lesions occur every day. Unrepaired DNA damage can lead to deleterious health consequences, including cancer and aging. Therefore, an essential endpoint in cell-based chemical safety testing is the assessment of a compound's genotoxic potential. In this work, we developed a CometChip platform that addresses two major areas that are lacking in genotoxicity testing: 1. rapid and sensitive detection of bulky DNA adducts, and 2. robust and physiologically relevant metabolism of test compounds. The assay uses two DNA repair synthesis inhibitors, hydroxyurea and 1-β-D-arabinofuranosyl cytosine, to cause strand-break accumulation and HepaRG™ cells to provide high levels of liver-specific functions. We also conducted extensive validation studies and a small chemical screen to demonstrate the platform's applicability in genotoxicity testing.

One of the most important decisions of proliferating cells under stresses is to divide, senesce, or die. Therefore, *in vitro* measurements of cell survival after a toxic exposure are among the most fundamental and broadly used endpoints in biology. The gold standard for cell survival testing is the colony forming assay, which is exquisitely sensitive but sees limited uses due its low-throughput nature and requirement of large dishes. We have developed MicroColonyChip as a high-throughput platform that can directly measure a cell's ability to divide and has the potential to provide highly sensitive and rapid toxicity assessment of chemicals of interest. The technology is based on the use of a microcolony array where the size distributions for different conditions provide a direct measure of cell survival. We have results showing that MicroColonyChip is as sensitive as the gold standard assay, reduces ~80% incubation time, and requires ~250x less surface area for cell growth.

In addition to detecting genotoxic agents, it is also important to understand how an individual responds to internal and external assaults to DNA as a necessary first step for assessment of human health outcomes. There is a high variability in DNA repair capacity among people, and more studies are needed to elucidate whether a causal relationship between DNA repair capacity and clinical outcomes exists. We applied CometChip to study repair kinetics in human primary

lymphocytes. In order to account for the extensive crosstalk and competition between different repair pathways, repair of different types of DNA damage was measured. To test the assay's sensitivity and reproducibility, a small population of 56 healthy volunteers were recruited to give blood samples. Isolated lymphocytes from different individuals show significant differences in repair kinetics of oxidative damage and a sevenfold variation in repair rates.

Taken together, the work described here represents significant technological advances in addressing a number of major challenges in chemical toxicity testing as well as in the evaluation of health outcome variability across populations. The technologies also open doors to exciting opportunities in personalized strategies for disease prevention and intervention.

Thesis Supervisor: Bevin P. Engelward
Title: Professor of Biological Engineering

Thesis Supervisor: Leona D. Samson
Title: Professor of Biological Engineering and Biology

Contents

List of Figures

List of Tables

List of Abbreviations

5'-dRP	5'-deoxyribophosphate
8oxoG	8-oxoguanine
A	Adenine
AAG	Alkyladenine glycosylase
AFB_1	Aflatoxin B_1
ALKBH	AlkB homolog
ANF	α-naphthoflavone
AP	Apurinic/Apyrimidinic Site
APE1	AP endonuclease 1
ara-C	1-β-D-arabinofuranosyl cytosine
ATM	Ataxia telangiectasia mutated
ATR	Ataxia telangiectasia Rad3-related protein
B[a]P	Benzo[a]pyrene
BER	Base Excision Repair
bp	Base pairs
C	Cytosine
CPDs	cyclobutane pyrimidine dimers
CTG®	CellTiter-Glo®
DNA	Deoxyribonucleic acid
DNA-PK	DNA protein kinase
DNA-PKcs	DNA-PK catalytic subunit
DR	Direct reversal
DSB	Double strand break
FapyG	2,6-diamino-4-hydroxy-5-formamidopyrimidine
FEN1	Flap endonuclease 1
F/M	Integrated fluorescence intensity per microcolony
FYDR	Fluorescent yellow direct repeat
G	Guanine
GSH	Glutathione
H_2O_2	Hydrogen peroxide
HR	Homologous recombination
HU	Hydroxyurea
KET	Ketoconazole
LPO	Lipid peroxidation
MGMT	O^6-methylguanine methyltransferase
MMR	Mismatch repair
MMS	Methylmethane sulfonate
NAD^+	Nicotinamide adenine dinucleotide

NER	Nucleotide excision repair
NHEJ	Non-homologous end joining
$O^{\bullet}_2^-$	Superoxide radical
$^{\bullet}OH$	Hydroxyl radical
O^6meG	O^6-methylguanine
OGG1	8-oxo-guanine glycosylase
PARP1	Poly-ADP ribose polymerase 1
PBS	Phosphate buffered saline
PCNA	Proliferating cell nuclear antigen
PNKP	Polynucleotide kinase phosphatase
POLβ	Polymerase Beta
RONS	Reactive oxygen and nitrogen species
RPA	Replication protein A
SDSA	Synthesis-dependent strand annealing
SP	Spironolactone
SSB	Single strand break
T	Thymine
TLS	Translesion synthesis
U	Uracil
WT	Wild type
γH2AX	Phosphorylated Serine-139 on Histone H2AX
γIR	γ Ionizing radiation
εA	Ethenoadenine
εC	Ethenocytosine
εG	Ethenoguanine
μCC	MicroColonyChip

Chapter 1

Background and Introduction

The large number of novel compounds produced every year and the vast reservoir of existing chemicals pose an enormous public health challenge that traditional approaches for chemical safety testing have failed to meet. Recent coordinated efforts from governmental programs recognize this challenge and are working to change the way safety testing is conducted. More than ever, innovations that enable rapid and reproducible analyses of large numbers of samples are needed. As a contribution to this effort, this dissertation focuses on the development of two high-throughput platforms for assessment of genotoxicity as well as cellular sensitivity to test compounds.

The effect on human health is the net result of the interactions between the chemicals and the individual's molecular responses, which can vary widely across the population. In order to fully assess the consequences of an exposure, it is therefore crucial to understand the differences in molecular responses among individuals. DNA damage is a fundamental step toward a number of human diseases and aging, and there is increasing evidence showing that the ability to repair DNA damage is one of the key determining factors for health outcomes. This work demonstrates a potential use of CometChip, a high-throughput platform for DNA damage detection, to assess the differences in individuals' repair capacity in response to DNA damaging agents.

1.1. DNA DAMAGE AND HUMAN HEALTH

For each human cell, about 100,000 DNA lesions occur every day (1, 2), and the majority come from three different sources. First, spontaneous chemical reactions, such as hydrolysis, can result in base losses and deamination. Examples are the loss of purines due to hydrolysis of their N-glycosyl linkages (depurination) and deamination of cytosine to uracil (3). Endogenous metabolism and inflammation are the second and main source of DNA damage via reactive metabolites, such as reactive oxygen and nitrogen

species (RONS), lipid peroxidation products, and reactive aldehydes (4, 5). The third source comes from exogenous physical and chemical agents (5), such as ultraviolet light, pollutants, and ionizing radiation. Paradoxically, a large number of cancer therapies kill tumor cells by inducing DNA damage, which can result in secondary cancers.

Unrepaired DNA damage can lead to deleterious consequences (5). Damaged bases that mispair during replication leave a permanent change in the genetic material (a mutation), which increases the risk of cancer. DNA nicks and DNA lesions may stall replication, causing fork collapse that can lead to large genomic changes (e.g. deletions/insertions, translocations, and amplifications) and increased cancer risk. On the other hand, DNA damage that blocks replication may trigger either cell death or cell senescence, contributing to aging (5).

To maintain genomic stability, the cells have evolved six major pathways for DNA repair (6, 7) (Fig. 1-1). Some base modifications can be directly reversed by several proteins, such as the ALKBH family and MGMT. Bases that mispair due to replication errors can be removed by mismatch repair (MMR). Base excision repair (BER) or nucleotide excision repair (NER) are also involved in the removal of DNA lesions. BER recognizes and removes bases with small adducts that minimally distort the double helix structure. In addition, BER is involved in the repair of single-strand breaks (SSBs) and abasic sites. NER is capable of removing bulky adducts that thermodynamically destabilize the DNA duplex. In addition to helix-distorting lesions, a sub-pathway of NER, transcription-coupled repair (TC-NER), has also been implicated in the repair of small lesions that block transcription (e.g. 3,N^4-ethenocytosine (8)). Double-strand breaks are primarily repaired by non-homologous end-joining (NHEJ) and homologous recombination (HR) (9). Although each major pathway is specialized to efficiently recognize and repair certain types of DNA damage, there is extensive overlapping of substrates between the pathways.

Following are descriptions of some of the most common types of DNA damage, their molecular and cellular consequences, the key repair pathways that act on them, and their effects on human health.

Types of DNA damage

Single-strand breaks (SSBs)

SSBs are the most common type of DNA damage (10). The main source of SSBs is oxidative attack by reactive oxygen species (ROS), such as superoxide, hydrogen peroxide, and hydroxyl radical. Heavily regulated vital processes, such as transcription and translation, employ specialized enzymes (e.g. DNA topoisomerases) to create SSBs. On the other hand, unregulated SSBs can form as intermediates in DNA excision repair pathways or via direct breakage of the sugar-phosphate backbone due to oxidative attack.

Most SSBs are repaired by a global SSB repair process, which involves SSB detection, DNA end processing, DNA gap filling, and DNA ligation steps. Many of the enzymes and processes involved in the global SSB repair are shared with BER. Unrepaired SSBs can lead to devastating consequences to the cell (10). In proliferating cells, SSBs can stall the replication fork, causing fork collapse, which results in double-strand breaks (DSBs). DSBs can result in cell cycle arrest, which may trigger cell death or cellular senescence. In non-proliferating cells, SSBs block RNA polymerases, triggering cell death (11-13). Excessive SSBs can lead to cell death via hyperactivation of the protein poly(ADP-ribose) polymerase 1 (PARP1), which depletes cellular NAD+ and ATP and causes energetic failure (14, 15). This type of cell death contributes to the pathology of conditions associated with oxidative stress, such as post-ischemic brain or heart damage (10).

Double-strand breaks (DSBs)

DSBs are the most deleterious type of DNA damage (16), being highly cytotoxic and cytostatic (5). In dividing cells, it is estimated that about 10 DSBs occur per cell per day (17-20). DSBs are introduced mainly by oxidative attacks that result in breakage of the sugar-phosphate backbone (21). These attacks can come from exogenous sources, such as ionizing radiation, or endogenous radicals generated during cellular metabolism (17). DSBs also form as a consequence of replication fork collapse when it encounters SSBs or unrepaired lesions (16, 17). During meiosis, DSBs are created to facilitate recombination (16, 17).

Regulated rearrangements, such as V(D)J recombination and immunoglobulin class-switch recombination, produce DSBs as intermediates (16, 17).

Chromosomal rearrangements that come from misrepair of DSBs lead to large genomic alterations, such as deletions/insertions, translocations, loss of heterozygosity, and amplifications. Chromosomal aberration is highly associated with increased risk of cancer. For example, the Philadelphia chromosome (22) comes from a translocation between chromosomes 9 and 22 that results in a fusion between the *BCR* and *ABL1* genes. The fusion gene (*BCR-ABL1*) codes for a tyrosine kinase that is constitutively active, leading to unregulated cell division (22). The Philadelphia chromosome is associated with acute lymphoblastic leukemia and chronic myeloid leukemia.

There are two main pathways that repair DSBs: NHEJ and HR. In recent years, two micro-homology directed repair pathways have emerged to play important roles in DSB repair and associated diseases: alternative end joining (alt-EJ) and single-strand annealing (SSA) (23). The molecular mechanism for the pathway choice decision is not completely understood although recent studies have shed many insights into the process (23). The initiation of 5'- 3' end resection commits the cell to HR and inhibits repair by NHEJ. End resection proteins are tightly regulated by the cell cycle. As a consequence, the cell cycle appears to play a crucial role in pathway choice. NHEJ is favored in non-proliferating cells and during M/G1 phases while HR and the other two pathways are used primarily during S/G2 phases (24). In addition, DSBs formed during meiosis are mainly resolved by HR (17).

DNA base damage

A large number of DNA damage involves chemical modifications of the nucleobases. Most DNA damaging agents induce a spectrum of DNA lesions with diverse chemical structures and biological consequences. Following is a discussion of a few groups of DNA base damage that are both prevalent and important in the context of human health.

Base oxidation comes predominantly from ROS induced by oxidative stress. The main endogenous sources of ROS are cellular metabolisms, including oxidative phosphorylation by mitochondria, metabolism by cytochrome P450s, and inflammatory cell activation (25). ROS are also produced in response to exogenous sources, such as ionizing radiation (IR), ultraviolet light, chlorinated compounds, and metal ions (25). Dietary intakes have also been shown to modulate the level of ROS in the body and subsequently the level of oxidative damage. For example, consumption of kiwifruit (26) and carotenoids (27, 28) significantly reduces the level of 8-oxoguanine (8-oxoG), an established biomarker for oxidative stress.

Examples of common oxidative base lesions are shown in Fig. 1-2 (29, 30) . High levels of 8-oxoG and thymine glycol have been used as biomarkers of persistent oxidative stress, which is associated with aging and human diseases, including chronic inflammation, neurodegenerative diseases, and cancer (31). Unrepaired, these lesions are also highly mutagenic (31). For example, 8-oxoG can mispair with A, causing G-to-T transversion mutations (30, 31). The majority of oxidative base lesions are corrected by base excision repair (BER), which has six glycosylases dedicated to the recognition and removal of oxidative base lesions in mammalian cells (32).

Another prevalent type of base modification is DNA alkylation damage, which is caused by the transfer of alkyl groups from alkylating agents onto DNA nucleobases or the sugar phosphate backbone. Alkylating agents are ubiquitous. Endogenous sources include lipid peroxidation (LPO) and cellular methyl donors, such as S-adenosylmethionine (6). Major external sources of alkylating agents are contaminants in air or drinking water (e.g. N-nitrosodimethylamine) and pollutants (e.g. polycyclic aromatic hydrocarbons) (6). Importantly, alkylating agents are routinely used as anticancer drugs, such as temozolomide, bis-chloroethylnitrosourea (BCNU) (6).

The ring nitrogen (N) and the extracyclic oxygen (*O*) atoms are particularly vulnerable to reactions with alkylating agents via either S_N1 or S_N2 nucleophilic substitutions (examples of lesions in Fig. 1-3A). S_N1 agents react readily with both N and *O* positions while S_N2 agents mainly target the ring nitrogen atoms.

Examples of strong S_N1 agents are nitrosoureas, many of which are used in chemotherapy (6). Examples of S_N2 are alkane sulfonates, such as methyl methanesulfonate (MMS) (33). In addition, alkylating agents can be either monofunctional or bifunctional. Monofunctional agents have one reactive group while bifunctional agents have two reactive groups that can form covalent bonds with two DNA bases, generating intrastrand and interstrand crosslinks (6).

Alkylated lesions have significant biological effects. For example, about 10% of alkylated lesions are N3-methyl adenine (3meA), which blocks most DNA polymerases, triggering cell death (6, 34, 35). About 60-80% of lesions are N7-methyl guanine (7meG), which is neither mutagenic nor cytotoxic. However, 7meG is prone to hydrolysis, generating AP sites that are both mutagenic and cytotoxic (6, 34, 35). S_N1 agents induce a small number of O^6-methyl guanine (O^6meG) lesions (~5%), which can mispair with thymine during replication and cause a G-to-A mutation (6, 34, 35). On the other hand, the O^6meG:T mismatch can activate MMR, which acts on the newly synthesized DNA strand and removes the mispaired thymine. MMR then reinserts a thymine across O^6meG, creating a futile cycle. During the next replication cycle, the persistent strand break generated by the repeated base removal and insertion process causes fork collapse, resulting in chromosome aberrations, cell cycle arrest, and cell death (6).

Attacks of RONS on lipids, especially polyunsaturated fatty acids, generate lipid peroxides as primary products and reactive aldehydes as secondary products (36). These aldehydes are potent DNA alkylating agents, some examples of which are 4-hydroxy-2-nonenal (4-HNE), malondialdehyde (MDA), acrolein, and crotonaldehyde. Their reactions with DNA bases can generate mutagenic exocyclic DNA lesions, such as etheno adducts (five-member ring) and propano adducts (six-member ring) (37). Etheno adducts (Fig. 1-3B) are highly mutagenic and thought to underlie the carcinogenicity of vinyl chloride and urethane (37). Bulky adducts that distort the DNA duplex such as those induced by LPO (Fig. 1-3C) block replication and can also be mutagenic (36, 37).

Alkylated bases are repaired by a number of different pathways. Small N-alkyl lesions (eg. 3meA, 7meG) are removed by the alkyladenine DNA glycosylase (AAG, also known as MPG) in mammalian cells

as part of BER (32). AP sites are also repaired by BER. O^6meG can be directly reversed by the MGMT alkyltransferase in mammalian cells (6). In fact, increased MGMT expression has been implicated as a potential mechanism for resistance to alkylating agents in cancer treatment (38-41). Bulky lesions (HNE-dG and M_1dG) are repaired by NER (36, 37). ALKBH enzymes can directly remove the etheno group in some adducts [e.g, 1,N6-ethenoadenine (εA) and 1,N^2-ethenoguanine] (42, 43). εA can also be removed by AAG (44, 45), and as mentioned above, TC-NER contributes to the repair of εC (8). DNA crosslinks are removed by a combination of HR and NER components (46).

An important group of DNA damage is comprised of bulky adducts that significantly disrupt base-pairing and thermodynamically destabilize the DNA duplex. Some alkylated bases, such as the propano adducts induced by LPO, belong to this group. Bulky lesions underlie the carcinogenicity of many known environmental carcinogens (Fig. 1-4). Common examples include UV-induced adducts, cyclobutane pyrimidine dimers (CPDs) and pyrimidine-pyrimidone photoproducts (6-4PPs), which are both cytotoxic and mutagenic. 6-4PPs are efficiently removed by NER with a half-life of ~2-3 hours while it takes ~10-24 hours for NER to remove half of CPDs (47). People diagnosed with xeroderma pigmentosum (XP) disorder were born with a defect in one of the seven NER proteins or in DNA polymerase η (48). XP patients are reported to have 10,000-fold increase in skin cancer under 20 years of age, and 25% of the patients also develop progressive neurological degeneration (48).

Another important class of DNA modifications is DNA crosslinks, which can be between bases of opposing strands (interstrand) or between adjacent bases on the same DNA strand (intrastrand). Interstrand crosslinks (ICLs) are highly toxic DNA modifications because they prevent the separation of DNA strands in the double helix. Strand separation is essential for many molecular processes, including DNA replication and transcription, and the blockage of these processes by ICLs triggers cell death (46). Intrastrand crosslinks are much less cytotoxic because they can be bypassed by translesion DNA synthesis (TLS) (46). However, they can mispair during this process and result in point mutations. Endogenous sources of DNA crosslinks come from byproducts of LPO, such as acrolein and crotonaldehyde (49). Consumption of alcohol and a

high-fat diet is shown to increase LPO and subsequently the level of DNA crosslinks (50-52). Currently, the most prevalent class of chemotherapeutics is ICL-based, and many are bifunctional alkylating agents. Some examples are cyclophosphamide, BCNU, and cisplatin. DNA crosslinks induced by ICL-based chemotherapeutics are mostly intrastrand (e.g. 80-90% by cisplatin), which are partially repaired by NER or bypassed by TLS (46). In most cases, only a small number of ICLs are induced (e.g. ~5% by cisplatin), and these are primarily repaired by the Fanconi anaemia (FA) complex, which coordinates components from HR, NER, and TLS (46). FA disorder results from genetic defects in key components of the FA complex (46).

Common assays for DNA damage detection

Immunoassays

Antibodies against number of biomarkers for DNA damage provide highly sensitive tools for DNA damage assessment (53). Some important examples include antibodies against oxidative damage (e.g. 8-oxoG), alkylation damage (e.g. O^6meG, 7meG), bulky lesions (e.g. benzo[a]pyrene-DNA adducts, aflatoxin B_1-DNA adducts), markers of DSBs [e.g. γH2AX, p53-binding protein 1 (53BP1) (54)], and DNA repair proteins [e.g. X-ray repair cross complementing 1 (XRCC1) (55)]. Different types of immunoassays have been applied in numerous studies where levels of DNA adducts were monitored following specific environmental or clinical exposures (53). Immunoassays can range from highly quantitative methods, such as the enzyme-linked immunosorbent assay (ELISA), to mostly qualitative techniques, such as immunohistochemistry. There are assays that measure the level of DNA damage markers from cell and tissue lysates, such as immunoblotting and ELISA. On the other hands, methods have been developed to perform detection and/or quantification directly for each cell, e.g. fluorescent microscopy, fluorescence-activated cell sorting (FACS) (53). Following is a brief discussion of the most commonly used biomarker for DNA damage and repair, γH2AX foci, for which many sensitive and robust immunoassays have been established.

γH2AX

The most common method for detection and quantification of DSBs is via immunostaining for γH2AX (56). A crucial component in repair of DSBs is the histone protein H2AX, which becomes phosphorylated on serine 139 by PI3K-like kinases (e.g. ATM, ATR, DNA-PK) to form γH2AX at nascent DSB sites (54). Within minutes after DSBs arise, a large number of H2AX molecules are phosphorylated in the chromatin near the break site, covering a stretch of DNA as long as 30 Mbp (54). The amplification of γH2AX signal serves as a focus to recruit chromatin remodeling and DNA repair proteins. Importantly, the high concentration of γHA2X near the break site enables the detection of a single DSB using an antibody for γH2AX.

There are generally two different approaches for quantification of γH2AX levels. The first approach measures γH2AX levels in cell or tissue lysates. Common techniques for this approach include immunoblotting and enzyme-linked immunosorbent assay (ELISA) (57, 58). ELISA is a much more sensitive method, and several high-throughput assays have been adapted to use in genotoxicity screening and clinical trials (57, 59). The second and most common approach in measuring γHA2X is via immunofluorescence and based on assessment directly in cells and tissues. The number of γH2AX foci has been shown to correlate well with the number of DSBs (54, 60, 61), and the fluorescent foci can be counted for each cell, manually or with a software, via fluorescent microscopy. The total level of γH2AX in each cell can also be quantified with flow cytometry. While flow cytometry is faster and more quantitative, fluorescent microscopy provides structural information that is missed in flow cytometry. One important example is the difference between distinct foci, which are indicative of DSBs, and pan-staining, which is a characteristic of apoptotic cells (62).

Advantages. A large body of evidence shows that γH2AX is a highly sensitive and robust measure of DSBs. γH2AX is also an established biomarker for DNA damage (62) and cellular sensitivity to toxic agents (63). In addition, γH2AX holds powerful potential for use in cancer diagnostics, cancer progression and treatment

monitoring (54), and clinical pharmacodynamic studies (59). High-throughput and sensitive assays tailored for different applications have been developed, facilitating ease of use.

Disadvantages. The majority of DNA damaging agents do not directly cause DSBs. In many cases, DSBs are an indirect consequence of fork collapse due to replication blockage by DNA lesions. In these situations, the result from γH2AX assay may differ significantly between resting cells and proliferative cells. Another major concern in using the assay is the interpretation of the foci. It is still unclear whether every γH2AX focus represents a DSB (64). In fact, formation of γH2AX foci have been observed in cells undergoing apoptosis (65) as well as cells exposed to UV light (66). Small γH2AX foci also appear in certain cell types (67, 68) and may interfere with the quantification of DSB-associated γH2AX foci.

Comet assays

Developed in 1984 (69), the comet assay has since become a classic tool in a number of fields, including environmental biomonitoring, DNA repair studies, and genotoxicity screening (70, 71). The comet assay is based upon electrophoretic migration of nuclear DNA in the presence of strand breaks (SBs). DNA from cells exists as supercoiled loops, and a single SB relaxes the supercoiling, enabling the movement of the free ends under electrophoresis (70). The result is a comet-like shape, where different parameters of the comet tail can be quantified as a measure of DNA damage level. There are two main basic versions of the comet assay. The alkaline comet assay detects DNA SSBs and alkali-labile sites while the neutral comet assay mainly detects DSBs (72). The underlying principle of the comet assay dictates that detectable DNA lesions must be convertible to SBs chemically, enzymatically, or biologically. Chemical conversion includes transforming alkali-labile sites to SBs under high pH conditions (pH >13) (72). Enzymatically, incubation with lesion-specific enzymes to create nicks or generate alkali-labile abasic sites at the damage positions is an efficient method to improve sensitivity and specificity (e.g. Fpg, Endo III, hOGG1, T4 Endo V, DpnI, AlkA, UDG) (72). Biological conversion is based on cellular repair of DNA damage, which often involves multiple steps, including incisions to remove the damage base or a nucleotide

fragment surrounding the damage site. Repair intermediates that contain DNA SBs are generated through this process and can be detected by the comet assay (72).

The comet assay has been used with human primary samples to assess DNA damage levels of people who have been exposed to genotoxic chemicals. The level of DNA damage has been demonstrated as a sensitive biomarker for several types of exposure (73). For example, antioxidant diet reduces oxidative damage (26-28) while tobacco smoke increases both oxidative damage (74, 75) and aromatic bulky DNA lesions (76). In fact, many studies have found that smoking status is highly correlated with the level of aromatic bulky adducts found in peripheral blood lymphocytes (PBLs), a high level of which is associated with more than threefold increase in lung cancer risk (77, 78). In addition, concomitant exposure to AFB_1 and Hepatitis B synergistically increases risk of liver cancer (79).

Potential clinical applications of the comet assay have been demonstrated in a number of studies. Specifically, cancer incidence can be monitored using the comet assay to examine DNA damage levels in PBLs. Supporting evidence for the feasibility of this application includes results showing that PBLs of cancer patients (e.g. head and neck, breast, bladder, and so on) have elevated basal DNA damage compared to control groups (80). In addition, high chromosome aberration frequency in PBLs has been established as a reliable biomarker for cancer incidence (81), suggesting that it is feasible to monitor for cancer incidence via measures of DNA damage in PBLs. Besides diagnostics, another potential clinical application of the comet assay lies in early prediction of tumor response to a cancer treatment regimen. Because only a small number of surviving tumor cells is sufficient for a treatment to fail, it is important to be able to predict early the tumor response and design an effective treatment regimen accordingly. In fact, strong correlation has been observed between DNA damage susceptibility measured by the alkaline comet assay and sensitivity to γ-radiation and several chemotherapeutics (e.g. cisplatin, mitomycin C) in cancer cell lines (80, 82).

Advantages. The key advantages of the comet assay include simple procedures, sensitivity to low levels of DNA damage, affordability, use of a small number of cells, and small amounts of test compounds. In addition, different versions of the comet assays have been developed tailored for detection of specific types

of DNA damage. DNA repair synthesis inhibitors have also been used to enhance the sensitivity of strand break detection.

Disadvantages. The disadvantages of the comet assay lie in its low-throughput nature, poor reproducibility, and slow image processing and analysis methods. Problems with reproducibility stem from both technical problems and human errors/bias. Recently, CometChip was invented in the Engelward laboratory to address these challenges (83, 84). CometChip increases throughput by more than 5,000 fold and also significantly improves reproducibility (85). Another disadvantage is the potential interference from cytotoxicity. SBs can arise from cell death processes, such as apoptosis, and comet assays may overestimate the level of DNA damage-induced SBs.

1.2. CELL SURVIVAL QUANTIFICATION

In vitro measurements of cell survival after a toxic exposure are among the most fundamental and broadly used endpoints in biology (86, 87). As a basic research tool, cytotoxicity assays enable analysis of molecular pathways and gene functions (88, 89). Viability assays are also a mainstay assay in the pharmaceutical industry where they are used to predict adverse effects as well as establishing efficacy of compounds designed to kill cells, such as chemotherapeutics (90). Furthermore, from the perspective of environmental health, cytotoxicity assays are critical for identifying agents in our environment that are potentially toxic. There is an acute need for faster and better cytotoxicity assays by environmental health sciences given the challenge of the more than 2,000 new compounds that are introduced annually into our environment by industry (91).

The gold standard for cell survival testing is the colony forming assay, wherein cells are exposed to a cytotoxic agent and the ability of single cells to form colonies is quantified (92, 93). This assay was developed decades ago, and is still performed in most laboratories using essentially the same approach wherein surviving colonies are stained and counted by eye. The power of the colony forming assay is that it provides a direct measure of the ability of cells to divide, and it has an impressive dynamic range,

spanning over several orders of magnitude. Nevertheless, this assay is performed relatively infrequently compared to other cytotoxicity assays (described below) because it is low-throughput (often requiring 10-21 days of incubation), it is prone to bias, there is significant variation from laboratory to laboratory, and large dishes with large volumes of media are generally required. Importantly, the requirement for large plates renders the assay incompatible with high-throughput screening technologies that require a 96 or 384 well format, and also serves as a barrier for analysis of novel compounds wherein only small quantities are available.

A popular class of viability assays rely upon membrane integrity and mitochondrial functions as endpoints. Several assays, such as the trypan blue or propidium iodide exclusion assay, quantify the loss in cell viability by measuring the proportion of cells that have lost membrane integrity. A drawback of this approach is that membrane permeability does not always accurately reflect cell viability. For example, cells going through early apoptosis would be counted as viable using this assay.

Another approach for estimating viability is to measure mitochondrial functions via metabolism-based endpoints. For example, the MTT/XTT assays are based upon the underlying principle that a live cell can reduce tetrazolium salts to formazan derivatives, accompanied by a change in color that can be measured by absorbance. Analogously, the CellTiter-Glo® (CTG®) assay (from Promega) is based on quantification of intracellular ATP as a measure of viable cells (94). Although these assays are highly prevalent in toxicity screening (eg. services offered by CROs, drug development in pharma), they have significant shortcomings, such as artifacts as a result of changes in pH, factors that affect cellular metabolism, and constituents in cell media (e.g. reducing agents) (86).

1.3. INTERINDIVIDUAL VARIATION IN DNA REPAIR CAPACITY

There is a high variability in how an individual responds to DNA damaging agents. This variation manifests in several important contexts. First, the risk of cancer associated with environmental and occupational exposures to genotoxic agents varies widely among individuals. For example, only 10% of heavy smokers develop lung cancer (95). Second, cancer patients undergoing treatment suffer different

degrees of side effects, which can be mild or severe. Third, tumor response to a treatment regimen is also highly variable (96). Therefore, the ability to predict how an individual responds to a DNA damaging agent may enable more accurate assessment of cancer risk and provide useful information to design tailored treatment regimens in order to minimize side effects while maximizing treatment effectiveness.

Many lines of evidence point toward an association between aberrant DNA repair capacity and risk of cancer as well as sensitivity to treatment. Xeroderma pigmentosum represents a classic example where genetic defects in a major repair pathway, NER, lead to ~2,000-fold increased risk of skin cancer (48). Fanconi anaemia (FA) patients, who carry genetic defects in the FANC repair pathway, are hypersensitive to chemotherapeutics that induce interstrand crosslinks (ICLs) (46). An example highlighting the role of DNA repair in treatment efficacy is the case of breast and ovarian cancers, where BRCA1/2-deficiency confers sensitivity to PARPT inhibitors (97-99).

Over the past two decades, there is mounting evidence showing significant interindividual variations in DNA repair capacity, which are associated with differences in disease risk and treatment outcomes. The evidence has been contributed by methods that indirectly or directly measure DNA repair capacity. Examples of major indirect methods include gene variant association and gene expression studies. Important results from gene variant association studies include a large number of correlations between common single nucleotide polymorphisms in genes in major DNA repair pathways and cancer risks (56). There are also important examples from gene expression studies. Reduced expression levels of XPG or CSB are associated with higher risk of lung cancer (100). In some cases, the expression level of a single DNA repair gene can predict the outcomes for certain cancer treatments [e.g. MGMT (101), ERCC1 (102)]. A major challenge with indirect methods of measurement is that they may fail to predict protein functions due to the complexity of biological processes that govern the transition from a gene to a functional protein.

Direct or functional methods for measurements of DNA repair capacity include enzyme activity assays performed on cell-free extracts, quantification of DNA damage (e.g. ^{32}P-postlalebling, comet assays), and quantification of repair efficiency of damaged reporter plasmid DNA [host-cell reactivation

assays (HCR)]. Activity assays using cell lysates have revealed wide variations among important repair enzymes. Examples include a tenfold variation in MGMT activity (103) and AAG activity (104) in cell-free extracts prepared from human lymphocytes. The comet assays allow detection and quantification of overall DNA damage levels or specific DNA lesions, enabling direct monitoring of DNA damage disappearance over time as a measure of DNA repair efficiency as well as repair kinetics. A number of studies using comet assays demonstrate a wide range of variation in repair among people and associated cancer risks (105-107). Results from studies using HCR assays show interindividual variations across most of the major DNA repair pathways (108, 109) and provide further evidence of the association between DNA repair capacity and cancer risks (110-113).

Despite the significance of interindividual variation in DNA repair capacity and the importance of functional methods, clinical applications have been limited. Specifically, clinical applications of DNA repair capacity have been realized mostly in genetic testing of known mutations for genes associated with DNA repair defects and diseases (114). There are only infrequent uses of certain cell-based assays, such as chromosomal aberration and UV-induced unscheduled DNA synthesis, for diagnostics in the clinics (115, 116). Furthermore, although genetic defects in DNA repair proteins have been exploited to improve cancer treatment outcomes (102, 117), interindividual variation in DNA repair capacity has not been considered in cohort selection for clinical trials or in designing treatment regimens.

It is evident that more studies are needed to further elucidate the relationship between DNA repair capacity and clinical outcomes. Larger and more prospective studies are especially crucial since it is unclear whether the altered DNA repair capacity associated with cancer risk and response to treatment is the cause or the effect. The extensive crosstalk and competition between the major DNA repair pathways also needs to be taken into account in these studies. To these ends, high-throughput assays capable of measuring multiple repair pathways in parallel, such as CometChip (83, 84) and a multiplexed fluorescence-based flow cytometric HCR assay (FM-HCR) (109, 118), have been developed. Efforts to demonstrate their applications in large-scale population studies are under way.

1.4. OBJECTIVE AND SPECIFIC AIMS

The objective of this dissertation is to establish and validate cell-based platforms for HT evaluation of chemical toxicity. To that end, the following specific aims are pursued, and the next chapters are devoted to comprehensive descriptions and in-depth discussions of the experimental results.

Aim 1. Development of a CometChip platform for detection of DNA adducts induced by metabolic activation. The work detailed in chapter 2 addresses two major areas that are lacking in genotoxicity testing: 1. rapid and sensitive detection of bulky DNA adducts, and 2. robust and physiologically relevant metabolism of test compounds. With the advent of the CometChip platform (83, 84), it becomes possible to measure DNA damage in a high-throughput and reproducible fashion (85). To overcome the first challenge, a technique commonly used to enhance SB persistence in the alkaline sucrose sedimentation assay is adopted into a CometChip procedure. Bulky DNA adducts are primarily repaired by the NER pathway, which generates transient SB intermediates (Fig. 1-5). Two DNA repair synthesis inhibitors, hydroxyurea (HU) and 1-β-D-arabinofuranosyl cytosine (ara-C), are used to inhibit the gap filling step of NER, causing accumulation of SBs easily detectable by the alkaline comet assay. The use of HepaRG™, a unique human hepatocyte cell line that maintains high levels of liver-specific functions, provides a possible solution to the second challenge. Extensive validation studies and results from a small chemical screen to demonstrate the platform's applicability in genotoxicity testing are also described in details.

Aim 2. Development of a microarray colony formation platform, MicroColonyChip, for high-throughput cell survival quantification. Chapter 3 showcases the establishment of a cell survival assay that addresses major shortcomings of commonly used methods. The gold standard is the colony formation assay, which is exquisitely sensitive but requires a long incubation and large amounts of valuable test compounds. On the other hand, many popular assays that are fast and compatible with microtiter plates rely on indirect biomarkers of cell viability, which can result in lack of sensitivity in addition to viability-independent interferences. The MicroColonyChip exploits the microarray platform originally developed

for CometChip to grow non-overlapping colonies that are evenly spaced from one another, substantially reducing the surface area required for colony formation. The assay also relies on automated analysis of colony size distributions to measure relative cell survival, achieving similar sensitivity as the gold standard assay within a few days instead of weeks. This chapter describes how MicroColonyChip works, how it compares to commonly used assays, and potential applications for toxicity testing.

Aim 3. Application of CometChip in human lymphocytes to study interindividual variation in DNA repair capacity. Chapter 4 describes the initial efforts to apply CometChip for population studies. The chapter begins with the work to optimize CometChip assays for measuring DNA repair kinetics in response to different types of DNA damage, including oxidative damage, alkylation damage, bulky adducts, and DSBs, in human primary lymphocytes. Next, a small pilot study of ten volunteers comparing intraindividual and interindividual variations in repair of oxidative damage is described. The chapter ends with results obtained from lymphocytes isolated from 46 healthy volunteers and preliminary analyses showing a sevenfold variation in repair rates of oxidative damage.

Chapter 5 offers a discussion of the experimental achievements, the limitations, and future work to further establish the methods for chemical safety testing and population studies.

1.5. REFERENCES

1. Lindahl T. Instability and decay of the primary structure of DNA. Nature. 1993;362(6422):709-15.
2. Sander M, Cadet J, Casciano DA, Galloway SM, Marnett LJ, Novak RF, Pettit SD, Preston RJ, Skare JA, Williams GM, Van Houten B, Gollapudi BB. Proceedings of a workshop on DNA adducts: biological significance and applications to risk assessment Washington, DC, April 13-14, 2004. Toxicol Appl Pharmacol. 2005;208(1):1-20. doi: 10.1016/j.taap.2004.12.012. PubMed PMID: 16164957.
3. Alberts B. Molecular biology of the cell. 4th ed. New York: Garland Science; 2002. xxxiv, 1463, 86 p. p.
4. De Bont R, van Larebeke N. Endogenous DNA damage in humans: a review of quantitative data. Mutagenesis. 2004;19(3):169-85. PubMed PMID: 15123782.
5. Hoeijmakers JH. DNA damage, aging, and cancer. N Engl J Med. 2009;361(15):1475-85. doi: 10.1056/NEJMra0804615. PubMed PMID: 19812404.
6. Fu D, Calvo JA, Samson LD. Balancing repair and tolerance of DNA damage caused by alkylating agents. Nat Rev Cancer. 2012;12(2):104-20. doi: 10.1038/nrc3185. PubMed PMID: 22237395; PMCID: PMC3586545.
7. Lord CJ, Ashworth A. The DNA damage response and cancer therapy. Nature. 2012;481(7381):287-94. doi: 10.1038/nature10760. PubMed PMID: 22258607.
8. Chaim IA, Gardner A, Wu J, Iyama T, Wilson DM, 3rd, Samson LD. A novel role for transcription-coupled nucleotide excision repair for the in vivo repair of 3,N4-ethenocytosine. Nucleic Acids Res. 2017;45(6):3242-52. doi: 10.1093/nar/gkx015. PubMed PMID: 28115629; PMCID: PMC5389632.
9. Jackson SP, Bartek J. The DNA-damage response in human biology and disease. Nature. 2009;461(7267):1071-8. doi: 10.1038/nature08467. PubMed PMID: 19847258; PMCID: PMC2906700.
10. Caldecott KW. Single-strand break repair and genetic disease. Nat Rev Genet. 2008;9(8):619-31. doi: 10.1038/nrg2380. PubMed PMID: 18626472.
11. Kathe SD, Shen GP, Wallace SS. Single-stranded breaks in DNA but not oxidative DNA base damages block transcriptional elongation by RNA polymerase II in HeLa cell nuclear extracts. J Biol Chem. 2004;279(18):18511-20. doi: 10.1074/jbc.M313598200. PubMed PMID: 14978042.
12. Zhou W, Doetsch PW. Effects of abasic sites and DNA single-strand breaks on prokaryotic RNA polymerases. Proc Natl Acad Sci U S A. 1993;90(14):6601-5. PubMed PMID: 8341674; PMCID: PMC46980.

13. Zhou W, Doetsch PW. Transcription bypass or blockage at single-strand breaks on the DNA template strand: effect of different 3' and 5' flanking groups on the T7 RNA polymerase elongation complex. Biochemistry. 1994;33(49):14926-34. PubMed PMID: 7993919.
14. Heeres JT, Hergenrother PJ. Poly(ADP-ribose) makes a date with death. Curr Opin Chem Biol. 2007;11(6):644-53. doi: 10.1016/j.cbpa.2007.08.038. PubMed PMID: 17936669.
15. Moroni F. Poly(ADP-ribose)polymerase 1 (PARP-1) and postischemic brain damage. Curr Opin Pharmacol. 2008;8(1):96-103. doi: 10.1016/j.coph.2007.10.005. PubMed PMID: 18032109.
16. Khanna KK, Jackson SP. DNA double-strand breaks: signaling, repair and the cancer connection. Nat Genet. 2001;27(3):247-54. doi: 10.1038/85798. PubMed PMID: 11242102.
17. Lieber MR. The mechanism of double-strand DNA break repair by the nonhomologous DNA end-joining pathway. Annu Rev Biochem. 2010;79:181-211. doi: 10.1146/annurev.biochem.052308.093131. PubMed PMID: 20192759; PMCID: PMC3079308.
18. Lieber MR, Karanjawala ZE. Ageing, repetitive genomes and DNA damage. Nat Rev Mol Cell Biol. 2004;5(1):69-75. doi: 10.1038/nrm1281. PubMed PMID: 14708011.
19. Lieber MR, Ma Y, Pannicke U, Schwarz K. Mechanism and regulation of human non-homologous DNA end-joining. Nat Rev Mol Cell Biol. 2003;4(9):712-20. doi: 10.1038/nrm1202. PubMed PMID: 14506474.
20. Martin GM, Smith AC, Ketterer DJ, Ogburn CE, Disteche CM. Increased chromosomal aberrations in first metaphases of cells isolated from the kidneys of aged mice. Isr J Med Sci. 1985;21(3):296-301. PubMed PMID: 3997491.
21. Weterings E, Chen DJ. The endless tale of non-homologous end-joining. Cell Res. 2008;18(1):114-24. doi: 10.1038/cr.2008.3. PubMed PMID: 18166980.
22. Koretzky GA. The legacy of the Philadelphia chromosome. J Clin Invest. 2007;117(8):2030-2. doi: 10.1172/JCI33032. PubMed PMID: 17671635; PMCID: PMC1934583.
23. Ceccaldi R, Rondinelli B, D'Andrea AD. Repair Pathway Choices and Consequences at the Double-Strand Break. Trends Cell Biol. 2016;26(1):52-64. doi: 10.1016/j.tcb.2015.07.009. PubMed PMID: 26437586; PMCID: PMC4862604.
24. Symington LS, Gautier J. Double-strand break end resection and repair pathway choice. Annu Rev Genet. 2011;45:247-71. doi: 10.1146/annurev-genet-110410-132435. PubMed PMID: 21910633.
25. Klaunig JE, Kamendulis LM. The role of oxidative stress in carcinogenesis. Annu Rev Pharmacol Toxicol. 2004;44:239-67. doi: 10.1146/annurev.pharmtox.44.101802.121851. PubMed PMID: 14744246.

26. Collins BH, Horska A, Hotten PM, Riddoch C, Collins AR. Kiwifruit protects against oxidative DNA damage in human cells and in vitro. Nutr Cancer. 2001;39(1):148-53. doi: 10.1207/S15327914nc391_20. PubMed PMID: 11588897.
27. Lorenzo Y, Azqueta A, Luna L, Bonilla F, Dominguez G, Collins AR. The carotenoid beta-cryptoxanthin stimulates the repair of DNA oxidation damage in addition to acting as an antioxidant in human cells. Carcinogenesis. 2009;30(2):308-14. doi: 10.1093/carcin/bgn270. PubMed PMID: 19056931.
28. Pool-Zobel BL, Bub A, Muller H, Wollowski I, Rechkemmer G. Consumption of vegetables reduces genetic damage in humans: first results of a human intervention trial with carotenoid-rich foods. Carcinogenesis. 1997;18(9):1847-50. PubMed PMID: 9328185.
29. Krokan HE, Bjoras M. Base excision repair. Cold Spring Harb Perspect Biol. 2013;5(4):a012583. doi: 10.1101/cshperspect.a012583. PubMed PMID: 23545420; PMCID: PMC3683898.
30. Evans MD, Dizdaroglu M, Cooke MS. Oxidative DNA damage and disease: induction, repair and significance. Mutat Res. 2004;567(1):1-61. doi: 10.1016/j.mrrev.2003.11.001. PubMed PMID: 15341901.
31. Kryston TB, Georgiev AB, Pissis P, Georgakilas AG. Role of oxidative stress and DNA damage in human carcinogenesis. Mutat Res. 2011;711(1-2):193-201. doi: 10.1016/j.mrfmmm.2010.12.016. PubMed PMID: 21216256.
32. Wallace SS. Base excision repair: a critical player in many games. DNA Repair (Amst). 2014;19:14-26. doi: 10.1016/j.dnarep.2014.03.030. PubMed PMID: 24780558; PMCID: PMC4100245.
33. Jones GD, Le Pla RC, Farmer PB. Phosphotriester adducts (PTEs): DNA's overlooked lesion. Mutagenesis. 2010;25(1):3-16. doi: 10.1093/mutage/gep038. PubMed PMID: 19920061.
34. Beranek DT. Distribution of methyl and ethyl adducts following alkylation with monofunctional alkylating agents. Mutat Res. 1990;231(1):11-30. PubMed PMID: 2195323.
35. Beranek DT, Weis CC, Swenson DH. A comprehensive quantitative analysis of methylated and ethylated DNA using high pressure liquid chromatography. Carcinogenesis. 1980;1:595-606.
36. Ayala A, Munoz MF, Arguelles S. Lipid peroxidation: production, metabolism, and signaling mechanisms of malondialdehyde and 4-hydroxy-2-nonenal. Oxid Med Cell Longev. 2014;2014:360438. doi: 10.1155/2014/360438. PubMed PMID: 24999379; PMCID: PMC4066722.
37. Nair U, Bartsch H, Nair J. Lipid peroxidation-induced DNA damage in cancer-prone inflammatory diseases: a review of published adduct types and levels in humans. Free Radic Biol Med. 2007;43(8):1109-20. doi: 10.1016/j.freeradbiomed.2007.07.012. PubMed PMID: 17854706.

38. Bobola MS, Berger MS, Ellenbogen RG, Roberts TS, Geyer JR, Silber JR. O6-Methylguanine-DNA methyltransferase in pediatric primary brain tumors: relation to patient and tumor characteristics. Clin Cancer Res. 2001;7(3):613-9. PubMed PMID: 11297257.

39. Christmann M, Verbeek B, Roos WP, Kaina B. O(6)-Methylguanine-DNA methyltransferase (MGMT) in normal tissues and tumors: enzyme activity, promoter methylation and immunohistochemistry. Biochim Biophys Acta. 2011;1816(2):179-90. doi: 10.1016/j.bbcan.2011.06.002. PubMed PMID: 21745538.

40. Hegi ME, Diserens AC, Gorlia T, Hamou MF, de Tribolet N, Weller M, Kros JM, Hainfellner JA, Mason W, Mariani L, Bromberg JE, Hau P, Mirimanoff RO, Cairncross JG, Janzer RC, Stupp R. MGMT gene silencing and benefit from temozolomide in glioblastoma. N Engl J Med. 2005;352(10):997-1003. doi: 10.1056/NEJMoa043331. PubMed PMID: 15758010.

41. Hongeng S, Brent TP, Sanford RA, Li H, Kun LE, Heideman RL. O6-Methylguanine-DNA methyltransferase protein levels in pediatric brain tumors. Clin Cancer Res. 1997;3(12 Pt 1):2459-63. PubMed PMID: 9815647.

42. Ringvoll J, Moen MN, Nordstrand LM, Meira LB, Pang B, Bekkelund A, Dedon PC, Bjelland S, Samson LD, Falnes PO, Klungland A. AlkB homologue 2-mediated repair of ethenoadenine lesions in mammalian DNA. Cancer Res. 2008;68(11):4142-9. Epub 2008/06/04. doi: 68/11/4142 [pii]

10.1158/0008-5472.CAN-08-0796. PubMed PMID: 18519673.

43. Zdzalik D, Domanska A, Prorok P, Kosicki K, van den Born E, Falnes PO, Rizzo CJ, Guengerich FP, Tudek B. Differential repair of etheno-DNA adducts by bacterial and human AlkB proteins. DNA Repair (Amst). 2015;30:1-10. doi: 10.1016/j.dnarep.2015.02.021. PubMed PMID: 25797601; PMCID: PMC4451939.

44. Lee CY, Delaney JC, Kartalou M, Lingaraju GM, Maor-Shoshani A, Essigmann JM, Samson LD. Recognition and processing of a new repertoire of DNA substrates by human 3-methyladenine DNA glycosylase (AAG). Biochemistry. 2009;48(9):1850-61. doi: 10.1021/bi8018898. PubMed PMID: 19219989; PMCID: PMC2883313.

45. Saparbaev M, Kleibl K, Laval J. *Escherichia coli*, *Saccharomyces cerevisiae*, rat and human 3-methyladenine DNA glycosylases repair 1,N^6-ethenoadenine when present in DNA. Nucleic Acids Res. 1995;23(18):3750-5.

46. Deans AJ, West SC. DNA interstrand crosslink repair and cancer. Nat Rev Cancer. 2011;11(7):467-80. doi: 10.1038/nrc3088. PubMed PMID: 21701511; PMCID: PMC3560328.

47. Mitchell DL, Haipek CA, Clarkson JM. (6-4)Photoproducts are removed from the DNA of UV-irradiated mammalian cells more efficiently than cyclobutane pyrimidine dimers. Mutat Res. 1985;143(3):109-12. PubMed PMID: 4010689.

48. DiGiovanna JJ, Kraemer KH. Shining a light on xeroderma pigmentosum. J Invest Dermatol. 2012;132(3 Pt 2):785-96. doi: 10.1038/jid.2011.426. PubMed PMID: 22217736; PMCID: PMC3279615.
49. Kozekov ID, Nechev LV, Moseley MS, Harris CM, Rizzo CJ, Stone MP, Harris TM. DNA interchain cross-links formed by acrolein and crotonaldehyde. J Am Chem Soc. 2003;125(1):50-61. doi: 10.1021/ja020778f. PubMed PMID: 12515506.
50. Brooks PJ, Theruvathu JA. DNA adducts from acetaldehyde: implications for alcohol-related carcinogenesis. Alcohol. 2005;35(3):187-93. doi: 10.1016/j.alcohol.2005.03.009. PubMed PMID: 16054980.
51. Folmer V, Soares JC, Gabriel D, Rocha JB. A high fat diet inhibits delta-aminolevulinate dehydratase and increases lipid peroxidation in mice (Mus musculus). J Nutr. 2003;133(7):2165-70. PubMed PMID: 12840172.
52. Stone MP, Cho YJ, Huang H, Kim HY, Kozekov ID, Kozekova A, Wang H, Minko IG, Lloyd RS, Harris TM, Rizzo CJ. Interstrand DNA cross-links induced by alpha,beta-unsaturated aldehydes derived from lipid peroxidation and environmental sources. Accounts of chemical research. 2008;41(7):793-804. doi: 10.1021/ar700246x. PubMed PMID: 18500830; PMCID: PMC2785109.
53. Santella RM. Immunological methods for detection of carcinogen-DNA damage in humans. Cancer Epidemiol Biomarkers Prev. 1999;8(9):733-9. PubMed PMID: 10498391.
54. Bonner WM, Redon CE, Dickey JS, Nakamura AJ, Sedelnikova OA, Solier S, Pommier Y. GammaH2AX and cancer. Nat Rev Cancer. 2008;8(12):957-67. doi: 10.1038/nrc2523. PubMed PMID: 19005492; PMCID: PMC3094856.
55. Figueroa-Gonzalez G, Perez-Plasencia C. Strategies for the evaluation of DNA damage and repair mechanisms in cancer. Oncol Lett. 2017;13(6):3982-8. doi: 10.3892/ol.2017.6002. PubMed PMID: 28588692; PMCID: PMC5452911.
56. Jalal S, Earley JN, Turchi JJ. DNA repair: from genome maintenance to biomarker and therapeutic target. Clin Cancer Res. 2011;17(22):6973-84. doi: 10.1158/1078-0432.CCR-11-0761. PubMed PMID: 21908578; PMCID: PMC3218201.
57. Matsuzaki K, Harada A, Takeiri A, Tanaka K, Mishima M. Whole cell-ELISA to measure the gammaH2AX response of six aneugens and eight DNA-damaging chemicals. Mutat Res. 2010;700(1-2):71-9. doi: 10.1016/j.mrgentox.2010.05.009. PubMed PMID: 20580854.
58. Wang LH, Pfister TD, Parchment RE, Kummar S, Rubinstein L, Evrard YA, Gutierrez ME, Murgo AJ, Tomaszewski JE, Doroshow JH, Kinders RJ. Monitoring drug-induced gammaH2AX as a pharmacodynamic biomarker in individual circulating tumor cells. Clin Cancer Res. 2010;16(3):1073-84. doi: 10.1158/1078-0432.CCR-09-2799. PubMed PMID: 20103672; PMCID: PMC2818670.

59. Redon CE, Nakamura AJ, Zhang YW, Ji JJ, Bonner WM, Kinders RJ, Parchment RE, Doroshow JH, Pommier Y. Histone gammaH2AX and poly(ADP-ribose) as clinical pharmacodynamic biomarkers. Clin Cancer Res. 2010;16(18):4532-42. doi: 10.1158/1078-0432.CCR-10-0523. PubMed PMID: 20823146; PMCID: PMC2940983.

60. Rogakou EP, Boon C, Redon C, Bonner WM. Megabase chromatin domains involved in DNA double-strand breaks in vivo. J Cell Biol. 1999;146(5):905-16. PubMed PMID: 10477747; PMCID: PMC2169482.

61. Sedelnikova OA, Rogakou EP, Panyutin IG, Bonner WM. Quantitative detection of (125)IdU-induced DNA double-strand breaks with gamma-H2AX antibody. Radiat Res. 2002;158(4):486-92. PubMed PMID: 12236816.

62. Ivashkevich A, Redon CE, Nakamura AJ, Martin RF, Martin OA. Use of the gamma-H2AX assay to monitor DNA damage and repair in translational cancer research. Cancer Lett. 2012;327(1-2):123-33. doi: 10.1016/j.canlet.2011.12.025. PubMed PMID: 22198208; PMCID: PMC3329565.

63. Olive PL, Banath JP. Phosphorylation of histone H2AX as a measure of radiosensitivity. Int J Radiat Oncol Biol Phys. 2004;58(2):331-5. PubMed PMID: 14751500.

64. Rothkamm K, Lobrich M. Evidence for a lack of DNA double-strand break repair in human cells exposed to very low x-ray doses. Proc Natl Acad Sci USA. 2003;100(9):5057-62. PubMed PMID: 12679524.

65. Solier S, Sordet O, Kohn KW, Pommier Y. Death receptor-induced activation of the Chk2- and histone H2AX-associated DNA damage response pathways. Mol Cell Biol. 2009;29(1):68-82. doi: 10.1128/MCB.00581-08. PubMed PMID: 18955500; PMCID: PMC2612481.

66. Marti TM, Hefner E, Feeney L, Natale V, Cleaver JE. H2AX phosphorylation within the G1 phase after UV irradiation depends on nucleotide excision repair and not DNA double-strand breaks. Proc Natl Acad Sci U S A. 2006;103(26):9891-6. doi: 10.1073/pnas.0603779103. PubMed PMID: 16788066; PMCID: PMC1502549.

67. McManus KJ, Hendzel MJ. ATM-dependent DNA damage-independent mitotic phosphorylation of H2AX in normally growing mammalian cells. Molecular biology of the cell. 2005;16(10):5013-25. doi: 10.1091/mbc.E05-01-0065. PubMed PMID: 16030261; PMCID: PMC1237100.

68. Sedelnikova OA, Horikawa I, Zimonjic DB, Popescu NC, Bonner WM, Barrett JC. Senescing human cells and ageing mice accumulate DNA lesions with unrepairable double-strand breaks. Nature cell biology. 2004;6(2):168-70. doi: 10.1038/ncb1095. PubMed PMID: 14755273.

69. Ostling O, Johanson KJ. Microelectrophoretic study of radiation-induced DNA damages in individual mammalian cells. Biochem Biophys Res Commun. 1984;123(1):291-8. PubMed PMID: 6477583.

70. Olive PL, Banath JP. The comet assay: a method to measure DNA damage in individual cells. Nat Protoc. 2006;1(1):23-9. doi: 10.1038/nprot.2006.5. PubMed PMID: 17406208.
71. Hartmann A, Agurell E, Beevers C, Brendler-Schwaab S, Burlinson B, Clay P, Collins A, Smith A, Speit G, Thybaud V, Tice RR. Recommendations for conducting the in vivo alkaline Comet assay. 4th International Comet Assay Workshop. Mutagenesis. 2003;18(1):45-51. PubMed PMID: 12473734.
72. Collins A, A. OA, Brunborg G, Gaivao I, Giovannelli L, Kruszewski M, Smith CC, Stetina R. The comet assay: topical issues. Mutagenesis. 2008;23:143-51.
73. Moller P. The alkaline comet assay: towards validation in biomonitoring of DNA damaging exposures. Basic Clin Pharmacol Toxicol. 2006;98(4):336-45. doi: 10.1111/j.1742-7843.2006.pto_167.x. PubMed PMID: 16623855.
74. Arora A, Willhite CA, Liebler DC. Interactions of beta-carotene and cigarette smoke in human bronchial epithelial cells. Carcinogenesis. 2001;22(8):1173-8. PubMed PMID: 11470745.
75. Pryor WA. Cigarette smoke radicals and the role of free radicals in chemical carcinogenicity. Environ Health Perspect. 1997;105 Suppl 4:875-82. PubMed PMID: 9255574; PMCID: PMC1470037.
76. Pfeifer GP, Denissenko MF, Olivier M, Tretyakova N, Hecht SS, Hainaut P. Tobacco smoke carcinogens, DNA damage and p53 mutations in smoking-associated cancers. Oncogene. 2002;21(48):7435-51. doi: 10.1038/sj.onc.1205803. PubMed PMID: 12379884.
77. Tang D, Phillips DH, Stampfer M, Mooney LA, Hsu Y, Cho S, Tsai WY, Ma J, Cole KJ, She MN, Perera FP. Association between carcinogen-DNA adducts in white blood cells and lung cancer risk in the physicians health study. Cancer Res. 2001;61(18):6708-12. PubMed PMID: 11559540.
78. Veglia F, Matullo G, Vineis P. Bulky DNA adducts and risk of cancer: a meta-analysis. Cancer Epidemiol Biomarkers Prev. 2003;12(2):157-60. PubMed PMID: 12582026.
79. Henry SH, Bosch FX, Bowers JC. Aflatoxin, hepatitis and worldwide liver cancer risks. Adv Exp Med Biol. 2002;504:229-33. PubMed PMID: 11922091.
80. McKenna DJ, McKeown SR, McKelvey-Martin VJ. Potential use of the comet assay in the clinical management of cancer. Mutagenesis. 2008;23(3):183-90. doi: 10.1093/mutage/gem054. PubMed PMID: 18256034.
81. Hagmar L, Bonassi S, Stromberg U, Brogger A, Knudsen LE, Norppa H, Reuterwall C. Chromosomal aberrations in lymphocytes predict human cancer: a report from the European Study Group on Cytogenetic Biomarkers and Health (ESCH). Cancer Res. 1998;58(18):4117-21. PubMed PMID: 9751622.
82. Bowman KJ, Al-Moneef MM, Sherwood BT, Colquhoun AJ, Goddard JC, Griffiths TR, Payne D, Singh S, Butterworth PC, Khan MA, Summerton DJ, Steward WP, McKelvey-Martin VJ, McKeown SR, Kockelbergh RC, Mellon JK, Symonds RP, Jones GD. Comet assay measures of DNA damage

are predictive of bladder cancer cell treatment sensitivity in vitro and outcome in vivo. Int J Cancer. 2014;134(5):1102-11. doi: 10.1002/ijc.28437. PubMed PMID: 23959905.

83. Weingeist DM, Ge J, Wood DK, Mutamba JT, Huang Q, Rowland EA, Yaffe MB, Floyd S, Engelward BP. Single-cell microarray enables high-throughput evaluation of DNA double-strand breaks and DNA repair inhibitors. Cell Cycle. 2013;12(6):907-15. doi: 10.4161/cc.23880. PubMed PMID: 23422001; PMCID: PMC3637349.
84. Wood DK, Weingeist DM, Bhatia SN, Engelward BP. Single cell trapping and DNA damage analysis using microwell arrays. Proc Natl Acad Sci U S A. 2010;107(22):10008-13. doi: 10.1073/pnas.1004056107. PubMed PMID: 20534572; PMCID: PMC2890454.
85. Ge J, Chow DN, Fessler JL, Weingeist DM, Wood DK, Engelward BP. Micropatterned comet assay enables high throughput and sensitive DNA damage quantification. Mutagenesis. 2015;30(1):11-9. doi: 10.1093/mutage/geu063. PubMed PMID: 25527723; PMCID: PMC4272061.
86. Sumantran VN. Cellular chemosensitivity assays: an overview. Methods Mol Biol. 2011;731:219-36. doi: 10.1007/978-1-61779-080-5_19. PubMed PMID: 21516411.
87. Riss TL, Moravec RA, Niles AL, Benink HA, Worzella TJ, Minor L, Storts D, Reid Y. Cell Viability Assays. In: Sittampalam GS, Coussens NP, Nelson H, Arkin M, Auld D, Austin C, Bejcek B, Glicksman M, Inglese J, Iversen PW, Li Z, McGee J, McManus O, Minor L, Napper A, Peltier JM, Riss T, Trask OJ, Jr., Weidner J, editors. Assay Guidance Manual. Bethesda (MD)2004.
88. Brown JM, Attardi LD. The role of apoptosis in cancer development and treatment response. Nat Rev Cancer. 2005;5(3):231-7. doi: 10.1038/nrc1560. PubMed PMID: 15738985.
89. Galluzzi L, Aaronson SA, Abrams J, Alnemri ES, Andrews DW, Baehrecke EH, Bazan NG, Blagosklonny MV, Blomgren K, Borner C, Bredesen DE, Brenner C, Castedo M, Cidlowski JA, Ciechanover A, Cohen GM, De Laurenzi V, De Maria R, Deshmukh M, Dynlacht BD, El-Deiry WS, Flavell RA, Fulda S, Garrido C, Golstein P, Gougeon ML, Green DR, Gronemeyer H, Hajnoczky G, Hardwick JM, Hengartner MO, Ichijo H, Jaattela M, Kepp O, Kimchi A, Klionsky DJ, Knight RA, Kornbluth S, Kumar S, Levine B, Lipton SA, Lugli E, Madeo F, Malomi W, Marine JC, Martin SJ, Medema JP, Mehlen P, Melino G, Moll UM, Morselli E, Nagata S, Nicholson DW, Nicotera P, Nunez G, Oren M, Penninger J, Pervaiz S, Peter ME, Piacentini M, Prehn JH, Puthalakath H, Rabinovich GA, Rizzuto R, Rodrigues CM, Rubinsztein DC, Rudel T, Scorrano L, Simon HU, Steller H, Tschopp J, Tsujimoto Y, Vandenabeele P, Vitale I, Vousden KH, Youle RJ, Yuan J, Zhivotovsky B, Kroemer G. Guidelines for the use and interpretation of assays for monitoring cell death in higher eukaryotes. Cell Death Differ. 2009;16(8):1093-107. doi: 10.1038/cdd.2009.44. PubMed PMID: 19373242; PMCID: PMC2757140.

90. Blumenthal RD, Goldenberg DM. Methods and goals for the use of in vitro and in vivo chemosensitivity testing. Mol Biotechnol. 2007;35(2):185-97. PubMed PMID: 17435285.
91. Shukla SJ, Huang R, Austin CP, Xia M. The future of toxicity testing: a focus on in vitro methods using a quantitative high-throughput screening platform. Drug Discov Today. 2010;15(23-24):997-1007. doi: 10.1016/j.drudis.2010.07.007. PubMed PMID: 20708096; PMCID: 2994991.
92. Puck TT, Marcus PI. A Rapid Method for Viable Cell Titration and Clone Production with Hela Cells in Tissue Culture: The Use of X-Irradiated Cells to Supply Conditioning Factors. Proc Natl Acad Sci U S A. 1955;41(7):432-7. PubMed PMID: 16589695; PMCID: 528114.
93. Puck TT, Marcus PI. Action of x-rays on mammalian cells. J Exp Med. 1956;103:653-66.
94. Crouch SP, Kozlowski R, Slater KJ, Fletcher J. The use of ATP bioluminescence as a measure of cell proliferation and cytotoxicity. J Immunol Methods. 1993;160(1):81-8. PubMed PMID: 7680699.
95. Wu X, Zhao H, Suk R, Christiani DC. Genetic susceptibility to tobacco-related cancer. Oncogene. 2004;23(38):6500-23. doi: 10.1038/sj.onc.1207811. PubMed PMID: 15322521.
96. Cox JD, Stetz J, Pajak TF. Toxicity criteria of the Radiation Therapy Oncology Group (RTOG) and the European Organization for Research and Treatment of Cancer (EORTC). Int J Radiat Oncol Biol Phys. 1995;31(5):1341-6. doi: 10.1016/0360-3016(95)00060-C. PubMed PMID: 7713792.
97. Byrski T, Gronwald J, Huzarski T, Grzybowska E, Budryk M, Stawicka M, Mierzwa T, Szwiec M, Wisniowski R, Siolek M, Dent R, Lubinski J, Narod S. Pathologic complete response rates in young women with BRCA1-positive breast cancers after neoadjuvant chemotherapy. J Clin Oncol. 2010;28(3):375-9. doi: 10.1200/JCO.2008.20.7019. PubMed PMID: 20008645.
98. Fong PC, Boss DS, Yap TA, Tutt A, Wu P, Mergui-Roelvink M, Mortimer P, Swaisland H, Lau A, O'Connor MJ, Ashworth A, Carmichael J, Kaye SB, Schellens JH, de Bono JS. Inhibition of poly(ADP-ribose) polymerase in tumors from BRCA mutation carriers. N Engl J Med. 2009;361(2):123-34. doi: 10.1056/NEJMoa0900212. PubMed PMID: 19553641.
99. Konecny GE, Kristeleit RS. PARP inhibitors for BRCA1/2-mutated and sporadic ovarian cancer: current practice and future directions. Br J Cancer. 2016;115(10):1157-73. doi: 10.1038/bjc.2016.311. PubMed PMID: 27736844; PMCID: PMC5104889 participated in advisory boards for Genentech, Clovis Oncology, and Medivation. RSK was involved in the development of rucaparib, participated in olaparib trials, and served an advisory role to Clovis Oncology.
100. Li C, Wang LE, Wei Q. DNA repair phenotype and cancer susceptibility--a mini review. Int J Cancer. 2009;124(5):999-1007. doi: 10.1002/ijc.24126. PubMed PMID: 19065660; PMCID: PMC4349428.
101. Amatu A, Sartore-Bianchi A, Moutinho C, Belotti A, Bencardino K, Chirico G, Cassingena A, Rusconi F, Esposito A, Nichelatti M, Esteller M, Siena S. Promoter CpG island hypermethylation of the DNA repair enzyme MGMT predicts clinical response to dacarbazine in a phase II study for

metastatic colorectal cancer. Clin Cancer Res. 2013;19(8):2265-72. doi: 10.1158/1078-0432.CCR-12-3518. PubMed PMID: 23422094.

102. Olaussen KA, Mountzios G, Soria JC. ERCC1 as a risk stratifier in platinum-based chemotherapy for nonsmall-cell lung cancer. Curr Opin Pulm Med. 2007;13(4):284-9. doi: 10.1097/MCP.0b013e32816b5c63. PubMed PMID: 17534174.

103. O'Donnell PN, Barber PV, Margison GP, Povey AC. Association between O6-alkylguanine-DNA-alkyltransferase activity in peripheral blood lymphocytes and bronchial epithelial cells. Cancer Epidemiol Biomarkers Prev. 1999;8(7):641-5. PubMed PMID: 10428203.

104. Calvo JA, Moroski-Erkul CA, Lake A, Eichinger LW, Shah D, Jhun I, Limsirichai P, Bronson RT, Christiani DC, Meira LB, Samson LD. Aag DNA glycosylase promotes alkylation-induced tissue damage mediated by Parp1. PLoS genetics. 2013;9(4):e1003413. doi: 10.1371/journal.pgen.1003413. PubMed PMID: 23593019; PMCID: 3617098.

105. Gaivao I, Piasek A, Brevik A, Shaposhnikov S, Collins AR. Comet assay-based methods for measuring DNA repair in vitro; estimates of inter- and intra-individual variation. Cell biology and toxicology. 2009;25(1):45-52. doi: 10.1007/s10565-007-9047-5. PubMed PMID: 18058031.

106. El-Zein RA, Monroy CM, Cortes A, Spitz MR, Greisinger A, Etzel CJ. Rapid method for determination of DNA repair capacity in human peripheral blood lymphocytes amongst smokers. BMC cancer. 2010;10:439. doi: 10.1186/1471-2407-10-439. PubMed PMID: 20718982; PMCID: PMC2933626.

107. Palyvoda O, Polanska J, Wygoda A, Rzeszowska-Wolny J. DNA damage and repair in lymphocytes of normal individuals and cancer patients: studies by the comet assay and micronucleus tests. Acta Biochim Pol. 2003;50(1):181-90. doi: 035001181. PubMed PMID: 12673358.

108. Nagel ZD, Chaim IA, Samson LD. Inter-individual variation in DNA repair capacity: a need for multi-pathway functional assays to promote translational DNA repair research. DNA Repair (Amst). 2014;19:199-213. doi: 10.1016/j.dnarep.2014.03.009. PubMed PMID: 24780560; PMCID: PMC4071454.

109. Nagel ZD, Margulies CM, Chaim IA, McRee SK, Mazzucato P, Ahmad A, Abo RP, Butty VL, Forget AL, Samson LD. Multiplexed DNA repair assays for multiple lesions and multiple doses via transcription inhibition and transcriptional mutagenesis. Proc Natl Acad Sci U S A. 2014;111(18):E1823-32. doi: 10.1073/pnas.1401182111. PubMed PMID: 24757057; PMCID: PMC4020053.

110. Cheng L, Eicher SA, Guo Z, Hong WK, Spitz MR, Wei Q. Reduced DNA repair capacity in head and neck cancer patients. Cancer Epidemiol Biomarkers Prev. 1998;7(6):465-8. PubMed PMID: 9641488.

111. Shi Q, Wang LE, Bondy ML, Brewster A, Singletary SE, Wei Q. Reduced DNA repair of benzo[a]pyrene diol epoxide-induced adducts and common XPD polymorphisms in breast cancer patients. Carcinogenesis. 2004;25(9):1695-700. doi: 10.1093/carcin/bgh167. PubMed PMID: 15090466.

112. Wang L, Wei Q, Shi Q, Guo Z, Qiao Y, Spitz MR. A modified host-cell reactivation assay to measure repair of alkylating DNA damage for assessing risk of lung adenocarcinoma. Carcinogenesis. 2007;28(7):1430-6. doi: 10.1093/carcin/bgm029. PubMed PMID: 17341660.

113. Wei Q, Lee JE, Gershenwald JE, Ross MI, Mansfield PF, Strom SS, Wang LE, Guo Z, Qiao Y, Amos CI, Spitz MR, Duvic M. Repair of UV light-induced DNA damage and risk of cutaneous malignant melanoma. J Natl Cancer Inst. 2003;95(4):308-15. PubMed PMID: 12591987.

114. Ellis CN, SpringerLink (Online service). Obtaining and Using Genetic Information. 2011. In: Inherited cancer syndromes [Internet]. New York ; London: Springer,. 2nd. [p1-21]. Available from: SpringerLink http://dx.doi.org/10.1007/978-1-4419-6821-0 MIT Access Only.

115. Alter BP. Diagnostic evaludation of FA. In: Eiler ME, Frohnmayer D, Larsen K, Owen J, editors. Fanconi Anemia: Guidelines for Diagnosis and Management. 3rd ed: Fanconi Anemia Reserach Fund, Inc.; 2008.

116. Bernstam VA. CRC Handbook of Gene Level Diagnostics in Clinical Practice. Boca Raton, FL: CRC Press; 1992.

117. Rouleau M, Patel A, Hendzel MJ, Kaufmann SH, Poirier GG. PARP inhibition: PARP1 and beyond. Nat Rev Cancer. 2010;10(4):293-301. doi: 10.1038/nrc2812. PubMed PMID: 20200537; PMCID: PMC2910902.

118. Chaim IA, Nagel ZD, Jordan JJ, Mazzucato P, Ngo LP, Samson LD. In vivo measurements of interindividual differences in DNA glycosylases and APE1 activities. Proc Natl Acad Sci U S A. 2017;114(48):E10379-E88. doi: 10.1073/pnas.1712032114. PubMed PMID: 29122935.

119. Marteijn JA, Lans H, Vermeulen W, Hoeijmakers JH. Understanding nucleotide excision repair and its roles in cancer and ageing. Nat Rev Mol Cell Biol. 2014;15(7):465-81. doi: 10.1038/nrm3822. PubMed PMID: 24954209.

120. Li CL, Golebiowski FM, Onishi Y, Samara NL, Sugasawa K, Yang W. Tripartite DNA Lesion Recognition and Verification by XPC, TFIIH, and XPA in Nucleotide Excision Repair. Mol Cell. 2015;59(6):1025-34. doi: 10.1016/j.molcel.2015.08.012. PubMed PMID: 26384665; PMCID: PMC4617536.

121. Dunand-Sauthier I, Hohl M, Thorel F, Jaquier-Gubler P, Clarkson SG, Scharer OD. The spacer region of XPG mediates recruitment to nucleotide excision repair complexes and determines substrate

specificity. J Biol Chem. 2005;280(8):7030-7. doi: 10.1074/jbc.M412228200. PubMed PMID: 15590680.

122. Hohl M, Thorel F, Clarkson SG, Scharer OD. Structural determinants for substrate binding and catalysis by the structure-specific endonuclease XPG. J Biol Chem. 2003;278(21):19500-8. doi: 10.1074/jbc.M213155200. PubMed PMID: 12644470.

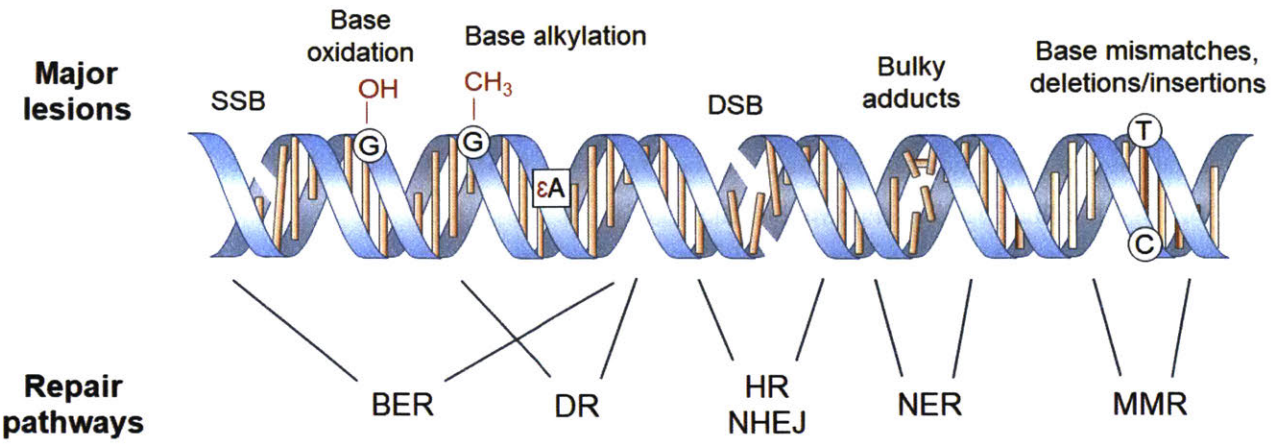

Figure 1-1. Major types of DNA damage and DNA repair mechanisms (adapted from (7)). SSB = single-strand break, DSB = double-strand break, BER = base excision repair, DR = direct reversal, HR = homologous recombination, NHEJ = non-homologous end joining, NER = nucleotide excision repair, MMR = mismatch repair.

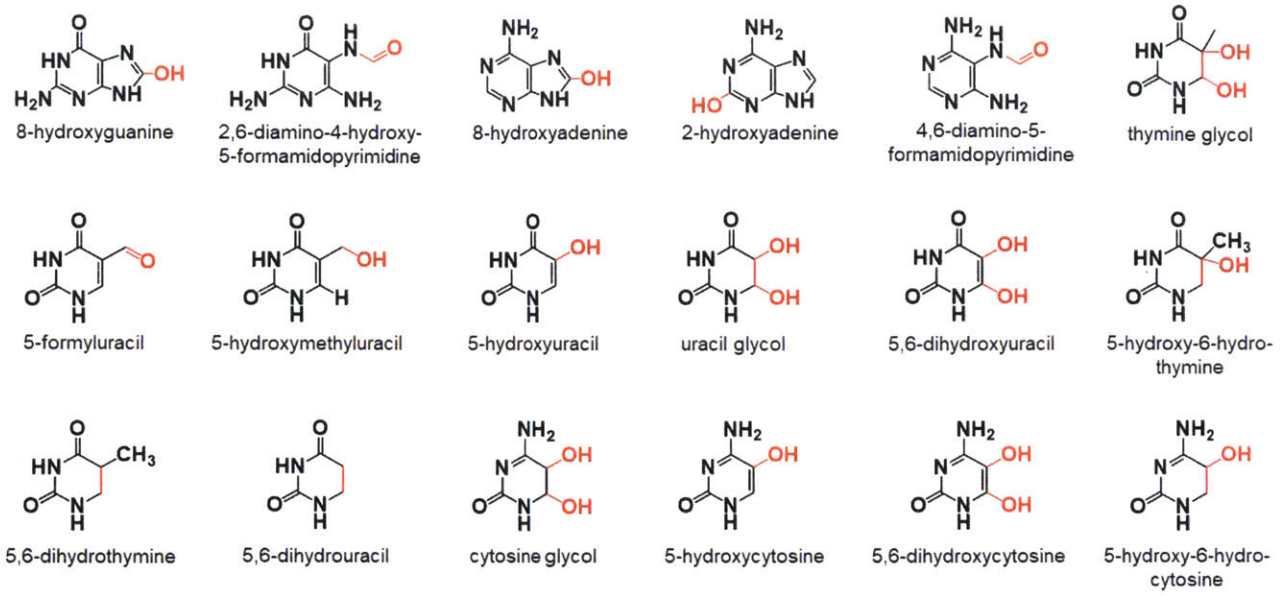

Figure 1-2. Examples of common oxidative nucleobase lesions.

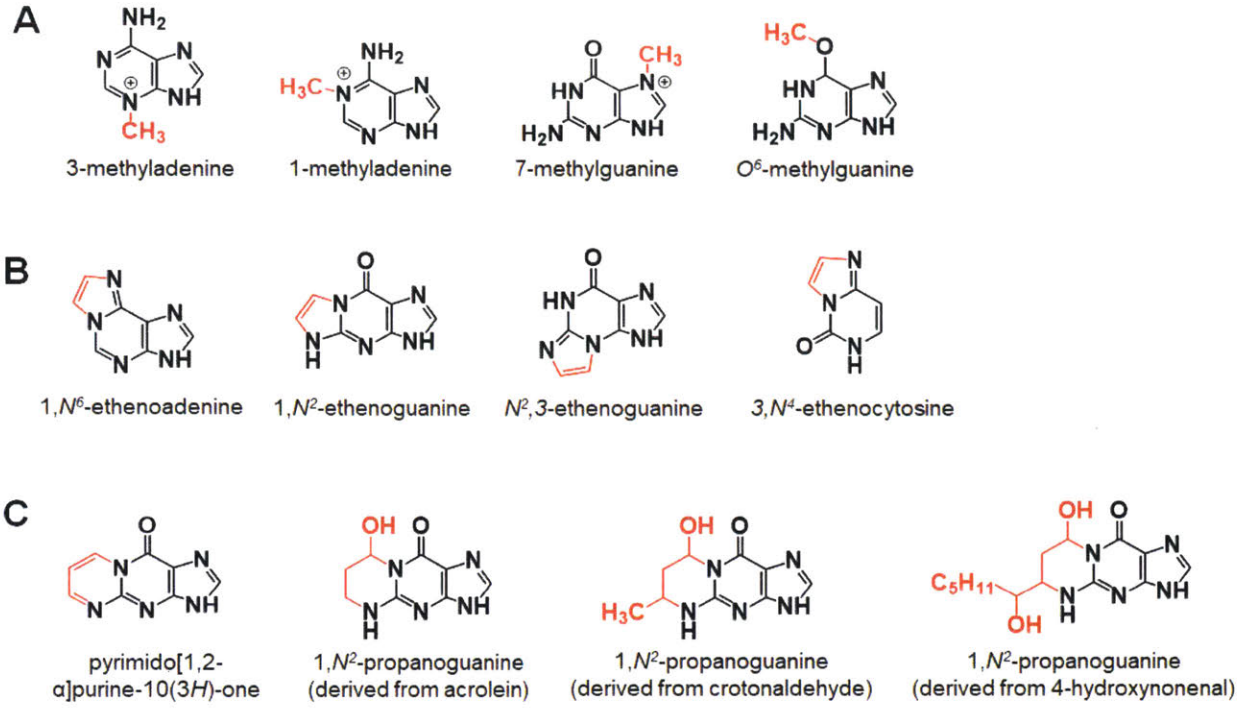

Figure 1-3. Examples of major alkylated nucleobases. **A.** Common methylated bases. **B.** Etheno DNA adducts. **C.** Propano DNA adducts.

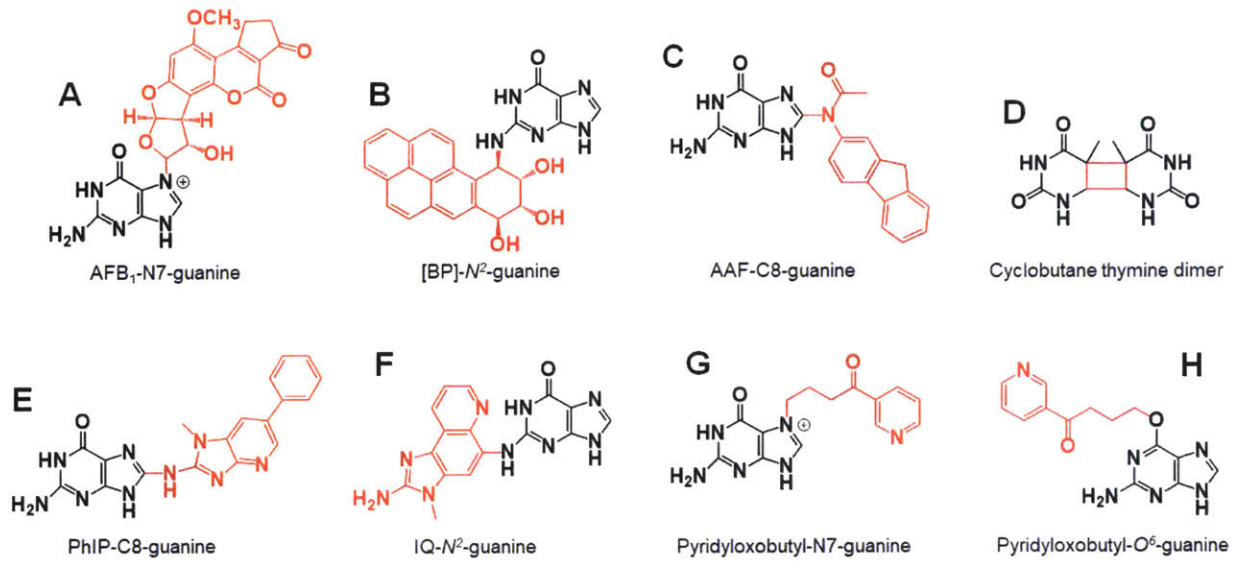

Figure 1-4. Examples of bulky lesions induced by environmental carcinogens: **A.** Mycotoxin aflatoxin B_1 (AFB_1); **B.** Benzo[a]pyrene (B[a]P), a polycyclic aromatic hydrocarbon; **C.** 2-Acetylaminofluorene (2-AAF), previously used in insecticides; **D.** Ultraviolet radiation; **E.** 2-Amino-1-methyl-6-phenylimidazo[4,5-*b*]pyridine (PhIP) and **F.** 2-amino-3-methylimidazo[4,5-*f*]quinoline (IQ), major heterocyclic amines in cooked meat; **G** and **H.** 4-(methylnitrosamino)-1-(3-pyridyl)-1-butanone (NNK), a *N*-nitrosamine from tobacco smoke.

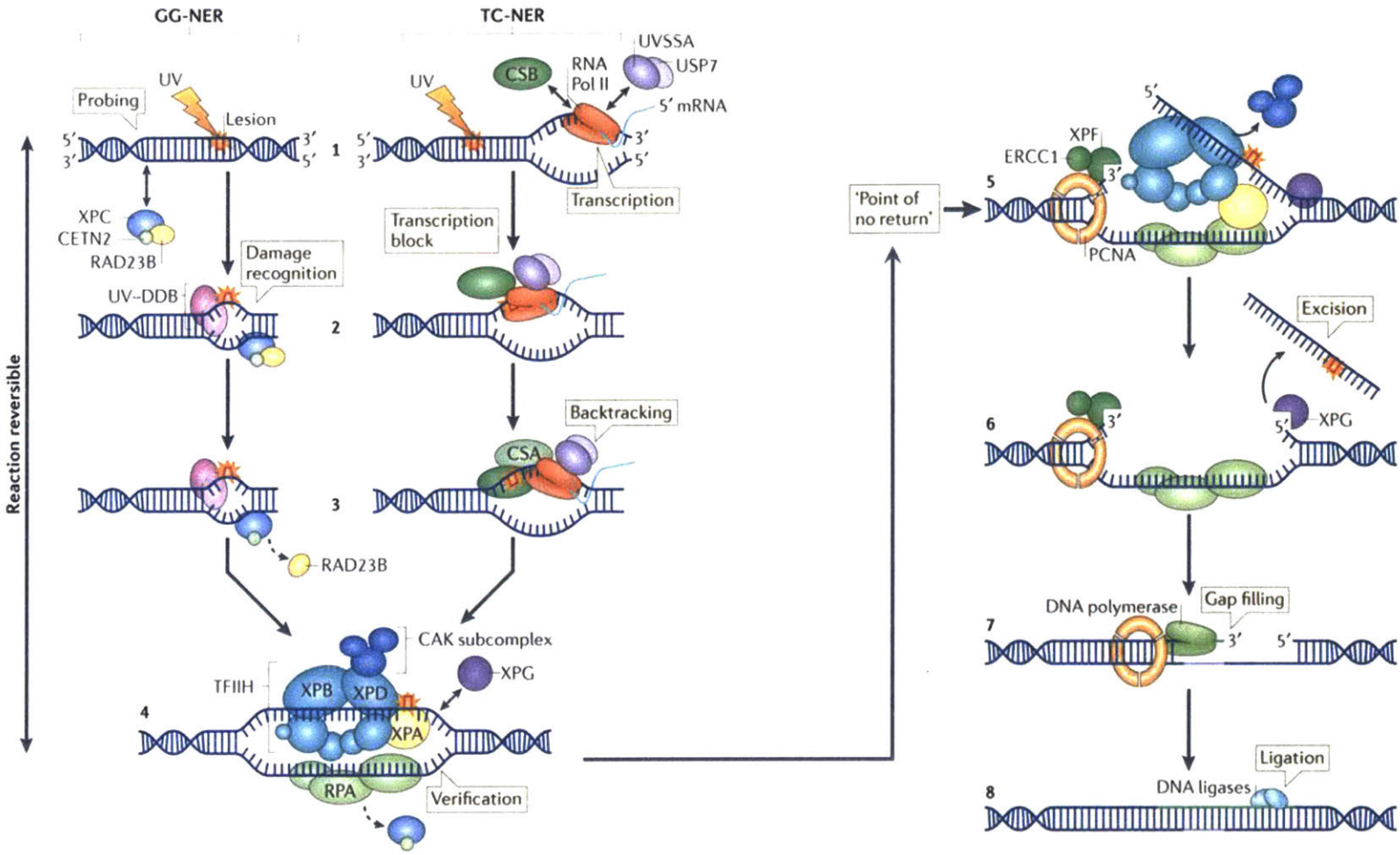

Figure 1-5. Nucleotide excision repair (adapted from (119) by permission from RightsLink Permissions Springer Customer Service Centre GmbH: Springer Nature, Nature Reviews Molecular Cell Biology). There are two separate NER subpathways, global-genomic (GG-NER) and transcription-coupled (TC-NER). The two subpathways differ in the initial damage recognition (**steps 1, 2,** and **3**). GG-NER relies on the damage sensor XPC in complex with RAD23 and CETN2 to constantly probe for disrupted base-pairing. Once detected, the XPC complex binds to the DNA strand opposite the lesion. The diversity of NER substrates is partially due to the fact that the XPC complex does not depend on direct contact with the lesion for damage recognition. In TC-NER, a damage site is indirectly recognized when transcription is blocked. The Cockayne syndrome protein CSB transiently interacts with RNA polymerase II during transcription elongation and binds the stalled RNA polymerase II with a higher affinity. The CSA protein is recruited to form the CSA-CSB complex, which potentially facilitates the backtracking of the stalled RNA polymerase II, making the lesion accessible for repair. After damage recognition, the two NER subpathways converge. The transcriptional initiation factor II helicase (TFIIH) complex is recruited to the damage site by XPC (**step 4**). Upon binding, the CAK module dissociates from the TFIIH complex, leaving behind a seven-subunit core (Core7). In a recent study, the CAK module has been shown to inhibit DNA binding by TFIIH, thereby enhancing the specificity of XPC-dependent recruitment (120). Core7 includes two ATP-dependent helicases, XPB and XPD, which are essential in unwinding the DNA around the lesion to form a DNA bubble. Furthermore, a recent finding shows that XPB and XPD potentially provide an additional damage verification step since the presence of bulky lesions inhibits their helicase activity (120). While the same study also finds that AP sites do not inhibit the helicase activity, it is unclear whether this result applies to other small base lesions. The damage verification step is believed to be further aided by the XPA protein, which preferentially binds to single-stranded, modified nucleotides (119). TFIIH also

mediates the recruitment of a structure-specific endonuclease, XPG, to the NER preincision complex (121). Once the lesion is verified, XPA recruits the structure-specific endonuclease complex, XPF-ERCC1, which makes a 5' incision to the damage site (**step 5**). Gap filling DNA synthesis by DNA polymerases δ, κ, and ε can happen immediately after this step. XPG is activated, potentially by the conformational change in the NER complex (122), and cleaves the DNA strand 3' to the lesion site (**step 6**). Consequently, the lesion is excised along with a DNA single strand of 22-30 nucleotides. DNA polymerases continue to fill in the gap (**step 7**), and the final nick is sealed by DNA ligase 1 or 3 (**step 8**).

Chapter 2

High-Throughput Platform for Detection of DNA Adducts Induced by Metabolic Activation of Xenobiotics

2.1. ABSTRACT

The comet assay is a well-known sensitive method used for measuring DNA damage that can lead to or can be converted into strand breaks in DNA. One blind spot of the comet assay is its poor sensitivity to detect bulky DNA adducts induced by the metabolism of xenobiotics, such as benzo[a]pyrene (B[a]P) and aflatoxin B_1 (AFB_1). CometChip, a high-throughput comet platform recently invented in the Engelward laboratory, increases throughput by more than 5,000 fold and also increases reproducibility. The advantages provided by CometChip enable our work aimed at optimizing conditions for high-throughput detection of bulky DNA damage. We optimized CometChip conditions using DNA repair synthesis inhibitors [hydroxyurea (HU) and 1-β-D-arabinofuranosyl cytosine (ara-C)] to prevent completion of nucleotide excision repair (NER) of bulky DNA adducts (the HU/ara-C approach). We also leveraged the metabolic capacity of the HepaRG™ cell line for genotoxic assessment that is relevant in a human context. Here, we demonstrated the use of our approach for detection of bulky DNA adducts induced by bioactivation in HepaRG™ cells. We used B[a]P and AFB_1 as model DNA damaging agents that require bioactivation to be reactive with DNA. Using specific CYP450 inhibitors, we validated that DNA damage detected is dependent upon bioactivation of B[a]P and AFB_1. Importantly, inhibiting NER initiation resulted in a reduction in the detected signal, confirming the mechanism of DNA damage detection in the HU/ara-C approach is via NER-induced strand-break (SB) intermediates. Taken together, this approach provides a rapid and sensitive method for genotoxicity assessment of chemicals in human-relevant metabolic conditions.

2.2. INTRODUCTION

Injuries to genetic material can lead to debilitating heritable diseases, cancers, and aging (1-4). It is required that all pharmaceuticals are comprehensively tested for their genotoxic potential (5). On the other hand, people are exposed to an unknown number of chemicals every day, most of which have not been tested for safety. Current genotoxicity tests recognized by the regulatory authorities (e.g. Ames test, chromosome aberration test, *in vitro* mouse lymphoma thymidine kinase mutation assay) are slow, laborious, and often require large quantities of expensive test compounds (6). Significantly, there are about 100,000 synthetic chemicals in consumer products (7), and more than 2,000 new chemicals are released every year (8), increasing the urgent need for testing methods that are not only reliable and sensitive but also adaptable for high-throughput (HT) screens.

Although there have been many advances in the ability to screen for genotoxicity (6), many HT technologies depend on indirect measures of DNA damage, such as γH2AX formation (9) or p53 activation (10). To identify genotoxic agents, a number of methods are used for detecting DNA damage, including the unscheduled DNA synthesis assay, alkaline elution method, and the single-cell gel electrophoresis assay (comet assay). Developed in 1984 (11), the comet assay has since become a classic tool in a number of fields, including environmental biomonitoring, DNA repair mechanisms, and genotoxicity (12, 13). The key advantages of the comet assay include simple procedures, sensitivity to low levels of DNA damage, affordability, use of a small number of cells, and small amounts of test compounds. The disadvantages of the comet assay lie in its low-throughput nature, poor reproducibility, and slow image processing and analysis methods. Problems with reproducibility stem from both technical problems and human errors/bias. Recently, CometChip was invented in the Engelward laboratory to address these challenges of the conventional comet assay (14, 15). CometChip increases throughput by more than 5,000 fold and also significantly improves reproducibility (16).

The comet assay is based upon electrophoretic migration of nuclear DNA in the presence of SBs. DNA from cells exists as supercoiled loops, and a single SB relaxes the supercoiling, enabling the

movement of the free ends under electrophoresis (12). The result is a comet-like shape, where different parameters of the comet tail can be quantified as a measure of DNA damage level. There are two main basic versions of the comet assay. In the context of genotoxicity testing, the most relevant version is the alkaline assay (pH >13) due to its sensitivity to a broader range of DNA damage than the neutral comet assay (13). The alkaline comet assay detects DNA strand breaks and alkali-labile sites, such as abasic sites. Abasic sites are the result of spontaneous loss of a damage base (most often alkylated purines) or are intermediates in the base excision repair pathway (BER) (17). For this study, we opted to use the alkaline comet version to maximize our platform's sensitivity.

The underlying principle of the comet assay dictates that detectable DNA lesions must be convertible to SBs chemically, enzymatically, or biologically. Chemical conversion includes converting alkali-labile sites to SBs under high pH conditions (pH >13) (17). Enzymatically, incubation with lesion-specific enzymes creates nicks or generates alkali-labile abasic sites at the damage positions, which is an efficient method to improve sensitivity and specificity (e.g. oxidized bases or alkylated bases) (17). Biological conversion is based on cellular repair of DNA damage, which often involves multiple steps, including incisions to remove the damage base or a nucleotide fragment surrounding the damage site. Repair intermediates that contain DNA SBs are generated through this process and can be detected by the comet assay (17).

Many environmental carcinogens have been shown to cause bulky DNA adducts (3, 18, 19). DNA adducts are considered "bulky" when the damage thermodynamically destabilizes the DNA double helix, distorting the DNA structure (18, 19). Examples are ultraviolet radiation (UVR)-induced lesions, including cyclobutane pyrimidine dimers (CPDs) and pyrimidine-pyrimidones (6-4PPs) (20), and adducts induced by bioactivated polycyclic aromatic hydrocarbons (PAHs) (21). Unrepaired adducts can block replication and transcription, which leads to cell-cycle arrest that can result in cell death (22), as well as promote mutagenesis and carcinogenesis (23-27). In fact, high levels of bulky DNA adducts have been shown to

correlate with an increased risk of cancer in humans (28, 29). Therefore, a method enabling sensitive and rapid detection of bulky adducts has the potential to make a positive and significant impact on human health.

The conventional comet assay has relatively poor sensitivity bulky DNA lesions because these lesions are difficult to convert to SBs. There are currently no robust methods using endonucleases to create lesion-specific nicks. Therefore, these lesions are often indirectly detected via SB repair intermediates of NER (17). Having the widest range of substrates among the repair pathways, NER is the main pathway that recognizes and removes bulky DNA lesions (18-20). NER operates following an efficient "cut-patch-cut-patch" model, minimizing the presence of SB intermediates (30). The incision 5' to the damage site made by the ERCC1-XPF endonuclease is followed by DNA repair synthesis, which in turn activates 3' incision by the XPG endonuclease. DNA repair synthesis continues to fill in the resulting gap, and the nick is sealed by DNA ligases (31, 32).

Importantly, inhibition of DNA repair synthesis has been shown by a number of techniques to enhance SB accumulation in cells treated with UV light and PAHs, including the alkaline sucrose sedimentation assay (33, 34), alkaline unwinding (35), alkaline elution assay (36, 37), and the alkaline comet assay (38-40). A combination of HU and ara-C is often employed. HU depletes the deoxyribonucleotide triphosphate (dNTP) pool by inhibiting the activity of ribonucleotide reductase (41-45). Ara-C is a deoxycytidine structural analog (46), which can be incorporated into DNA (47-50), inhibiting DNA elongation by DNA polymerases and causing early chain termination (47, 51-54)

The HU/ara-C combination enhances the comet assay's sensitivity in detecting DNA damage and has the potential to be used as an efficient tool in genotoxicity testing (38-40). However, little has been done to validate the contribution of bulky adducts in the detected signals as well as develop conditions for a HT approach. Here, we aimed to develop a HT platform based on CometChip for sensitive detection of bulky DNA adducts by using HU and ara-C to amplify the level of SBs generated by NER.

In the human body, foreign substances (xenobiotics) are extensively metabolized, mainly by hepatocytes in the liver (55). Bioactivation is the metabolic process whereby a chemical is converted into reactive or toxic metabolites. Therefore, in order for chemical toxicity assessment to be physiologically relevant, it is essential to have a testing system that can provide appropriate levels of xenobiotic metabolism.

Many environmental procarcinogens are hydrophobic, allowing for passive diffusion through the cell membrane (56). Kidney clearance of the parent chemicals requires that they are converted to a more hydrophilic form to be soluble in aqueous urine (55). The biotransformation process of xenobiotics is typically divided into two phases. Phase I includes oxidation/reduction of parent chemicals, increasing their hydrophilicity by adding polar groups, such as hydroxyl or amine (55, 56). The cytochrome P450 enzymes (CYP450s), or microsomal mixed-function mono-oxygenases, account for ~75% of all phase I enzymes (56) and are involved in ~95% of oxidative biotransformation (55). Phase II further increases the polarity of the metabolites from phase I (or chemicals containing moieties appropriate for conjugation reactions) by adding hydrophilic groups (e.g. glucuronic acid, glutathione, and so on) (55). In many cases, the oxidation products of CYP450s carry highly unstable and reactive moieties (e.g. epoxide) that readily react with DNA, forming covalent adducts. Therefore, any assessment of chemical genotoxicity needs to take into consideration the genotoxic potential of both the parent chemicals and their metabolites.

A major drawback of current *in vitro* genotoxicity assays is the lack of a standard system that can provide consistent and human relevant levels of metabolic enzymes. In regulatory settings, rat liver S9 fraction is recommended in most *in vitro* toxicity tests to provide metabolic activation (5). The use of rat S9 fraction has a few critical disadvantages, including the interspecies difference between rat and human metabolisms, large batch-to-batch metabolic variability, and overrepresentation of CYP450s (57-61). For these reasons, a system that uses a human cell model is preferable. Currently, primary human hepatocytes are considered the gold standard (62). The drawbacks are high costs and low reproducibility due to inter-individual variation in metabolic capacity (63). To circumvent these advantages, a number of cell lines have been established, some of which were derived from human liver cancers (e.g. HepG2, Fa2N-4, BC2) while

some were engineered to express metabolic enzymes (e.g. MCL-5). Human liver-derived cell lines tend to express very low levels of metabolic enzymes (63). For example, the classic human hepatoblastoma-derived HepG2 cell line, which was established nearly 40 years ago (64), has been widely used in a large number of studies with references in more than 9,000 scientific articles (65). Although HepG2 cells retain many liver specific functions, they exhibit very low basal and inducible levels of P450s, with the exception of CYP1 family. Engineered cell lines, on the other hand, often express a narrow set of CYP450s and do not exhibit the regulation of gene expression in primary hepatocytes (63, 66).

In 2002, the hepatoma cell line HepaRG was established from a hepatocellular hepatoma as a cell model for Hepatitis B infection studies (67). HepaRG cells can undergo extensive differentiation, exhibiting hepatocyte-like morphology as well as displaying substantial liver-specific functions. Differentiated HepaRG cells (commercialized as HepaRG™) express broad-spectrum Phase I and Phase II enzymes, many of which are maintained at levels within the normal range of human hepatocytes and are significantly higher than in HepG2 cells. Since establishment, HepaRG™ cells have gained popularity as an *in vitro* model for a number of drug metabolism and hepatototixicty studies (60, 68-78).

In this study, we developed an alkaline CometChip platform for genotoxicity HT screening by incorporating the use of two DNA repair synthesis inhibitors, HU and ara-C, and HepaRG™ cells. We describe here the use of this platform in detection of bulky DNA adducts induced by bioactivation. We used B[a]P and AFB_1 as model DNA damaging agents that require bioactivation to be reactive with DNA. Using CYP450 inhibitors, we validated that DNA damage detected using our approach is dependent upon metabolic activation of B[a]P and AFB_1. Importantly, we inhibited NER initiation, which results in a reduction in SB levels, indicating the contribution of NER intermediates to detected SBs. Furthermore, we demonstrated that the platform has superior sensitivity compared to the conventional alkaline comet procedure using a small screen of nine known *in vivo* genotoxins.

Taken together, we have leveraged the HT advantage of CometChip, the enhanced sensitivity of the HU/ara-C combination, and the metabolic capacity of HepaRG™ cells to develop a screening platform

for DNA damage induced by the metabolism of xenobiotics. We believe this platform provides a rapid and sensitive tool to help overcome an important public health challenge, which is HT genotoxicity assessment in human-relevant metabolic conditions.

2.3. MATERIAL AND METHODS

Chemicals

Reduced L-glutathione (GSH, G6013), hydroxyurea (HU, H8627), and cytosine arabinoside (ara-C, C1768) were obtained from MilliporeSigma, St. Louis, MO. 1X GSH solution (10 mM) was prepared by dissolving GSH powder in warm culture medium and used immediately within 30 minutes of preparation. 1,000X HU (1 M) and 1,000X ara-C (10 mM) stock solutions were prepared by dissolving crystal HU and ara-C in cell culture grade water and stored in 30-50 µL aliquots at -20°C for no more than one year.

30% w/w hydrogen peroxide (H_2O_2) solution was obtained from MilliporeSigma, St. Louis, MO (H1009) and was stored at 4°C, protected from light. H_2O_2 dilutions were freshly prepared from the 30% stock immediately before use. 99% methyl methanesulfonate (MMS) solution was obtained from MilliporeSigma, St. Louis, MO (129925) and was stored at room temperature. MMS dilutions were freshly prepared from the 99% stock less than 15 minutes before use. 100% dimethyl sulfoxide (DMSO) was obtained from MilliporeSigma, St. Louis, MO (D8418).

Other chemicals (Table 2-1) were purchased in powder form and dissolved to prepare stock solutions, and their aliquots were stored at -20°C for up to one year. To use, an aliquot was slowly thawed at room temperature.

Cell culture

Dulbecco's phosphate-buffered saline (DPBS), high-glucose Dulbecco's Modified Eagle's Medium (DMEM, high glucose, 11965092), RMPI-1640 with GlutaMAX™ (61870), 200 mM L-glutamine (A2916801), 10,000 U/ml Pen-Strep (15140), 100X GlutaMAX™ supplement (35050061), William's E Medium (WEM, A1217601), HepaRG™ Thaw, Plate, & General Purpose Medium Supplement (HPRG670), HepaRG™ Maintenance/Metabolism Medium Supplement (HPRG620), 0.25% Trypsin-EDTA with phenol red (25200), and 96-well plate coated with collagen I (A1142803) were purchased from ThermoFisher Scientific, Waltham, MA. Fetal bovine serum was obtained from Atlanta Biologicals, Inc., Flowery Branch, GA.

All the cells were cultured in an incubator set at 37°C with 5% CO_2.

TK6 (79, 80), a human B-lymphoblastoid cell line, was a gift from W. Thilly. TK6 was cultured in RPMI 1640 medium with GlutaMAX™ supplemented with 100 U/ml Pen-Strep. TK6 cell suspension was directly obtained from the suspension culture.

The XPG cell lines were gifts from O. Scharer. These include XPG-deficient, XPG/WT, and XPG/E791A. The XPG-deficient cell line was obtained from SV40-transformation of the primary human skin fibroblasts from patient XPCS1RO (81). XPG/WT and XPG/E791A cells were obtained from the stable transfection of the lentiviral vector containing XPG WT cDNA or XPG-E791A cDNA in the XPG-deficient cell line (30). The XPG cell lines were cultured in high-glucose DMEM supplemented with 10% FBS, 2 mM L-glutamine, and 100 U/ml Pen-Strep.

HepG2 (ATCC® HB-8065™), an immortalized cell line derived from human hepatocellular carcinoma, was obtained from the American Type Culture Collection (Manassas, VA). The cells were cultured in high-glucose DMEM supplemented with 10% FBS, 1X GlutaMAX™, and 100 U/ml Pen-Strep. For chemical exposures, exponentially growing cells were plated in a tissue cultured treated 96-well plate two days before treatment. The seeding density was 50,000 cells/well.

Cryopreserved HepaRG™ (HPRGC10), a terminally differentiated hepatic cell line, was purchased from ThermoFisher Scientific (Waltham, MA). HepaRG™ was thawed and cultured according to the supplier's manual. Briefly, the general purpose working medium was WEM supplemented with 1X GlutaMAX™ and 1X HepaRG™ Thaw, Plate, & General Purpose Medium Supplement. The metabolism working medium was WEM supplemented with 1X GlutaMAX™ and HepaRG™ Maintenance/Metabolism Medium Supplement. HepaRG™ cells were thawed in the general purpose working medium and plated in a 96-well plate coated with collagen I at 100,000 cells/well. For *same-day chemical treatments*, the final volume per well after plating was 50 µL. Cells were allowed to attach for 1-1.5 hr. 50 µL of chemical solution in 2X concentration (prepared in the general purpose working medium) was added to each well to obtain a final concentration of 1X and a final volume of 100 µL. For *day-7 chemical treatments*, the final volume per well after plating was 100 µL. One day after plating, the general purpose working medium was changed to the metabolism working medium. The metabolism working medium was renewed on day 4 and day 6 after plating. On day 7, the cells were treated with 100 µL of 1X test chemical prepared in the metabolism working medium.

To obtain cell suspension for the XP-G cell lines, HepG2, and HepaRG, the monolayer culture was incubated with 0.25% Trypsin-EDTA at 37°C. For XPG cell lines, the incubation time was 1-2 minutes. For HepG2 and HepaRG, the incubation time was 5-10 minutes. Detached cells were then suspended in complete working media. Cell viability and cell number were analyzed using an automated Trypan Blue exclusion system [Vi-CELL™ cell counter (Beckman Coulter Life Sciences, Brea, CA)].

CometChip fabrication

Sylgar™ 184 silicone elastomer kit (102092-312) and bottomless 96-well plates (82050-714) were purchased from VWR, Radnor, PA. GelBond® Film (53761) was obtained from Lonza, Portsmouth, NH. UltraPure™ agarose (16500100) and UltraPure™ low melting point agarose (16520100) were purchased from ThermoFisher Scientific, Waltham, MA.

The microwells were fabricated as described previously (14-16, 82). Briefly, 1% w/v agarose solution in DPBS was prepared. A polydimethylsiloxane (PDMS) stamp with an array of micropegs was fabricated using the Sylgar™ 184 kit as described previously (15). The stamp was pressed into the molten agarose solution on top of the hydrophilic side of a sheet of GelBond® Film. The agarose was allowed to gel at room temperature for ~15 minutes. The stamp was removed to reveal an array of microwells with ~40-50 μm in both diameter and depth. The microwells were spaced 240 μm apart. A bottomless 96-well plate was pressed on top of the agarose chip to form 96 macrowells. The bottom of each macrowell was an array of ~300 microwells.

To load cells into microwells, ~2,000 – 200,000 cells in suspension were placed into each macrowell, and the chip was incubated at 37°C in the presence of 5% CO_2 for 15 minutes. This time is sufficient for most cell types to have fully loaded into the microwells by gravity. Excess cells were then washed off with DPBS by shear force. The chip was covered with a layer of overlay agarose (1% w/v low-melting point agarose solution in DPBS, kept molten at 43°C until use). For complete solidification of the overlay agarose, the chip was kept at room temperature for 2 minutes followed by 2 minutes at 4°C.

Alkaline comet assay

Sodium chloride (NaCl, 7581), disodium EDTA (Na_2EDTA, 4931), and sodium hydroxide pellets (NaOH, 7708) were purchased from VWR, Radnor, PA. Trizma® base (T1503), Trizma® HCl (T5941), and Triton X-100 (X-100) were obtained from MilliporeSigma, St. Louis, MO. 10,000X SYBR™ Gold nucleic acid gel stain was obtained from ThermoFisher Scientific, Waltham, MA.

The alkaline lysis buffer (pH ~ 10) was a solution of 2.5 M NaCl, 100 mM Na_2EDTA, 10 mM Trizma® base, and 1% v/v Triton X-100 dissolved in de-ionized H_2O (dI H_2O). The alkaline unwinding buffer (pH ~ 13.5) was prepared by diluting NaOH and Na_2EDTA stock solutions in dI H_2O to final concentrations of 0.3 M and 1 mM, respectively. The neutralization buffer (pH ~ 7.5) was prepared by dissolving Trizma® HCl in distilled H_2O to a final concentration of 0.4 M.

Cells encapsulated in CometChip were lysed in the alkaline lysis buffer overnight at 4°C. The nuclei were unwound in the alkaline unwinding buffer for 40 minutes at 4°C, and the DNA was electrophoresed in the same buffer at the same temperature for 30 minutes at 1 V/cm and ~300 mA. The CometChip was then washed three times in the neutralization buffer by submerging for five minutes each time.

Afterward, the DNA on ComeChip was stained for 15 minutes at room temperature with 1X of SYBR™ Gold diluted in DPBS, protected from light. Fluorescent images of the comets were captured at 40X magnification using an epifluorescence microscope (Nikon Eclipse 80i, Nikon Instruments, Inc., Melville, NY) with a 480 nm excitation filter. Image acquisition was achieved by automatic scanning using a motorized XY stage. Comet images were automatically analyzed using Guicometanalyzer, a custom software developed in MATLAB (The MathWorks Inc., Natick, MA) as previously described (15). Outputs from Guicometanalyzer were processed and imported to a spreadsheet (Microsoft Excel, Microsoft Office Suite 2016) using Comet2Excel, an in-house software developed in Python (Python Software Foundation, Python version 2.7.10).

Liver perfusion and hepatocyte culture on CometChip

100X Gibco® Antibiotic-Antimycotic (15240) was purchased from ThermoFisher Scientific, Waltham, MA. Insulin-transferrin-sodium selenite supplement (ITS) (11074547001), aprotinin (A3428), HEPES (H4034), dexamethasone (D4902), and Percoll® (P4937) were obtained from MilliporeSigma, St. Louis, MO.

Isolation medium was WEM supplemented with 1X GlutaMAX™, 1X Gibco® Antibioti-Antimycotic, 10 μg/mL IST, 1 μg/mL aprotinin, 10 mM HEPES, 0.1 μM dexamethasone, and 10% FBS. Maintenance medium was isolation medium without 10% FBS.

Primary mouse hepatocytes were obtained from 10-14 week old C57Bl6 mice using a standard two-step collagenase liver perfusion procedure with minor changes (83, 84). The isolated cells were suspended

in the isolation medium and were enriched for viable hepatocytes by centrifugation using a 45% Percoll® solution. Cell viability and cell number were analyzed using an automated Trypan Blue exclusion system [Vi-CELL™ cell counter (Beckman Coulter Life Sciences, Brea, CA)]. The perfusion procedure yielded ~20-50 million cells per liver and ~80-90% cell viability.

Microwell array in agarose chip was fabricated as described in the Alkaline CometChip section with some changes. Specifically, the 1% w/v agarose solution and the overlay agarose solution were supplemented with 2X Gibco® Antibiotic-Antimycotic. Hepatocytes in suspension were loaded into microwells by incubating at 37°C for a maximum of 10 minutes. After the agarose overlay step, cells were incubated in isolation medium (50 µL/macrowell) at 37°C in the presence of 5% CO_2. After four hours, isolation medium was exchanged for maintenance medium, and cells were incubated overnight at 37°C in the presence of 5% CO_2. After the overnight incubation, chemical treatments were performed by exposing cells to 1X solution of test compounds diluted in the maintenance medium (50 µL/macrowell).

Ultraviolet (UV) light exposure

Prior to UV irradiation, cells embedded in CometChip were incubated for 40 minutes at 37°C in working medium supplemented with 10 mM GSH. Exposure to 254 nm UV light radiation (UVC) was administered via a handheld UV lamp that had a dose-rate of 14 $J/m^2/s$ at a distance of 7.6 cm (UVP 95001614, ThermoFisher Scientific, Waltham, MA). The UV irradiation procedure was carried out in the dark at 4°C.

To query the level of bulky adducts induced by UV exposure, we used a combination of 1 mM HU and 10 µM ara-C to inhibit NER repair synthesis. Specifically, 500X HU/ara-C solution was prepared by combining one volume of 1 M HU and one volume of 10 mM ara-C. Before UV exposure, cells were pretreated with 1X HU/ara-C prepared in working medium supplemented with 10 mM GSH for 40 minutes at 37°C. Following UV exposure, cells were incubated in working medium supplemented with 10 mM GSH

and 1X HU/ara-C for one hour and four hours at 37°C. Cells were lysed in the alkaline lysis buffer and the level of DNA strand breaks were analyzed following the alkaline comet assay described above.

To study NER efficiency, we examined the the repair rate of CPDs induced by UV irradiation. The bacterial T4 endonuclease V (M0308S, New England BioLabs, Ipswich, MA) was used in combination with the alkaline comet assay to query the level of CPDs (85) over 24 hours of repair. Briefly, UV-exposed cells were incubated in working medium supplemented with 10 mM GSH for one hour, four hours, and 24 hours. Cells embedded in CometChip were lysed overnight in the alkaline lysis buffer. The CometChip was then washed three times with the enzyme reaction buffer (1 mM EDTA, 100 mM NaCl, 25 mM Na_2HPO_4, 100 μg/mL BSA, pH 7.2) by submerging for 15 minutes each time. The enzyme reaction was performed by incubating the CometChip with 50 U/mL T4 Endonuclease V in the enzyme reaction buffer for 15 minutes at 37°C. Afterward, the CometChip was placed in the alkaline unwinding buffer and processed following the remaining steps of the alkaline comet assay.

AFB_1 and B[a]P treatments

For each dose of the test compound, a 200X solution was prepared by diluting the stock solution (4 mM AFB_1 or 20 mM B[a]P) in DMSO. The 1X solution was prepared by diluting the 200X with cell culture medium. A vehicle control condition was included by diluting DMSO in cell culture medium to get a final concentration of 0.5%. Cells were incubated with the 1X solution for 24 hours at 37°C in the presence of 5% CO_2. To reveal the level of DNA damage induced by the test compound, cells were also exposed to 1X HU/ara-C at the same time. After treatment, cells were analyzed with the alkaline comet assay.

Inhibition of AFB_1 or B[a]P bioactivation

5 μM KET or 25 μM ANF was added to culture medium at the start of the AFB_1 or B[a]P treatment to inhibit AFB_1 or B[a]P bioactivation, respectively. The maximum final concentration of DMSO was 0.6%. The remaining steps were similar to the AFB_1 and B[a]P treatments.

Inhibition of NER initiation with spironolactone (SP)

Cells were pretreated with 20 μM SP for 5 hours at 37°C. For UV-treatment, 20 μM was also added to the 40-min incubated period prior to UV exposure and in the medium for repair following the irradiation. The maximum concentration of DMSO was 0.1%, and the remaining steps were similar to the UV exposure experiment. For AFB_1 and B[a]P, 20 μM SP was also added to the culture medium during the treatment period. The maximum final concentration of DMSO was 0.6%. The remaining steps were similar to the AFB_1 and B[a]P treatments.

CellTiter-Glo® assay (CTG®) for cell viability

The CellTiter-Glo® luminescent cell viability assay kit (G7570) was obtained from Promega, Madison, WI. Cell viability after 24 hours of chemical treatment was measured according to the manufacturer's manual. Luminescent signals were recorded using a SpectraMax M2e microplate reader (Molecular Devices, Sunnyvale, CA). Control wells with no cells were included to obtain background luminescence, which was then subtracted from the signals measured in the sample wells.

P450-Glo™ assays for CYP3A4 and CYP1A2 activity

The P450-Glo™ CYP3A4 assay with luciferin-IPA (V9001) and the P450-Glo™ CYP1A2 assay with luciferin-1A2 (V8421) were purchased from Promega, Madison, WI. The activity levels of CYP3A4 and CYP1A2 in cells were measured according to the manufacturer's protocol for non-lytic cell-based assays. Luminescent signals were recorded using a SpectraMax M2e microplate reader (Molecular Devices, Sunnyvale, CA). Control wells with no cells were included to obtain background luminescence. The net signal for each sample was obtained by subtracting the background luminescence value.

CYP3A4 or CYP1A2 activity per cell can be obtained by normalizing P450-Glo™ values with cell numbers. After a sample was analyzed for CYP3A4 or CYP1A2 activity, the CTG® assay was performed to obtain an estimate of the number of viable cells in the sample. The result from P450-Glo™ was then divided by the CTG® value to obtain CYP3A4 or CYP1A2 activity per cell.

Hydrogen peroxide (H_2O_2) treatment

Doses of H_2O_2 were prepared immediately before use by diluting 30% stock solution (10 M) with cold PBS. Suspension of TK6 cells was obtained directly from exponentially growing culture and loaded onto CometChip (see "CometChip fabrication"). A new bottomless 96-well was placed on top of the CometChip. 100 μL of H_2O_2 solution was pipetted into each well, and the CometChip was incubated at 4°C for 20 minutes, protected from light. Afterward, the H_2O_2 solution was aspirated, and the bottomless plate was taken off. The CometChip was rinsed by submerging in cold PBS. To analyzed DNA damage immediately after treatment, the CometChip was placed in cold alkaline lysis buffer and processed following the remaining steps of the alkaline comet assay. To study repair kinetics, the CometChip was cut into ~5 cm x 5 cm pieces using a pair of sterile surgical scissors and incubated in culture medium at 37°C for up to two hours. At each time point, a piece of CometChip was removed and placed in cold alkaline lysis buffer. The remaining steps followed the alkaline comet assay procedure.

Methylmethane sulfonate (MMS) treatment

Doses of MMS were prepared ~15 minutes before use by diluting 99% stock solution (11.8 M) with warm serum-free media (pre-warmed by incubation at 37°C). Suspension of TK6 cells was obtained directly from exponentially growing culture, and 1 mL of cell suspension was placed in a 15 mL conical tube. The tube was centrifuged (200 x g, 5 minutes), and the supernatant was aspirated. The cell pellet in each well was re-suspended in 1 mL of MMS solution, and the tube was incubated for 30 minutes or one hour at 37°C. Next, the tube was again centrifuged (200 x g, 5 minutes), and MMS supernatant was aspirated. Each cell pellet was washed three times by re-suspending in 1 mL PBS, spinning down (200 x g, 5 minutes), and aspirating the supernatant. After the last wash, each pellet was re-suspended in 1 mL culture medium. To analyzed DNA damage immediately after treatment, 50 μL of cell suspension was transfer to a macrowell on CometChip. After the cells loaded into the microwells (see "CometChip fabrication"), they were immediately placed in cold alkaline lysis buffer and processed following the remaining steps of the alkaline comet assay. To analyze repair kinetics, remaining cells in the tube were incubated at 37°C for up

to 24 hours. At each time point, 50 μL of cell suspension was transfer to a macrowell on CometChip and processed as above.

2.4. RESULTS

Modification of alkaline CometChip for sensitive detection of bulky DNA adducts (HU/ara-C approach)

Many environmental carcinogens, such as ultraviolet light, aflatoxins, PAHs, and heterocyclic amines, induce DNA lesions that are considered "bulky" (18, 19). Bulky adducts thermodynamically destabilize the double helix, making them good substrates of NER (19). After the damage site is recognized and verified, dual incisions are made to excise a 22-30 nucleotide fragment surrounding the damage site (20). As a consequence, NER produces a number of SB intermediates as part of the repair pathway. These intermediates are, in principle, detectable by the alkaline comet assay. However, it has been reported that the frequency of SBs is relatively low in high UV doses (86), which suggests that NER SB intermediates are transient and difficult to detect with the alkaline comet assay.

To improve throughput and reproducibility, in this study we performed the alkaline comet procedure using CometChip as described previously (15, 16, 82) (Fig. 2-1, see **Methods**). In order to investigate the sensitivity of the alkaline CometChip in detecting bulky DNA lesions, we exposed immortalized human fibroblasts with UV-C, which is known to induce mostly CPDs and 6-4PPs (20), as well as oxidative damage (87, 88). Both CPD and 6-4PP are known to destabilize the DNA duplex and are substrates for NER (18-20). To minimize oxidative damage induced by UV radiation, the cells were pre-treated with reduced glutathione (10 mM GSH). After exposure to UV-C, the cells were allowed to repair for up to four hours in fresh medium supplemented with GSH. As shown in Fig. 2-2A, the level of DNA SBs analyzed by the alkaline comet assay increases following UV exposure, reaching a maximum of ~20% tail DNA after one hour and slowly going down to ~15% at the 4-hour time point. Both of these numbers

are only slightly above the basal damage level (~10% tail DNA) and well below the alkaline comet assay's saturation level (~75% tail DNA), indicating that the assay is relatively insensitive to bulky adducts.

SB intermediates from DNA repair are transient, and the level of SBs is a function of both break generation (incision) and gap filling (DNA repair synthesis and ligation). Therefore, slowing down or inhibiting gap filling can theoretically enhance the level of SBs, thereby improving the assay's sensitivity. To test this hypothesis, we irradiated XPG/E791A cells (30) with UV-C and measured the resulting SBs. The E791A mutation renders the XPG enzyme catalytically inactive but still allows DNA binding (30, 89). Because the 5' incision by ERCC1-XPF is not affected (30) XPG/E791A cells are able to generate NER SB intermediates. However, XPG-E791A is not able to cleave 3' to the damage site, leading to a 5' overhang and preventing ligation. In fact, we observed that SBs accumulate in XPG/E791A cells overtime following UVR, exhibiting >2.5-fold the level of SBs in XPG/WT (Fig. 2-2B).

An implication from Fig. 2-2B is that NER's efficient gap filling contributes to the transient state of the SB intermediates. As a consequence, the result suggests that it is possible to increase the assay's sensitivity by inhibiting gap filling. In fact, classic SB detection methods, such as the alkaline sucrose sedimentation technique (33, 34) and alkaline elution assay (36), employ the use of DNA repair synthesis inhibitors to obtain more SBs for DNA repair studies of UV-induced damage. We adapted this technique and employed a combination of the inhibitors HU and ara-C. In the presence of HU/ara-C (short for "a mixture of 1 mM HU and 10 μM ara-C"), the level of accumulated SBs reaches a steady state of ~73-78% tail DNA after one hour following UVR (Fig. 2-2C), which is ~four times higher than the control condition without HU/ara-C (Fig. 2-2A). Since 75% tail DNA is the alkaline comet assay's saturation limit, it is possible that a higher number of SBs are generated but not reflected in the comet result.

HU/ara-C eliminates strand break formation by NER

To validate that the use of the HU and ara-C combination inhibits NER gap filling while allowing NER incision, we compared the results from XPG-deficient and XPG/WT cells (see **Methods**). Cells

defective in XPG are unable to initiate NER and generate SB intermediates in the presence of DNA lesions (30). Here, we show that SB accumulation in XPG-deficient cells is significantly less than in XPG/WT in both the absence and presence of HU and ara-C (Fig. 2-2D). The difference is revealed to be more than three-fold in the presence of the repair synthesis inhibitors, showing that most of the detected SBs using HU/ara-C are NER intermediates.

Dose-response to UV treatment using HU/ara-C approach

We also investigated the ability to study dose-response to a genotoxic agent using HU/ara-C. TK6 (human lymphoblastoid) and HepG2 (human hepatocyte cell line) were incubated in medium supplemented with GSH, HU, and ara-C for ~40 minutes and irradiated with various doses of UV-C. The cells were allowed to repair in the same medium for one hour after UV exposure to facilitate maximum SB accumulation. The HU/ara-C combination displays a strong dose-response to UV-C treatment in both cell lines, ranging from the basal level of ~10% to ~75% tail DNA (Fig. 2-2E). In contrast, the control condition without HU/ara-C shows significant increase in SBs only at the highest dose in HepG2 cells (~20% tail DNA).

Application of the HU/ara-C method to detect damage induced by metabolic activation of AFB_1 and B[a]P

Many environmental carcinogens are metabolically activated upon entering the body, mainly by hepatocytes in the liver (55). To study DNA damage in physiologically relevant metabolism conditions, we aimed to optimize an alkaline CometChip procedure using the HU/ara-C method together with metabolically competent human cell lines. We demonstrated the efficacy of the method by treating HepaRG™, HepG2, and primary mouse hepatocytes with the carcinogens aflatoxin B_1 (AFB_1) and benzo[a]pyrene (B[a]P), both of which are known to become DNA reactive upon metabolic activation by CYP450s. To control for bioactivation, we included a negative control cell line, TK6, which has been shown to have no expression of CYP450s (90).

Aflatoxin B_1 treatment in cell lines

The mycotoxin AFB_1 is a potent environmental human carcinogen (91). It is produced by the molds *Aspergillus flavus* and *A. parasiticus*, which are frequent contaminants in peanuts and maize in certain regions of the world (92). Exposure to AFB_1 increases the risk of hepatocellular carcinoma (HCC) about three times, and co-exposure with hepatitis B elevates the risk approximately 60-fold (23). AFB_1 requires bioactivation to become reactive to DNA. Several CYP450 enzymes (93), such as CYP3A4 and CYP1A2, are known to oxidize AFB_1, producing a number of metabolites (94-97). The highly mutagenic metabolite, AFB_1-exo-8,9-epoxide, is very unstable, with a half-life of ~1 s in neutral pH at room temperature (98). The metabolite readily reacts with the N7 position of guanine to form DNA adducts. The most ubiquitous are AFB_1-N7-dG and AFB_1-Fapy-dG, both of which can lead to G-to-T transversions (24, 25). AFB_1-N7-dG highly distorts the double helix and has been shown to be excised by NER (99). In addition, a recent study shows that AFB_1-Fapy-dG is partially repaired by BER (recognized and excised by the glycosylase NEIL1) in mammalian cells (100).

Because CYP3A4 and CYP1A2 are essential in bioactivation of AFB_1, we compared the activity levels of these two enzymes in HepaRG™ and HepG2 cells using the P450-Glo™ assay (see **Methods**). As expected, HepaRG™ exhibits much higher activity levels for both of these P450s. Specifically, HepaRG™ shows >100-fold higher CYP3A4 activity (Fig. 2-S1) and >10-folder higher CYP1A2 activity compared to HepG2 cells (Fig. 2-S2). Consistent with the difference in P450 activity, HU/ara-C reveals a strong dose-response relationship to AFB_1 treatment in HepaRG™ cells while HepG2 cells show relatively little increase in SBs (Fig. 2-3A). The negative control cell line for bioactivation, TK6, has CYP3A4 and CYP1A2 activity levels below the detectable range of the P450-Glo assay and shows no response to AFB_1 treatment in both the absence and presence of HU/ara-C, further supporting the role of metabolic activation in SB formation. In addition, while HepG2 cells display a slight trend toward increased DNA damage with higher doses of AFB_1, no such trend is observed in TK6 cells (Fig. 2-3A). In the presence of HU/ara-C,

there is ~2-fold increase in background damage in TK6 cells, potentially due to either background NER activity or because of the cells' sensitivity toward the repair inhibitors themselves.

Benzo[a]pyrene treatment in cell lines

B[a]P, another human carcinogen (91), is the best known PAH. Many other PAHs are known carcinogens (26, 27). PAHs naturally occur in coal, oil, and gasoline and are produced by incomplete combustion of organic material. Common routes of exposure include breathing in fuel exhaust, cigarette smoke, and burning wood smoke, or consuming charred meat or other types of charred food (27). B[a]P, like other PAHs, is an inducer of the aryl hydrocarbon receptor (AHR), which is a transcription factor regulating a number of phase I and phase II enzymes, including the CYP1 family (CYP1A1, CYP1A2, and CYP1B1) (101). B[a]P is bioactivated by the CYP1 family. The most genotoxic metabolite is the diolepoxide (+)-anti-B[a]P-7,8-diol-9,10-epoxide (BPDE), which is formed in a series of reactions: B[a]P → B[a]P-7,8-oxide (by CYP1s) → B[a]P-7,8-diol (by epoxide hydrolase) → B[a]P-7,8-diol-9,10-epoxide (by CYP1s). BPDE covalently binds to the exocyclic N^2 of guanine, forming DNA adducts that can lead to G-to-T transversions (27).

In both HepaRG™ and HepG2 cells, HU/ara-C reveals dose-dependent increase of SBs with B[a]P treatment (Fig. 2-3B). HepaRG™ cells display overall higher levels of strand breaks, consistent with higher CYP1A2 activity level (Fig. 2-S2). For example, exposure to 1 μM B[a]P induces ~3 times more breaks in HepaRG than in HepG2. On the other hand, B[a]P treatment does not induce additional strand breaks in TK6 cells, which are consistent with the lack of an inducible CYP450 system in TK6 cells (90).

Application of HU/ara-C in primary mouse hepatocytes

Primary hepatocytes are the gold standard for metabolism studies. We wanted to show that HU/ara-C works well with these cells. Mouse hepatocytes were isolated using a standard two-step collagenase liver perfusion (see **Methods**). The cells were immediately loaded into CometChip microwells and allowed to recover overnight before AFB_1 or B[a]P treatment. HU/ara-C is able to show consistent dose-responses to

both chemicals (Fig. 2-3C and 3D). AFB_1 appears to induce SBs that are detectable even in the absence of HU and ara-C although the use of the repair inhibitors still improves the overall level of detected SBs. In contrast, B[a]P shows a strong dose-response in the presence of HU and ara-C while displaying a minimal increase in SBs in the absence of the inhibitors.

Bioactivation modulates the level of strand breaks detected using HU/ara-C approach

To further validate that strand breaks induced by AFB_1 and BaP using HU/ara-C in the alkaline CometChip are due to bioactivation of the carcinogens, we exploited the use of P450 inhibitors. We expected that inhibiting the key P450 enzyme responsible for the metabolism of each chemical would reduce the level of DNA adducts, which in turn would suppress the formation of NER SBs.

To reduce metabolic activation of AFB_1, we treated cells with ketoconazole (KET), a potent inhibitor of CYP3A4 (38, 102-105). At 5 μM KET, CYP3A4 activity level in HepaRG™ cells is reduced by ~100-fold and HepG2 level is reduced by ~10-fold (Fig. 2-S1). By itself, 5 μM KET does not induce detectable DNA damage in TK6, HepaRG™, and HepG2 (Fig. 2-4A, 4B, and 4C). When HepaRG™ cells are exposed to AFB_1 in the presence of KET, the level of SBs across all AFB_1 doses is reduced to near the background level (Fig. 2-4B). There is no apparent effect of KET in TK6 and HepG2 cells (Fig. 2-4A and 4C), which is most likely because the AFB_1 induces no damage in TK6 cells and minimal damage in HepG2 cells (Fig. 2-3A). The results show that HepaRG™ cells have the ability to metabolically activate AFB_1 and that the vast majority of AFB_1-induced damage is due to CYP3A4 activity.

To inhibit the metabolism of B[a]P, we used the small molecule α-naphthoflavone (ANF), a potent antagonist of CYP1A2 (106, 107). In addition, ANF also binds to AHR and inhibits its activation, thereby preventing the upregulation of AHR targets, including the CYP1 family (101, 108, 109). B[a]P induces CYP1A2 activity in a dose-dependent manner (Fig. 2-S2), consistent with activation of the AHR pathway by PAHs. Interestingly, B[a]P increases CYP1A2 activity in HepG2 cells up to ~12 times above the background level while the induction is only ~three times in HepaRG™ cells. Treatment of the cells with

25 μM ANF leads to ~40% reduction in background CYP1A2 activity in HepaRG™ cells and no apparent reduction in HepG2 cells. Furthermore, ANF completely suppresses the induction of CYP1A2 activity by B[a]P in both cell lines (Fig. 2-S2). Significantly, we observed in parallel that the same dose of ANF reduces the level of B[a]P-induced SBs to near the background level in both HepaRG™ and HepG2 (Fig. 2-4D, 4E, and 4F). Taken together, these results show that both HepaRG™ and HepG2 cells are capable of inducible metabolic activation of B[a]P and that CYP1A2 activity is essential for B[a]P's genotoxicity.

Contribution of NER to strand break formation

In the case of UV exposure, we have shown that the majority of SBs detected by HU/ara-C are NER intermediates (Fig. 2-2D), indicating the repair synthesis inhibitors can be used to reveal bulky lesions. Similarly, we wanted to investigate whether bulky lesions induced by AFB_1 and B[a]P contribute to detected SBs by HU/ara-C. To do this, we studied the contribution of NER SB intermediates following exposure to AFB_1 and B[a]P.

Our approach was to inhibit NER initiation and query whether SB formation is affected. Recently, the small molecule pharmaceutical spironolactone (SP) has been shown to inhibit the repair of 6-4PP induced by UV light via induction of XPB degradation (110). XPB is an essential component of the transcription factor 2 helicase complex (TFIIH) (111). The TFIIH complex plays a key role in the damage verification step of NER, which takes place prior to DNA incisions (18-20, 111). Consequently, we expected a reduction in SBs generated by NER in cells treated with SP, which would result in an overall reduction of SBs detected by HU/ara-C.

To investigate the effect of SP on SB generation by NER, we irradiated cells with UV-C to induce bulky adducts. Prior to UV-C exposure, cells were treated for five hours with 20 μM SP. Following UV-C irradiation, cells were allowed to repair in the presence of 20 μM SP for one hour. The results show that cells treated with SP exhibit more than three-fold reduction in SBs in both TK6 and HepG2 (Fig. 2-S3), indicating that the number of NER incision events is significantly reduced. On the other hand, there are

residual SBs revealed by HU/ara-C that are significantly higher than the basal levels in both cell types (Fig. 2-S3C and S3D). These results together show that SP partially inhibits NER initiation and can be used to reveal the contribution of NER intermediates to detected SBs in the presence of HU/ara-C.

We employed SP to explore the role of NER in SBs induced by AFB_1 and B[a]P. Similar to the UV experiment described above, HepaRG™, HepG2, and TK6 cells were pretreated with SP for five hours before exposure to AFB_1 or B[a]P for 24 hours. To maintain inhibition of NER initiation, SP was also added to the treatment solution.

In AFB_1 treatment, SP significantly reduces the level of SBs in HepaRG™ cells incubated with HU/ara-C, revealing that ~25-50% of detected SBs are NER intermediates (Fig. 2-5B). This result is potentially an underestimation of NER contribution since SP inhibition of NER is likely partial (Fig. 2-S3C and S3D). Therefore, residual NER activity may account for the remaining SBs. In addition, since the DNA damage spectrum of AFB_1 is complex and the mechanisms of HU and ara-C are not specific to NER, it is likely that other repair pathways partially contribute to the detected SBs. Furthermore, SP appears to have a relatively small, although not statistically significant, inhibitory effect on CYP3A4 activity in HepaRG™ cells (Fig. 2-S4A), which may contribute to the observed reduction in SBs in Fig. 2-5B. Finally, because the negative control cells, TK6 and HepG2, display no additional SB formation in response to AFB_1, SP shows no inhibitory effect in these cells (Fig. 2-5A and 5C).

Results from B[a]P treatment show that SP displays no inhibition of B[a]P-induced SB formation in HepaRG™ cells (Fig 2-5E) whereas SP reduces SBs to near the background level in HepG2 cells (Fig. 2-5F). The results in HepG2 indicate that the majority of strand breaks detected by HU/ara-C come from NER of B[a]P-induced bulky adducts. There appears to be a relatively small but significant reduction of CYP1A2 activity by SP in HepG2 cells (Fig. 2-S5B), which may partially account for the reduction in SB formation. The dramatic difference in the effect of SP in HepaRG™ and HepG2 may be due to a difference in the levels of NER suppression achieved by SP in the two cell lines. SP is known to be extensively metabolized in the liver to produce metabolites that are active for treatment of hypertension and congestive

heart failure (112). Although SP has been shown to induce XPB degradation (110), the effects of SP's metabolites on NER machinery are unknown. Since HepaRG™ cells have a much higher metabolic capacity than HepG2, it is possible that there is less available NER-inhibiting SP in HepaRG™ compared to HepG2.

Altogether, the results from SP treatment suggest at least a partial contribution of NER to SBs induced by AFB_1 and potentially B[a]P. To accurately quantify the contribution of NER SB intermediates, we used an *Xpa*$^{-/-}$ mouse model to completely abolish NER (113). The XPA protein is an essential component of the NER preincision complex, interacting with a number of NER proteins (e.g. TFIIH, RPA, ERCC1-XPF, and PCNA) and facilitating the correct formation of the complex so that incision can occur (19). Therefore, XPA deficiency results in a complete loss of NER. As a consequence, *Xpa*$^{-/-}$ mice are prone to developing tumors upon UV exposure (113) and have been a popular mouse model for NER studies.

In order to provide the necessary metabolism, we used primary mouse hepatocytes for AFB_1 and B[a]P treatments. For AFB_1 doses higher than 1 μM, the SB level in WT hepatocytes is more than twice the level in *Xpa*$^{-/-}$ cells in the presence of HU/ara-C (Fig. 2-6A). These results indicate that NER intermediates contribute more than half of the SBs induced by AFB_1, which is consistent with the results obtained in HepaRG™ cells using SP (Fig. 2-5B). Significantly, the results also show that a significant portion of SBs are NER-independent and therefore likely intermediates from other repair pathways. Furthermore, a similar dose-response to AFB_1 is observed in both WT and *Xpa*$^{-/-}$ in the absence of HU and ara-C, which strengthens the argument that some of AFB_1-induced damage is repaired by NER-independent pathways. Our most likely candidate is BER with NEIL1 as the glycosylase that can recognize and excise a portion of AFB_1-Fapy-dG adducts (100). Alkali-labile abasic sites formed by spontaneous hydrolysis of AFB_1-Fapy-dG adducts may also contribute to detected strand breaks (114). In addition, the process of AFB_1 metabolic activation by CYP450s is also known to produce reactive oxygen species and induce lipid peroxidation (115-117), which can result in a mixture of DNA lesions (117) that require the participation of different DNA repair pathways.

For B[a]P treatment, while WT hepatocytes show a dose-dependent increase in SBs, there is virtually no SB formation in *Xpa*$^{-/-}$ hepatocytes in the presence of HU/ara-C (Fig. 2-6B). These results are consistent with the data obtained from HepG2 cells (Fig. 2-5F), further supporting that the majority of SBs detected in the presence of HU/ara-C are NER intermediates and that the lack of SB reduction by SP observed in HepaRG™ cells (Fig. 2-5E) may be due to insufficient reduction of NER activity.

HU/ara-C inhibits repair of oxidative and alkylation damage

We have demonstrated that the use of HU and ara-C is efficient at inhibiting the gap-filling step of NER. However, the molecular mechanisms of HU and ara-C suggest that gap filling of BER, particularly long-patch BER, may also be affected. Specifically, HU leads to a depletion of the dNTP pool (41-45), which is likely to affect any DNA synthesis-dependent process. There is a body of evidence showing that ara-C blocks DNA repair synthesis by Pol β (47, 51-53), which participates in BER (118). Therefore, we postulated that the HU/ara-C combination can also be used to enhanced sensitivity for detection of oxidative and alkylation damage, both of which are mainly repaired by BER in mammalian cells (118).

To investigate the effect of HU/ara-C on SBs induced by oxidative damage, we treated TK6 cells with hydrogen peroxide (H_2O_2) for 20 minutes at 4°C to minimize repair activity. Cells were then allowed to repair for one hour. Immediately after the H_2O_2 challenge, TK6 cells show a dose-dependent increase in SBs (Fig. 2-7A, *left* – gray line). Interestingly, immediately after H_2O_2 treatment, HU/ara-C leads to a small but statistically significant increase in SBs for the top three H_2O_2 doses (Fig. 2-7A, left – red line). The most striking result is observed after one hour of repair following the H_2O_2 challenge. In the absence of the repair synthesis inhibitors, SBs are rapidly rejoined, and by one hour of repair, their level has reduced to near the basal level across all doses (Fig. 2-7A, *right* – gray line). In contrast, cells incubated with HU and ara-C maintain the same initial level of SBs, suggesting that oxidative damage repair is inhibited (Fig. 2-7A, *right* – red line).

To induce alkylation damage, we challenged TK6 cells with the chemotherapeutic methyl methane sulfonate (MMS) for 30 minutes at 37°C. While a dose-response to MMS treatment is observed in the absence of HU/ara-C, the presence of the repair inhibitors increases the SB level by ~2-fold (Fig. 2-7B, *left* – red line). A significant observation is that while 0.5 mM MMS does not appear genotoxic in the absence of HU and ara-C, the addition of the repair synthesis inhibitors reveals a damage level more than twice the background level. After one hour of repair following MMS treatment, the damage level is maintained in both the absence and presence of HU/ara-C. In fact, the repair of MMS-induced damage in TK6 cells is relatively slow, with a half-time of ~6 hours, which is ~12 times slower than the repair of H_2O_2-induced damage (half-time ~28 min) (Fig. 2-S6).

All in all, we conclude that the combination of the repair synthesis inhibitors HU and ara-C can be used to improve the overall sensitivity of the alkaline comet assay for DNA damage detection by amplifying the number of SBs induced by the repair of bulky DNA adducts, oxidative damage, and alkylation damage. The implication is that not only a broader range of genotoxic agents can be uncovered but a wider range of genotoxic doses can also be revealed.

HU/ara-C improves overall detection sensitivity for DNA damaging agents

For performance assessment of *in vitro* genotoxicity tests, the European Reference Laboratory for Alternatives to Animal Testing (EURL ECVAM) published recommendations of chemicals that should give either positive results or negative results in an *in vitro* test (119, 120). To assess the sensitivity of the alkaline CometChip using HU/ara-C, we treated HepaRG™ cells with nine known *in vivo* genotoxins from Group 1 of the ECVAM's recommendation (120) (Table 2-1, No. 5 – 13) and compared the results of the alkaline CometChip assay in the absence and presence of HU/ara-C.

The identities of the test compounds were blinded until all data were collected and analyzed. Stock solutions were prepared to be 100X of the top doses recommended for *in vitro* genotoxic assessment (120). The treatment time was 24 hours for all chemicals. In parallel, cell viability for each condition was also

collected using CTG® (see **Methods**). Remarkably, whereas only one chemical shows positive results for DNA damage [N-nitrosodimethylamine (NDMA)] in the absence of HU/ara-C, the presence of the repair inhibitors reveal significant DNA damage for seven (out of nine) compounds (Table 2-2, second and third columns). In addition, four of the test compounds are known to be metabolically activated [cyclophosphamide, B[a]P, NDMA, and 2,4-diaminotoluene (2,4-DAT) (120)], and all four are scored as positives in the presence of HU/ara-C.

Hydroquinone (HQ) and chloramphenicol (CAM) induce high levels of cytotoxicity for doses that show significant DNA damage in the presence of HU/ara-C. Specifically, the highest dose for HQ exhibits significant increase in SBs but kills more than 50% of the cells (Fig. 2-S7F). Similarly, the two highest doses for CAM (3.1 and 6.2 mM) induce high levels of cytotoxicity (~53% and ~3% survival, respectively – Fig. 2-S7H) as well as significant DNA damage. There is no formal threshold for cell viability in scoring the comet assay. Nonetheless, cytotoxicity may contribute to DNA fragmentation, which can lead to overestimation of genotoxicity (13). Therefore, cytotoxicity needs to be considered in assessing comet data. In the cases of HQ and CAM, because there appear to be dose-response trends (although not all doses reach statistical significance), we decided to score both chemicals as positives. However, if a 50% cell viability threshold is applied, then HQ and the highest CAM dose will be excluded from the positive results.

The two compounds with definite negative results are *para*-chloroaniline (PCA) and cisplatin. PCA is used in a number of industrial processes, such as dye production (121). It is extensively metabolized in the body as part of the detoxification process, but it is unclear whether genotoxic metabolites are generated (121). Although PCA is an *in vivo* genotoxin (119, 120), a rodent carcinogen (121), and a possible human carcinogen (91) (Table 2-2), there are conflicting data about PCA's *in vitro* genotoxic potential (121, 122). Notably, although the highest dose (5 mM) induces ~50% cell death, no significant increase in DNA damage is detected (Fig. 2-S7D). The implication is that PCA induces cell death via a DNA damage-independent pathway.

Cisplatin is a commonly used platinum-based chemotherapeutic for different types of cancers, including bladder cancer, ovarian cancer, head and neck cancer, and non-small-cell lung cancer (123-126). Upon entering the cell, the chloride ligands hydrolyze, generating aquated cisplatin that can bind to the N7 atom of purine bases in DNA to form monoadducts and subsequent crosslinks (123). Notably, more than 85% of the adducts are intrastrand crosslinks, and about 4-5% are interstrand crosslinks (123, 124). Although crosslinks can be repaired by NER, our results show no increase in DNA migration with cisplatin treatment (Fig. 2-S7I). These observations indicate that despite their small number, the interstrand crosslinks are able to prevent migration of DNA ends generated by NER, possibly by holding the two DNA strands of the double helix together (127).

In the absence of HU and ara-C, only N-nitrosodimethyl amine (NDMA) shows positive results for DNA damage (Table 2-2). NDMA is bioactivated in the body mainly by CYP2E1 (128) to yield an α-hydroxymethyl nitrosamine that forms a reactive methyl diazonium ion (129), which alkylates nucleobases irreversibly via S_N1 nucleophilic substitution (130). Unlike MMS, which is an S_N2 alkylator (131), NDMA does not exhibit additional increase in SBs in the presence of HU/ara-C (Fig. 2-S7E).

In summary, the repair synthesis inhibitors HU and ara-C significantly improve the sensitivity of the alkaline comet assay. In the context of chemical genotoxicity testing, we propose the use of the alkaline CometChip with HepaRG™ cells in the presence of HU/ara-C as a screening platform to achieve high throughput and low false positive rates. To further assess the platform, we will proceed to test its specificity with non-genotoxic chemicals from the ECVAM's recommendations (chemicals from Group 2 and Group 3) (119, 120).

2.5. DISCUSSION

Although DNA damage can drive the initiation and progression of carcinogenesis and other diseases (1-4), there have been relatively few advances in techniques for detection of DNA damage. There

is currently no HT assay for detection of bulky DNA adducts, and metabolic activation of chemicals is still routinely achieved through incubation with liver S9 fractions (5, 57). The most commonly used is the comet assay, which relies on DNA strand breaks to measure the level of DNA damage. However, it is low-throughput, has high laboratory variation, and is relatively insensitive toward bulky DNA lesions. To overcome these challenges, we combined the HT nature of CometChip, the metabolic capacity of HepaRG™ cells, and enhanced sensitivity for DNA damage using DNA repair synthesis inhibitors. We demonstrated in this study a platform for genotoxicity screening that is significantly more sensitive and >5,000 fold faster compared to the conventional comet assay.

With its broad spectrum metabolism and its high basal and inducible metabolic enzyme levels, HepaRG™ has the potential to be the gold standard as a robust and reliable cell model for genotoxicity testing. We compared HepaRG™ with HepG2, a classic human hepatocyte cell line, and found that HepaRG™ exhibit orders of magnitude higher activity levels of CYP3A4 and CYP1A2, which is consistent with the difference in gene expression levels found in other studies (70, 71, 76). We found that the higher CYP3A4 and CYP1A2 activities in HepaRG™ cells translate to higher levels of DNA damage induced by AFB_1 and B[a]P compared to HepG2. Significantly, the difference in DNA damage between the two cell lines is revealed only in the presence of the repair synthesis inhibitors HU and ara-C.

Using the alkaline CometChip, we showed here that the HU/ara-C combination enables superior sensitivity to bulky DNA adducts induced by metabolic activation. Specifically, the HU/ara-C combination elevates the level of SBs in cells upon exposure to UV, AFB_1, and B[a]P. Using CYP450 inhibitors in HepaRG™ and HepG2 cells, we verified that formation of SBs upon AFB_1 and B[a]P treatments is dependent on specific CYP450 enzyme activity. Furthermore, we confirmed that the majority of SBs induced by UV, AFB_1, and B[a]P treatment in the presence of HU/ara-C are intermediates of NER by inhibiting NER incisions. These results indicate that HU/ara-C is sensitive for detection of NER substrates, which include a wide range of DNA lesions (19).

In addition, we demonstrated that the HU/ara-C combination can be applied to inhibit completion of the repair of oxidative damage (H_2O_2 treatment), resulting in sustained SB level after one hour of repair. Because oxidative base lesions (e.g. 8-oxoG) are primarily repaired by the BER (132), it is likely that HU/ara-C inhibits the gap filling step of BER. On the other hand, there is evidence that NER also participates in removing oxidative "non-bulky" adducts, such as 8-oxoG and thymine glycol (133). Furthermore, reactive oxygen species can initiate lipid peroxidation, which produces a number of unsaturated aldehydes or enals (134). Some of these products (e.g. trans-4-hydroxynonenal, crotonaldehyde, acetaldehyde (117, 134)) react with DNA to form bulky adducts (e.g. 1,N^2-propano-2'-deoxyguanosine) (135), which can be repaired by NER (136). It is therefore possible that NER intermediates also contribute to the observed SBs induced by H_2O_2.

While we have not yet tested the level of DNA damage in MMS-treated cells after a sufficient repair period in the presence of HU/ara-C (e.g. 24 hours), we were able to show that the inhibitors HU and ara-C enhance the initial damage by a factor of ~two. The reason is likely because during the 30 minutes of MMS treatment, DNA repair by BER is active. The presence of HU/ara-C likely inhibits the gap filling step of BER during this period, resulting in SB accumulation. On the other hand, while HU/ara-C leads to additional MMS-induced SBs, the same effect is not observed in another alkylating agent, NDMA. Both NDMA and MMS are alkylating agents, capable of methylating the ring nitrogen atoms in DNA bases (130). On the other hand, as an S_N1 alkylator, NDMA is more likely to target both the extracyclic oxygen groups in the DNA bases (130) and the oxygen atoms of the sugar-phosphate backbone (131, 137). Therefore, the relationship between alklation damage repair and HU/ara-C is potentially complicated and dependent on the types of alkalyted lesions.

Despite high variability in metabolic enzyme expressions in primary hepatocytes obtained from different individuals, primary hepatocytes remain an essential tool in toxicity testing and metabolism studies. We demonstrated here a procedure where primary mouse hepatocytes are loaded onto CometChip immediately following isolation, exposed to genotoxins in the presence of HU/ara-C, and analyzed for SBs

directly on chip. This procedure significantly simplifies cell handling and eliminates the need to detach the cells from culturing vessels (usually via trypsinization), minimizing the stress on the cells. We demonstrated here that the hepatocytes recovered on CometChip maintained their ability to bioactivate the carcinogens AFB_1 and B[a]P, indicating that CometChip can potentially be used as a suitable culturing vessel for primary hepatocytes. Further studies are needed to characterize the viability of the cells as well as quantifying liver-specific protein levels over time. On the other hand, because CometChip is fabricated with agarose, which provides a hydrophilic and neutrally charged surface, we expect that the effect is similar to the ultra-low attachment plates (e.g. Corning® Ultra-Low Attachment Spheroid Microplates) that are routinely used for hepatocyte spheroid formation and culture (138).

As demonstrated in the study with cisplatin, the platform developed here is potentially insensitive to some DNA crosslinking agents. Although DNA crosslinks induced by cisplatin can be repaired by NER (124), the results suggest that perhaps a small portion of unrepaired interstrand crosslinks (ICLs) holds the DNA ends generated from NER in place, preventing electrophoretic migration. There is already an established comet procedure to detect ICLs, where the reduction in DNA migration after treatment with a SB-inducing agent, such as γ-radiation, is a measure of the level of ICLs (127). We envision that this approach can be easily incorporated into our platform as an additional step in the procedure to verify the existence of the highly toxic ICLs.

The comet assay is a popular tool in human biomonitoring studies, where DNA damage can be used as a biomarker for occupational and environmental exposures and dietary effects (139-145). The HT nature of CometChip and the enhanced sensitivity for DNA damage using the HU/ara-C combination can be a valuable tool for these types of studies. There is one caveat, which is that a difference in the level of SBs across samples may reflect the inter-individual variation in both DNA damage level and NER or BER incision activity. Therefore, to quantify the contribution of the variation in DNA repair capacity, we recommend including an independent assay to monitor DNA repair capacity in parallel (e.g. fluorescence-based multiplex host cell reactivation assay (146)).

Because an understanding of the types of DNA lesions helps elucidate a chemical's mode of actions, it can be useful to learn if bulky adducts are formed. The use of HU/ara-C is sensitive but not specific to bulky adducts, so the technique itself is not capable of discerning whether a chemical induces bulky adducts. However, as demonstrated in this work, it is possible to determine the presence of bulky adducts by including a condition where NER incision is inhibited either by a small molecule (e.g. SP) or by deleting key proteins of the preincision complex (e.g. XPA, XPG). The resulting reduction of strand breaks indicates participation of NER and therefore supports the presence of bulky adducts.

Determining whether the metabolism of a compound results in genotoxic metabolites is important in the contexts of both environmental exposures and drug development. We showed here that inhibitors for specific CYP450s can be employed in our platform to investigate the role of the enzymes in producing the genotoxic effect of test compounds. As a potential application, our platform can be used to screen a panel of CYP450 inhibitors to differentiate between parent- and metabolite-based genotoxicity and to determine the contribution of specific CYP450s for novel compounds with unknown metabolisms.

In conclusion, using a combination of the DNA repair synthesis inhibitors HU and ara-C and a metabolically competent human cell line HepaRG™, we developed a CometChip platform for HT genotoxicity testing that has enhanced sensitivity to a broad range of DNA damaging agents. The platform can be used as a powerful HT tool for screening of large chemical libraries, which finds applications in both the pharmaceutical industry and the chemical industry. The use of HU/ara-C together with CometChip is also a promising tool for clinical applications, where DNA damage level can be monitored as an early surrogate endpoint for tumor response. In addition, CometChip is compatible with HT screening facilities, enabling testing of thousands of treatment conditions at the same time in a matter of 2-3 days.

2.6. REFERENCES

1. Hoeijmakers JH. Genome maintenance mechanisms for preventing cancer. Nature. 2001;411(6835):366-74. doi: 10.1038/35077232. PubMed PMID: 11357144.
2. Hoeijmakers JH. DNA damage, aging, and cancer. N Engl J Med. 2009;361(15):1475-85. doi: 10.1056/NEJMra0804615. PubMed PMID: 19812404.
3. Poirier MC. Chemical-induced DNA damage and human cancer risk. Nat Rev Cancer. 2004;4(8):630-7. doi: 10.1038/nrc1410. PubMed PMID: 15286742.
4. Jackson SP, Bartek J. The DNA-damage response in human biology and disease. Nature. 2009;461(7267):1071-8. doi: 10.1038/nature08467. PubMed PMID: 19847258; PMCID: PMC2906700.
5. Food and Drug Administration, Center for Drug Evaluation and Research (CDER), Center for Biologics Evaluation and Research (CBER). Guidance for Industry: S2(R1) Genotoxicity Testing and Data Interpretation for Pharmaceuticals Intended for Human Use In: Services USDoHaH, editor. Silver Spring, MD, USA2012.
6. Knight AW, Little S, Houck K, Dix D, Judson R, Richard A, McCarroll N, Akerman G, Yang C, Birrell L, Walmsley RM. Evaluation of high-throughput genotoxicity assays used in profiling the US EPA ToxCast chemicals. Regul Toxicol Pharmacol. 2009;55(2):188-99. doi: 10.1016/j.yrtph.2009.07.004. PubMed PMID: 19591892.
7. Hartung T, Rovida C. Chemical regulators have overreached. Nature. 2009;460(7259):1080-1. doi: 10.1038/4601080a. PubMed PMID: 19713914.
8. National Toxicology Program. About NTP [cited 2017 November 3rd]. Available from: https://ntp.niehs.nih.gov/about/.
9. Garcia-Canton C, Anadon A, Meredith C. Assessment of the in vitro gammaH2AX assay by High Content Screening as a novel genotoxicity test. Mutat Res. 2013;757(2):158-66. doi: 10.1016/j.mrgentox.2013.08.002. PubMed PMID: 23988589.
10. Vernetti L, Irwin W, Giuliano KA, Gough A, Johnston K, Taylor DL. Cellular systems biology applied to preclinical safety testing: A case study of CellCiPhr profiling. In: Ekins S, Xu JJ, editors. Drug Efficacy, Safety, and Biologics Discovery: Emerging Technologies and Tools. Hoboken, N.J: John Wiley & Sons; 2009.
11. Ostling O, Johanson KJ. Microelectrophoretic study of radiation-induced DNA damages in individual mammalian cells. Biochem Biophys Res Commun. 1984;123(1):291-8. PubMed PMID: 6477583.
12. Olive PL, Banath JP. The comet assay: a method to measure DNA damage in individual cells. Nat Protoc. 2006;1(1):23-9. doi: 10.1038/nprot.2006.5. PubMed PMID: 17406208.

13. Hartmann A, Agurell E, Beevers C, Brendler-Schwaab S, Burlinson B, Clay P, Collins A, Smith A, Speit G, Thybaud V, Tice RR, th International Comet Assay W. Recommendations for conducting the in vivo alkaline Comet assay. 4th International Comet Assay Workshop. Mutagenesis. 2003;18(1):45-51. PubMed PMID: 12473734.
14. Weingeist DM, Ge J, Wood DK, Mutamba JT, Huang Q, Rowland EA, Yaffe MB, Floyd S, Engelward BP. Single-cell microarray enables high-throughput evaluation of DNA double-strand breaks and DNA repair inhibitors. Cell Cycle. 2013;12(6):907-15. doi: 10.4161/cc.23880. PubMed PMID: 23422001; PMCID: PMC3637349.
15. Wood DK, Weingeist DM, Bhatia SN, Engelward BP. Single cell trapping and DNA damage analysis using microwell arrays. Proc Natl Acad Sci U S A. 2010;107(22):10008-13. doi: 10.1073/pnas.1004056107. PubMed PMID: 20534572; PMCID: PMC2890454.
16. Ge J, Chow DN, Fessler JL, Weingeist DM, Wood DK, Engelward BP. Micropatterned comet assay enables high throughput and sensitive DNA damage quantification. Mutagenesis. 2015;30(1):11-9. doi: 10.1093/mutage/geu063. PubMed PMID: 25527723; PMCID: PMC4272061.
17. Collins AR, Oscoz AA, Brunborg G, Gaivao I, Giovannelli L, Kruszewski M, Smith CC, Stetina R. The comet assay: topical issues. Mutagenesis. 2008;23(3):143-51. doi: 10.1093/mutage/gem051. PubMed PMID: 18283046.
18. Gillet LC, Scharer OD. Molecular mechanisms of mammalian global genome nucleotide excision repair. Chem Rev. 2006;106(2):253-76. doi: 10.1021/cr040483f. PubMed PMID: 16464005.
19. Scharer OD. Nucleotide excision repair in eukaryotes. Cold Spring Harb Perspect Biol. 2013;5(10):a012609. doi: 10.1101/cshperspect.a012609. PubMed PMID: 24086042; PMCID: PMC3783044.
20. Marteijn JA, Lans H, Vermeulen W, Hoeijmakers JH. Understanding nucleotide excision repair and its roles in cancer and ageing. Nat Rev Mol Cell Biol. 2014;15(7):465-81. doi: 10.1038/nrm3822. PubMed PMID: 24954209.
21. Xue W, Warshawsky D. Metabolic activation of polycyclic and heterocyclic aromatic hydrocarbons and DNA damage: a review. Toxicol Appl Pharmacol. 2005;206(1):73-93. doi: 10.1016/j.taap.2004.11.006. PubMed PMID: 15963346.
22. Nagel ZD, Chaim IA, Samson LD. Inter-individual variation in DNA repair capacity: a need for multi-pathway functional assays to promote translational DNA repair research. DNA Repair (Amst). 2014;19:199-213. doi: 10.1016/j.dnarep.2014.03.009. PubMed PMID: 24780560; PMCID: PMC4071454.

23. Qian GS, Ross RK, Yu MC, Yuan JM, Gao YT, Henderson BE, Wogan GN, Groopman JD. A follow-up study of urinary markers of aflatoxin exposure and liver cancer risk in Shanghai, People's Republic of China. Cancer Epidemiol Biomarkers Prev. 1994;3(1):3-10. PubMed PMID: 8118382.
24. Johnson WW, Guengerich FP. Reaction of aflatoxin B1 exo-8,9-epoxide with DNA: kinetic analysis of covalent binding and DNA-induced hydrolysis. Proc Natl Acad Sci U S A. 1997;94(12):6121-5. PubMed PMID: 9177180; PMCID: PMC21012.
25. Smela ME, Hamm ML, Henderson PT, Harris CM, Harris TM, Essigmann JM. The aflatoxin B(1) formamidopyrimidine adduct plays a major role in causing the types of mutations observed in human hepatocellular carcinoma. Proc Natl Acad Sci U S A. 2002;99(10):6655-60. doi: 10.1073/pnas.102167699. PubMed PMID: 12011430; PMCID: PMC124458.
26. Baird WM, Hooven LA, Mahadevan B. Carcinogenic polycyclic aromatic hydrocarbon-DNA adducts and mechanism of action. Environ Mol Mutagen. 2005;45(2-3):106-14. doi: 10.1002/em.20095. PubMed PMID: 15688365.
27. International Agency for Research on Cancer. Chemical Agents and Related Occupations IARC Monographs on the Evaluation of Carcinogenic Risks to Humans, volume 100F. Lyon, France: IARC; 2012.
28. Otteneder M, Lutz WK. Correlation of DNA adduct levels with tumor incidence: carcinogenic potency of DNA adducts. Mutat Res. 1999;424(1-2):237-47. PubMed PMID: 10064864.
29. Veglia F, Matullo G, Vineis P. Bulky DNA adducts and risk of cancer: a meta-analysis. Cancer Epidemiol Biomarkers Prev. 2003;12(2):157-60. PubMed PMID: 12582026.
30. Staresincic L, Fagbemi AF, Enzlin JH, Gourdin AM, Wijgers N, Dunand-Sauthier I, Giglia-Mari G, Clarkson SG, Vermeulen W, Scharer OD. Coordination of dual incision and repair synthesis in human nucleotide excision repair. EMBO J. 2009;28(8):1111-20. doi: 10.1038/emboj.2009.49. PubMed PMID: 19279666; PMCID: PMC2683701.
31. Moser J, Kool H, Giakzidis I, Caldecott K, Mullenders LH, Fousteri MI. Sealing of chromosomal DNA nicks during nucleotide excision repair requires XRCC1 and DNA ligase III alpha in a cell-cycle-specific manner. Mol Cell. 2007;27(2):311-23. doi: 10.1016/j.molcel.2007.06.014. PubMed PMID: 17643379.
32. Shivji MK, Podust VN, Hubscher U, Wood RD. Nucleotide excision repair DNA synthesis by DNA polymerase epsilon in the presence of PCNA, RFC, and RPA. Biochemistry. 1995;34(15):5011-7. PubMed PMID: 7711023.
33. Cleaver JE. Normal reconstruction of DNA supercoiling and chromatin structure in cockayne syndrome cells during repair of damage from ultraviolet light. Am J Hum Genet. 1982;34(4):566-75. PubMed PMID: 7102674; PMCID: PMC1685362.

34. Hiss EA, Preston RJ. The effect of cytosine arabinoside on the frequency of single-strand breaks in DNA of mammalian cells following irradiation or chemical treatment. Biochim Biophys Acta. 1977;478(1):1-8. PubMed PMID: 407935.
35. Erixon K, Ahnstrom G. Single-strand breaks in DNA during repair of UV-induced damage in normal human and xeroderma pigmentosum cells as determined by alkaline DNA unwinding and hydroxylapatite chromatography: effects of hydroxyurea, 5-fluorodeoxyuridine and 1-beta-D-arabinofuranosylcytosine on the kinetics of repair. Mutat Res. 1979;59(2):257-71. PubMed PMID: 35744.
36. Kinley JS, Brunborg G, Moan J, Young AR. Detection of UVR-induced DNA damage in mouse epidermis in vivo using alkaline elution. Photochem Photobiol. 1995;61(2):149-58. PubMed PMID: 7899504.
37. Park JK, Lee JS, Lee HH, Choi IS, Park SD. Accumulation of polycyclic aromatic hydrocarbon-induced single strand breaks is attributed to slower rejoining processes by DNA polymerase inhibitor, cytosine arabinoside in CHO-K1 cells. Life Sci. 1991;48(13):1255-61. PubMed PMID: 2002753.
38. Meredith CG, Maldonado AL, Speeg KV, Jr. The effect of ketoconazole on hepatic oxidative drug metabolism in the rat in vivo and in vitro. Drug Metab Dispos. 1985;13(2):156-62. PubMed PMID: 2859162.
39. Martin FL, Cole KJ, Orme MH, Grover PL, Phillips DH, Venitt S. The DNA repair inhibitors hydroxyurea and cytosine arabinoside enhance the sensitivity of the alkaline single-cell gel electrophoresis ('comet') assay in metabolically-competent MCL-5 cells. Mutat Res. 1999;445(1):21-43. PubMed PMID: 10521689.
40. Gedik CM, Ewen SW, Collins AR. Single-cell gel electrophoresis applied to the analysis of UV-C damage and its repair in human cells. Int J Radiat Biol. 1992;62(3):313-20. PubMed PMID: 1356133.
41. Gandhi V, Plunkett W, Kantarjian H, Talpaz M, Robertson LE, O'Brien S. Cellular pharmacodynamics and plasma pharmacokinetics of parenterally infused hydroxyurea during a phase I clinical trial in chronic myelogenous leukemia. J Clin Oncol. 1998;16(7):2321-31. doi: 10.1200/JCO.1998.16.7.2321. PubMed PMID: 9667246.
42. Skoog L, Bjursell G. Nuclear and cytoplasmic pools of deoxyribonucleoside triphosphates in Chinese hamster ovary cells. J Biol Chem. 1974;249(20):6434-8. PubMed PMID: 4472692.
43. Skoog L, Nordenskjold B. Effects of hydroxyurea and 1-beta-D-arabinofuranosyl-cytosine on deoxyribonucleotide pools in mouse embryo cells. Eur J Biochem. 1971;19(1):81-9. PubMed PMID: 5573224.

44. Snyder RD. The role of deoxynucleoside triphosphate pools in the inhibition of DNA-excision repair and replication in human cells by hydroxyurea. Mutat Res. 1984;131(3-4):163-72. PubMed PMID: 6717470.
45. Tyrsted G. Effect of hydroxyurea and 5-fluorodeoxyuridine on deoxyribonucleoside triphosphate pools early in phytohemagglutinin-stimulated human lymphocytes. Biochem Pharmacol. 1982;31(19):3107-13. PubMed PMID: 6216891.
46. Galmarini CM, Mackey JR, Dumontet C. Nucleoside analogues: mechanisms of drug resistance and reversal strategies. Leukemia. 2001;15(6):875-90. PubMed PMID: 11417472.
47. Ohno Y, Spriggs D, Matsukage A, Ohno T, Kufe D. Effects of 1-beta-D-arabinofuranosylcytosine incorporation on elongation of specific DNA sequences by DNA polymerase beta. Cancer Res. 1988;48(6):1494-8. PubMed PMID: 3345522.
48. Kufe DW, Major PP, Egan EM, Beardsley GP. Correlation of cytotoxicity with incorporation of ara-C into DNA. J Biol Chem. 1980;255(19):8997-900. PubMed PMID: 7410404.
49. Major PP, Egan EM, Beardsley GP, Minden MD, Kufe DW. Lethality of human myeloblasts correlates with the incorporation of arabinofuranosylcytosine into DNA. Proc Natl Acad Sci U S A. 1981;78(5):3235-9. PubMed PMID: 6942429; PMCID: PMC319536.
50. Major PP, Egan EM, Herrick DJ, Kufe DW. Effect of ARA-C incorporation on deoxyribonucleic acid synthesis in cells. Biochem Pharmacol. 1982;31(18):2937-40. PubMed PMID: 7138584.
51. Matsukage A, Ono K, Ohashi A, Takahashi T, Nakayama C, Saneyoshi M. Inhibitory effect of 1-beta-D-arabinofuranosylthymine 5'-triphosphate and 1-beta-D-arabinofuranosylcytosine 5'-triphosphate on DNA polymerases from murine cells and oncornavirus. Cancer Res. 1978;38(9):3076-9. PubMed PMID: 79444.
52. Miller MR, Chinault DN. Evidence that DNA polymerases alpha and beta participate differentially in DNA repair synthesis induced by different agents. J Biol Chem. 1982;257(1):46-9. PubMed PMID: 6171569.
53. Mutsukage A, Takahashi T, Nakayama C, Saneyoshi M. Inhibition of mouse myeloma DNA polymerase alpha by 5-triphosphates of 1-beta-D-arabinofuranosylthymine and 1-beta-D-arabinofuranosylcytosine. J Biochem. 1978;83(5):1511-5. PubMed PMID: 566267.
54. Townsend AJ, Cheng YC. Sequence-specific effects of ara-5-aza-CTP and ara-CTP on DNA synthesis by purified human DNA polymerases in vitro: visualization of chain elongation on a defined template. Mol Pharmacol. 1987;32(3):330-9. PubMed PMID: 2444869.
55. Golan DE, Tashjian AH. Principles of pharmacology : the pathophysiologic basis of drug therapy. 3rd ed. Philadelphia: Wolters Kluwer Health/Lippincott Williams & Wilkins; 2012. xxi, 954 p. p.

56. Nebert DW, Dalton TP. The role of cytochrome P450 enzymes in endogenous signalling pathways and environmental carcinogenesis. Nat Rev Cancer. 2006;6(12):947-60. doi: 10.1038/nrc2015. PubMed PMID: 17128211.

57. Brandon EF, Raap CD, Meijerman I, Beijnen JH, Schellens JH. An update on in vitro test methods in human hepatic drug biotransformation research: pros and cons. Toxicol Appl Pharmacol. 2003;189(3):233-46. PubMed PMID: 12791308.

58. Guengerich FP, Dannan GA, Wright ST, Martin MV, Kaminsky LS. Purification and characterization of liver microsomal cytochromes p-450: electrophoretic, spectral, catalytic, and immunochemical properties and inducibility of eight isozymes isolated from rats treated with phenobarbital or beta-naphthoflavone. Biochemistry. 1982;21(23):6019-30. PubMed PMID: 6758842.

59. Ku WW, Bigger A, Brambilla G, Glatt H, Gocke E, Guzzie PJ, Hakura A, Honma M, Martus HJ, Obach RS, Roberts S, Strategy Expert Group I. Strategy for genotoxicity testing--metabolic considerations. Mutat Res. 2007;627(1):59-77. doi: 10.1016/j.mrgentox.2006.10.004. PubMed PMID: 17141553.

60. Le Hegarat L, Dumont J, Josse R, Huet S, Lanceleur R, Mourot A, Poul JM, Guguen-Guillouzo C, Guillouzo A, Fessard V. Assessment of the genotoxic potential of indirect chemical mutagens in HepaRG cells by the comet and the cytokinesis-block micronucleus assays. Mutagenesis. 2010;25(6):555-60. doi: 10.1093/mutage/geq039. PubMed PMID: 20675360.

61. Obach RS, Dobo KL. Comparison of metabolite profiles generated in Aroclor-induced rat liver and human liver subcellular fractions: considerations for in vitro genotoxicity hazard assessment. Environ Mol Mutagen. 2008;49(8):631-41. doi: 10.1002/em.20416. PubMed PMID: 18626997.

62. Gomez-Lechon MJ, Tolosa L, Conde I, Donato MT. Competency of different cell models to predict human hepatotoxic drugs. Expert Opin Drug Metab Toxicol. 2014;10(11):1553-68. doi: 10.1517/17425255.2014.967680. PubMed PMID: 25297626.

63. Guillouzo A, Guguen-Guillouzo C. Evolving concepts in liver tissue modeling and implications for in vitro toxicology. Expert Opin Drug Metab Toxicol. 2008;4(10):1279-94. doi: 10.1517/17425255.4.10.1279. PubMed PMID: 18798698.

64. Aden DP, Fogel A, Plotkin S, Damjanov I, Knowles BB. Controlled synthesis of HBsAg in a differentiated human liver carcinoma-derived cell line. Nature. 1979;282(5739):615-6. PubMed PMID: 233137.

65. Lopez-Terrada D, Cheung SW, Finegold MJ, Knowles BB. Hep G2 is a hepatoblastoma-derived cell line. Hum Pathol. 2009;40(10):1512-5. doi: 10.1016/j.humpath.2009.07.003. PubMed PMID: 19751877.

66. Castell JV, Jover R, Martinez-Jimenez CP, Gomez-Lechon MJ. Hepatocyte cell lines: their use, scope and limitations in drug metabolism studies. Expert Opin Drug Metab Toxicol. 2006;2(2):183-212. doi: 10.1517/17425255.2.2.183. PubMed PMID: 16866607.

67. Gripon P, Rumin S, Urban S, Le Seyec J, Glaise D, Cannie I, Guyomard C, Lucas J, Trepo C, Guguen-Guillouzo C. Infection of a human hepatoma cell line by hepatitis B virus. Proc Natl Acad Sci U S A. 2002;99(24):15655-60. doi: 10.1073/pnas.232137699. PubMed PMID: 12432097; PMCID: PMC137772.

68. Aninat C, Piton A, Glaise D, Le Charpentier T, Langouet S, Morel F, Guguen-Guillouzo C, Guillouzo A. Expression of cytochromes P450, conjugating enzymes and nuclear receptors in human hepatoma HepaRG cells. Drug Metab Dispos. 2006;34(1):75-83. doi: 10.1124/dmd.105.006759. PubMed PMID: 16204462.

69. Antherieu S, Chesne C, Li R, Camus S, Lahoz A, Picazo L, Turpeinen M, Tolonen A, Uusitalo J, Guguen-Guillouzo C, Guillouzo A. Stable expression, activity, and inducibility of cytochromes P450 in differentiated HepaRG cells. Drug Metab Dispos. 2010;38(3):516-25. doi: 10.1124/dmd.109.030197. PubMed PMID: 20019244.

70. Guillouzo A, Corlu A, Aninat C, Glaise D, Morel F, Guguen-Guillouzo C. The human hepatoma HepaRG cells: a highly differentiated model for studies of liver metabolism and toxicity of xenobiotics. Chem Biol Interact. 2007;168(1):66-73. doi: 10.1016/j.cbi.2006.12.003. PubMed PMID: 17241619.

71. Hart SN, Li Y, Nakamoto K, Subileau EA, Steen D, Zhong XB. A comparison of whole genome gene expression profiles of HepaRG cells and HepG2 cells to primary human hepatocytes and human liver tissues. Drug Metab Dispos. 2010;38(6):988-94. doi: 10.1124/dmd.109.031831. PubMed PMID: 20228232; PMCID: PMC2879958.

72. Hoekstra R, Nibourg GA, van der Hoeven TV, Ackermans MT, Hakvoort TB, van Gulik TM, Lamers WH, Elferink RP, Chamuleau RA. The HepaRG cell line is suitable for bioartificial liver application. Int J Biochem Cell Biol. 2011;43(10):1483-9. doi: 10.1016/j.biocel.2011.06.011. PubMed PMID: 21726661.

73. Josse R, Aninat C, Glaise D, Dumont J, Fessard V, Morel F, Poul JM, Guguen-Guillouzo C, Guillouzo A. Long-term functional stability of human HepaRG hepatocytes and use for chronic toxicity and genotoxicity studies. Drug Metab Dispos. 2008;36(6):1111-8. doi: 10.1124/dmd.107.019901. PubMed PMID: 18347083.

74. Josse R, Rogue A, Lorge E, Guillouzo A. An adaptation of the human HepaRG cells to the in vitro micronucleus assay. Mutagenesis. 2012;27(3):295-304. doi: 10.1093/mutage/ger076. PubMed PMID: 22058015.

75. Kanebratt KP, Andersson TB. Evaluation of HepaRG cells as an in vitro model for human drug metabolism studies. Drug Metab Dispos. 2008;36(7):1444-52. doi: 10.1124/dmd.107.020016. PubMed PMID: 18385292.

76. Kanebratt KP, Andersson TB. HepaRG cells as an in vitro model for evaluation of cytochrome P450 induction in humans. Drug Metab Dispos. 2008;36(1):137-45. doi: 10.1124/dmd.107.017418. PubMed PMID: 17954527.

77. Le Hegarat L, Mourot A, Huet S, Vasseur L, Camus S, Chesne C, Fessard V. Performance of comet and micronucleus assays in metabolic competent HepaRG cells to predict in vivo genotoxicity. Toxicol Sci. 2014;138(2):300-9. doi: 10.1093/toxsci/kfu004. PubMed PMID: 24431211.

78. Szabo M, Veres Z, Baranyai Z, Jakab F, Jemnitz K. Comparison of human hepatoma HepaRG cells with human and rat hepatocytes in uptake transport assays in order to predict a risk of drug induced hepatotoxicity. PLoS One. 2013;8(3):e59432. doi: 10.1371/journal.pone.0059432. PubMed PMID: 23516635; PMCID: PMC3597610.

79. Liber HL, Thilly WG. Mutation assay at the thymidine kinase locus in diploid human lymphoblasts. Mutat Res. 1982;94(2):467-85. PubMed PMID: 6810168.

80. Skopek TR, Liber HL, Penman BW, Thilly WG. Isolation of a human lymphoblastoid line heterozygous at the thymidine kinase locus: possibility for a rapid human cell mutation assay. Biochem Biophys Res Commun. 1978;84(2):411-6. PubMed PMID: 214074.

81. Ellison AR, Nouspikel T, Jaspers NG, Clarkson SG, Gruenert DC. Complementation of transformed fibroblasts from patients with combined xeroderma pigmentosum-Cockayne syndrome. Exp Cell Res. 1998;243(1):22-8. doi: 10.1006/excr.1998.4147. PubMed PMID: 9716445.

82. Ge J, Wood DK, Weingeist DM, Prasongtanakij S, Navasumrit P, Ruchirawat M, Engelward BP. Standard fluorescent imaging of live cells is highly genotoxic. Cytometry A. 2013;83(6):552-60. doi: 10.1002/cyto.a.22291. PubMed PMID: 23650257; PMCID: PMC3677558.

83. Buck LD, Inman SW, Rusyn I, Griffith LG. Co-regulation of primary mouse hepatocyte viability and function by oxygen and matrix. Biotechnol Bioeng. 2014;111(5):1018-27. doi: 10.1002/bit.25152. PubMed PMID: 24222008; PMCID: PMC4110975.

84. Martinez SM, Bradford BU, Soldatow VY, Kosyk O, Sandot A, Witek R, Kaiser R, Stewart T, Amaral K, Freeman K, Black C, LeCluyse EL, Ferguson SS, Rusyn I. Evaluation of an in vitro toxicogenetic mouse model for hepatotoxicity. Toxicol Appl Pharmacol. 2010;249(3):208-16. doi: 10.1016/j.taap.2010.09.012. PubMed PMID: 20869979; PMCID: PMC2980592.

85. Collins AR, Mitchell DL, Zunino A, de Wit J, Busch D. UV-sensitive rodent mutant cell lines of complementation groups 6 and 8 differ phenotypically from their human counterparts. Environ Mol Mutagen. 1997;29(2):152-60. PubMed PMID: 9118967.

86. Smith CA, Okumoto DS. Nature of DNA repair synthesis resistant to inhibitors of polymerase alpha in human cells. Biochemistry. 1984;23(7):1383-91. PubMed PMID: 6426505.
87. Zhang X, Rosenstein BS, Wang Y, Lebwohl M, Mitchell DM, Wei H. Induction of 8-oxo-7,8-dihydro-2'-deoxyguanosine by ultraviolet radiation in calf thymus DNA and HeLa cells. Photochem Photobiol. 1997;65(1):119-24. PubMed PMID: 9066291.
88. Zhang X, Rosenstein BS, Wang Y, Lebwohl M, Wei H. Identification of possible reactive oxygen species involved in ultraviolet radiation-induced oxidative DNA damage. Free Radic Biol Med. 1997;23(7):980-5. PubMed PMID: 9358240.
89. Constantinou A, Gunz D, Evans E, Lalle P, Bates PA, Wood RD, Clarkson SG. Conserved residues of human XPG protein important for nuclease activity and function in nucleotide excision repair. J Biol Chem. 1999;274(9):5637-48. PubMed PMID: 10026181.
90. McGregor DB, Edwards I, Wolf CR, Forrester LM, Caspary WJ. Endogenous xenobiotic enzyme levels in mammalian cells. Mutat Res. 1991;261(1):29-39. PubMed PMID: 1715512.
91. International Agency for Research on Cancer WHO. IARC Monographs on the Evaluation of Carcinogenic Risks to Humans - List of Classifications, Volumes 1-120 [cited 2017 November 10]. Available from: http://monographs.iarc.fr/ENG/Classification/latest_classif.php.
92. International Agency for Research on Cancer. Some Traditional Herbal Medicines, Some Mycotoxins, Naphthalene and Styrene. IARC Monographs on the Evaluation of Carcinogenic Risks to Humans, volume 82. Lyon, France: IARC; 2002.
93. Aoyama T, Yamano S, Guzelian PS, Gelboin HV, Gonzalez FJ. Five of 12 forms of vaccinia virus-expressed human hepatic cytochrome P450 metabolically activate aflatoxin B1. Proc Natl Acad Sci U S A. 1990;87(12):4790-3. PubMed PMID: 2162057; PMCID: PMC54203.
94. Gallagher EP, Kunze KL, Stapleton PL, Eaton DL. The kinetics of aflatoxin B1 oxidation by human cDNA-expressed and human liver microsomal cytochromes P450 1A2 and 3A4. Toxicol Appl Pharmacol. 1996;141(2):595-606. doi: 10.1006/taap.1996.0326. PubMed PMID: 8975785.
95. Gallagher EP, Wienkers LC, Stapleton PL, Kunze KL, Eaton DL. Role of human microsomal and human complementary DNA-expressed cytochromes P4501A2 and P4503A4 in the bioactivation of aflatoxin B1. Cancer Res. 1994;54(1):101-8. PubMed PMID: 8261428.
96. Langouet S, Coles B, Morel F, Becquemont L, Beaune P, Guengerich FP, Ketterer B, Guillouzo A. Inhibition of CYP1A2 and CYP3A4 by oltipraz results in reduction of aflatoxin B1 metabolism in human hepatocytes in primary culture. Cancer Res. 1995;55(23):5574-9. PubMed PMID: 7585637.
97. Raney KD, Meyer DJ, Ketterer B, Harris TM, Guengerich FP. Glutathione conjugation of aflatoxin B1 exo- and endo-epoxides by rat and human glutathione S-transferases. Chem Res Toxicol. 1992;5(4):470-8. PubMed PMID: 1391613.

98. Johnson WW, Harris TM, Guengerich FP. Kinetics and Mechanism of Hydrolysis of Aflatoxin B_1 exo-8,9-Epoxide and Rearrangement of the Dihydrodiol. Journal of the American Chemical Society. 1996;118(35):8213-20. Epub September 4, 1996. doi: 10.1021/ja960525k.

99. Bedard LL, Massey TE. Aflatoxin B1-induced DNA damage and its repair. Cancer Lett. 2006;241(2):174-83. doi: 10.1016/j.canlet.2005.11.018. PubMed PMID: 16458422.

100. Vartanian V, Minko IG, Chawanthayatham S, Egner PA, Lin YC, Earley LF, Makar R, Eng JR, Camp MT, Li L, Stone MP, Lasarev MR, Groopman JD, Croy RG, Essigmann JM, McCullough AK, Lloyd RS. NEIL1 protects against aflatoxin-induced hepatocellular carcinoma in mice. Proc Natl Acad Sci U S A. 2017;114(16):4207-12. doi: 10.1073/pnas.1620932114. PubMed PMID: 28373545; PMCID: PMC5402411.

101. Murray IA, Patterson AD, Perdew GH. Aryl hydrocarbon receptor ligands in cancer: friend and foe. Nat Rev Cancer. 2014;14(12):801-14. doi: 10.1038/nrc3846. PubMed PMID: 25568920; PMCID: PMC4401080.

102. Crespi CL, Miller VP, Penman BW. Microtiter plate assays for inhibition of human, drug-metabolizing cytochromes P450. Anal Biochem. 1997;248(1):188-90. doi: 10.1006/abio.1997.2145. PubMed PMID: 9177742.

103. Eagling VA, Tjia JF, Back DJ. Differential selectivity of cytochrome P450 inhibitors against probe substrates in human and rat liver microsomes. Br J Clin Pharmacol. 1998;45(2):107-14. PubMed PMID: 9491822; PMCID: PMC1873357.

104. Maurice M, Pichard L, Daujat M, Fabre I, Joyeux H, Domergue J, Maurel P. Effects of imidazole derivatives on cytochromes P450 from human hepatocytes in primary culture. FASEB J. 1992;6(2):752-8. PubMed PMID: 1371482.

105. Sheets JJ, Mason JI. Ketoconazole: a potent inhibitor of cytochrome P-450-dependent drug metabolism in rat liver. Drug Metab Dispos. 1984;12(5):603-6. PubMed PMID: 6149911.

106. Chang TK, Gonzalez FJ, Waxman DJ. Evaluation of triacetyloleandomycin, alpha-naphthoflavone and diethyldithiocarbamate as selective chemical probes for inhibition of human cytochromes P450. Arch Biochem Biophys. 1994;311(2):437-42. PubMed PMID: 8203907.

107. Cho US, Park EY, Dong MS, Park BS, Kim K, Kim KH. Tight-binding inhibition by alpha-naphthoflavone of human cytochrome P450 1A2. Biochim Biophys Acta. 2003;1648(1-2):195-202. PubMed PMID: 12758162.

108. Gasiewicz TA, Rucci G. Alpha-naphthoflavone acts as an antagonist of 2,3,7, 8-tetrachlorodibenzo-p-dioxin by forming an inactive complex with the Ah receptor. Mol Pharmacol. 1991;40(5):607-12. PubMed PMID: 1658599.

109. Merchant M, Arellano L, Safe S. The mechanism of action of alpha-naphthoflavone as an inhibitor of 2,3,7,8-tetrachlorodibenzo-p-dioxin-induced CYP1A1 gene expression. Arch Biochem Biophys. 1990;281(1):84-9. PubMed PMID: 2166479.

110. Alekseev S, Ayadi M, Brino L, Egly JM, Larsen AK, Coin F. A small molecule screen identifies an inhibitor of DNA repair inducing the degradation of TFIIH and the chemosensitization of tumor cells to platinum. Chem Biol. 2014;21(3):398-407. doi: 10.1016/j.chembiol.2013.12.014. PubMed PMID: 24508195.

111. Coin F, Oksenych V, Egly JM. Distinct roles for the XPB/p52 and XPD/p44 subcomplexes of TFIIH in damaged DNA opening during nucleotide excision repair. Mol Cell. 2007;26(2):245-56. doi: 10.1016/j.molcel.2007.03.009. PubMed PMID: 17466626.

112. Los LE, Pitzenberger SM, Ramjit HG, Coddington AB, Colby HD. Hepatic metabolism of spironolactone. Production of 3-hydroxy-thiomethyl metabolites. Drug Metab Dispos. 1994;22(6):903-8. PubMed PMID: 7895608.

113. de Vries A, van Oostrom CT, Hofhuis FM, Dortant PM, Berg RJ, de Gruijl FR, Wester PW, van Kreijl CF, Capel PJ, van Steeg H, Verbeek SJ. Increased susceptibility to ultraviolet-B and carcinogens of mice lacking the DNA excision repair gene XPA. Nature. 1995;377(6545):169-73. doi: 10.1038/377169a0. PubMed PMID: 7675086.

114. Alekseyev YO, Hamm ML, Essigmann JM. Aflatoxin B1 formamidopyrimidine adducts are preferentially repaired by the nucleotide excision repair pathway in vivo. Carcinogenesis. 2004;25(6):1045-51. doi: 10.1093/carcin/bgh098. PubMed PMID: 14742311.

115. Shen HM, Shi CY, Lee HP, Ong CN. Aflatoxin B1-induced lipid peroxidation in rat liver. Toxicol Appl Pharmacol. 1994;127(1):145-50. doi: 10.1006/taap.1994.1148. PubMed PMID: 8048046.

116. Shen HM, Shi CY, Shen Y, Ong CN. Detection of elevated reactive oxygen species level in cultured rat hepatocytes treated with aflatoxin B1. Free Radic Biol Med. 1996;21(2):139-46. PubMed PMID: 8818628.

117. Weng MW, Lee HW, Choi B, Wang HT, Hu Y, Mehta M, Desai D, Amin S, Zheng Y, Tang MS. AFB1 hepatocarcinogenesis is via lipid peroxidation that inhibits DNA repair, sensitizes mutation susceptibility and induces aldehyde-DNA adducts at p53 mutational hotspot codon 249. Oncotarget. 2017;8(11):18213-26. doi: 10.18632/oncotarget.15313. PubMed PMID: 28212554; PMCID: PMC5392321.

118. Krokan HE, Bjoras M. Base excision repair. Cold Spring Harb Perspect Biol. 2013;5(4):a012583. doi: 10.1101/cshperspect.a012583. PubMed PMID: 23545420; PMCID: PMC3683898.

119. Kirkland D, Kasper P, Martus HJ, Muller L, van Benthem J, Madia F, Corvi R. Updated recommended lists of genotoxic and non-genotoxic chemicals for assessment of the performance of new or improved

genotoxicity tests. Mutat Res Genet Toxicol Environ Mutagen. 2016;795:7-30. doi: 10.1016/j.mrgentox.2015.10.006. PubMed PMID: 26774663.

120. Kirkland D, Kasper P, Muller L, Corvi R, Speit G. Recommended lists of genotoxic and non-genotoxic chemicals for assessment of the performance of new or improved genotoxicity tests: a follow-up to an ECVAM workshop. Mutat Res. 2008;653(1-2):99-108. doi: 10.1016/j.mrgentox.2008.03.008. PubMed PMID: 18539078.
121. International Agency for Research on Cancer. IARC Monographs on the Evaluation of Carcinogenic Risks to Humans, volume 57. Occupational Exposures of Hairdressers and Barbers and Personal Use of Hair Colourants; Some Hair Dyes, Cosmetic Colourants, Industrial Dyestuffs and Aromatic Amines1993.
122. World Health Organization. 4-Chloroaniline, Concise International Chemical Assessment Document 48. Geneva, Switzerland: WHO; 2003.
123. Jamieson ER, Lippard SJ. Structure, Recognition, and Processing of Cisplatin-DNA Adducts. Chem Rev. 1999;99(9):2467-98. PubMed PMID: 11749487.
124. Siddik ZH. Cisplatin: mode of cytotoxic action and molecular basis of resistance. Oncogene. 2003;22(47):7265-79. doi: 10.1038/sj.onc.1206933. PubMed PMID: 14576837.
125. Deans AJ, West SC. DNA interstrand crosslink repair and cancer. Nat Rev Cancer. 2011;11(7):467-80. doi: 10.1038/nrc3088. PubMed PMID: 21701511; PMCID: PMC3560328.
126. Hoebers FJ, Pluim D, Verheij M, Balm AJ, Bartelink H, Schellens JH, Begg AC. Prediction of treatment outcome by cisplatin-DNA adduct formation in patients with stage III/IV head and neck squamous cell carcinoma, treated by concurrent cisplatin-radiation (RADPLAT). Int J Cancer. 2006;119(4):750-6. doi: 10.1002/ijc.21919. PubMed PMID: 16550603.
127. Olive PL, Banath JP. Kinetics of H2AX phosphorylation after exposure to cisplatin. Cytometry B Clin Cytom. 2009;76(2):79-90. doi: 10.1002/cyto.b.20450. PubMed PMID: 18727058.
128. Yamazaki H, Inui Y, Yun CH, Guengerich FP, Shimada T. Cytochrome P450 2E1 and 2A6 enzymes as major catalysts for metabolic activation of N-nitrosodialkylamines and tobacco-related nitrosamines in human liver microsomes. Carcinogenesis. 1992;13(10):1789-94. PubMed PMID: 1423839.
129. World Health Organization. N-Nitrosodimethylamine, Concise International Chemical Assessment Document 38. Geneva, Switzerland: WHO; 2002.
130. Fu D, Calvo JA, Samson LD. Balancing repair and tolerance of DNA damage caused by alkylating agents. Nat Rev Cancer. 2012;12(2):104-20. doi: 10.1038/nrc3185. PubMed PMID: 22237395; PMCID: PMC3586545.

131. Jones GD, Le Pla RC, Farmer PB. Phosphotriester adducts (PTEs): DNA's overlooked lesion. Mutagenesis. 2010;25(1):3-16. doi: 10.1093/mutage/gep038. PubMed PMID: 19920061.

132. Berquist BR, Wilson DM, 3rd. Pathways for repairing and tolerating the spectrum of oxidative DNA lesions. Cancer Lett. 2012;327(1-2):61-72. doi: 10.1016/j.canlet.2012.02.001. PubMed PMID: 22353689; PMCID: PMC3389563.

133. Reardon JT, Bessho T, Kung HC, Bolton PH, Sancar A. In vitro repair of oxidative DNA damage by human nucleotide excision repair system: possible explanation for neurodegeneration in xeroderma pigmentosum patients. Proc Natl Acad Sci U S A. 1997;94(17):9463-8. PubMed PMID: 9256505; PMCID: PMC23224.

134. Esterbauer H, Schaur RJ, Zollner H. Chemistry and biochemistry of 4-hydroxynonenal, malonaldehyde and related aldehydes. Free Radic Biol Med. 1991;11(1):81-128. PubMed PMID: 1937131.

135. Chung FL, Chen HJ, Nath RG. Lipid peroxidation as a potential endogenous source for the formation of exocyclic DNA adducts. Carcinogenesis. 1996;17(10):2105-11. PubMed PMID: 8895475.

136. Choudhury S, Pan J, Amin S, Chung FL, Roy R. Repair kinetics of trans-4-hydroxynonenal-induced cyclic 1,N2-propanodeoxyguanine DNA adducts by human cell nuclear extracts. Biochemistry. 2004;43(23):7514-21. doi: 10.1021/bi049877r. PubMed PMID: 15182193; PMCID: PMC2711554.

137. Den Engelse L, Menkveld GJ, De Brij RJ, Tates AD. Formation and stability of alkylated pyrimidines and purines (including imidazole ring-opened 7-alkylguanine) and alkylphosphotriesters in liver DNA of adult rats treated with ethylnitrosourea or dimethylnitrosamine. Carcinogenesis. 1986;7(3):393-403. PubMed PMID: 3948325.

138. Bell CC, Hendriks DF, Moro SM, Ellis E, Walsh J, Renblom A, Fredriksson Puigvert L, Dankers AC, Jacobs F, Snoeys J, Sison-Young RL, Jenkins RE, Nordling A, Mkrtchian S, Park BK, Kitteringham NR, Goldring CE, Lauschke VM, Ingelman-Sundberg M. Characterization of primary human hepatocyte spheroids as a model system for drug-induced liver injury, liver function and disease. Sci Rep. 2016;6:25187. doi: 10.1038/srep25187. PubMed PMID: 27143246; PMCID: PMC4855186.

139. Collins A, Dusinska M, Franklin M, Somorovska M, Petrovska H, Duthie S, Fillion L, Panayiotidis M, Raslova K, Vaughan N. Comet assay in human biomonitoring studies: reliability, validation, and applications. Environ Mol Mutagen. 1997;30(2):139-46. PubMed PMID: 9329638.

140. Collins BH, Horska A, Hotten PM, Riddoch C, Collins AR. Kiwifruit protects against oxidative DNA damage in human cells and in vitro. Nutr Cancer. 2001;39(1):148-53. doi: 10.1207/S15327914nc391_20. PubMed PMID: 11588897.

141. Garaj-Vrhovac V, Kopjar N. The alkaline Comet assay as biomarker in assessment of DNA damage in medical personnel occupationally exposed to ionizing radiation. Mutagenesis. 2003;18(3):265-71. PubMed PMID: 12714692.

142. Lebailly P, Vigreux C, Lechevrel C, Ledemeney D, Godard T, Sichel F, LeTalaer JY, Henry-Amar M, Gauduchon P. DNA damage in mononuclear leukocytes of farmers measured using the alkaline comet assay: modifications of DNA damage levels after a one-day field spraying period with selected pesticides. Cancer Epidemiol Biomarkers Prev. 1998;7(10):929-40. PubMed PMID: 9796639.

143. Lorenzo Y, Azqueta A, Luna L, Bonilla F, Dominguez G, Collins AR. The carotenoid beta-cryptoxanthin stimulates the repair of DNA oxidation damage in addition to acting as an antioxidant in human cells. Carcinogenesis. 2009;30(2):308-14. doi: 10.1093/carcin/bgn270. PubMed PMID: 19056931.

144. Moller P. The alkaline comet assay: towards validation in biomonitoring of DNA damaging exposures. Basic Clin Pharmacol Toxicol. 2006;98(4):336-45. doi: 10.1111/j.1742-7843.2006.pto_167.x. PubMed PMID: 16623855.

145. Moller P, Knudsen LE, Loft S, Wallin H. The comet assay as a rapid test in biomonitoring occupational exposure to DNA-damaging agents and effect of confounding factors. Cancer Epidemiol Biomarkers Prev. 2000;9(10):1005-15. PubMed PMID: 11045781.

146. Nagel ZD, Margulies CM, Chaim IA, McRee SK, Mazzucato P, Ahmad A, Abo RP, Butty VL, Forget AL, Samson LD. Multiplexed DNA repair assays for multiple lesions and multiple doses via transcription inhibition and transcriptional mutagenesis. Proc Natl Acad Sci U S A. 2014;111(18):E1823-32. doi: 10.1073/pnas.1401182111. PubMed PMID: 24757057; PMCID: PMC4020053.

147. Nakanomyo H, Hiraoka M, Shiraya M. [Mutagenicity tests of etoposide and teniposide]. J Toxicol Sci. 1986;11 Suppl 1:301-10. PubMed PMID: 3761399.

148. Gold LS, Zeiger E. Handbook of carcinogenic potency and genotoxicity databases. Boca Raton: CRC Press; 1997. 754 p. p.

149. Ashby J, Richardson CR, Lefevre PA, Callander RD, Styles JA. Chloracetamide-N-metholol: an example of an in vitro and in vivo clastogen which is non-mutagenic to Salmonella. Mutat Res. 1985;156(1-2):19-32. PubMed PMID: 3889624.

150. Hannan MA, al-Dakan AA, Hussain SS, Amer MH. Mutagenicity of cisplatin and carboplatin used alone and in combination with four other anticancer drugs. Toxicology. 1989;55(1-2):183-91. PubMed PMID: 2652378.

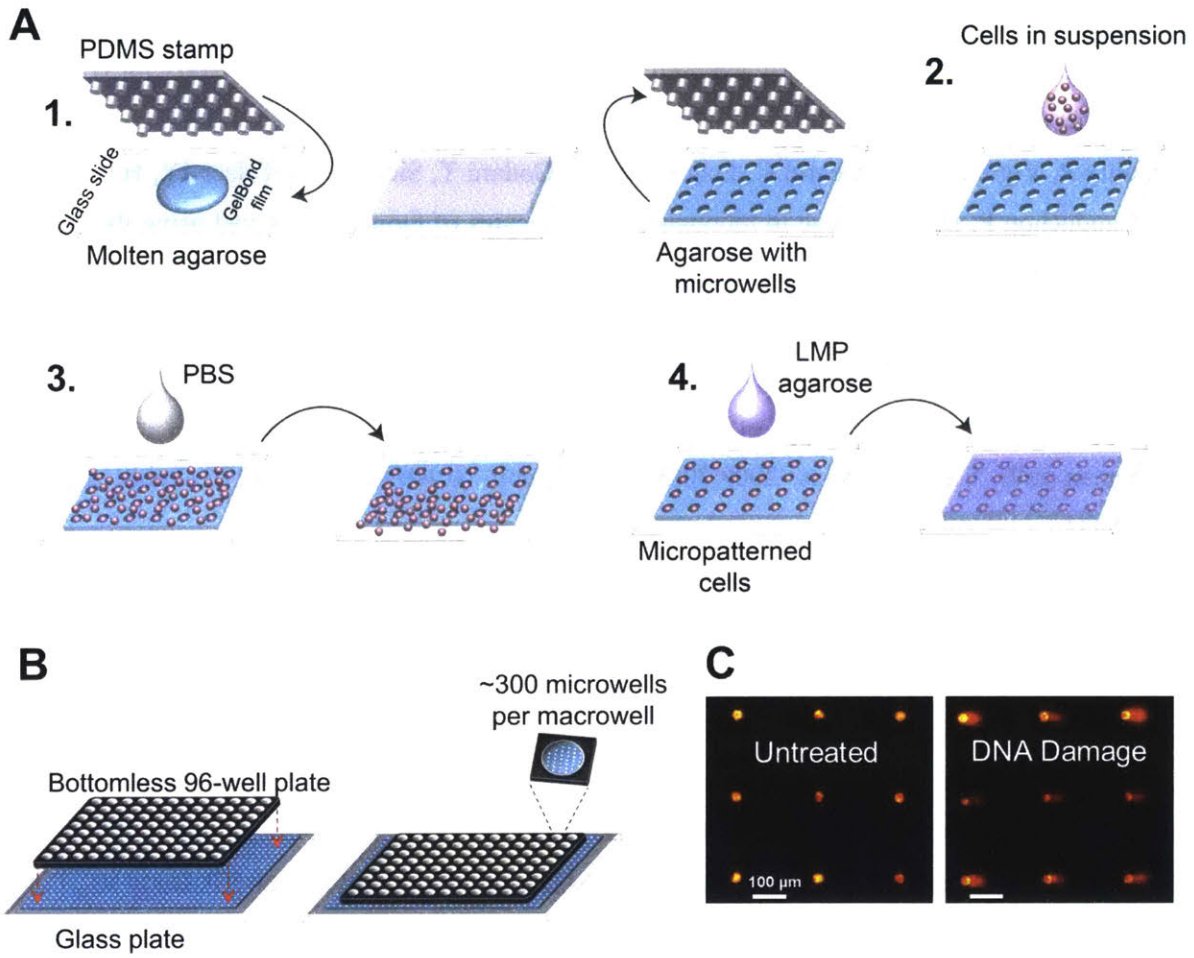

Figure 2-1. CometChip for high-throughput assessment of DNA damage. **A.** CometChip fabrication. **1.** A PDMS stamp with an array of micropegs is pressed into molten agarose. Once the agarose cools down and solidifies, the stamp is lifted to reveal an array of microwells (~40-50 µm in both diameter and depth, spaced 240 µm from each other). **2.** Cells in suspension are loaded directly into microwells via gravity. **3.** Excess cells are washed off by shear force, revealing an array of micropatterned cells. **4.** Low-melting point (LMP) agarose kept molten at ~37°C is placed on top of the micropatterned cells and allowed to solidify by a brief incubation at 4°C (~two minutes). **B.** Macrowells are formed by clamping a bottomless 96-well plate on top of a microwell array. The bottom surface of each macrowell contains up to 300 microwells. Macrowells can be used both to load multiple cell types at the same time and to perform parallel treatments. C. Example fluorescent images of comets on alkaline CometChip. Images were taken at 40X magnification (see **Methods**). Each frame can capture ~60 to more than 100 comet images. *Left*: untreated TK6 cells yield comets with little to no tail. *Right*: comets from TK6 cells treated with a high dose of a DNA damaging agent (50 µM H_2O_2) have visibly large tails.

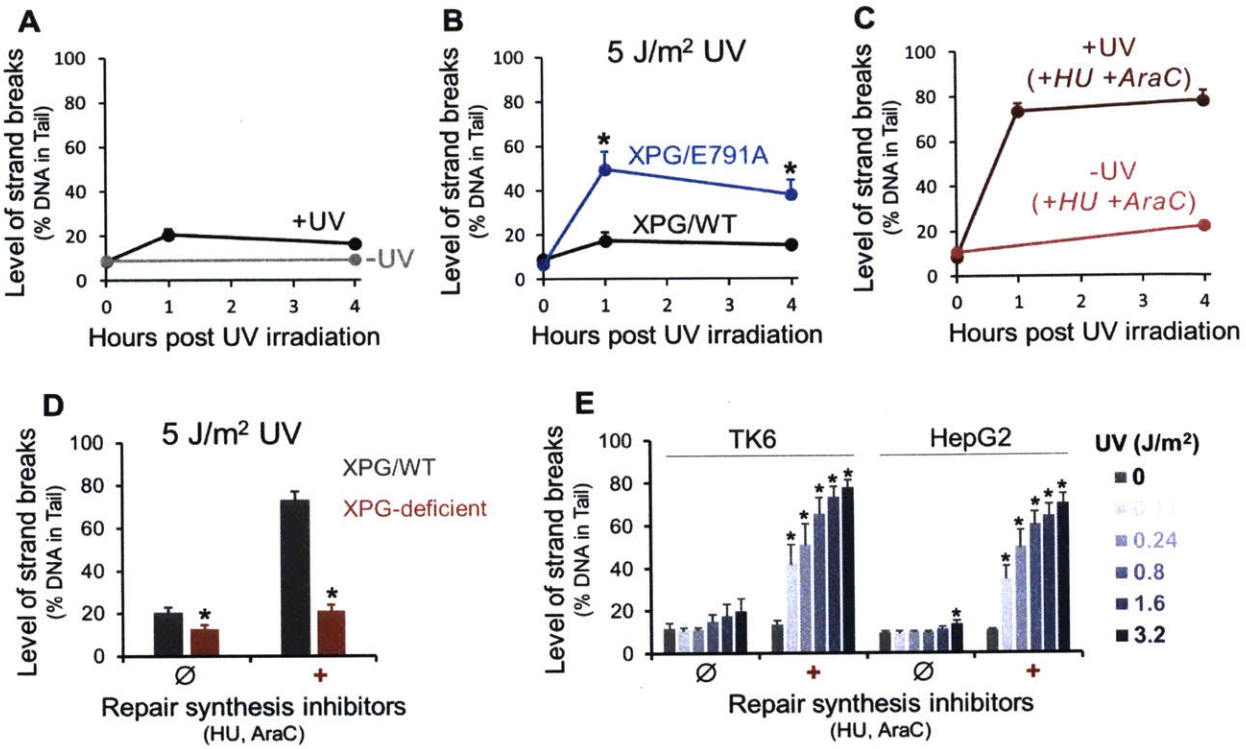

Figure 2-2. Analysis of strand breaks (SBs) by the alkaline CometChip as a measure of UV-induced lesions. Cells were pre-incubated with 10 mM GSH for 40 minutes at 37°C before UV irradiation and kept in the presence of 10 mM GSH for any subsequent incubation following UV exposure. **A**. Comparison of SB levels in human skin fibroblast cell line (XPG/WT) between untreated cells (-UV) and cells irradiated with 5 J/m^2 UV-C (+UV). **B**. SB levels in XPG/WT and XPG/E791A cells up to four hours following 5 J/m2 UV-C exposure. **C**. SBs in XPG/WT cells incubated with DNA repair synthesis inhibitors, HU and ara-C. Cells were pre-incubated with 1 mM HU, and 10 μM ara-C for 40 minutes at 37°C, irradiated with 5 J/m^2 UV-C (dark red line), and then incubated with the same HU and ara-C concentrations for up to four hours after exposure. Untreated control cells were kept in the same HU and ara-C conditions (light red line). **D**. Contribution of NER SB intermediates to detected SBs. XPG/WT and XPG-deficient cells were exposed to 5 J/m^2 UV-C and allowed to repair for one hour following irradiation. Cells were either incubated with the repair synthesis inhibitors (1 mM HU, 10 μM ara-C) for 40 minutes prior to UV irradiation and one hour of repair after exposure (+) or were incubated in regular medium without the inhibitors (Ø). *$p < 0.05$, Student's t-test, 2-tailed, paired (between the two cell lines for each inhibitor condition). **E.** HU/ara-C approach reveals dose-response to UV exposure. TK6 and HepG2 cells were irradiated with different doses of UV-C and analyzed for SBs one hour following exposure. Cells were either incubated with the repair synthesis inhibitors (1 mM HU, 10 μM ara-C) for 40 minutes prior to UV irradiation and one hour of repair after exposure (+) or were incubated in regular medium without the inhibitors (Ø). *$p < 0.05$, Student's t-test, 2-tailed, paired (between each UV dose and the untreated control). All data represent the average of ≥ 3 independent experiments. Error bars are standard errors of the means.

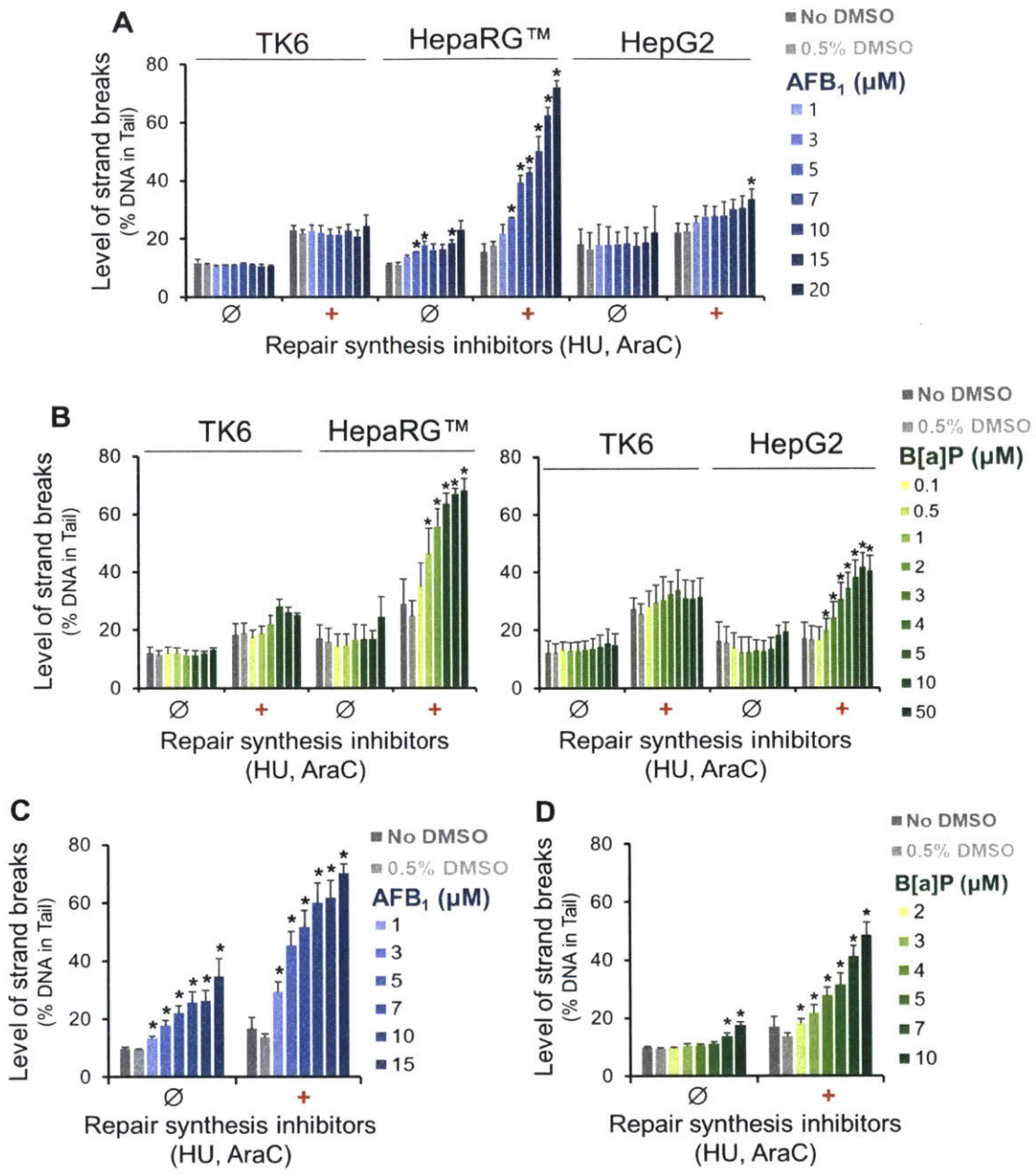

Figure 2-3. Application of HU/ara-C approach on alkaline CometChip to detect DNA damage induced by bioactivation of AFB_1 and B[a]P. Cells were treated with either AFB_1 or B[a]P in the absence (Ø) or presence (+) of 1 mM HU and 10 μM ara-C for 24 hours at 37°C and analyzed with the alkaline CometChip. **A.** Dose-response to AFB_1 in TK6, HepaRG™ (same-day treatment, see **Methods**), and HepG2. All three cell lines were treated in parallel. **B.** Dose-response to B[a]P in TK6, HepaRG™ (day-7 treatment, see **Methods**), and HepG2. HepaRG™ and HepG2 cells were treated on different days. TK6 was analyzed in parallel as a control for each treatment. $n \geq 3$. Error bars are standard errors of the means. **C and D.** Dose-response to AFB_1 (**C**) and B[a]P (**D**) in primary mouse hepatocytes (see **Methods**). All data represent the average of six mice (C57Bl6, 10-14 weeks old). Error bars are standard errors of the means. *$p<0.05$, Student's t-test, 2-tailed, paired [between treated dose and vehicle control (0.5% DMSO)].

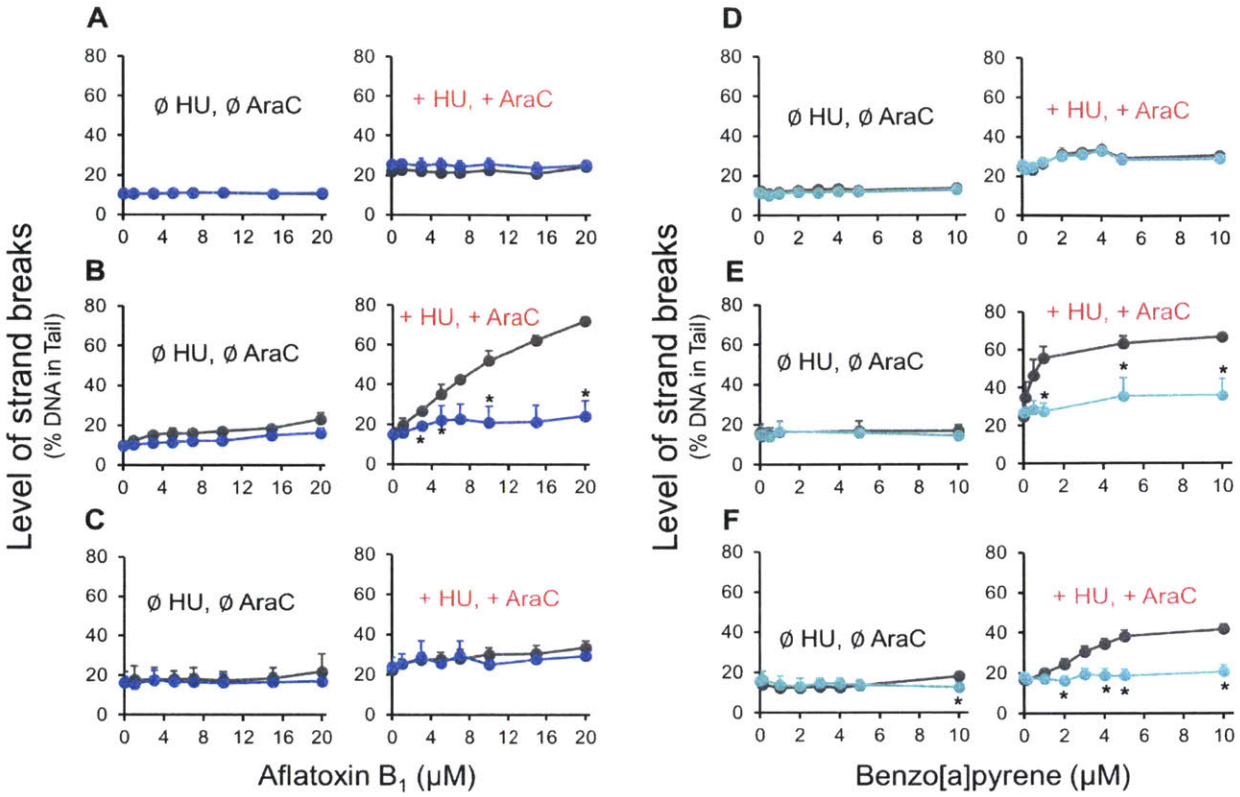

Figure 2-4. Role of metabolic activation in induction of SBs by AFB_1 and B[a]P. Cells were treated with AFB_1 or B[a]P for 24 hours in the absence or presence of 1 mM HU and 10 μM ara-C and analyzed with the alkaline CometChip. To inhibit AFB_1 metabolic activation, 5 μM KET was added to AFB_1 treatment (blue lines in **A**, **B**, and **C**). To inhibit B[a]P bioactivaion, 25 μM ANF was added to B[a]P treatment (teal lines in **D**, **E**, and **F**). Gray lines represent treatment conditions without KET and ANF. **A** and **D**. TK6 cells. **B**. HepaRG™ cells (same-day treatment). **E**. HepaRG™ (day-7 treatment). **C** and **F**. HepG2 cells. $n \geq 3$. Error bars are standard errors of the means. *$p<0.05$, Student's t-test, 2-tailed, paired.

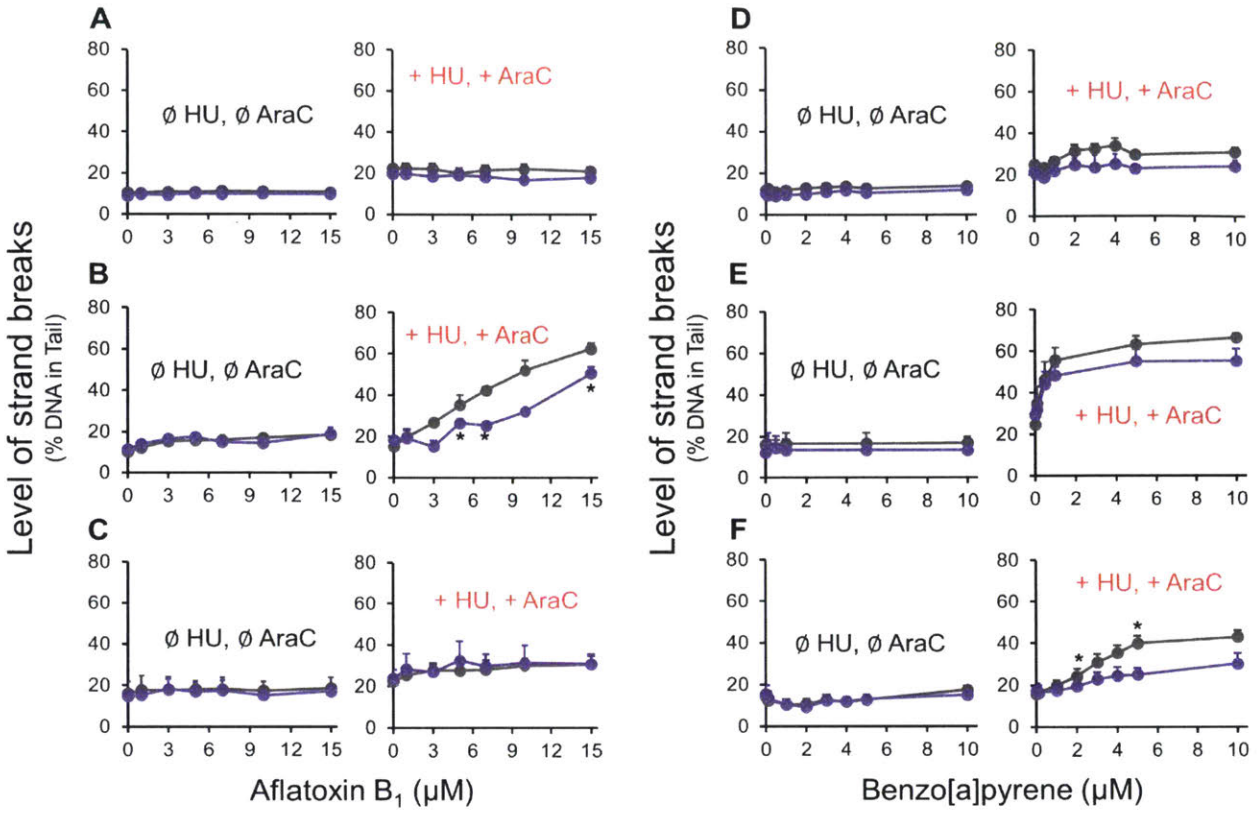

Figure 2-5. Using SP to study contribution of NER intermediates to SBs detected by HU/ara-C approach. Cells were treated with AFB_1 or B[a]P for 24 hours in the absence or presence of 1 mM HU and 10 μM ara-C and analyzed with the alkaline CometChip. To inhibit NER initiation, cells were incubated with 20 μM SP for five hours are 37°C prior to AFB_1 and B[a]P challenge. 20 μM SP was also added during AFB_1 and B[a]P treatment. Gray lines represent treatment conditions without SP. Purple lines represent treatment conditions with 20 μM SP. **A** and **D**. TK6 cells. **B**. HepaRG™ cells (same-day treatment). **E**. HepaRG™ (day-7 treatment). **C** and **F**. HepG2 cells. $n \geq 3$. Error bars are standard errors of the means. *$p<0.05$, Student's t-test, 2-tailed, paired.

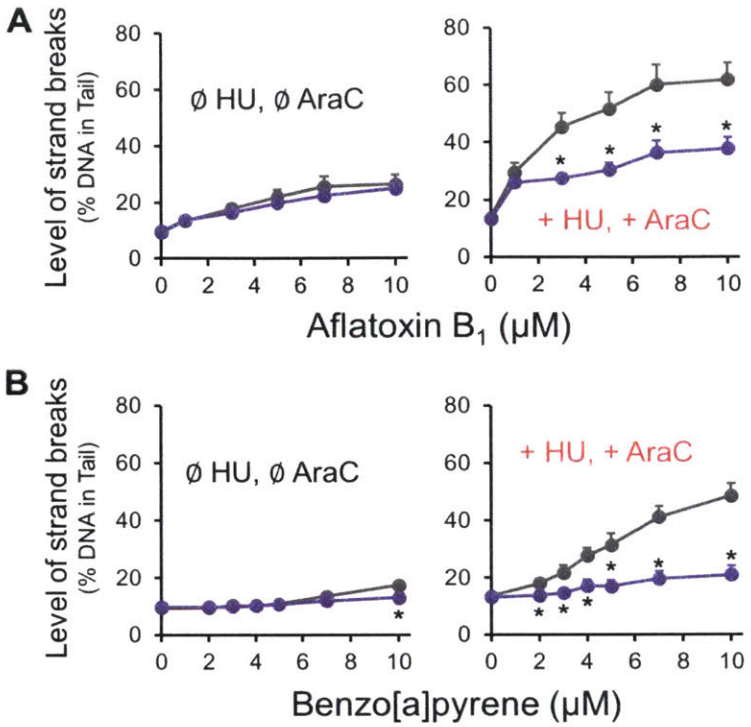

Figure 2-6. Using *Xpa*$^{-/-}$ mouse hepatocytes to study **c**ontribution of NER intermediates to SBs detected by HU/ara-C approach. Primary hepatocytes from six pairs of WT and *Xpa*$^{-/-}$ mice (C57Bl6, 10-14 weeks old) were isolated via two-step collagenase liver perfusion and incubated at 37°C overnight on CometChip (see **Methods**). Cells were then treated with AFB_1 (**A**) or B[a]P (**B**) for 24 hours in the absence or presence of 1 mM HU and 10 μM ara-C and analyzed with the alkaline CometChip. Gray lines represent the average of six WT mice. Purple lines represent the average of six *Xpa*$^{-/-}$ mice. Error bars are standard errors of the means. *$p<0.05$, Student's t-test, 2-tailed, paired.

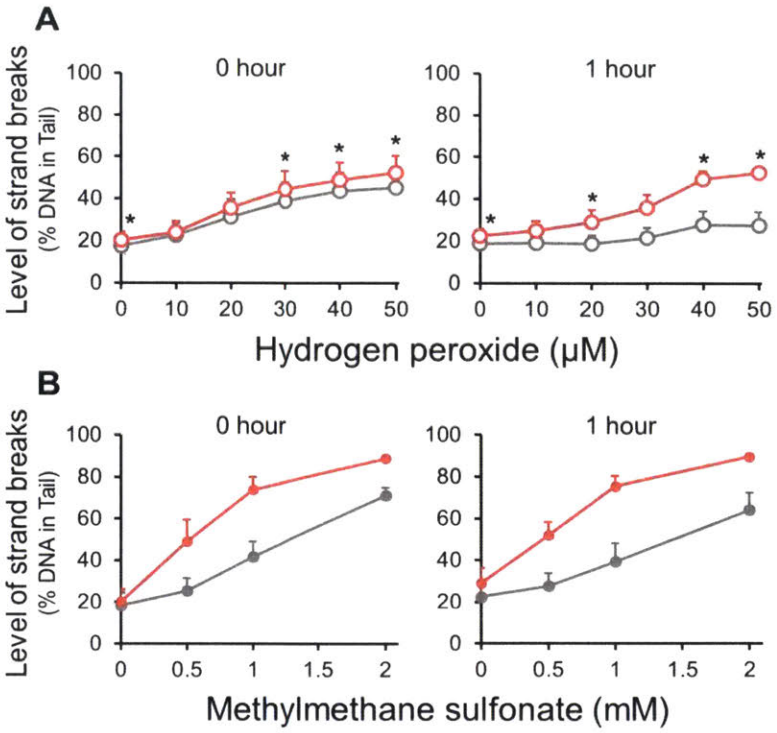

Figure 2-7. Testing the effects of HU/ara-C on repair of oxidative damage and alkylation damage in TK6 cells using the alkaline CometChip. Cells were incubated in culture medium in the absence or presence of 1 mM HU and 10 μM ara-C for 40 minutes at 37°C prior to H_2O_2 and MMS treatment. **A**. Cells were incubated with H_2O_2 for 20 minutes at 4°C, protected from light, in the absence or presence of 1 mM HU and 10 μM ara-C. After treatment, H_2O_2 was rinsed off. Half of the cells were placed in regular culture medium and the other half in medium supplemented with 1 mM HU and 10 μM ara-C for one hour at 37°C. n = 3. Error bars are standard errors of the means. *$p<0.05$, Student's t-test, 2-tailed, paired. **B**. Cells were incubated with MMS for 30 minutes at 37°C in the absence or presence of 1 mM HU and 10 μM ara-C. After treatment, MMS was rinsed off. Half of the cells were placed in regular culture medium and the other half in medium supplemented with 1 mM HU and 10 μM ara-C for one hour at 37°C. n = 2. Error bars are standard errors of the means. "0 hour" are cells analyzed immediately after treatment. "1 hour" are cells analyzed after one hour of repair. Gray lines are cells unexposed to HU/ara-C, and red lines are cells treated with HU/ara-C.

Table 2-1. List of chemicals used in this study that were prepared from powder form.

No.	Chemical	Abbreviation	Source	Catalog number	Stock concentration	Solvent
1	Aflatoxin B_1	AFB_1	MilliporeSigma, St. Louis, MO	AF10	4 mM	DMSO
2	Ketoconazole	KET	MilliporeSigma, St. Louis, MO	K1003	20 mM	DMSO
3	α-naphthoflavone	ANF	MilliporeSigma, St. Louis, MO	N5757	20 mM	DMSO
4	Spironolactone	SP	MilliporeSigma, St. Louis, MO	S3378	20 mM	DMSO
5	Benzo[a]pyrene	B[a]P	MilliporeSigma, St. Louis, MO	B1760	20 mM and 1 mM	DMSO
6	Etoposide		MilliporeSigma, St. Louis, MO	E1383	1 mM	DMSO
7	2,4-Diaminotoluene	2,4-DAT	TCI America, Portland, OR	D0123	1 M	DMSO
8	Cyclophosphamide monohydrate	CP	MilliporeSigma, St. Louis, MO	C0768	1 M	DMSO
9	*para*-Chloroaniline	PCA	MilliporeSigma, St. Louis, MO	C22415	500 mM	DMSO
10	N-Nitrosodimethylamine	NDMA	MilliporeSigma, St. Louis, MO	48552	1 M	H_2O
11	Hydroquinone	HQ	MilliporeSigma, St. Louis, MO	H17902	100 mM	H_2O
12	Chloramphenicol	CAM	MilliporeSigma, St. Louis, MO	C0378	200 mg/ml (619 mM)	DMSO
13	cis-Diamineplatinum(II) dichloride	cisplatin	MilliporeSigma, St. Louis, MO	479306	1 mM	H_2O

Table 2-2. Results of alkaline CometChip for genotoxicity screen of nine known *in vivo* genotoxins (120) and summary of known information about these toxins. "-" means no statistically significant measure of DNA damage. "+" means at least one dose shows statistically significant DNA damage. Numbers in parentheses represent the range of doses that score "+".

	Genotoxicity			Carcinogenicity
In vivo genotoxins	Ames test	Alkaline CometChip HepaRG™	Alkaline CometChip HepaRG™ + HU + ara-C	IARC classification (91)
Etoposide	+ (147)	-	+ (10 μM)	Group 1
2,4-DAT	+ (148)	-	+ (10 mM)	Group 2B
CP	+ (148)	-	+ (5-10 mM)	Group 1
PCA	+ (148)	-	-	Group 2B
NDMA	+ (148)	+ (2.5 - 20 mM)	+ (2.5 - 20 mM)	Group 2A
HQ	- (148)	-	+ (0.33 mM)	Group 3
B[a]P	+ (148)	-	+ (5-10 μM)	Group 1
CAM	- (149)	-	+ (3.1 mM)	Group 2A
Cisplatin	+ (150)	-	-	Group 2A

IARC classification (91): Group 1: human carcinogen, Group 2A: probably human carcinogen, Group 2B: possible human carcinogen, Group 3: not classifiable as to its carcinogenicity to humans.

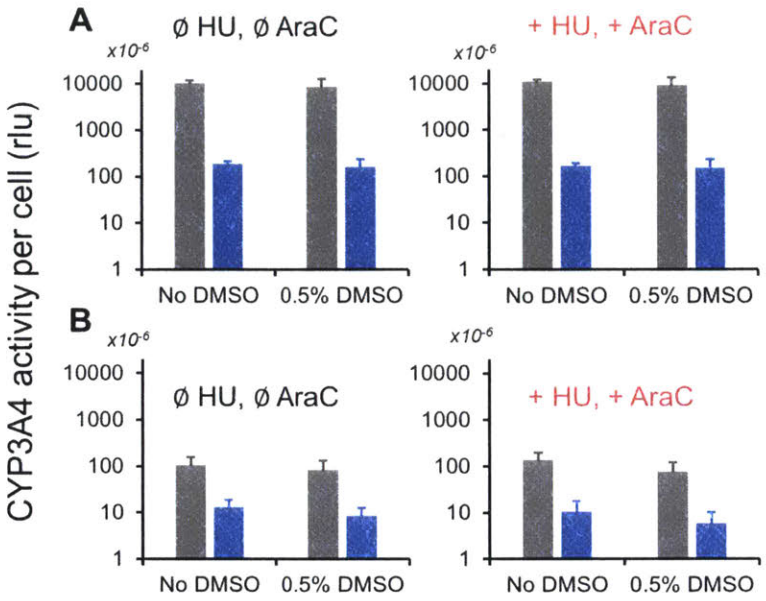

Figure 2-S1. Effects of ketoconazole (KET) on CYP3A4 activity per cell measured by P450-Glo™ assay (see **Methods**). Cells were incubated with 5 μM KET for 24 hours at 37°C in the absence or presence of 1 mM HU and 10 μM ara-C. Gray bars: basal CYP3A4 activity levels for both untreated (No DMSO) and vehicle control (0.5% DMSO). Blue bars: CYP3A4 activity levels in the presence of 5 μM KET. **A.** HepaRG™ cells. **B.** HepG2 cells. rlu: relative light unit. All data represent the average of three independent experiments. Error bars are standard errors of the means.

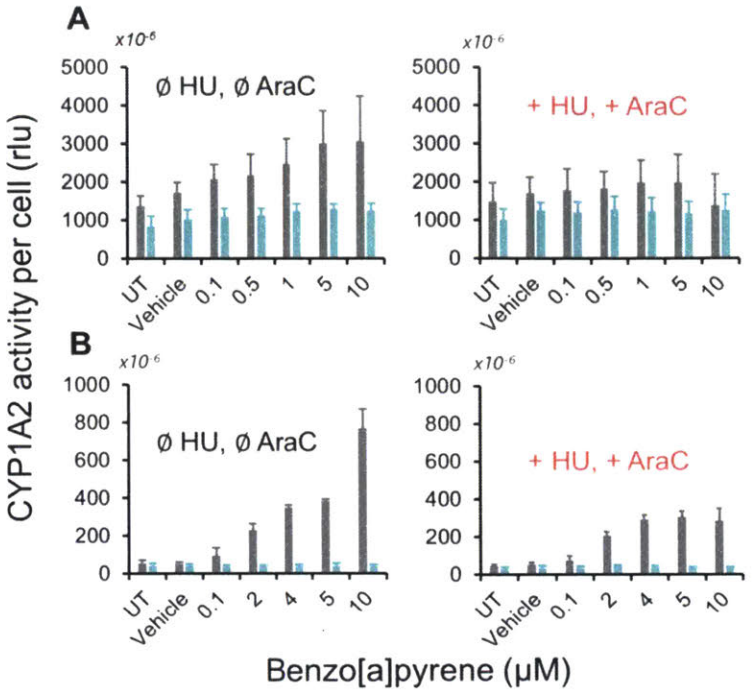

Figure 2-S2. Effects of α-naphthoflavone (ANF) on CYP1A2 activity per cell measured by P450-Glo™ assay (see **Methods**). Cells were incubated with B[a]P together with 25 μM ANF for 24 hours at 37°C in the absence or presence of 1 mM HU and 10 μM ara-C. Gray bars: CYP1A2 activity levels corresponding to untreated control (UT), vehicle control (0.5% DMSO), and B[a]P doses. Teal bars: CYP1A2 activity levels in the presence of 25 μM ANF. **A.** HepaRG™ cells. **B.** HepG2 cells. rlu: relative light unit. All data represent the average of three independent experiments. Error bars are standard errors of the means.

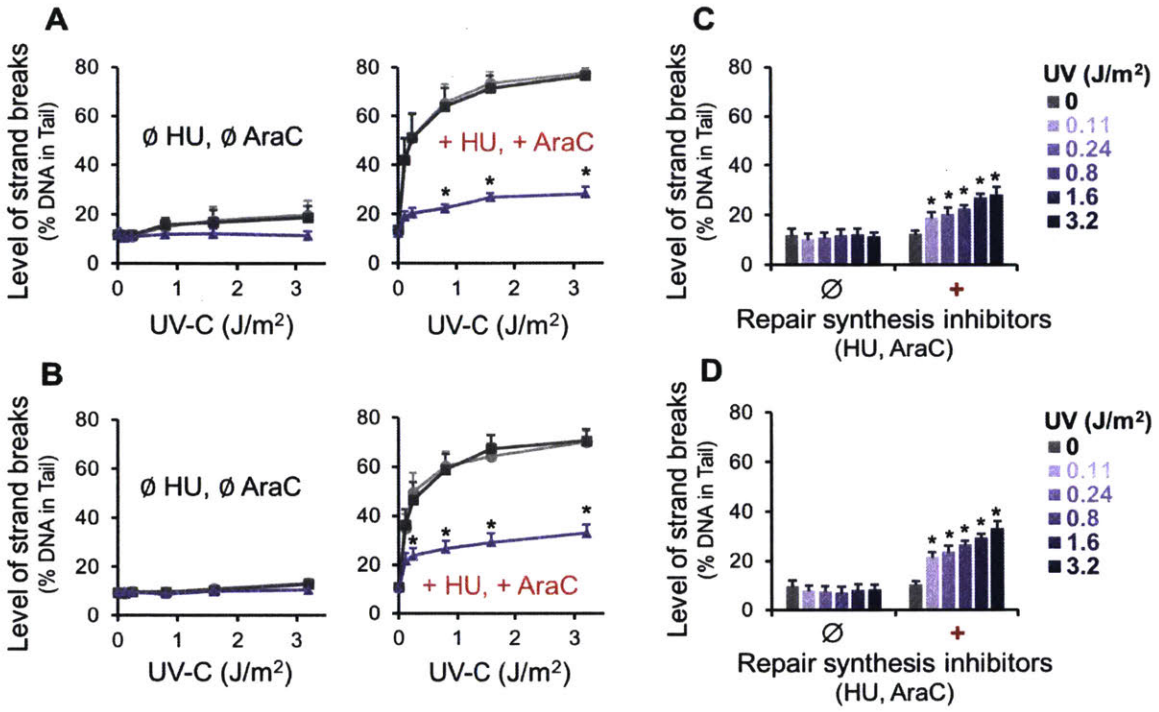

Figure 2-S3. A and B. Effects of spironolactone (SP) on NER initiation. Cells were exposed to UV light and allowed to repair for one hour at 37°C. SBs were analyzed using the alkaline CometChip. 1 mM HU and 10 μM ara-C were either absent or present at all time in the experiment. *Purple*: 20 μM SP (see **Methods**). *Dark gray*: vehicle control (0.1% DMSO). *Light gray*: untreated control (no DMSO). **A.** TK6 cells. **B.** HepG2 cells. All data represent the average of four independent experiments. Error bars are standard errors of the means. *$p<0.05$, Student's t-test, 2-tailed, paired (between 20 μM SP and vehicle control).

C and D. UV-induced SBs in the presence of 20 μM SP. **C.** TK6 cells. **D.** HepG2 cells. All data represent the average of four independent experiments. Error bars are standard errors of the means. *$p<0.05$, Student's t-test, 2-tailed, paired (between each UV dose and untreated control (0 J/m^2)).

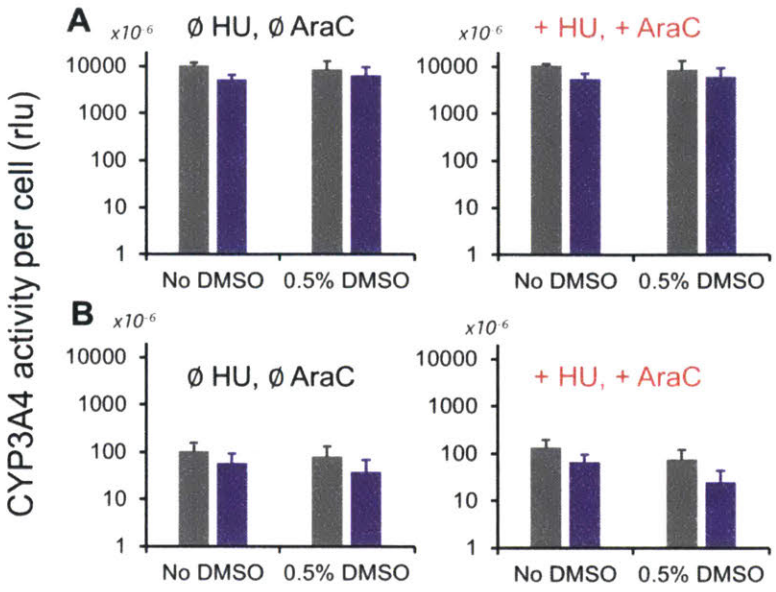

Figure 2-S4. Effects of spironolactone (SP) on CYP3A4 activity per cell measured by P450-Glo™ assay (see **Methods**). Cells were incubated with 20 μM SP for 24 hours at 37°C in the absence or presence of 1 mM HU and 10 μM ara-C. Gray bars: basal CYP3A4 activity levels for both untreated (No DMSO) and vehicle control (0.5% DMSO). Purple bars: CYP3A4 activity levels in the presence of 20 μM SP. **A.** HepaRG™ cells. **B.** HepG2 cells. rlu: relative light unit. All data represent the average of three independent experiments. Error bars are standard errors of the means.

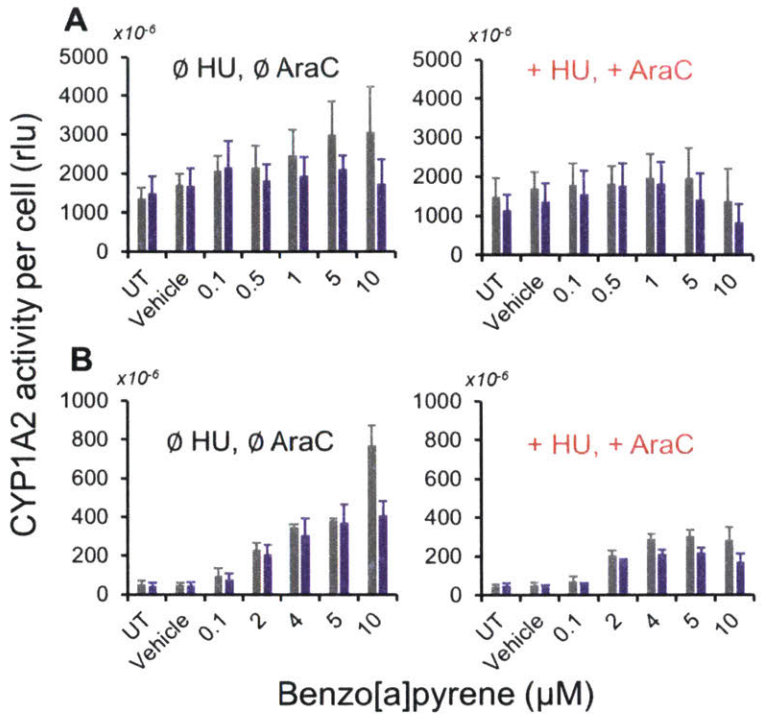

Figure 2-S5. Effects of SP on CYP1A2 activity per cell measured by P450-Glo™ assay (see **Methods**). Cells were incubated with B[a]P together with 20 μM SP for 24 hours at 37°C in the absence or presence of 1 mM HU and 10 μM ara-C. Gray bars: CYP1A2 activity levels corresponding to untreated control (UT), vehicle control (0.5% DMSO), and B[a]P doses. Purple bars: CYP1A2 activity levels in the presence of 20 μM SP. **A.** HepaRG™ cells. **B.** HepG2 cells. rlu: relative light unit. All data represent the average of three independent experiments. Error bars are standard errors of the means.

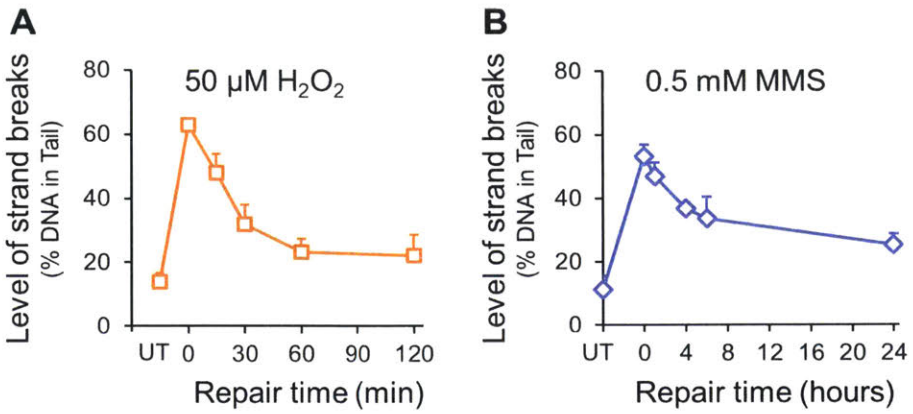

Figure 2-S6. DNA repair kinetics of oxidative damage and alkylation damage in TK6 cells. **A.** TK6 cells were loaded onto CometChip and exposed to 50 μM H_2O_2 for 20 min at 4°C, protected from light. After treatment, cells were allowed to repair in culture medium at 37°C. Cells were analyzed for SB levels using the alkaline CometChip for basal damage (UT), immediately after treatment (0 min), and at 15, 30, 60, and 120 min of repair. **B.** TK6 cells in suspension were treated with 0.5 mM MMS for one hour at 37°C. After treatment and washing, cells in suspension were allowed to repair in culture medium at 37°C. Cells were loaded onto CometChip and analyzed for background SB level (UT), SBs immediately after treatment (0 hour), and 1, 4, 6, and 24 hours of repair. All data represent the average of three independent experiments. Error bars are standard errors of the means.

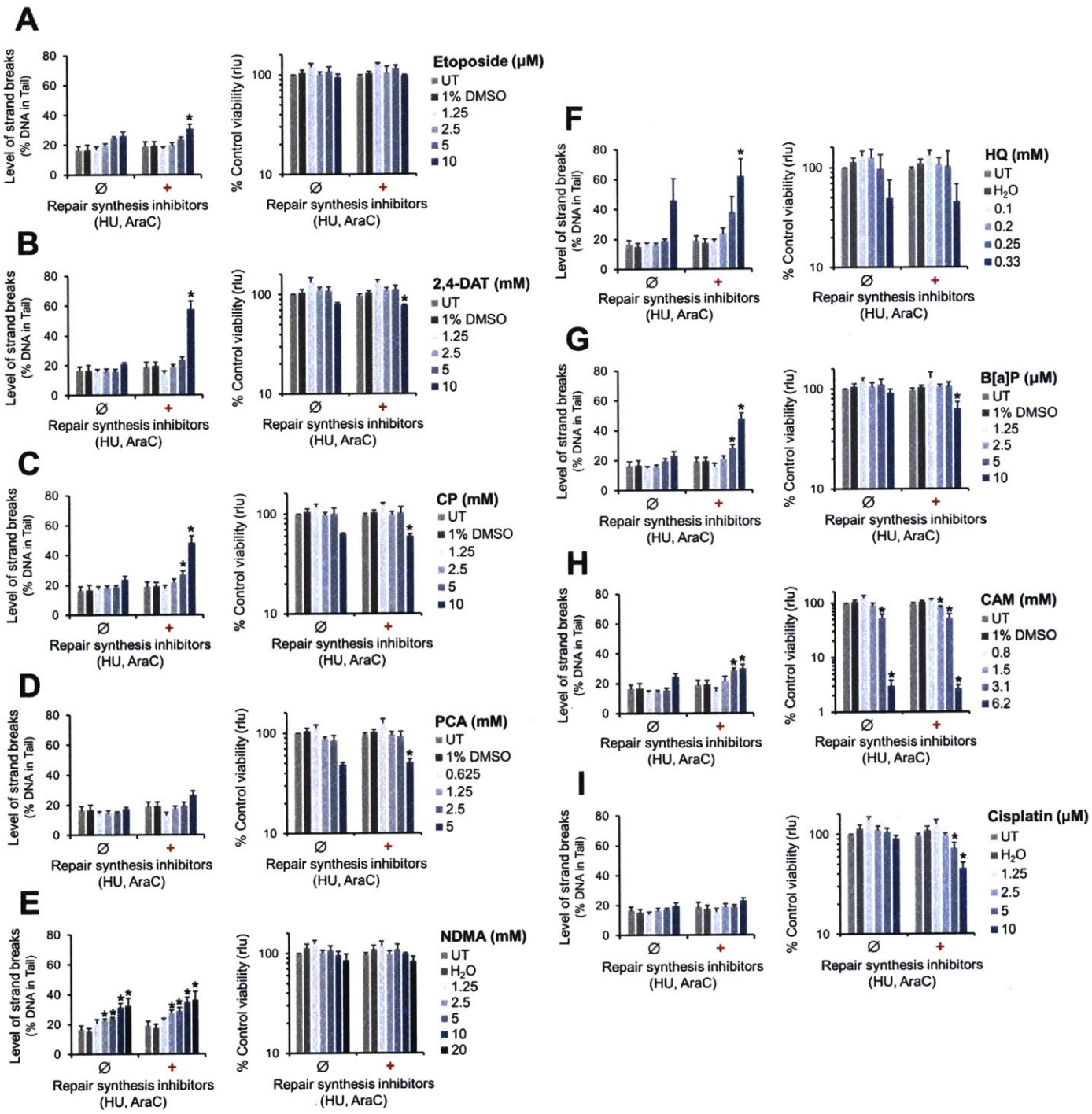

Figure 2-S7. DNA damage in HepaRG™ cells induced by nine *in vivo* genotoxins, measured by the alkaline CometChip using the repair synthesis inhibitors HU and ara-C. HepaRG™ cells were exposed to test compounds for 24 hours at 37°C using the same-day treatment procedure (see **Methods**). 1 mM HU and 10 μM ara-C were either absent (Ø) or present (+) in the same treatment. At the end of the exposure period, half of the cells were analyzed for SB levels with the alkaline CometChip (left plot of each figure), and the other half were analyzed for cell viability using the CTG® assay (see **Methods**) (right plot of each figure). "UT" represents background damage. Vehicle controls are "1% DMSO" or "H_2O". **A.** Etoposide. **B.** 2,4-Diaminotoluene. **C.** Cyclophosphamide. **D.** para-Chloroaniline. **E.** N-Nitrosodimethylamine. **F.**

Hydroquinone. **G.** Benzo[a]pyrene. **H.** Chloramphenicol. **I.** cis-Diamineplatinum (II) dichloride. rlu: relative light unit. All data represent the average of three independent experiments. Error bars are standard errors of the means. $*p<0.05$, Student's t-test, 2-tailed, paired (between a treatment dose and the corresponding vehicle control).

Chapter 3

Novel Microarray Colony Formation Platform for High-Throughput Cell Survival Quantification

3.1. ABSTRACT

Quantification of cell survival is one of the most fundamental and broadly used endpoints in biology. The gold standard for cell survival quantification is the colony formation assay. While the assay has an impressive dynamic range over several orders of magnitude, it is relatively low-throughput (10-21 days), laborious, and consumes large amounts of test compounds. On the other hand, XTT and CellTiter-Glo® (CTG®), two of the most popular high-throughput assays, use indirect measures of cell viability to estimate the extent of cytotoxicity. The XTT assay suffers from low sensitivity and an inferior dynamic range compared to the colony formation assay. In addition, because indirect markers do not always correlate directly with viability, both XTT and CTG® are susceptible to viability-independent interferences. To overcome the major limitations of commonly used assays, we developed MicroColony Chip (μCC) to measure directly a cell's ability to divide (similar to the colony formation assay) with the scale and speed of microtiter assays. μCC is a miniaturized colony formation platform, wherein microcolonies grow in an array and toxicity is calculated based on the change in the distribution of the microcolony sizes. We show here that μCC achieves the same sensitivity as the colony formation assay with ~250-fold reduction in growth surface area and ~80% reduction in incubation time. We also show that μCC is more sensitive than the XTT assay and that it has comparable sensitivity to CellTiter-Glo® while being more robust. Finally, we show that the μCC can be used for studies of xenobiotics in metabolically relevant conditions.

3.2. INTRODUCTION

Quantification of cell survival is one of the most fundamental and broadly used endpoints in biology. Cell viability assays are a basic research tool enabling molecular pathway analysis and definition of gene function. Cell survival assessment is also essential in chemical safety studies. There are more than 100,000 synthetic chemicals used in consumer products, many of which have not been tested for safety (1). In addition, more than 2,000 new compounds are introduced each year (2), increasing the urgent need for sensitive, reliable, and rapid methods for toxicity assessment. Viability assays are also a mainstay assay in the pharmaceutical industry where they are used to predict adverse effects as well as establishing efficacy of compounds designed to target cancer cells (3). In these contexts and others, accurate cell survival testing has significant implications. For example, in terms of public health, a false negative for toxicity could mean that hundreds of people are exposed to a hazardous chemical. For the pharmaceutical industry, a false positive could mean that an effective drug does not make it to the market, while a false negative could mean that patients get exposed to toxic pharmaceuticals.

The gold standard for cell survival quantification is the colony formation assay (4), wherein cells are exposed to a toxic agent and the ability of single cells to form colonies is quantified (5, 6). About 2-3 weeks following exposure, the surviving cells form colonies that can be counted by eye when stained. Comparison of the colony numbers between the treated and untreated cells yields the relative toxicity of the treatment condition. While the assay has an impressive dynamic range over several orders of magnitude, it is inconvenient and relatively low-throughput due to long incubations. In addition, to prevent colony overlapping, cells are plated in large dishes, which require large amounts of media. High volumes of media consume more test compounds. Small molecule libraries are generally limited in quantities, and therefore the colony formation assay cannot be used. Further, manual colony counting is time consuming and can be prone to bias (4).

Due to the significant limitations of the colony formation assay, viability assays that are compatible with microtiter plates or have a rapid assay time of 1-4 days have become popular alternatives. Loss of

membrane integrity has been the most common indicator of cell death for many viability assays, such as the trypan blue and propidium iodide exclusion assays (3). Cells considered viable are those with intact membrane and can exclude the stains. A drawback of this approach is that membrane integrity does not always accurately reflect viability. Cells going through early stage programmed cell death may still have intact plasma membrane (4, 6). On the other hand, severely damaged cells can disintegrate before the assay is performed and will not be counted (7).

Another approach for estimating viability is to measure mitochondrial function via metabolism-based endpoints. For example, tetrazolium assays (eg. MTT and XTT) are based upon the underlying principle that a live cell can reduce tetrazolium salts to formazan derivatives, accompanied by a change in color that can be measured by absorbance (8-11). Because of its relative ease of use and affordability, tetrazolium assays are commonly used despite their low sensitivity (4, 9, 10). Importantly, artifacts can arise from spontaneous reduction of the tetrazolium salts by reducing agents in cell media (4) or changes in the absorbance spectrum of the formazan products induced by pH changes in the culture medium (12, 13). Analogously, intracellular ATP levels can be quantified as a measure of viable cells (14-18). The most popular assay for this approach is the CellTiter-Glo® (CTG®) assay (Promega), which quantifies ATP levels with luciferin-luciferase luminescence. CTG® is exquisitely sensitive and is able to measure ATP levels in a single mammalian cell (6). However, ATP assays are affected by viability-independent perturbations, such as nutrient depletion and pH changes (3, 13, 19), and can underestimate toxicity for short incubation periods (6). Importantly, we have found in this work that CTG® can yield highly different results depending on initial cell density (described in detail below).

Here, we aimed to create an alternative approach to cell survival testing that combines the advantages of existing assays. The result is "MicroColonyChip" (μCC), which requires ~250 times less surface area than the colony formation assay and reduces ~80% incubation time while achieving similar sensitivity. μCC is based upon the ability of microcolonies to grow in a microarray, enabling the miniaturization of the traditional colony formation assay. Specifically, being able to grow cells in a

microarray suppresses colony overlap, making it possible to move from large dishes to a 96-well plate format. Rather than manual counting of colonies, μCC uses DNA fluorescent staining combined with an in-house software to measure microcolony sizes, enabling a significant reduction of assay time. For most cell types, it takes ~2-3 weeks for colonies to be countable by eye. On the other hand, after ~3-4 days we have observed significant differences between the distributions of microcolony sizes in the untreated control and in the exposed population. Based on this observation, we developed methods to extract key parameters that reflect the portion of surviving cells. These variables form the basis of a highly sensitive toxicity test.

We demonstrate in this work that the μCC has sensitivity comparable to the gold standard colony formation assay. Furthermore, we find that the μCC is significantly more sensitive than the XTT assay, and that it has comparable sensitivity to CTG®, while being more robust against culturing conditions. Finally, we show that the μCC can be applied for studies of xenobiotics in metabolically relevant conditions.

3.3. MATERIAL AND METHODS

Chemicals

1,3-Bis(2-chloroethyl)-1-nitrosourea (BCNU) was obtained from Sigma-Aldrich, St. Louis, MO (C0400) and dissolved in 100% ethanol to make a 99 mM stock solution. Aflatoxin B_1 from *Aspergillus flavus* (A6636) and ketoconazole (K1003) were purchased from Sigma-Aldrich, St. Louis, MO (A6636) and dissolved in 100% dimethyl sulfoxide (DMSO) to make 20 mM stock solutions. 10% formalin, RPMI 1640 medium with GlutaMAX™, and Pen-Strep were obtained from Thermo Fisher Scientific, Waltham, MA (61870). Fetal Bovine Serum (FBS) was obtained from Atlanta Biologicals, Inc., Flowery Branch, GA.

Cell culture

TK6 (20, 21), TK6+MGMT (22), and MCL-5 (23) human B-lymphoblastoid cell lines were cultured in 1X RPMI 1640 medium with GlutaMAX™ supplemented with 10% FBS and 1% Pen-Strep. All cell lines were incubated in an incubator set at 37°C with 5% atmospheric CO_2. Cell growth in liquid

culture was measured by counting cell density of the same culture every day for four days using the Vi-CELL™ cell counter (Beckman Coulter Life Sciences, Brea, CA).

μCC fabrication

The microwells were fabricated as described previously (24-27). Briefly, 1% w/v agarose solution in phosphate-buffered saline (PBS) was prepared. When the molten agarose solution cooled down to ~65°C, Pen-Strep was aseptically added to a final concentration of 2%. A polydimethylsiloxane (PDMS) mold with an array of micropegs was pressed into the molten agarose solution on top of the hydrophilic side of a sheet of GelBond® Film (Lonza, Hopkinton, MA). The agarose was allowed to gel at room temperature for ~15 minutes. After the mold was removed, a bottomless 96-well plate was pressed on top of the agarose chip.

A 0.6% w/v low melting point agarose stock solution in PBS was kept molten at 43°C. A culture medium stock (RPMI 1640 with GlutaMAX™ supplemented with 20% FBS and 2% Pen-Strep) was kept at 37°C. To prepare the 0.3% w/v overlay agarose solution, one volume of the agarose stock solution was combined with one volume of the culture medium stock.

Cells were loaded into the microwells by gravity, and the gel was then covered with a thin layer of 0.3% w/v overlay agarose prepared as described above. The gel was kept at room temperature for 15 minutes and another layer of the overlay agarose was added. After 15 more minutes at room temperature, the gel was transferred to 4°C for 15 minutes to ensure maximal solidification of the overlay agarose.

Microcolony culture and treatment with DNA damaging agents

The μCC gel attached to GelBond® Film was cut into 5 cm x 5 cm pieces using a pair of sterile surgical scissors. The μCC pieces were submerged in fresh culture medium and incubated at 37°C and 5% atmospheric CO_2 overnight before toxic treatments.

For chemical treatments, the compounds were added to the medium at different concentrations, and the μCC pieces were then submerged in the medium. Immediately after the treatment time, an unexposed μCC piece was removed from culture medium and placed in 10% formalin (starting population). The rest of the μCC pieces were allowed to recover in fresh culture medium with no compounds for three or four additional days before fixation in 10% formalin.

μCC pieces were submerged in 10% formalin for cell fixation and kept at 4°C for at least 2 hours before staining for DNA content. After fixation, μCC pieces were transferred to PBS and kept at 4°C until staining.

γ radiation treatment

While submerged in culture medium, cells encapsulated in μCC were irradiated at room temperature using γ-rays from a ^{137}Cesium source at 1 Gy/min (Gammacell 40 Exactor, Best Theratronics Model C-440).

N,N'-bis (2-chloroethyl)-N-nitrosourea (BCNU) treatment

μCCs were removed from culture medium and rinsed by submerging in PBS for 5 minutes. PBS was aspirated and replaced with BCNU diluted in warm RPMI 1640 (+ GlutaMAX™) supplemented with 1% Pen-Strep. The maximum final concentration of ethanol was 0.1%. BCNU exposure was for one hour at 37°C with 5% atmospheric CO_2; the BCNU solution was aspirated and residual BCNU was rinsed off twice by submerging the μCC pieces in PBS for 5 minutes each time.

Aflatoxin B_1 (AFB_1) treatment

μCCs were submerged in culture medium supplemented with AFB_1 and incubated at 37°C and 5% atmospheric CO_2. The maximum final concentration of DMSO was 0.5%. After 24 hours of incubation, the AFB_1-supplemented medium was removed. The μCC pieces were washed three times by submerging in PBS for 5 minutes.

Inhibition of AFB_1 metabolism with ketoconazole (KET)

To inhibit AFB_1 metabolism, 5 μM KET was added to culture medium at the start of AFB_1 treatment. The maximum final concentration of DMSO was 0.53%. The remaining steps were similar to the AFB_1 treatment.

Fluorescence imaging and analysis

After cell fixation with 10% formalin, the μCCs were rinsed once with PBS solution and stained with Vybrant® DyeCycle™ Green (Thermo Fisher Scientific, Waltham, MA) (dissolved in PBS to a final concentration of 1.5 μM) at 4°C overnight. As a membrane permeable dye, Vybrant® DyeCycle™ Green

maximizes the chance of capturing the total DNA content of a microcolony, which may contain both live and dead cells. Fluorescent images were captured using an epifluorescence microscope (Nikon Eclipse 80i, Nikon Instruments, Inc., Melville, NY) with a 480 nm excitation filter and automatically analyzed using a custom software written in MATLAB (The MathWorks Inc., Natick, MA) as previously described (24) with modifications to enable quantification of integrated fluorescence intensity per microcolony (F/M) (Figure 2A). Distributions of F/M values were automatically generated and exported into spreadsheet files using a custom software written in Python (Python Software Foundation, Python version 2.7.10). Analyses of F/M distributions for excess microcolonies and excess growth were performed in Microsoft Excel (Microsoft Office Suite 2016).

Colony formation assay in microtiter plates

The colony formation assay in microtiter plates was performed as previously described (28, 29) to determine survival of TK6 cells 3 weeks after ionizing radiation treatment. Briefly, TK6 cells growing in suspension were analyzed for viability and cell number using an automated Trypan Blue exclusion system [Vi-CELL^{TM} cell counter (Beckman Coulter Life Sciences, Brea, CA)]. A fixed number of TK6 cells were distributed over U-bottom 96-well plates after ionizing radiation treatment. After 3 weeks, the wells were scored for absence of colony growth, and the fraction of wells with no growth was calculated (a best estimate for P(0), the probability of any well having no colony). The number of viable cells per 96 well follows a Poisson distribution, therefore the mean number of viable cells per well can be calculated from the estimated P(0). The surviving fraction was then calculated by dividing by the number obtained for untreated cells and multiplying by a dilution factor. Bright field pictures of the bottom of 96-well plates were taken with an Olympus TG-860 Tough Stylus Digital Camera (Olympus America, Inc., Center Valley, PA) at 5X magnification.

XTT assay

The XTT cell viability kit was purchased from Cell Signaling Technology® (Danvers, MA). Three days after ionizing radiation treatment, the viability of TK6 cells was measured using the XTT kit according to the manufacturer's manual.

CellTiter-Glo® assay (CTG®)

The CTG® luminescent cell viability kit was purchased from Promega (Madison, WI). 3 days after ionizing radiation treatment, the viability of TK6 cells was measured using the CTG® kit according to the manufacturer's manual.

3.4. RESULTS

Patterning of cells using a microwell array platform

Arraying cells in a micropattern makes it possible to measure colony formation using a small area. Specifically, the microarray increases the density of colonies per cm^2 by ~250 times while eliminating most of colony overlap. In order to array cells, we use a cell microarray approach that has previously been described by our laboratory (24). Briefly, a PDMS mold (created by photolithography and soft lithography) is pressed into molten agarose. The agarose is allowed to gel, and the mold is removed to reveal an array of microwells. For the experiments described here, each microwell is ~40 μm in both diameter and depth, spaced 240 μm apart from one another. The microwell array platform provides a tunable physical distance between microcolonies and tunable well sizes. A bottomless 96-well plate is then compressed on top of the microwell array to create macrowells with about 300 microwells each. A suspension of cells is then placed in each macrowell and the cells are loaded into the microwells by gravity. Removal of excess cells by sheer force reveals a microarray of cells (Fig. 3-1A). Cells are then trapped by adding low melting point agarose in a layer above the cells. Due to the nature of the loading conditions where excess cells are washed away, we find that the wells work equally effectively across a remarkably broad range of cell numbers (2,000-200,000 cells/macrowell).

Non-adherent cells, such as lymphoblastoid cells, can be micropatterned using the microwell array (Fig. 3-1B). After the cells are loaded into the microwells, we observe a range between one and seven TK6 cells per microwell, using phase-contrast microscopy at 40X magnification (Fig. 3-1B – Day 0). To learn about the ability of the arrayed cells to form microcolonies, TK6 cells were incubated in cell culture media

at 37°C. Suspension cells that naturally grow without attachment have previously been shown to form colonies in soft agar (5, 30, 31). Consistent with these studies, here we show that TK6 cells also grow on the microwell array platform. Appearance of cells growing out of the microwell boundary was noted as soon as two days in culture (Fig. 3-1B, Day 2). By day four, most microwells had formed larger microcolonies with approximately more than ~60 cells, which is consistent with about a 20-hour doubling time and an average of three cells/well on Day 0 (manual approximation using phase-constrast) (Fig. 3-1B, Day 4) (28).

High-throughput quantification of microcolony size via nucleic acid fluorescence staining

We estimated individual microcolony sizes based on the total DNA content for each microcolony, since DNA content is a useful indicator of cell number (32-35). Although DNA content depends on the cell cycle phase, in a non-synchronous cultures, the average DNA content per cell stays relatively constant over time (34). We therefore labeled the DNA of the microcolonies (example in Fig. 3-1C, left) using a fluorescent nucleic acid stain that is membrane permeable (Vybrant® DyeCycle Green; see Methods). Fluorescent images of microcolonies were then captured (example in Fig. 3-1C, middle). To quantify total DNA staining for each microcolony, we used an in-house MATLAB program that integrates the fluorescence intensity for a given area (adapted from previous in-house software (24), see *Methods*). The program detects the locations of the microcolonies and generates images of individual microcolonies (example in Fig. 3-1C, middle). The software integrates the total fluorescence intensity for each microcolony (F/M) (example in Fig. 3-1C, right).

To validate the F/M parameter, the number of distinct fluorescent nuclei in a microcolony was counted manually as an estimate of total cell number for that microcolony (examples in Fig. 3-2A, see *Supplementary Procedures*). As shown in Fig. 3- 2B, the number of cells per microcolony increases linearly with the microcolony's F/M value ($R^2 = 1$), indicating F/M is a sensitive and robust measurement of cell number up to seven cells. F/M for a single cell, or fluorescence intensity per cell (F/C), is calculated to be 2300 ± 500 (arbitrary fluorescence unit).

We further tested the linearity of the F/M parameter for microcolony size beyond the cell number countable under phase-contrast microscopy (seven cells). We monitored the change in the median F/M value over four days in culture (Fig. 3-2C). Regression analysis shows that the median F/M for TK6 microcolonies increased exponentially between day 0 and day 4 (R^2 = 0.95) with a doubling time of approximately 21 hours. Similarly, we observed a doubling time of ~21 hours in TK6 cells growing in liquid culture (Fig. 3-2C, see *Methods*). We concluded that F/M is a sensitive and robust measurement of microcolony size and that the doubling time of TK6 cells cultured on μCC is not significantly altered.

Construction of microcolony size distribution using F/M values

To construct the distribution of microcolony sizes, we calculated the relative frequency of microcolonies with the same number of TK6 cells (Fig. 3-S1A). We monitored the growth of the TK6 microcolonies over the course of four days. Initially, the number of cells per microwell ranged between one and seven cells. On each day, a plate was removed for analysis, and microcolonies were stained for DNA content (Fig. 3-2D). As expected, some microcolonies remained very small while others had grown extensively. After four days, microcolony F/M values ranged from 1 F/C to 150 F/C, corresponding to ~one cell up to ~150. It is important to note that a colony that initially had seven cells could readily double to form a colony of more than 150 cells over the course of four days (approximately 4.5 doubling times). Fig. 3-2D shows that the F/M distribution of TK6 microcolonies is very tight on day 0 and that as the microcolonies grow, the distribution both shifts to the right and broadens. One can see more easily the extent to which the populations become broader when all plots have the same scale for the y-axis (Fig. 3-S2). We postulate that the broadening of F/M distributions is attributable to the difference in starting microcolony sizes, growth rates, and potential effects of cell-cell interactions.

Toxicity measurement with μCC.

To perform a toxicity assay, cells embedded in a μCC are exposed to a toxic agent for a fixed time (treatment period) and allowed to recover in fresh culture for at least three cell divisions following treatment (recovery period). As shown in Fig. 3-2D, microcolony growth leads to a shift of the microcolony size distribution toward higher frequencies of larger microcolonies compared to the initial microcolony

population. We define Excess Microcolonies to be the microcolonies that have grown beyond the starting population in size, and Excess Growth (EG) to be the total number of cells in Excess Microcolonies (Fig. 3-3A, *Supplementary Procedures*).

To explore the sensitivity of EG as a metric for toxicity, we treated micropatterned TK6 cells with γ-radiation. Exposure to γ-rays directly causes DNA single strand breaks and double strand breaks, which can be highly cytotoxic. Previous studies using the colony formation assay have shown that TK6 cells are highly sensitive to γ-radiation (36-39). We examined the microcolony size distributions for TK6 microcolonies three or four days after γ-radiation. Fig. 3-3B shows examples of TK6 microcolony size distributions in untreated condition (left) and after 3 Gy of γIR (right). As expected, non-irradiated cells (Fig. 3-3B, left) from small microcolonies (starting population – light green) readily grew into larger microcolonies after three days (dark green). They gave rise to a broad distribution of microcolony sizes with approximately a nine-fold increase in median colony size. In contrast, Fig. 3-3B (right) shows an example of microcolonies that were exposed to 3 Gy of γIR. Many of the irradiated cells were growth inhibited, due to either cell death or inability to divide, leading to overall smaller microcolonies after 3 days (dark green).

Having established EG as a new parameter for toxicity, we compared it to a more established metric of toxicity, the median microcolony size. In Fig. 3-3C, we detected more than two-log of killing using EG but only one-log using median size, establishing that EG is the more sensitive metric. For all the subsequent studies, all the microcolony size distributions are analyzed for EG values, and the method will simply be referred to as "μCC".

γIR Survival Curves: Comparison of μCC, XTT, CellTiter-Glo® (CTG®) and Colony Formation Assay

To investigate the sensitivity of μCC in measuring toxicity, we compared μCC and other assays for TK6 cells' sensitivity to γIR. Specifically, we compared μCC with the colony formation assay (28, 29) and two commercially available methods, XTT and CTG®. γ-irradiated TK6 microcolonies on μCC were

analyzed 3-4 days after exposure. The recovery periods for the other methods were varied to maximize their sensitivity.

We performed a direct comparison between the μCC approach to the gold standard colony formation assay (28, 29) (see *Methods*). γ-irradiated TK6 cells were analyzed for colony formation in microtiter plates three weeks after exposure. We tracked the appearance of colonies in 96-well plates over 18 days and observed that some colonies were not obvious until the last day (Fig. 3-S3). Therefore, we decided on a timescale of three weeks before counting the colonies in order to maximize the assay's sensitivity. In contrast, μCC data were obtained three days after γIR. μCC yields an exponential toxicity curve undistinguishable from the survival curve obtained from the colony formation assay (Fig. 3-4A). The result from μCC is also remarkably consistent with previously published studies using the colony formation assay (36-39). Specifically in 1998 study (36), the same cell type was analyzed using the traditional colony formation approach. Importantly, the μCC assay yielded nearly identical data (Fig. 3-4B). We conclude that the μCC assay is as sensitive as the colony formation assay while being ~80% faster.

Many microtiter-plate methods for measuring cell survival have been developed as faster and more convenient alternatives to the colony formation assay. We sought to compare μCC with two of the most popular assays, XTT and CTG®. The XTT method is a widely used colorimetric assay that estimates the number of viable cells by measuring the ability of cells to reduce the faint yellow salt (2,3-bis-(2-methoxy-4-nitro-5-sulfophenyl)-2H-tetrazolium-5-carboxanilide) (XTT) to a bright orange water-soluble formazan dye (40). γ-irradiated TK6 cells on microtiter plates were analyzed with XTT or μCC three days after exposure. Remarkably, the μCC assay is orders of magnitude more sensitive than the popular XTT assay (Fig. 3-4C).

The CTG® assay (from Promega) is based on luminescent quantification of cellular ATP as a measure of metabolically active cells (14). Specifically, beetle luciferin is added to lysed cells. ATP is rate limiting for beetle luciferin to be enzymatically converted to oxyluciferin by firefly luciferase, with the output of light. Thus, the amount of ATP in a sample (proportional to number of metabolically active cells) can be estimated by the extent to which light is emitted. We performed the CTG® assay with different

starting cell densities. Unexpectedly, the results are highly dependent on the initial cell number, which implies that there can be considerable variation in the results from one laboratory to another Fig. 3-S4A, Fig. 3-4D). Unlike CTG®, the μCC is highly consistent across cell loading densities ranging over two orders of magnitude (Fig. 3-S4B, Fig. 3-4E). The number of days in culture also changes the results of CTG® while having minimal effects on μCC (Fig. 3-S4).

Use of μCC to study the effects of a DNA repair gene on chemotherapeutic sensitivity

There is a great interest in DNA damaging agents because they can both cause cancer and be used to treat cancer. To combat problems posed by DNA damage, cells have evolved a network of DNA repair responses. Here, we explored the utility of μCC for studies of the role of DNA repair in preventing cytotoxicity caused by an important DNA damaging agent used for chemotherapy.

In this study, we used μCC to measure toxicity induced by N,N'-bis (2-chloroethyl)-N-nitrosourea (BCNU) and γIR using cells with different DNA repair capacity. BCNU is an chemotherapeutic alkylating agent used to treat brain cancers (31, 41, 42). BCNU induces highly cytotoxic DNA interstrand crosslinks (43). The DNA crosslinks are formed via a series of chemical reaction steps that start with the generation of O^6-chloroethylguanine lesions, which then react a second time with bases on the opposite strand (44). It is known that the O^6-methylguanine methyl transferase (MGMT) protein prevents the formation of the highly toxic interstrand crosslinks (45, 46).

The lymphoblastoid TK6 cells are deficient in MGMT and have been shown to be very sensitive to BCNU toxicity (31). The TK6+MGMT cells are TK6 cells stably transfected with cDNA expressing the MGMT protein and have been reported to be significantly more resistant to BCNU than the TK6 cells (31, 45, 46). As a control, we studied the effects of γ-radiation, for which MGMT is not expected to play a role. Results show that TK6 and TK6+MGMT are similarly sensitive to γIR-induced toxicity (Fig. 3-5A), consistent with the fact that MGMT is not involved in strand break repair induced by γ-radiation. In contrast, there is a significant difference in sensitivity to BCNU between TK6 and TK6+MGMT (Fig. 3-5B) (22, 31). This results shows that μCC can be used to reveal the role of DNA repair genes in modulating the sensitivity to chemotherapeutic agents.

Use of μCC to study toxicity of a metabolically activated carcinogen

In the human body, xenobiotics are extensively metabolized, mainly by hepatocytes in the liver (47). This process can result in reactive intermediates that can form adducts with DNA that may lead to mutations, tumorigenesis, and cell death (48). While viability assays are widely used to monitor potential health impact of industrial and pharmaceutical chemicals, a major drawback of current *in vitro* viability assays is the lack of an appropriate cell model that can provide capacity for metabolisms of foreign substances (xenobiotics). It is, therefore, essential to assess the toxicity of chemicals in metabolically relevant conditions. The cytochromes P450 (CYP450s) are a superfamily of metabolizing enzymes, responsible for ~70-80% of phase I metabolism in the liver (49). To provide μCC with the ability to measure toxicity of both parent chemicals and their metabolites, we incorporated a metabolically competent cell line, MCL-5. MCL-5 is an engineered human B-lymphoblastoid cell line that can stably express human cytochrome P450 CYP1A1, CYP1A2, CYP2A6, CYP2E1, CYP3A4, and microsomal epoxide hydrolase (mEH) (23). Together, these metabolic enzymes are responsible for approximately 50% of P450 activity in phase I metabolism (49).

In this study, we focus on aflatoxin B_1 (AFB_1). Millions of people worldwide are exposed to AFB_1, a procarcinogen present in the molds *Aspergillus flavus* and *A. parasiticus* usually found in grains. In combination with hepatitis B infection, AFB_1 has been reported to increase the risk of liver cancer approximately 60-fold and is thus the major cause of cancer in many regions of the world (50). Studies have shown AFB_1 is metabolized by a number of P450 enzymes (51). The most genotoxic metabolite, AFB_1 exo-8,9-epoxide, is generated via oxidation of AFB_1 mainly by CYP3A4 and CYP1A2 (52-55). AFB_1 exo-8,9-epoxide is highly unstable and readily reacts with guanine to form a number of bulky DNA adducts that can lead to mutations and carcinogenesis (56-58).

We applied μCC to measure the toxicity level of AFB_1 in MCL-5 cells three days following exposure. To control for the effects of metabolism, we included TK6 as a negative control cell line. As expected, TK6 cells are insensitive to AFB_1 due to their low metabolic capacity. In contrast, MCL-5 cells

are significantly more sensitive than TK6 to AFB_1 (more than two-log difference at the highest dose) (Fig. 3-5C). We were able to further test the hypothesis that MCL-5 sensitivity is due to metabolic activation of AFB_1 by using ketoconazole (KET). KET is a well-known potent inhibitor of CYP3A4 activity (59-61). Whereas MCL-5 cells are extremely sensitive to AFB_1, inhibition of metabolism by KET leads to significant rescue of MCL-5 cells (Fig. 3-5D). Taken together, the incorporation of MCL-5 cells into the μCC platform yields a rapid and sensitive method to test for toxicity of xenobiotics in a metabolically relevant context.

3.5. DISCUSSION

Despite the fact that millions of cytotoxicity tests are performed every year, there have been relatively few fundamental advances in cytotoxicity testing. The gold standard is the colony formation assay, which is slow, laborious, and not compatible with high-throughput screening. Alternative faster approaches have been developed, but they rely on indirect measures of cell viability. With nearly identical sensitivity and higher throughput, we show here that μCC rivals the colony formation assay, with the potential to become the new gold standard. The results presented in this work highlight a few important advantages of the μCC assay: (i) analysis of microcolony size distribution is a direct measure of cells' ability to divide, enabling quantification of toxicity using the same testing parameter as the colony formation assay in ~3-4 days instead of ~2-3 weeks; (ii) by arraying cells in microwells, μCC shrinks the colony formation assay to ~1/250 its area, enabling compatibility with the microtiter plate format; (iii) μCC is capable of measuring cell survival on a multi-log scale, enabling sensitive quantification of toxicity; (iv) μCC is robust against experimental noise introduced by differences in initial cell numbers. Perhaps the most important observation is that results from μCC are nearly identical to data from the traditional colony formation assay performed in our laboratory. Furthermore, the same experiment performed 20 years ago by a different laboratory yielded essentially the same results (36).

Today, commonly used assays are the tetrazolium assays and ATP assays. The underlying principle for these assays is that the number of viable cells is estimated by the cells' mitochondrial functions, either

to reduce a tetrazolium salt or to maintain intracellular ATP level. Developed in 1980s, tetrazolium assays have enjoyed popularity in academic labs as well as industry due to the convenient microtiter plate format and the wide availability of colorimetric plate readers. Tetrazolium assays, however, are known to be limited in sensitivity (4, 9, 10). On the other hand, μCC is capable of measuring multi-log survival levels. As demonstrated in this work, μCC is far more sensitive than the XTT assay, one of the most common tetrazolium assays, with more than 10-fold difference in dynamic range. Importantly, μCC relies solely on DNA content, which is a reliable and robust measure of cell number (32-35). In contrast, tetrazolium assays depend on mitochondrial activity, which can vary due to factors unrelated to cell division (4, 12, 13).

Similar to tetrazolium assays, ATP assays are also a staple in cell viability testing. The CTG® assay is amendable to microtiter plate format, highly sensitive, and the luminescence output is very convenient to measure. In this work, we observe that μCC yields consistent results across a 100-fold range of initial cell densities while CTG® results are highly susceptible to changes in both initial cell number and the number of days in culture. This observation is consistent with the fact that metabolic functions are highly influenced by non-lethal changes in culture conditions (3, 6, 13, 19, 62). In addition, the relationship between intracellular ATP level and cell viability is not always linear (63). Finally, ATP-based assays are not appropriate to assess toxicity of chemicals that interfere with ATP biosynthesis [e.g., atractyloside inhibits ADP/ATP translocases, inhibiting ATP biosynthesis (64)].

The advantages of μCC over commonly used cell viability assays can be leveraged to provide an efficient and sensitive screening platform in drug discovery. Quantification of cell survival provides a critical endpoint because the ability to modulate cell death is an effective therapeutic strategy. For example, in cancer therapy large chemical libraries are screened for their ability to induce cancer cell death or inhibit cell growth (65). On the other hand, cytoprotective compounds are selected for their ability to attenuate cell death in the context of ischemia and neurodegeneration (66). In these cases, μCC can provide highly sensitive and robust quantification of cell survival, which is critical in assessing the efficacy of a potential candidate drug. The short assay time and the compatibility with the microtiter-plate format also make μCC adaptable for high-throughput drug discovery screens.

In drug development, it is also important to understand the underlying cell death mechanism induced by a potential candidate (3). With their critical roles in human diseases, cell death modalities, such as apoptosis and necroptosis, and can be exploited as therapeutic targets. For example, necrosis inducers can be used to target apoptosis-resistant tumors (19, 67). In the context of drug discovery, μCC can be used in a multiplex fashion to both assess cell survival and study cell death mechanism. Besides excess growth, established viability biomarkers, such as membrane integrity (e.g., propidium idodide staining) and apoptosis (e.g., Annexin V staining), can also be probed simultaneously to provide information about cytotoxic levels as well as cell death modalities (data not shown).

In the broad context of chemical toxicity testing, the bottleneck of *in vitro* cell-based assays is biotransformation (68). Biotransformation is the process whereby a foreign substance (xenobiotic) is modified in the body to form metabolites, which can be transported to systemic circulation (47). Therefore, *in vitro* assays need to account for the toxic effects of both the parent chemicals and their metabolites (68). By incorporating MCL-5 cells, which have stable expressions of critical metabolic enzymes (23), μCC can provide a rapid and sensitive platform for primary toxicity screens that overcomes the bottleneck of *in vitro* assays.

μCC's compatibility with the microtiter plate format is potentially adaptable for high-throughput screening (HTS) for chemical safety testing in the context of environmental health. Due to the large number of chemicals that come in contact with humans and the environment, governmental agencies, such as the U.S. National Toxicology Program (NTP) and the EU's Registration, Evaluation, Authorisation, and Restriction of Chemicals (REACH), have heavily invested in large-scale chemical safety studies. Cell sensitivity is a critical endpoint in these studies, and microtiter plate viability assays are often the top choice due to their compatibility with HTS.

Because of its high-throughput capacity and its multi-log sensitivity, we anticipate that the μCC platform can be applied to detect subtle differences between people in population studies. Information about inter-individual variability in sensitivity to toxic exposures is useful in developing personalized disease

treatment as well as in understanding risk factors for environmentally-induced diseases. For example, studies have shown a wide range of variation in sensitivity toward different DNA damaging agents in lymphoblastoid cell lines derived from genetically diverse healthy individuals (31, 69). Many studies have also observed differences in radiosensitivity among mitogen-stimulated T lymphocytes obtained from different individuals (70). We anticipate that μCC is well suited to study dividing cells, such as mitogen-stimulated lymphocytes, because of its ability to yield sensitive measurements after only a few days in culture.

In this work, we focus on lymphoblastoid cells, which can grow in suspension. Further work is needed to demonstrate μCC's utility for other cell types. Although many cells can be grown in a non-adherent fashion (making it possible to grow them in the μCC agarose microwells), many other cell types are anchorage dependent and require a charged surface or a biological ligand for binding (71, 72). We have begun to explore several approaches for growing adherent cells on the μCC. For example, cells loaded into the agarose microwells can be overlaid with low melting point agarose mixed with collagen type 1. We found that HeLa cells and HepG2 cells appear to attach to the collagen ligands and form adherent microcolonies (Fig. 3-S5, top and middle). A limitation of this approach is that not all cells stay confined to the microwells, as they appear to elongate and spread during microcolony formation (Fig. 3-S5, bottom). To optimize the assay, it is ideal for the microcolonies to be compact so that there is not significant microcolony overlap. To overcome this limitation, further development to modify the growth conditions to foster growth within the microwell, rather than growth by attachment to the ligands in the upper layer, is necessary. Other ECM component proteins including laminin 1, fibronectin, vitronectin and various collagens (73) can also be added to the μCC. Additionally, varying microwell diameters and distances between the microwells can potentially acommodate different cell types. For example, for larger cells, a microwell with a larger diameter may be desireable, and for cells that migrate away from the microcolony, an increase in the inter-microwell distance may be advantageous.

In conclusion, we have described μCC, a rapid and sensitive cell survival assay that combines the

advantages of commonly used viability assays. With the short assay time and large dynamic range, the μCC platform provides an efficient alternative to the colony formation assay, which continues to be the gold standard in cell survival testing. The companion in-house software enables automated image analysis of thousands of microcolonies in a few minutes, making it easy for a new user to learn and use the assay. Finally, the high-throughput and potential multiplexing capacity make μCC a powerful tool for applications including screens for drug development, epidemiological studies, and chemical safety studies.

3.6. SUPPLEMENTARY PROCEDURES

Correlation of F/M values with cell numbers per microwell

We loaded TK6 cells into an array of 40-μm wells and immediately stained the cells with Vybrant® DyeCycle Green (see *Methods*). The microwells provide physical spaces with a defined volume that only allows a maximum number of ~7-8 TK6 cells per well. Fluorescent images of TK6 microcolonies were captured and analyzed using our in-house MATLAB program (see *Methods*). Because the cells had not been given time to grow after loading, the fluorescent nucleus of each cell in a microcolony can be clearly distinguished by eyes in the fluorescent images. The number of distinct nuclei was counted manually and compared to the F/M value of that microwell.

Calculation of Excess Microcolonies and Excess Growth

We can calculate the Excess Growth (EG) value for each treatment condition and compare to a negative control EG (unexposed cells) to obtain a toxicity measurement. To calculate EG, we first estimate Excess Microcolonies (EM), the portion of microcolonies that have grown in excess of the starting population, by subtracting the microcolony size distribution of the final population by that of the starting population. EG is the sum of the number of cells in these EM. To illustrate the calculation process, suppose a starting population has 100 microcolonies with the following distribution: 25 microcolonies have 1 cell each, 50 have 2 cells each, and 25 have 3 cells each (Fig. 3- S1B – light green). After growth, the final population of 100 microcolonies consists of 25 microcolonies with 2 cells each, 50 with 3 cells each, and

25 with 4 cells each (Fig. 3- S1B – dark green). For each microcolony size, we subtract the number of microcolonies in the final population by the starting population:

1-cell microcolonies: 0 - 25 = -25 microcolonies < 0

2-cell microcolonies: 25 - 50 = -25 microcolonies <0

3-cell microcolonies: 50 - 25 = 25 microcolonies **>0**

4-cell microcolonies: 25 - 0 = 25 microcolonies **>0**

We define the positive values of the subtractions to be the EM. In this case, EM consist of 25 of the 3-cell microcolonies and 25 of the 4-cell microcolonies. By our definition, the total number of cells in these microcolonies is EG:

EG = 25 microcolonies x 3 cells + 25 microcolonies x 4 cells = 175 cells.

In practice, the numbers of microcolonies collected for starting and final populations can differ. A normalization by the total number of microcolonies for each population is therefore required, and the subtraction is performed between the relative frequencies of microcolonies and not between the actual numbers of microcolonies.

Excess Growth

To quantify cell survival, we can compare different measures of growth between the treated population and the untreated. The median colony size of the 3-Gy is ~1/9 that of the untreated. In contrast, the 3-Gy's EG is only ~1/50, indicating a higher level of toxicity than revealed by the median colony size comparison. Exposure of TK6 microcolonies to a range of γIR doses reveals that toxicity measured by median colony size comparison plateaus around 10% of untreated. On the other hand, EG displays an exponential killing curve with a superior dynamic range of more than two orders of magnitude (Fig. 3- 3D).

3.7. REFERENCES

1. Hartung T, Rovida C. Chemical regulators have overreached. Nature. 2009;460(7259):1080-1. doi: 10.1038/4601080a. PubMed PMID: 19713914.
2. National Toxicology Program. About NTP [cited 2017 November 3rd]. Available from: https://ntp.niehs.nih.gov/about/.
3. Kepp O, Galluzzi L, Lipinski M, Yuan J, Kroemer G. Cell death assays for drug discovery. Nat Rev Drug Discov. 2011;10(3):221-37. doi: 10.1038/nrd3373. PubMed PMID: 21358741.
4. Cook JA, Mitchell JB. Viability measurements in mammalian cell systems. Anal Biochem. 1989;179(1):1-7. PubMed PMID: 2667390.
5. Franken NAP, Rodermond HM, Stap J, Haveman J, van Bree C. Clonogenic assay of cells in vitro. Nature Protocols. 2006;1(5):2315-9. doi: 10.1038/nprot.2006.339. PubMed PMID: WOS:000251155600018.
6. Sumantran VN. Cellular chemosensitivity assays: an overview. Methods Mol Biol. 2011;731:219-36. doi: 10.1007/978-1-61779-080-5_19. PubMed PMID: 21516411.
7. Weisenthal LM, Dill PL, Kurnick NB, Lippman ME. Comparison of dye exclusion assays with a clonogenic assay in the determination of drug-induced cytotoxicity. Cancer Res. 1983;43(1):258-64. PubMed PMID: 6571706.
8. Mosmann T. Rapid colorimetric assay for cellular growth and survival: application to proliferation and cytotoxicity assays. J Immunol Methods. 1983;65(1-2):55-63. PubMed PMID: 6606682.
9. Carmichael J, DeGraff WG, Gazdar AF, Minna JD, Mitchell JB. Evaluation of a tetrazolium-based semiautomated colorimetric assay: assessment of radiosensitivity. Cancer Res. 1987;47(4):943-6. PubMed PMID: 3802101.
10. Carmichael J, DeGraff WG, Gazdar AF, Minna JD, Mitchell JB. Evaluation of a tetrazolium-based semiautomated colorimetric assay: assessment of chemosensitivity testing. Cancer Res. 1987;47(4):936-42. PubMed PMID: 3802100.
11. Berridge MV, Herst PM, Tan AS. Tetrazolium dyes as tools in cell biology: new insights into their cellular reduction. Biotechnol Annu Rev. 2005;11:127-52. doi: 10.1016/S1387-2656(05)11004-7. PubMed PMID: 16216776.
12. Plumb JA, Milroy R, Kaye SB. Effects of the pH dependence of 3-(4,5-dimethylthiazol-2-yl)-2,5-diphenyl-tetrazolium bromide-formazan absorption on chemosensitivity determined by a novel tetrazolium-based assay. Cancer Res. 1989;49(16):4435-40. PubMed PMID: 2743332.
13. Petty RD, Sutherland LA, Hunter EM, Cree IA. Comparison of MTT and ATP-based assays for the measurement of viable cell number. J Biolumin Chemilumin. 1995;10(1):29-34. doi: 10.1002/bio.1170100105. PubMed PMID: 7762413.

14. Crouch SP, Kozlowski R, Slater KJ, Fletcher J. The use of ATP bioluminescence as a measure of cell proliferation and cytotoxicity. J Immunol Methods. 1993;160(1):81-8. PubMed PMID: 7680699.
15. Kangas L, Gronroos M, Nieminen AL. Bioluminescence of cellular ATP: a new method for evaluating cytotoxic agents in vitro. Med Biol. 1984;62(6):338-43. PubMed PMID: 6543460.
16. Lundin A, Hasenson M, Persson J, Pousette A. Estimation of biomass in growing cell lines by adenosine triphosphate assay. Methods Enzymol. 1986;133:27-42. PubMed PMID: 3821540.
17. Sevin BU, Peng ZL, Perras JP, Ganjei P, Penalver M, Averette HE. Application of an ATP-bioluminescence assay in human tumor chemosensitivity testing. Gynecol Oncol. 1988;31(1):191-204. PubMed PMID: 3410347.
18. Gerhardt RT, Perras JP, Sevin BU, Petru E, Ramos R, Guerra L, Averette HE. Characterization of in vitro chemosensitivity of perioperative human ovarian malignancies by adenosine triphosphate chemosensitivity assay. Am J Obstet Gynecol. 1991;165(2):245-55. PubMed PMID: 1872324.
19. Galluzzi L, Aaronson SA, Abrams J, Alnemri ES, Andrews DW, Baehrecke EH, Bazan NG, Blagosklonny MV, Blomgren K, Borner C, Bredesen DE, Brenner C, Castedo M, Cidlowski JA, Ciechanover A, Cohen GM, De Laurenzi V, De Maria R, Deshmukh M, Dynlacht BD, El-Deiry WS, Flavell RA, Fulda S, Garrido C, Golstein P, Gougeon ML, Green DR, Gronemeyer H, Hajnoczky G, Hardwick JM, Hengartner MO, Ichijo H, Jaattela M, Kepp O, Kimchi A, Klionsky DJ, Knight RA, Kornbluth S, Kumar S, Levine B, Lipton SA, Lugli E, Madeo F, Malomi W, Marine JC, Martin SJ, Medema JP, Mehlen P, Melino G, Moll UM, Morselli E, Nagata S, Nicholson DW, Nicotera P, Nunez G, Oren M, Penninger J, Pervaiz S, Peter ME, Piacentini M, Prehn JH, Puthalakath H, Rabinovich GA, Rizzuto R, Rodrigues CM, Rubinsztein DC, Rudel T, Scorrano L, Simon HU, Steller H, Tschopp J, Tsujimoto Y, Vandenabeele P, Vitale I, Vousden KH, Youle RJ, Yuan J, Zhivotovsky B, Kroemer G. Guidelines for the use and interpretation of assays for monitoring cell death in higher eukaryotes. Cell Death Differ. 2009;16(8):1093-107. doi: 10.1038/cdd.2009.44. PubMed PMID: 19373242; PMCID: PMC2757140.
20. Skopek TR, Liber HL, Penman BW, Thilly WG. Isolation of a human lymphoblastoid line heterozygous at the thymidine kinase locus: possibility for a rapid human cell mutation assay. Biochem Biophys Res Commun. 1978;84(2):411-6.
21. Liber HL, Thilly WG. Mutation assay at the thymidine kinase locus in diploid human lymphoblasts. Mutat Res. 1982;94(2):467-85.
22. Hickman MJ, Samson LD. Role of DNA mismatch repair and p53 in signaling induction of apoptosis by alkylating agents. Proc Natl Acad Sci U S A. 1999;96(19):10764-9. PubMed PMID: 10485900; PMCID: PMC17957.

23. Crespi CL, Gonzalez FJ, Steimel DT, Turner TR, Gelboin HV, Penman BW, Langenbach R. A metabolically competent human cell line expressing five cDNAs encoding procarcinogen-activating enzymes: application to mutagenicity testing. Chem Res Toxicol. 1991;4(5):566-72. PubMed PMID: 1793807.

24. Wood DK, Weingeist DM, Bhatia SN, Engelward BP. Single cell trapping and DNA damage analysis using microwell arrays. Proc Natl Acad Sci U S A. 2010;107(22):10008-13. Epub 2010/06/11. doi: 10.1073/pnas.1004056107. PubMed PMID: 20534572; PMCID: 2890454.

25. Weingeist DM, Ge J, Wood DK, Mutamba JT, Huang Q, Rowland EA, Yaffe MB, Floyd S, Engelward BP. Single-cell microarray enables high-throughput evaluation of DNA double-strand breaks and DNA repair inhibitors. Cell Cycle. 2013;12(6):907-15. Epub 2013/02/21. doi: 10.4161/cc.23880. PubMed PMID: 23422001.

26. Ge J, Wood DK, Weingeist DM, Prasongtanakij S, Navasumrit P, Ruchirawat M, Engelward BP. Standard fluorescent imaging of live cells is highly genotoxic. Cytometry A. 2013;83(6):552-60. Epub 2013/05/08. doi: 10.1002/cyto.a.22291. PubMed PMID: 23650257; PMCID: 3677558.

27. Ge J, Chow DN, Fessler JL, Weingeist DM, Wood DK, Engelward BP. Micropatterned comet assay enables high throughput and sensitive DNA damage quantification. Mutagenesis. 2015;30(1):11-9. doi: 10.1093/mutage/geu063. PubMed PMID: 25527723; PMCID: 4272061.

28. Furth EE, Thilly WG, Penman BW, Liber HL, Rand WM. Quantitative assay for mutation in diploid human lymphoblasts using microtiter plates. Anal Biochem. 1981;110(1):1-8. PubMed PMID: 7011090.

29. Kraemer KH, Waters HL, Buchanan JK. Survival of human lymphoblastoid cells after DNA damage measured by growth in microtiter wells. Mutat Res. 1980;72(2):285-94. PubMed PMID: 6160397.

30. Imamura T, Moore GE. Ability of Human Hematopoietic Cell Lines to Form Colonies in Soft Agar. P Soc Exp Biol Med. 1968;128(4):1179-&. PubMed PMID: WOS:A1968B870900065.

31. Valiathan C, McFaline JL, Samson LD. A rapid survival assay to measure drug-induced cytotoxicity and cell cycle effects. DNA Repair (Amst). 2012;11(1):92-8. Epub 2011/12/03. doi: 10.1016/j.dnarep.2011.11.002. PubMed PMID: 22133811; PMCID: 3408220.

32. Rago R, Mitchen J, Wilding G. DNA fluorometric assay in 96-well tissue culture plates using Hoechst 33258 after cell lysis by freezing in distilled water. Anal Biochem. 1990;191(1):31-4. PubMed PMID: 1706565.

33. Blaheta RA, Franz M, Auth MK, Wenisch HJ, Markus BH. A rapid non-radioactive fluorescence assay for the measurement of both cell number and proliferation. J Immunol Methods. 1991;142(2):199-206. PubMed PMID: 1717599.

34. Jones LJ, Gray M, Yue ST, Haugland RP, Singer VL. Sensitive determination of cell number using the CyQUANT cell proliferation assay. J Immunol Methods. 2001;254(1-2):85-98. PubMed PMID: 11406155.

35. Quent VM, Loessner D, Friis T, Reichert JC, Hutmacher DW. Discrepancies between metabolic activity and DNA content as tool to assess cell proliferation in cancer research. J Cell Mol Med. 2010;14(4):1003-13. doi: 10.1111/j.1582-4934.2010.01013.x. PubMed PMID: 20082656; PMCID: PMC3823131.

36. Wenz F, Azzam EI, Little JB. The response of proliferating cell nuclear antigen to ionizing radiation in human lymphoblastoid cell lines is dependent on p53. Radiat Res. 1998;149(1):32-40. PubMed PMID: 9421152.

37. Schwartz JL, Jordan R, Sedita BA, Swenningson MJ, Banath JP, Olive PL. Different sensitivity to cell killing and chromosome mutation induction by gamma rays in two human lymphoblastoid cell lines derived from a single donor: possible role of apoptosis. Mutagenesis. 1995;10(3):227-33. PubMed PMID: 7666775.

38. Amundson SA, Xia F, Wolfson K, Liber HL. Different cytotoxic and mutagenic responses induced by X-rays in two human lymphoblastoid cell lines derived from a single donor. Mutat Res. 1993;286(2):233-41. PubMed PMID: 7681535.

39. Schafer J, Bachtler J, Engling A, Little JB, Weber KJ, Wenz F. Suppression of apoptosis and clonogenic survival in irradiated human lymphoblasts with different TP53 status. Radiat Res. 2002;158(6):699-706. PubMed PMID: 12452772.

40. Scudiero DA, Shoemaker RH, Paull KD, Monks A, Tierney S, Nofziger TH, Currens MJ, Seniff D, Boyd MR. Evaluation of a soluble tetrazolium/formazan assay for cell growth and drug sensitivity in culture using human and other tumor cell lines. Cancer Res. 1988;48(17):4827-33. PubMed PMID: 3409223.

41. Hochberg FH, Parker LM, Takvorian T, Canellos GP, Zervas NT. High-dose BCNU with autologous bone marrow rescue for recurrent glioblastoma multiforme. J Neurosurg. 1981;54(4):455-60. doi: 10.3171/jns.1981.54.4.0455. PubMed PMID: 6259300.

42. Durando X, Lemaire JJ, Tortochaux J, Van-Praagh I, Kwiatkowski F, Vincent C, Bailly C, Verrelle P, Irthum B, Chazal J, Bay JO. High-dose BCNU followed by autologous hematopoietic stem cell transplantation in supratentorial high-grade malignant gliomas: a retrospective analysis of 114 patients. Bone Marrow Transplant. 2003;31(7):559-64. doi: 10.1038/sj.bmt.1703889. PubMed PMID: 12692621.

43. Gonzaga PE, Potter PM, Niu TQ, Yu D, Ludlum DB, Rafferty JA, Margison GP, Brent TP. Identification of the cross-link between human O6-methylguanine-DNA methyltransferase and chloroethylnitrosourea-treated DNA. Cancer Research. 1992;52(21):6052-8.

44. Tong WP, Kirk MC, Ludlum DB. Formation of the cross-link 1-[N3-deoxycytidyl),2-[N1-deoxyguanosinyl]ethane in DNA treated with N,N'-bis(2-chloroethyl)-N-nitrosourea. Cancer Research. 1982;42(8):3102-5.

45. Kaina B, Fritz G, Mitra S, Coquerelle T. Transfection and expression of human O^6-methylguanine-DNA methyltransferase (*MGMT*) cDNA in Chinese hamster cells: the role of *MGMT* in protection against the genotoxic effects of alkylating agents. Carcinogenesis. 1991;12(10):1857-67.

46. Gerson SL. MGMT: its role in cancer aetiology and cancer therapeutics. Nat Rev Cancer. 2004;4(4):296-307. doi: 10.1038/nrc1319. PubMed PMID: 15057289.

47. Golan DE, Tashjian AH. Principles of pharmacology : the pathophysiologic basis of drug therapy. 3rd ed. Philadelphia: Wolters Kluwer Health/Lippincott Williams & Wilkins; 2012. xxi, 954 p. p.

48. Nebert DW, Dalton TP. The role of cytochrome P450 enzymes in endogenous signalling pathways and environmental carcinogenesis. Nat Rev Cancer. 2006;6(12):947-60. doi: 10.1038/nrc2015. PubMed PMID: 17128211.

49. Evans WE, Relling MV. Pharmacogenomics: translating functional genomics into rational therapeutics. Science. 1999;286(5439):487-91. PubMed PMID: 10521338.

50. Henry SH, Bosch FX, Bowers JC. Aflatoxin, hepatitis and worldwide liver cancer risks. Adv Exp Med Biol. 2002;504:229-33. PubMed PMID: 11922091.

51. Aoyama T, Yamano S, Guzelian PS, Gelboin HV, Gonzalez FJ. Five of 12 forms of vaccinia virus-expressed human hepatic cytochrome P450 metabolically activate aflatoxin B1. Proc Natl Acad Sci U S A. 1990;87(12):4790-3. PubMed PMID: 2162057; PMCID: PMC54203.

52. Gallagher EP, Kunze KL, Stapleton PL, Eaton DL. The kinetics of aflatoxin B1 oxidation by human cDNA-expressed and human liver microsomal cytochromes P450 1A2 and 3A4. Toxicology and applied pharmacology. 1996;141(2):595-606. doi: 10.1006/taap.1996.0326. PubMed PMID: 8975785.

53. Gallagher EP, Wienkers LC, Stapleton PL, Kunze KL, Eaton DL. Role of human microsomal and human complementary DNA-expressed cytochromes P4501A2 and P4503A4 in the bioactivation of aflatoxin B1. Cancer Res. 1994;54(1):101-8. PubMed PMID: 8261428.

54. Langouet S, Coles B, Morel F, Becquemont L, Beaune P, Guengerich FP, Ketterer B, Guillouzo A. Inhibition of CYP1A2 and CYP3A4 by oltipraz results in reduction of aflatoxin B1 metabolism in human hepatocytes in primary culture. Cancer Res. 1995;55(23):5574-9. PubMed PMID: 7585637.

55. Raney KD, Shimada T, Kim DH, Groopman JD, Harris TM, Guengerich FP. Oxidation of aflatoxins and sterigmatocystin by human liver microsomes: significance of aflatoxin Q1 as a detoxication product of aflatoxin B1. Chem Res Toxicol. 1992;5(2):202-10. PubMed PMID: 1643250.

56. Johnson WW, Guengerich FP. Reaction of aflatoxin B1 exo-8,9-epoxide with DNA: kinetic analysis of covalent binding and DNA-induced hydrolysis. Proc Natl Acad Sci U S A. 1997;94(12):6121-5. PubMed PMID: 9177180; PMCID: PMC21012.

57. Smela ME, Hamm ML, Henderson PT, Harris CM, Harris TM, Essigmann JM. The aflatoxin B(1) formamidopyrimidine adduct plays a major role in causing the types of mutations observed in human hepatocellular carcinoma. Proc Natl Acad Sci U S A. 2002;99(10):6655-60. doi: 10.1073/pnas.102167699. PubMed PMID: 12011430; PMCID: PMC124458.

58. Kensler TW, Qian GS, Chen JG, Groopman JD. Translational strategies for cancer prevention in liver. Nat Rev Cancer. 2003;3(5):321-9. doi: 10.1038/nrc1076. PubMed PMID: 12724730.

59. Crespi CL, Miller VP, Penman BW. Microtiter plate assays for inhibition of human, drug-metabolizing cytochromes P450. Anal Biochem. 1997;248(1):188-90. doi: 10.1006/abio.1997.2145. PubMed PMID: 9177742.

60. Lorusso P, Heath EI, McGreivy J, Sun YN, Melara R, Yan L, Malburg L, Ingram M, Wiezorek J, Chen L, Pilat MJ. Effect of coadministration of ketoconazole, a strong CYP3A4 inhibitor, on pharmacokinetics and tolerability of motesanib diphosphate (AMG 706) in patients with advanced solid tumors. Invest New Drugs. 2008;26(5):455-62. doi: 10.1007/s10637-008-9144-1. PubMed PMID: 18574557.

61. Greenblatt DJ, Zhao Y, Venkatakrishnan K, Duan SX, Harmatz JS, Parent SJ, Court MH, von Moltke LL. Mechanism of cytochrome P450-3A inhibition by ketoconazole. J Pharm Pharmacol. 2011;63(2):214-21. doi: 10.1111/j.2042-7158.2010.01202.x. PubMed PMID: 21235585.

62. Ng KW, Leong DT, Hutmacher DW. The challenge to measure cell proliferation in two and three dimensions. Tissue Eng. 2005;11(1-2):182-91. doi: 10.1089/ten.2005.11.182. PubMed PMID: 15738673.

63. Huang H, Zhang X, Li S, Liu N, Lian W, McDowell E, Zhou P, Zhao C, Guo H, Zhang C, Yang C, Wen G, Dong X, Lu L, Ma N, Dong W, Dou QP, Wang X, Liu J. Physiological levels of ATP negatively regulate proteasome function. Cell Res. 2010;20(12):1372-85. doi: 10.1038/cr.2010.123. PubMed PMID: 20805844; PMCID: PMC2996470.

64. Schutt F, Aretz S, Auffarth GU, Kopitz J. Moderately reduced ATP levels promote oxidative stress and debilitate autophagic and phagocytic capacities in human RPE cells. Invest Ophthalmol Vis Sci. 2012;53(9):5354-61. doi: 10.1167/iovs.12-9845. PubMed PMID: 22789922.

65. Brown JM, Attardi LD. The role of apoptosis in cancer development and treatment response. Nat Rev Cancer. 2005;5(3):231-7. doi: 10.1038/nrc1560. PubMed PMID: 15738985.

66. Degterev A, Huang Z, Boyce M, Li Y, Jagtap P, Mizushima N, Cuny GD, Mitchison TJ, Moskowitz MA, Yuan J. Chemical inhibitor of nonapoptotic cell death with therapeutic potential for ischemic brain injury. Nat Chem Biol. 2005;1(2):112-9. doi: 10.1038/nchembio711. PubMed PMID: 16408008.

67. Guidicelli G, Chaigne-Delalande B, Dilhuydy MS, Pinson B, Mahfouf W, Pasquet JM, Mahon FX, Pourquier P, Moreau JF, Legembre P. The necrotic signal induced by mycophenolic acid overcomes apoptosis-resistance in tumor cells. PLoS One. 2009;4(5):e5493. doi: 10.1371/journal.pone.0005493. PubMed PMID: 19430526; PMCID: PMC2675064.

68. Coecke S, Ahr H, Blaauboer BJ, Bremer S, Casati S, Castell J, Combes R, Corvi R, Crespi CL, Cunningham ML, Elaut G, Eletti B, Freidig A, Gennari A, Ghersi-Egea JF, Guillouzo A, Hartung T, Hoet P, Ingelman-Sundberg M, Munn S, Janssens W, Ladstetter B, Leahy D, Long A, Meneguz A, Monshouwer M, Morath S, Nagelkerke F, Pelkonen O, Ponti J, Prieto P, Richert L, Sabbioni E, Schaack B, Steiling W, Testai E, Vericat JA, Worth A. Metabolism: a bottleneck in in vitro toxicological test development. The report and recommendations of ECVAM workshop 54. Alternatives to laboratory animals : ATLA. 2006;34(1):49-84. PubMed PMID: 16522150.

69. Fry RC, Svensson JP, Valiathan C, Wang E, Hogan BJ, Bhattacharya S, Bugni JM, Whittaker CA, Samson LD. Genomic predictors of interindividual differences in response to DNA damaging agents. Genes Dev. 2008;22(19):2621-6. PubMed PMID: 18805990.

70. Geara FB, Peters LJ, Ang KK, Wike JL, Sivon SS, Guttenberger R, Callender DL, Malaise EP, Brock WA. Intrinsic radiosensitivity of normal human fibroblasts and lymphocytes after high- and low-dose-rate irradiation. Cancer Res. 1992;52(22):6348-52. PubMed PMID: 1423281.

71. Gumbiner BM. Cell adhesion: the molecular basis of tissue architecture and morphogenesis. Cell. 1996;84(3):345-57. PubMed PMID: 8608588.

72. Giancotti FG, Ruoslahti E. Integrin signaling. Science. 1999;285(5430):1028-32. PubMed PMID: 10446041.

73. Geiger B, Bershadsky A, Pankov R, Yamada KM. Transmembrane crosstalk between the extracellular matrix-cytoskeleton crosstalk. Nat Rev Mol Cell Biol. 2001;2(11):793-805. doi: 10.1038/35099066. PubMed PMID: 11715046.

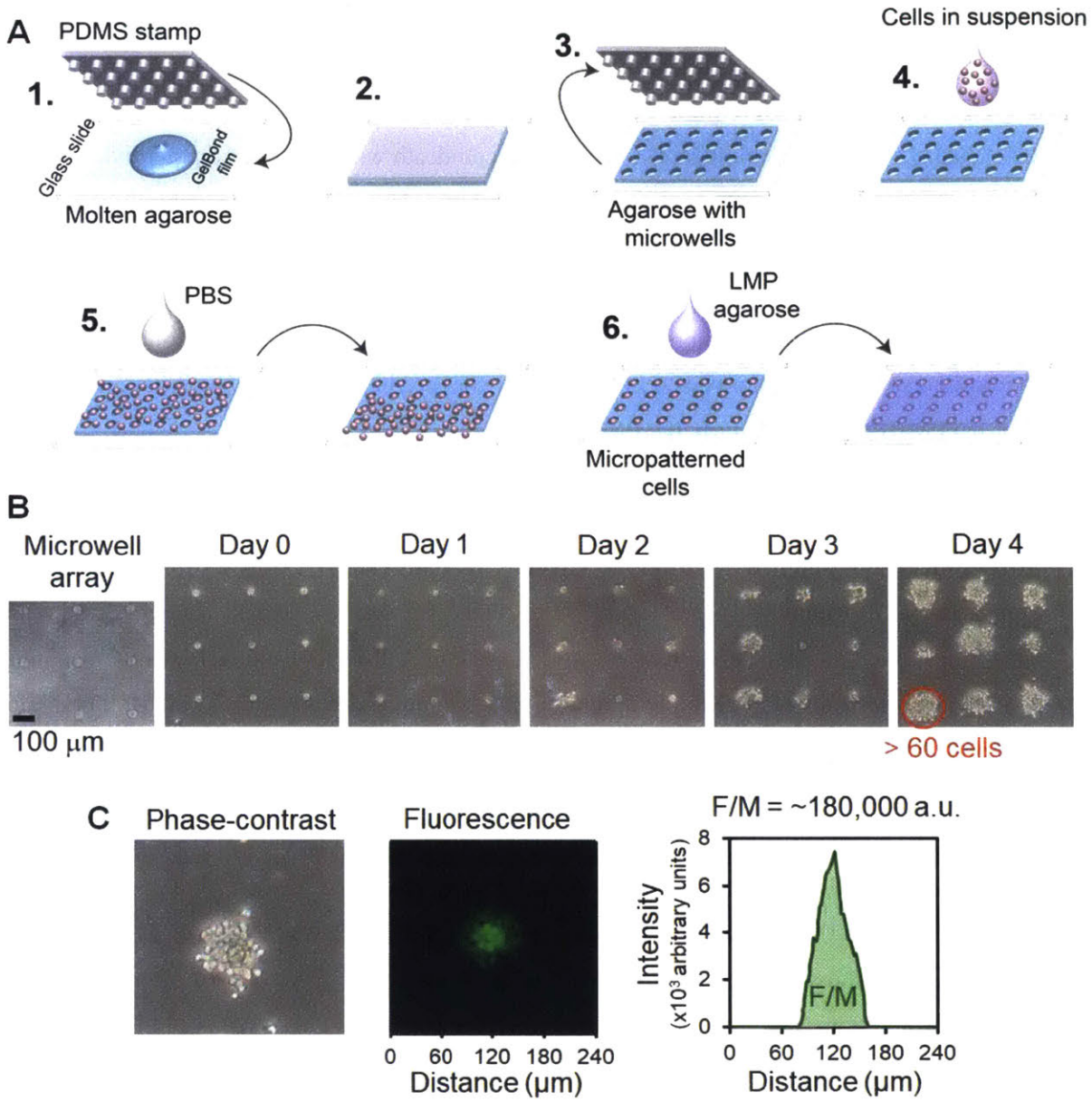

Figure 3-1. Construction of Microcolony Chip (μCC) and quantification of total DNA content. A. Steps in micropatterning cells in μCC. *1*. PDMS stamp with microposts is pressed into molten agarose. *2*. Agarose is allowed to cool and solidify. *3*. Stamp is lifted off to reveal patterned microwells on agarose chip. *4*. Cell suspension is placed directly onto agarose chip. *5*. Cells settle into microwells via gravity. Excess cells are washed off to reveal micropatterned cells. *6*. Cells are kept in microwells by an overlay layer of 0.3% low-melting point agarose. **B.** Phase-contrast pictures of example patterned TK6 microcolonies taken at 40X magnification. *Left*: empty agarose microwell array. *Day 0*: micropatterned cells after loading. *Day 1* - *Day 4*: growth of patterned microcolonies during 4 days in culture. **C.** Example calculation of integrated **f**luorescence intensity per **m**icrocolony (F/M) for one TK6 microcolony. *Left*: phase-contrast image of one TK6 microcolony after 4 days in culture. *Middle*: fluorescent image of a different TK6 microcolony stained with Vybrant® DyeCycle™ Green. *Right*: a plot of the average fluorescence intensity of each pixel column from the left to the right of the *Middle* image after background correction (binary mask using Otsu thresholding method). F/M is the total area under the curve.

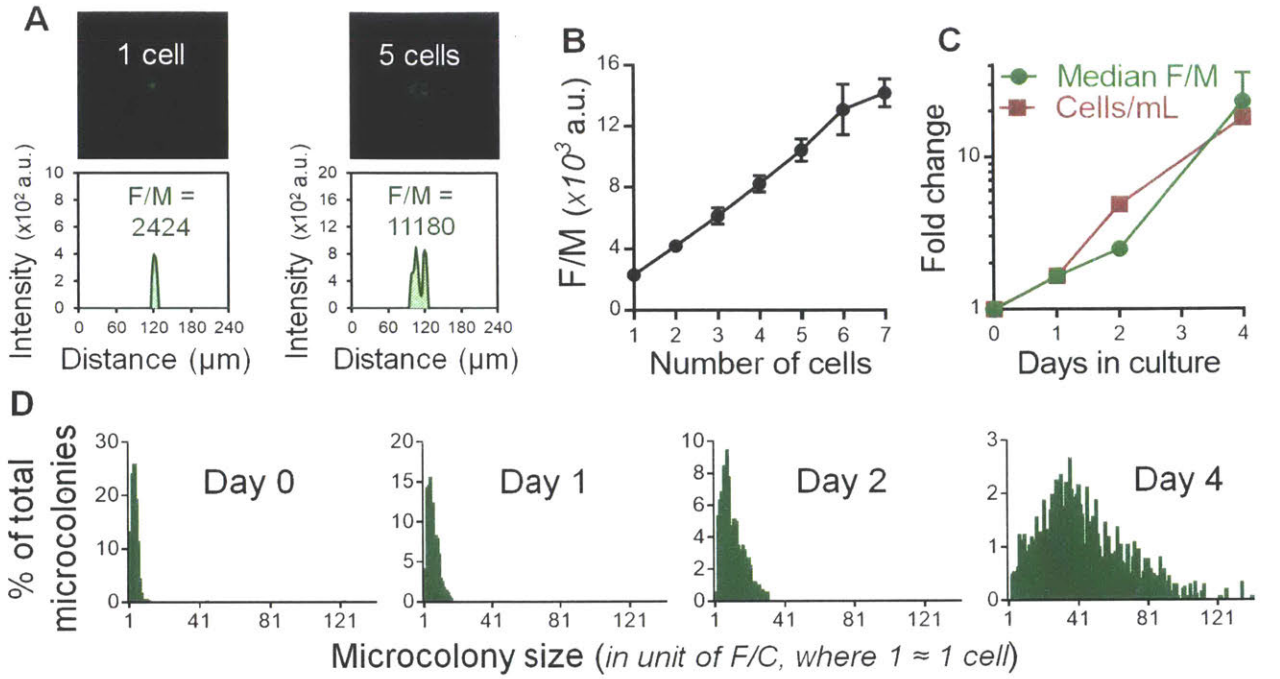

Figure 3-2. Total DNA content as a measure of microcolony size. A. Example calculation of F/M for microwells with one cell *(left)* and five cells *(right)*. *Top*: fluorescent images of TK6 cells in microwells stained with Vybrant® DyeCycle™ Green. *Bottom*: Fluorescence intensity plots of the corresponding fluorescent images after background correction (binary mask using Otsu thresholding method). F/M is the total area under the curve. **B.** Average F/M values for 1 to 7 TK6 cells. F/M for a single cell, or fluorescence intensity per cell (F/C), is calculated to be 2300 ± 500 (arbitrary fluorescence unit). Each data point is an average of 3 independent experiments. Error bars are standard errors of the means. **C.** Fold change of median F/M for TK6 microcolonies in μCC (green line) and TK6 cell density in liquid culture (red line) during 4 days of culture. Each data point is an average of at least 3 independent experiments. Error bars are standard errors of the means. **D.** Example of TK6 microcolony size distributions obtained from μCC during 4 days in culture. F/M values of >700 microcolonies were analyzed for each distribution and converted to cell numbers by dividing by the value of 1 F/C. y-axis for each plot is individually scaled.

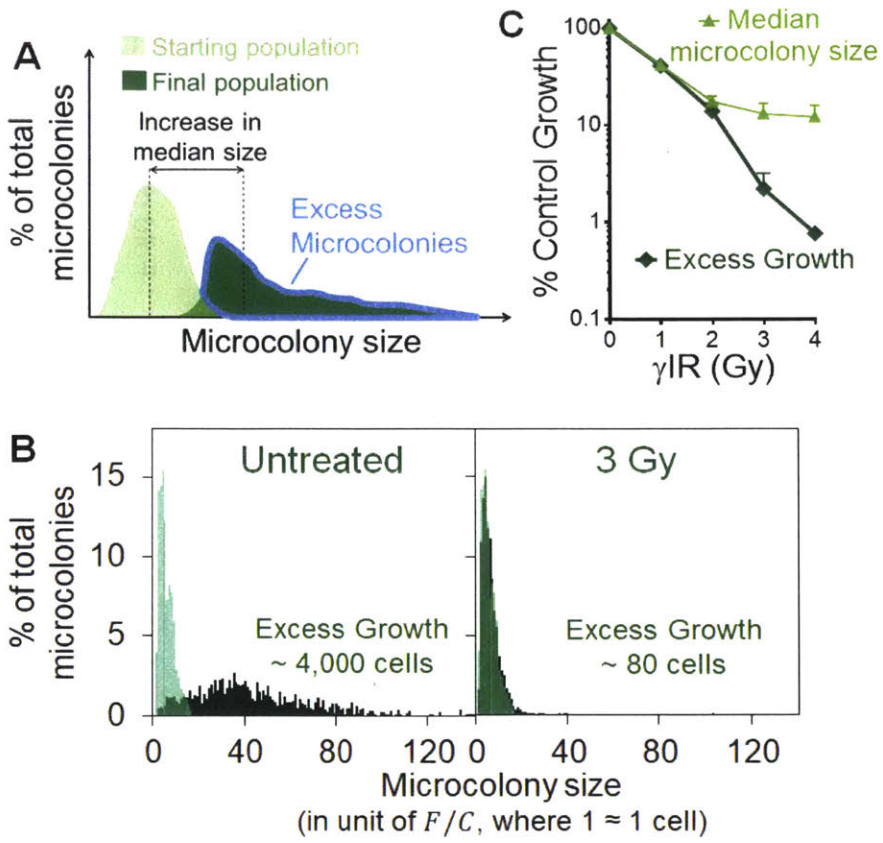

Figure 3-3. A. Illustrative example of microcolony size distributions before (starting population in light green) and after growth (final population in dark green). Excess Microcolonies (blue-outlined) are microcolonies in the final population that have grown beyond the starting population in size. Excess Growth (EG) is defined as the total number of cells in Excess Microcolonies. **B.** Example of microcolony size distributions derived from F/M values of TK6 cells. *Left*: distribution before γIR ("Starting population", light green) overlaying with untreated distribution after 3 days in culture ("Untreated", dark green). *Right*: distribution before γIR ("Starting population", light green) overlaying with γ-irradiated distribution after 3 days in culture ("3 Gy", dark green). **C.** γIR-induced toxicity (% Untreated) derived from normalization of γ-irradiated microcolonies by "Untreated" using median microcolony sizes (light green line) or Excess Growth values (dark green line).

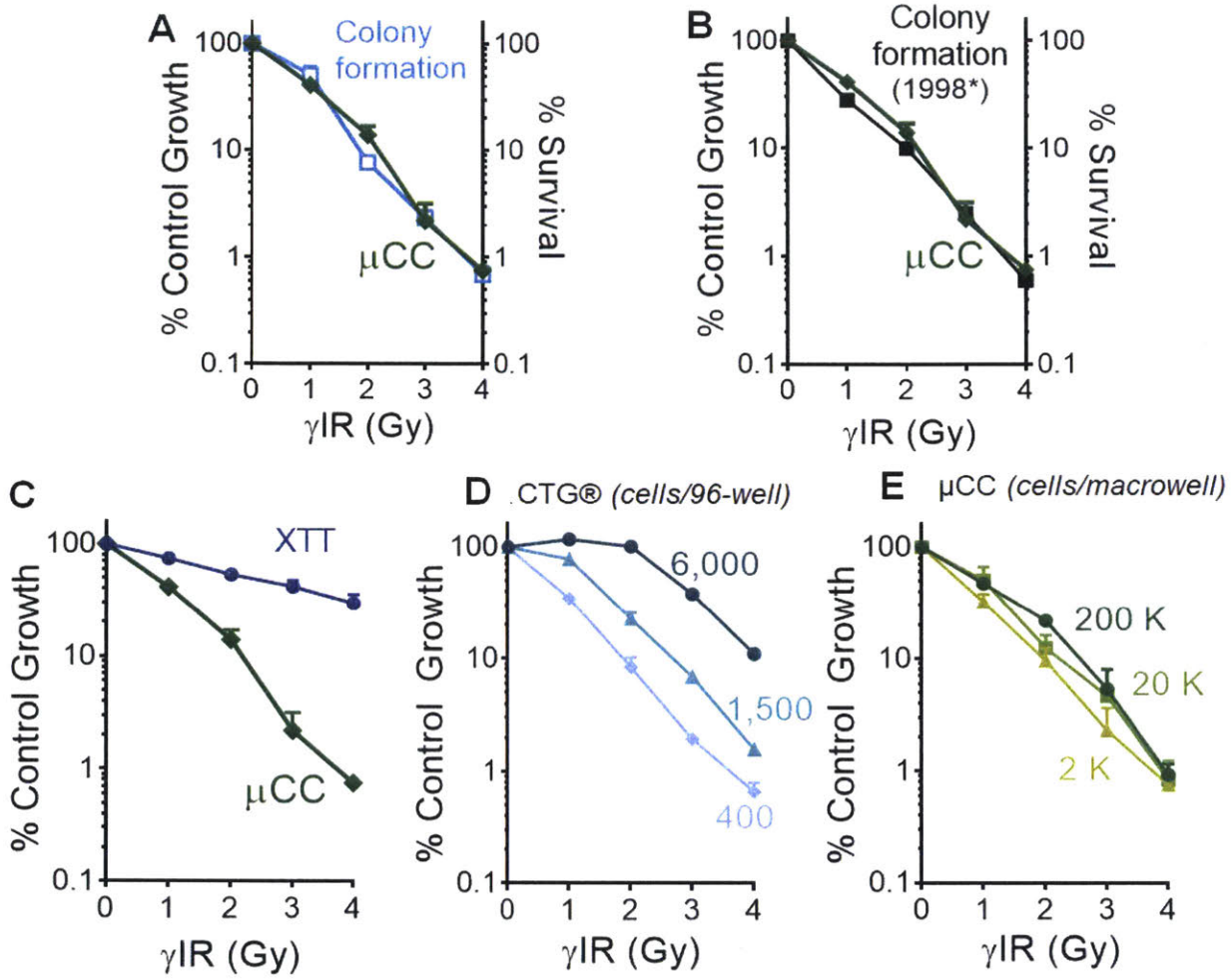

Figure 3-4. Compare μCC with other assays in measuring γIR-induced toxicity in TK6 cells. Toxicity is expressed as percent of γ-irradiated cells relative to untreated control cells. **A.** The colony formation assay data (light blue line, see Methods) were obtained 3 weeks after γ-irradiation. μCC data (dark green) were obtained 3 days post irradiation. **B.** Colony formation data from *Wenz F. et al, 1998 (black line, (36)) were reproduced with permission from *Radiation Research* journal. μCC data (dark green) were obtained 3 days post irradiation. **C.** XTT data (dark blue line) were obtained 3 days after exposure (see Methods). μCC data (dark green) were obtained 3 days post irradiation. **D.** γIR-induced toxicity in TK6 cells measured by CTG® with different cell seeding densities (*legend*: number of cells per 96-well) after a recovery period of 4 days. **E.** γIR-induced toxicity in TK6 cells measured by μCC with different cell loading densities (*legend*: number of cells per macrowell) after a recovery period of 4 days. $n \geq 3$, error bars are standard errors of the means.

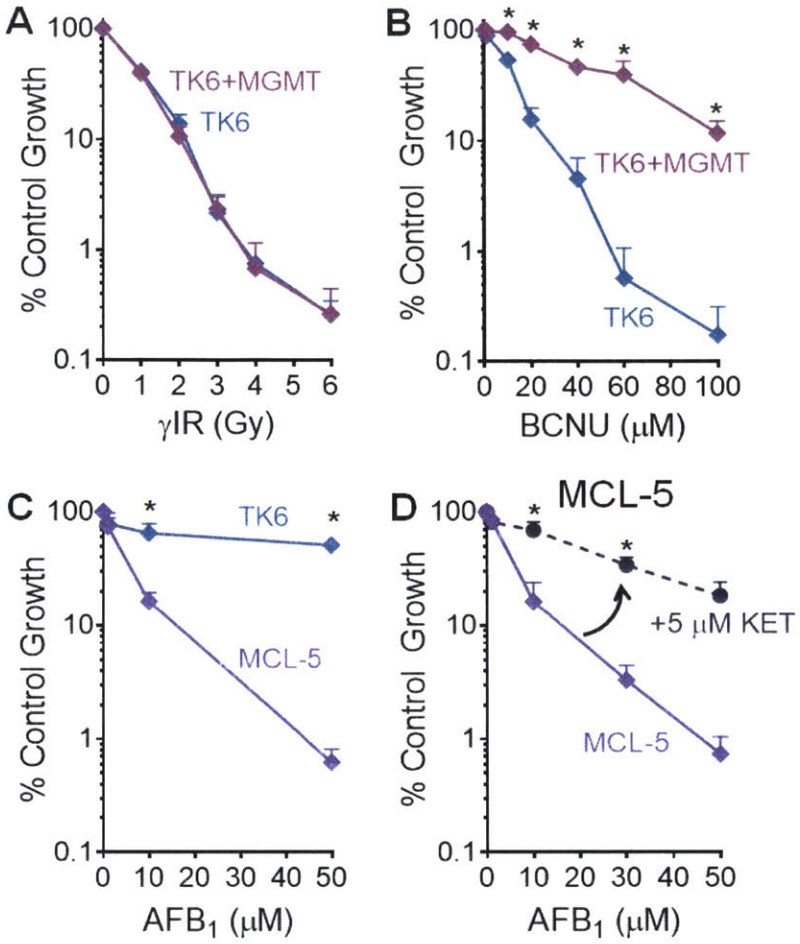

Figure 3-5. μCC analyses to measure toxicity presented as percent of treated cells relative to untreated control cells (% Control). **A.** γ radiation treatment (see Methods) for TK6 cells (blue) and TK6 + MGMT cells (pink). **B.** N,N'-bis (2-chloroethyl)-N-nitrosourea (BCNU) treatment (1 hour at 37^{0}C) for TK6 cells (blue) and TK6 + MGMT cells (pink). * $p < 0.05$, Student's t-test, 2-tailed, unequal variance. **C.** Aflatoxin B_1 (AFB_1) exposure (24 hours at 37^{0}C) for TK6 cells (blue) and MCL-5 cells (light purple). * $p < 0.05$, Student's t-test, 2-tailed, unequal variance. **D.** Parallel treatment of MCL-5 cells with AFB_1 or AFB_1 in conjunction with ketoconazole (KET). * $p < 0.05$, Student's t-test, 2-tailed, paired. All data points are means of ≥ 3 independent experiments. Error bars are standard errors of the means.

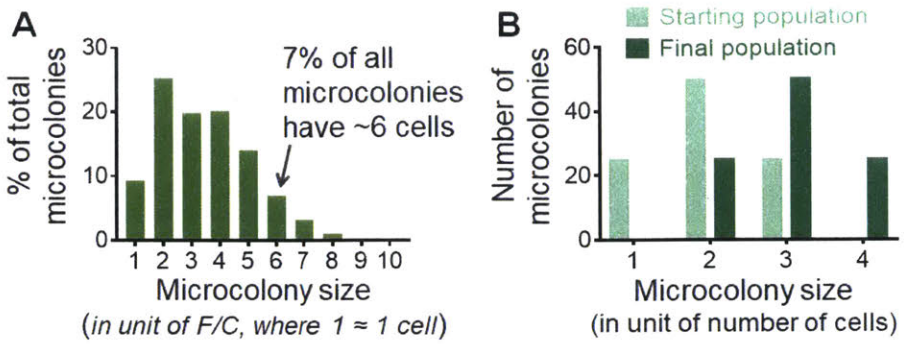

Figure 3-S1. **A.** We sorted microcolonies into F/M bins with equal widths of 2300 (arbitrary fluorescence unit) (1 F/C). These bins range from the expected F/M for ~one cell (1 F/C) to the expected F/M for ~150 cells (150 F/C's). We then derived the microcolony size distribution by quantifying the relative frequency of microcolonies with F/M values that fall within each specific F/M bin (example in Fig. S2). Illustration of the construction of a microcolony size distribution. Data are from untreated TK6 microcolonies after one day in culture. Each bin represents one microcolony size in unit of F/C (~number of cells). y-axis is the relative frequency of microcolonies with the same size. **B.** Simplified illustrative size distributions for 100 starting microcolonies (light green) and 100 final microcolonies (dark green). See **Supplementary Procedures** for step-by-step calculations for Excess Mircocolonies and Excess Growth.

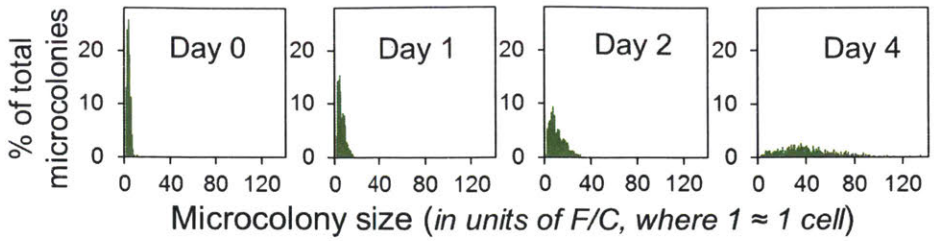

Figure 3-S2. Example of F/M distributions for TK6 cells on μCC at different times in culture (see Fig. 3-2D). y-axes for all distributions are set to the same scale.

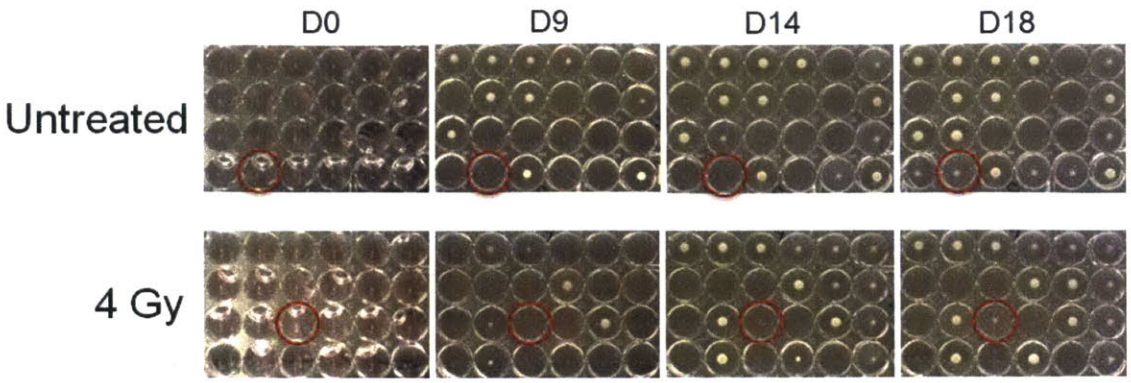

Figure 3-S3. Example bright-field pictures of wells with TK6 cells (untreated or γ-irradiated with 4 Gy) cultured in U-bottom 96-well plates over 18 days (D0 = immediately after exposure, D9 = 9 days after exposure, D14 = 14 days after, and D18 = 18 days after) (see Methods). Pictures are taken from the same 24 wells for each condition. Obvious colonies appear at different times across the wells. Red-circled wells represent examples of colonies that are not obvious until day 18 (D18).

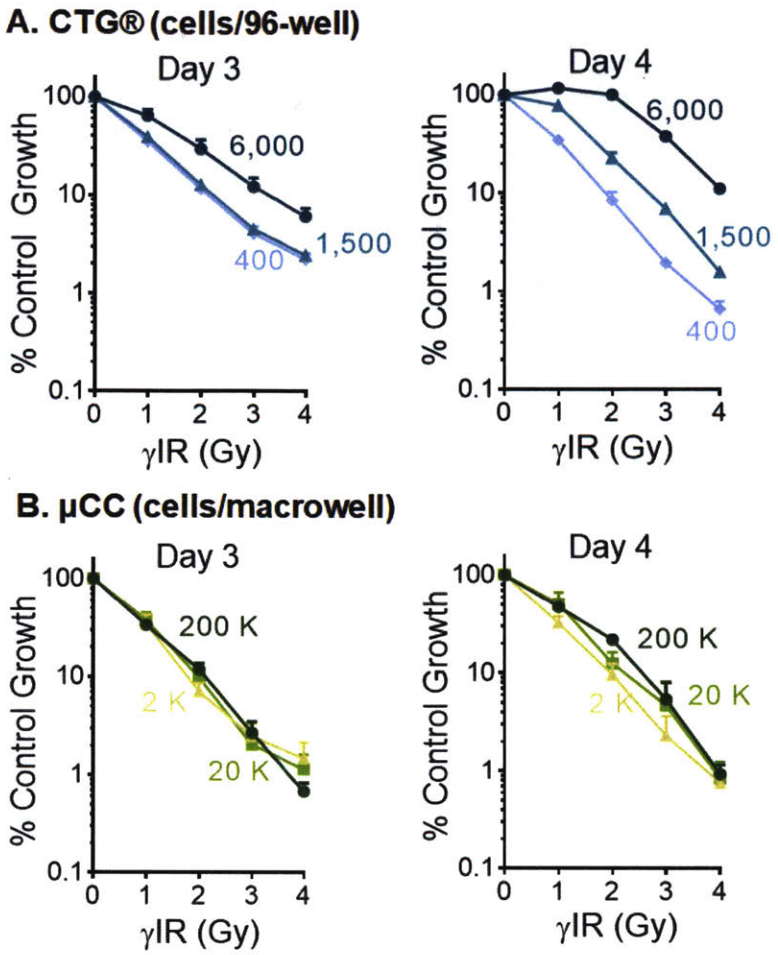

Figure 3-S4. **A**. γIR-induced toxicity in TK6 cells measured by CTG® with different cell seeding densities (*legend*: number of cells per 96-well) and 2 different recovery periods (*left*: 3 days; *right*: 4 days). **B**. γIR-induced toxicity in TK6 cells measured by μCC with different cell loading densities (*legend*: number of cells per macrowell) and 2 different recovery periods (*left*: 3 days; *right*: 4 days). n ≥ 3, error bars are standard errors of the means.

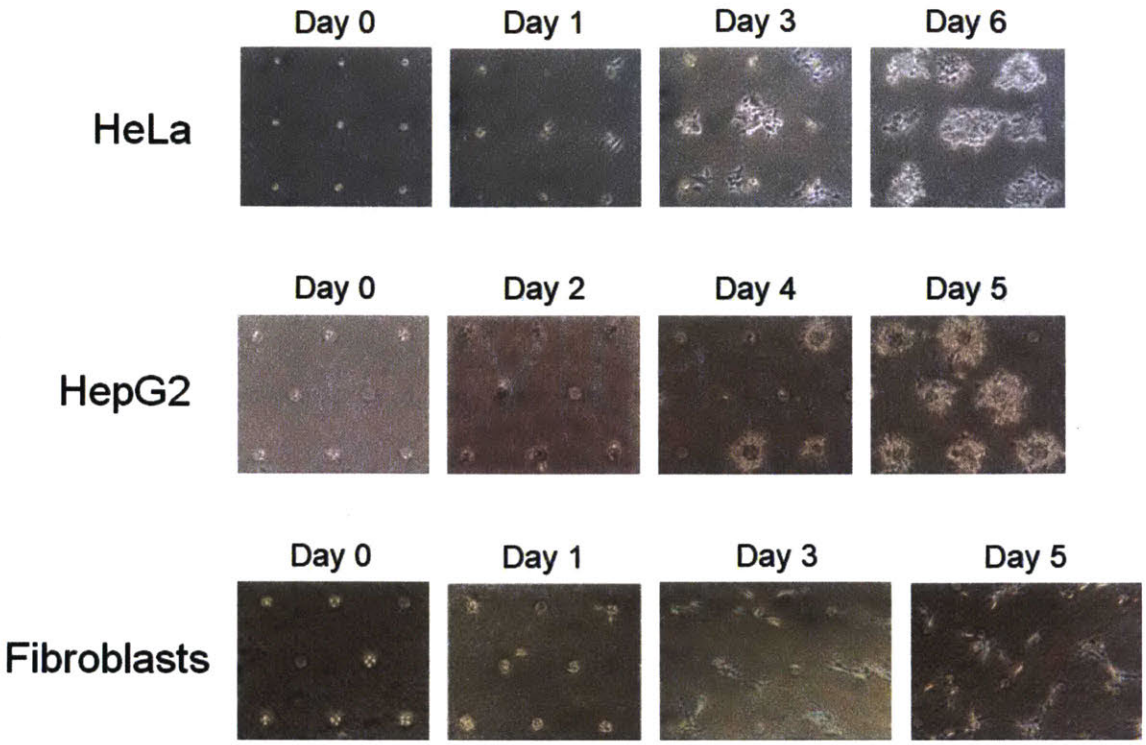

Figure 3-S5. Growth of adherent cells on modified μCC. A layer of Collagen I gel was sandwiched between the cells and the overlay agarose layer. Modified μCC with embedded cells was submerged in culture medium and monitored for cell growth. Phase-contrast pictures of HeLa cells, HepG2 cells, and human fibroblasts cells on modified μCC were taken at 40X magnification.

Chapter 4

Application of CometChip and Human Lymphocytes to Study Population Variation in DNA Repair Capacity

4.1. ABSTRACT

There is a high variability in how an individual responds to DNA damaging agents. Many lines of evidence point toward an association between aberrant DNA repair capacity and risk of cancer as well as sensitivity to anti-cancer treatment. Over the past two decades, there is mounting evidence showing significant interindividual variations in DNA repair capacity, which are associated with differences in disease risk and treatment outcomes. The evidence has been contributed by methods that indirectly or directly measure DNA repair capacity. Therefore, the ability to measure DNA capacity may allow for predictions of how an individual responds to a DNA damaging agent, enable more accurate assessment of cancer risk, and provide useful information to design tailored treatment regimens in order to minimize side effects while maximizing treatment effectiveness. CometChip, a high-throughput comet assay platform, can process ~3-4 orders of magnitude more samples than the conventional comet assay, opening doors to large population studies. In this study, we demonstrated how CometChip can be used to measure DNA repair kinetics of oxidative damage induced by γ ionizing radiation (γIR) and hydrogen peroxide (H_2O_2), alkylation damage induced by methyl methanesulfonate (MMS), cyclobutane pyrimidine dimers induced by ultraviolet (UV) light, and double-strand breaks (DSBs) formed upon γIR in human primary lymphocytes. We also conducted a small pilot study with primary lymphocytes isolated from 56 healthy volunteers, which shows a sevenfold variation in repair rates.

4.2. INTRODUCTION

Environmental DNA damaging agents, such as air pollution, tobacco smoke, and UV radiation, represent major causes of cancer, yet therapeutic DNA damaging agents, such as γ radiation and temozolomide, are standard cancer therapies. The health effects of exposure to DNA damaging agents vary greatly across populations. Among heavy smokers, only ~10% develop lung cancer (1), and among patients undergoing similar courses of cancer therapy, treatment outcomes highly diverge (2). The ability to identify individuals who are most susceptible to the health effects of DNA damage would open doors for personalized strategies for early detection or prevention of cancer and individualized dosing regimens that could make treatment more effective while minimizing its harmful side effects. Genetic and functional analyses indicate that cancer susceptibility and clinical treatment sensitivity can be associated with inefficient DNA repair (3-8), raising the possibility of tailoring individual treatment and prevention by measuring DNA repair capacity.

Despite the important role of DNA repair in modulating the health effects of DNA damage, clinical applications of DNA repair capacity have been limited to diagnostics via genetic testing of known polymorphisms in genes associated with DNA repair defects and diseases (9). Certain cell-based assays, such as chromosomal aberration and UV-induced unscheduled DNA synthesis, are occasionally used as confirmation tests (10, 11). Importantly, although genetic defects in DNA repair proteins have been exploited to improve cancer treatment outcomes (12, 13), interindividual variation in DNA repair capacity has not been considered in cohort selection for clinical trials or in designing treatment regimens.

More studies are needed to further elucidate the relationship between DNA repair capacity and health outcomes. Larger and more prospective studies are especially crucial since it is unclear whether the altered DNA repair capacity associated with cancer risk and treatment response variability is the cause or the effect. The extensive crosstalk and competition between the major DNA repair pathways also needs to be taken into account in these studies (14). To these ends, high-throughput assays capable of measuring

multiple repair pathways in parallel are essential. Recent examples include a multiplexed fluorescence-based flow cytometric host cell reactivation assay (FM-HCR) (15, 16) and CometChip (17, 18).

Developed in 1984 (19), the comet assay has since become a classic tool in a number of fields, including environmental biomonitoring, DNA repair studies, and genotoxicity testing (20, 21). The key advantages of the comet assay include simple procedures and sensitivity to a wide range of DNA damage. Importantly, only a small number of cells are required, making the assay particularly suitable for population studies where samples are usually rare and valuable. On the other hand, the conventional comet assay suffers from several major drawbacks, including low-throughput and high experimental variability. Only about 600 comets can be imaged within one hour, which limits the number of slides scored per day to 50 even when automated imaging systems are used (20). This practical challenge severely limits the use of the comet assay in large-scale sample size and is especially prohibitive in DNA repair kinetics studies where multiple time points are analyzed for several types of DNA damage.

CometChip, a high-throughput comet assay platform, was developed to overcome the limitations of the conventional comet assay (17, 18). The underlying principle of CometChip is based upon arraying cells in a grid on an agarose chip so that the resulting comets are on the same focal plane and are spaced at a fixed distance from one another. As a consequence, as many as 100 comets can be imaged in one field. In addition, a bottomless 96-well plate can be imposed on the agarose chip to create 96 isolated macrowells, each of which contains up to 300 comets. Each chip, therefore, corresponds to ~96 slides in the conventional comet assay, and one full chip can be imaged within ~15 minutes by automated systems. Finally, a companion in-house software enables automated analysis of more than 100 comet images per second. As a result, CometChip can process ~3-4 orders of magnitude more samples than the conventional comet assay, opening doors to large-scale population studies of DNA repair kinetics across multiple pathways.

This study focuses on establishing experimental CometChip conditions to measure DNA repair kinetics of multiple types of DNA damage in human peripheral blood lymphocytes. Human peripheral blood mononuclear cells (PBMCs) were isolated from fresh whole blood, and T-lymphocyte activation was

stimulated for three days with the mitogen phytohemagglutinin-L (PHA-L) (22, 23). The alkaline comet assay was used to study oxidative damage induced by γIR and H_2O_2 and alkylation damage induced by MMS. An additional incubation step with T4 endonuclease V was included in the alkaline comet assay to create nicks at CPDs formed upon short wavelength UV irradiation (UV-C). Finally, the repair of DSBs caused by γIR was monitored with the neutral comet assay. All five measures were conducted in parallel using the same sample of PHA-stimulated T-lymphocytes.

In a pilot study, we investigated CometChip's sensitivity and reproducibility to measure small differences in oxidative repair kinetics between individuals. Blood samples were taken from ten healthy volunteers on multiple visits in order to compare the variability within an individual and across the population. A larger study was also conducted with 46 healthy volunteers, each of whom had one single blood draw. Oxidative repair kinetics curves were obtained for the population, showing a sevenfold variation in repair rate.

4.3. MATERIALS AND METHODS

CometChip fabrication

Materials. Sylgar™ 184 silicone elastomer kit (102092-312) and bottomless 96-well plates (82050-714) were purchased from VWR, Radnor, PA. GelBond® Film (53761) was obtained from Lonza, Portsmouth, NH. UltraPure™ agarose (16500100) and UltraPure™ low melting point agarose (16520100) were purchased from ThermoFisher Scientific, Waltham, MA.

Procedure. The microwells were fabricated as described previously (17, 18, 24, 25). Briefly, 1% w/v agarose solution in DPBS was prepared. A polydimethylsiloxane (PDMS) stamp with an array of micropegs was fabricated using the Sylgar™ 184 kit as described previously (18). The stamp was pressed into the molten agarose solution on top of the hydrophilic side of a sheet of GelBond® Film. The agarose was allowed to gel at room temperature for ~15 minutes. The stamp was removed to reveal an array of

microwells with ~40-50 μm in both diameter and depth. The microwells were spaced 240 μm apart. A bottomless 96-well plate was pressed on top of the agarose chip to form 96 macrowells. The bottom of each macrowell was an array of ~300 microwells.

To load cells into microwells, ~2,000 – 200,000 cells in suspension were placed into each macrowell, and the chip was incubated at 37°C in the presence of 5% CO_2 for 15 minutes. This time is sufficient for most cell types to have fully loaded into the microwells by gravity. Excess cells were then washed off with DPBS by shear force. The chip was covered with a layer of overlay agarose (1% w/v low-melting point agarose solution in DPBS, kept molten at 43°C until use). For complete solidification of the overlay agarose, the chip was kept at room temperature for 2 minutes followed by 2 minutes at 4°C.

Alkaline CometChip assay

Chemicals. Sodium chloride (NaCl, 7581), disodium EDTA (Na_2EDTA, 4931), and sodium hydroxide pellets (NaOH, 7708) were purchased from VWR, Radnor, PA. Trizma® base (T1503), Trizma® HCl (T5941), and Triton X-100 (X-100) were obtained from MilliporeSigma, St. Louis, MO. 10,000X SYBR™ Gold nucleic acid gel stain was obtained from ThermoFisher Scientific, Waltham, MA.

Buffers. The alkaline lysis buffer (pH ~ 10) was a solution of 2.5 M NaCl, 100 mM Na_2EDTA, 10 mM Trizma® base, and 1% v/v Triton X-100 dissolved in de-ionized H_2O (dI H_2O). The alkaline unwinding buffer (pH ~ 13.5) was prepared by diluting NaOH and Na_2EDTA stock solutions in dI H_2O to final concentrations of 0.3 M and 1 mM, respectively. The neutralization buffer (pH ~ 7.5) was prepared by dissolving Trizma® HCl in distilled H_2O to a final concentration of 0.4 M.

Procedure. Cells encapsulated in CometChip were lysed in the alkaline lysis buffer overnight at 4°C. The nuclei were unwound in the alkaline unwinding buffer for 40 minutes at 4°C, and the DNA was electrophoresed in the same buffer at the same temperature for 30 minutes at 1 V/cm and ~300 mA. The CometChip was then washed three times in the neutralization buffer by submerging for five minutes each time.

Afterward, the DNA on ComeChip was stained for 15 minutes at room temperature with 1X of SYBR™ Gold diluted in DPBS, protected from light. Fluorescent images of the comets were captured at 40X magnification using an epifluorescence microscope (Nikon Eclipse 80i, Nikon Instruments, Inc., Melville, NY) with a 480 nm excitation filter. Image acquisition was achieved by automatic scanning using a motorized XY stage. Comet images were automatically analyzed using Guicometanalyzer, a custom software developed in MATLAB (The MathWorks Inc., Natick, MA) as previously described (18). Outputs from Guicometanalyzer were processed and imported to a spreadsheet (Microsoft Excel, Microsoft Office Suite 2016) using Comet2Excel, an in-house software developed in Python (Python Software Foundation, Python version 2.7.10).

Neutral CometChip assay

Chemicals. Sodium chloride (NaCl, 7581), disodium EDTA (Na_2EDTA, 4931), and sodium hydroxide pellets (NaOH, 7708) were purchased from VWR, Radnor, PA. N-lauroylsarcosine sodium salt (L9150), Trizma® base (T1503), Trizma® HCl (T5941), Triton X-100 (X-100), 100% dimethyl sulfoxide (DMSO, D8418) were obtained from MilliporeSigma, St. Louis, MO. 10,000X SYBR™ Gold nucleic acid gel stain was obtained from ThermoFisher Scientific, Waltham, MA. Boric acid (M139) was purchased from AMRESCO LLC, Solon, OH.

Buffers. The neutral lysis buffer (pH ~ 9.5) was prepared as a solution of 2.5 M NaCl, 100 mM Na_2EDTA, 10 mM Trizma® base, 1% N-lauroylsarcosine sodium salt, 0.5% v/v Triton X-100, and 10% DMSO in de-ionized H_2O (dI H_2O). The neutral electrophoresis buffer (TBE, pH ~ 8.5) comprised of 2 mM Na_2EDTA, 90 mM Trizma® base, and 90 mM boric acid in dI H_2O. The neutralization buffer (pH ~ 7.5) was prepared by dissolving Trizma® HCl in distilled H_2O to a final concentration of 0.4 M.

Procedure. Cells encapsulated in CometChip were lysed in the neutral lysis buffer overnight at 43°C. The CometChip was then washed vigorously three times by submerging in TBE and placed on an orbital shaker for 30 minutes at a slow speed (~50 rpm). Afterward, the chip was incubated in fresh TBE at

4°C for 60 minutes, and the DNA was electrophoresed in the same buffer at the same temperature for 60 minutes at a constant 0.6 V/cm and 6 mA. The CometChip was then washed three times in the neutralization buffer by submerging for five minutes each time.

Afterward, the DNA on CometChip was stained for 15 minutes at room temperature with 1X of SYBR™ Gold diluted in DPBS, protected from light. Fluorescent images of the comets were captured at 40X magnification using an epifluorescence microscope (Nikon Eclipse 80i, Nikon Instruments, Inc., Melville, NY) with a 480 nm excitation filter. Image acquisition was achieved by automatic scanning using a motorized XY stage. Comet images were automatically analyzed using Guicometanalyzer, a custom software developed in MATLAB (The MathWorks Inc., Natick, MA) as previously described (18). Outputs from Guicometanalyzer were processed and imported to a spreadsheet (Microsoft Excel, Microsoft Office Suite 2016) using Comet2Excel, an in-house software developed in Python (Python Software Foundation, Python version 2.7.10).

Culture of cell lines

Reagents. Dulbecco's phosphate-buffered saline (DPBS), high-glucose Dulbecco's Modified Eagle's Medium (DMEM, high glucose, 11965092), RMPI-1640 (11875093), 200 mM L-glutamine (A2916801), 10,000 U/ml Pen-Strep (15140), 0.25% Trypsin-EDTA with phenol red (25200) were purchased from ThermoFisher Scientific, Waltham, MA. Fetal bovine serum (FBS) was obtained from Atlanta Biologicals, Inc., Flowery Branch, GA.

Culture conditions. All the cells were cultured in an incubator set at 37°C with 5% CO_2.

Cell lines. TK6 (26, 27), a human B-lymphoblastoid cell line, was a gift from W. Thilly. TK6 was cultured in RPMI 1640 with GlutaMAX™ supplemented with 100 U/ml Pen-Strep. TK6 cell suspension was directly obtained from the suspension culture.

The XPG cell lines were gifts from O. Scharer. These include XPG-deficient, XPG/WT, and XPG/E791A. The XPG-deficient cell line was obtained from SV40-transformation of the primary human

skin fibroblasts from patient XPCS1RO (28). XPG/WT and XPG/E791A cells were obtained from the stable transfection of the lentiviral vector containing XPG WT cDNA or XPG-E791A cDNA in the XPG-deficient cell line (29). The XPG cell lines were cultured in high-glucose DMEM supplemented with 10% FBS, 2 mM L-glutamine, and 100 U/ml Pen-Strep. To obtain cell suspension for the XP-G cell lines, the monolayer culture was incubated with 0.25% Trypsin-EDTA for 1-2 minutes at 37°C. Detached cells were then suspended in complete working media. Cell viability and cell number were analyzed using an automated Trypan Blue exclusion system [Vi-CELL™ cell counter (Beckman Coulter Life Sciences, Brea, CA)].

Peripheral blood mononuclear cells (PBMCs)

Reagents. Ficoll-Paque PLUS solution (17144002) was purchased from GE Healthcare Bio-Sciences, Pittsburgh, PA. RMPI-1640 (11875093) and 10,000 U/ml Pen-Strep (15140) were purchased from ThermoFisher Scientific, Waltham, MA. Heat-inactivated fetal bovine serum (HI-FBS, 100-106) was obtained from Gemini Bio-Products, West Sacramento, CA. Phytohemagglutinin-L (PHA-L, L4144) and 100% dimethyl sulfoxide (DMSO, D8418) were obtained from MilliporeSigma, St. Louis, MO. D-Glucose (dextrose, BDH9230) was purchased from VWR, Radnor, PA.

Human whole blood. For assay optimization and internal controls, fresh whole blood from two anonymous healthy donors collected in sodium heparin Vacutainer collection tubes was purchased from Research Blood Components, Brighton, MA. For our population study, fresh whole blood from 56 healthy volunteers was collected in sodium heparin Vacutainer collection tubes by a clinical professional at the Clinical Research Center at Massachusetts Institute of Technology, Cambridge, MA. Ten of the 56 volunteers had multiple blood draws (up to five visits) while the remaining 46 had one single blood draw per person.

PBMC isolation. PBMCs were isolated using the standard Ficoll gradient density centrifugation (23, 30, 31). Briefly, 10 mL of fresh whole blood was diluted with 10 mL of warm RPMI-1640 solution. 8

mL of the Ficoll-Paque PLUS solution was gently injected underneath the diluted blood sample without mixing the two solutions. The whole tube was then centrifuged at 400 g for 40 minutes at 18°C with brakes off. The upper layer containing plasma and platelets was aspirated off, providing access to the PBMC layer (buffy coat). PBMCs were transferred to a new centrifuge tube. Cells isolated from the same original blood sample were pooled in one tube. PBMCs were washed by diluting in warm RPMI-1640 solution to a final volume of 50 mL and centrifuged at 600 g for 20 minutes at 18°C. The supernatant was aspirated, and the pellet was resuspended in 20 mL of warm RPMI-1640 solution. Cells from 10 µL of the suspension were stained with crystal violet, and the number of mononuclear cells were counted with a hemocytometer. The remaining suspension was centrifuged at 400 g for 15 minutes at 18°C. The supernatant was aspirated, and the pellet was suspended in the freezing medium (40% RPMI-1640 + 50% HI-FBS + 10% DMSO). The volume for the freezing medium was one-tenth the volume of the original blood sample (i.e. 1 mL freezing medium to suspend a pellet isolated from 10 mL of fresh whole blood). The average cell density was ~$10x10^6$ cells/mL.

PBMC cryopreservation and storage. 1 mL aliquots of PBMCs suspended in the freezing medium were transferred to separate cryovials. The vials were stored in a Styrofoam container and placed in a -80°C freezer. After 24 hours, the frozen vials were transferred to a Dewar containing liquid nitrogen.

PBMC recovery and T-lymphocyte stimulation. Cryopreserved PBMCs were rapidly thawed by placing the vial containing the cells in a 37°C water bath for ~one minute. Cells were transferred to a centrifuge tube containing 9 mL warm thawing medium (40% RPMI-1640 + 50% HI-FBS + 10% D-glucose) and centrifuged at 600 g for 5 minutes at room temperature. Supernatant was aspirated, and the pellet was resuspended in 10 mL of stimulation medium (RMPI-1640 + 20 % HI-FBS + 100 U/mL Pen-Strep + 5 µg/mL PHA-L). 500 µL of the suspension was analyzed for cell viability using an automated Trypan Blue exclusion system (Vi-CELL™ cell counter). The recovery procedure typically yielded more than 85% viable cells. T-lymphocytes were stimulated for three days by placing the remaining suspension in a tissue-culture incubator (37°C, 5% CO_2).

CometChip cell loading. For each experiment, $10x10^5$ of PHA-stimulated T-lymphocytes were harvested and suspended in 5 mL of complete medium (RPMI-1640 + 20% HI-FBS + 100 U/mL Pen-Strep). Cells were loaded into microwells by placing 50 µL of the suspension into a macrowell and incubating for 15 minutes at 37°C.

γ radiation treatment

Cells embedded in CometChip were irradiated with γ-rays from a ^{137}Cesium source delivered at ~1 Gy/min (Gammacell 40 Exactor, Best Theratronics Model C-440) for the alkaline comet assay. For the neutral comet assay, the γ-rays were delivered from a ^{60}Cobalt source at an approximate rate of 60 Gy/min (Gammacell 220 Excel, MDS Nordion). Cells were kept on ice during irradiation.

Hydrogen peroxide (H_2O_2)

Chemical. 30% w/w hydrogen peroxide (H_2O_2) solution was obtained from MilliporeSigma, St. Louis, MO (H1009) and was stored at 4°C, protected from light. H_2O_2 dilutions were freshly prepared from the 30% stock immediately before use.

H_2O_2 treatment. Doses of H_2O_2 were prepared immediately before use by diluting 30% stock solution (10 M) with cold PBS. Suspension of TK6 cells was obtained directly from exponentially growing culture and loaded onto CometChip (see "CometChip fabrication"). A new bottomless 96-well was placed on top of the CometChip. 100 µL of H_2O_2 solution was pipetted into each well, and the CometChip was incubated at 4°C for 20 minutes, protected from light. Afterward, the H_2O_2 solution was aspirated, and the bottomless plate was taken off. The CometChip was rinsed by submerging in cold PBS.

DNA damage and repair. To analyzed DNA damage immediately after treatment, the CometChip was placed in cold alkaline lysis buffer and processed following the remaining steps of the alkaline comet assay. To study repair kinetics, the CometChip was cut into ~5 cm x 5 cm pieces using a pair of sterile surgical scissors and incubated in culture medium at 37°C for up to two hours. At each time point, a piece

of CometChip was removed and placed in cold alkaline lysis buffer. The remaining steps followed the alkaline comet assay procedure.

Methyl methanesulfonate (MMS)

Chemical. 99% methyl methanesulfonate (MMS) solution was obtained from MilliporeSigma, St. Louis, MO (129925) and was stored at room temperature. MMS dilutions were freshly prepared from the 99% stock less than 15 minutes before use.

MMS treatment. Doses of MMS were prepared ~15 minutes before use by diluting 99% stock solution (11.8 M) with warm serum-free media (pre-warmed by incubation at 37°C). Suspension of TK6 cells was obtained directly from exponentially growing culture, and 1 mL of cell suspension was placed in a 15 mL conical tube. The tube was centrifuged (200 x g, 5 minutes), and the supernatant was aspirated. The cell pellet in each well was re-suspended in 1 mL of MMS solution, and the tube was incubated for 30 minutes or one hour at 37°C. Next, the tube was again centrifuged (200 x g, 5 minutes), and MMS supernatant was aspirated. Each cell pellet was washed three times by re-suspending in 1 mL PBS, spinning down (200 x g, 5 minutes), and aspirating the supernatant. After the last wash, each pellet was re-suspended in 1 mL culture medium.

DNA damage and repair analysis. To analyzed DNA damage immediately after treatment, 50 µL of cell suspension was transfer to a macrowell on CometChip. After the cells loaded into the microwells (see "CometChip fabrication"), they were immediately placed in cold alkaline lysis buffer and processed following the remaining steps of the alkaline CometChip assay. To analyze repair kinetics, remaining cells in the tube were incubated at 37°C for up to 24 hours. At each time point, 50 µL of cell suspension was transfer to a macrowell on CometChip and processed as above.

Ultraviolet (UV)

Chemical. Reduced L-glutathione (GSH, G6013) was obtained from MilliporeSigma, St. Louis, MO. 1X GSH solution (10 mM) was prepared by dissolving GSH powder in warm culture medium and used immediately within 30 minutes of preparation.

UV irradiation. Prior to UV irradiation, cells embedded in CometChip were incubated for 40 minutes at 37°C in working medium supplemented with 10 mM GSH. Exposure to 254 nm UV light radiation (UVC) was administered via a handheld UV lamp that had a dose-rate of 14 $J/m^2/s$ at a distance of 7.6 cm (UVP 95001614, ThermoFisher Scientific, Waltham, MA). The UV irradiation procedure was carried out in the dark at 4°C.

NER kinetics of CPDs. To study NER efficiency, we examined the repair rate of cyclobutane pyrimidine dimers (CPDs) induced by UV irradiation. The bacterial T4 endonuclease V (M0308S, New England BioLabs, Ipswich, MA) was used in combination with the alkaline CometChip assay to query the level of CPDs (32) over 24 hours of repair. Briefly, UV-exposed cells were incubated in working medium supplemented with 10 mM GSH for one hour, four hours, and 24 hours. Cells embedded in CometChip were lysed overnight in the alkaline lysis buffer. The CometChip was then washed three times with the enzyme reaction buffer (1 mM EDTA, 100 mM NaCl, 25 mM Na_2HPO_4, 100 μg/mL BSA, pH 7.2) by submerging for 15 minutes each time. The enzyme reaction was performed by incubating the CometChip with 50 U/mL T4 Endonuclease V in the enzyme reaction buffer for 15 minutes at 37°C. Afterward, the CometChip was placed in the alkaline unwinding buffer and processed following the remaining steps of the alkaline comet assay.

Data analysis of repair kinetics

Multiple comparisons between individuals. One-way ANOVA followed by Tukey-Kramer's multiple comparison test was performed using the Real Statistics Resource Pack software (Release 5.1). Copyright (2013-2017) Charles Zaiontz. www.real-statistics.com.

Mathematical modeling. Background-corrected data were obtained by subtracting the DNA damage level at each repair time point by the baseline level. Non-linear regression was performed using GraphPad Prism version 7.01 for Windows (GraphPad Software, La Jolla, CA, www. graphpad.com.) to fit the background-corrected data to a biphasic exponential decay model:

$$f(t) = F.e^{-k_f.t} + S.e^{-k_s.t},$$

where $f(t)$ is the level of DNA damage at time t, k_f and k_s are two rate constants corresponding to the fast and the slow phases of the repair kinetics, and $f(0) = F + S$ is the initial DNA damage level. Therefore, if $t_{1/2}$ is the time required to repair half of the initial damage (half-time), then

$$F.e^{-k_f.t_{1/2}} + S.e^{-k_s.t_{1/2}} - \frac{F+S}{2} = 0.$$

The value of $t_{1/2}$ was approximated using the Solver add-in in Microsoft Excel (Microsoft Office Suite 2016).

4.4. RESULTS

CometChip assays for PBMC repair kinetics

We aimed to optimize CometChip assay conditions to measure repair kinetics of lymphocytes against five different types of DNA damage: oxidative damage induced by H_2O_2, oxidative damage induced by γIR, alkylation damage induced by MMS, bulky lesions induced by UV light, and DSBs induced by γIR. PBMCs were isolated from purchased fresh whole blood collected from healthy individuals via Ficoll density gradient centrifugation (23, 30, 31) (Fig. 4-1). In whole blood, the total number of leukocytes varies between $4x10^6$ and $16x10^6$ cells/mL, with an average of $7x10^6$ cells/mL. The PBMC isolation procedure yields an average cell density of 1.4 x 10^6 cells/mL. After isolation, PBMCs were immediately suspended in media supplemented with 50% FBS and 10% DMSO and slowly cooled down to -80°C using insulated

containers. For long-term storage, cryopreserved cells were transferred to a liquid nitrogen tank and kept there until experiments. To recover PBMCs from cryopreservation, cells were rapidly thawed and transferred to warm media supplemented with 50% serum and 10% dextrose. On average, more than 85% of recovered PBMCs are viable. The recovered PBMCs were cultured with the mitogen PHA-L for three days to stimulate T-cell activation and proliferation (23) and then harvested for CometChip assays (Fig. 4-1).

Oxidative damage repair

Oxidative damage is the most common type of DNA damage, primarily caused endogenously by reaction of DNA with reactive oxygen species (ROS) that are byproducts of cellular metabolisms. In addition, external exposures to physical and chemical agents, such as γ-radiation, have also been shown to induce ROS, including superoxide ($O_2^{\bullet -}$), hydroxyl radical ($^{\bullet}OH$), and hydrogen peroxide (H_2O_2) (33). ROS can react with the sugar phosphate backbone and directly cause single-strand breaks (SSBs) (33). In addition, reactions of ROS with nucleobases result in a wide range of oxidative base lesions, such as 8oxoguanine, thymine glycol, 2,6-diamino-4-hydroxy-5-formamidopyrimidine (FapyG) (33).

The base excision repair pathway (BER) is involved in rejoining SSBs as well as correcting the majority of oxidative base lesions (34, 35). The first step in BER is damage recognition and base removal by DNA glycosylases (36). Monofunctional glycosylases remove the damaged base by cleaving the N-glycosidic linkage between the base and the sugar, leaving behind an abasic site (AP). On the other hand, bifunctional glycosylases not only remove the damaged base but also cleave the AP site, generating a SSB (35). Following N-glycosidic cleavage by a monofunctional glycosylase, AP endonuclease 1 (APE1) catalyzes the hydrolysis of the phosphodiester bond 5' of the AP site, creating a SSB flanked by a 5'-deoxyribose-5-phosphate (5'-dRP) and a 3'-hydroxyl (3'-OH) termini (37). In short-patch BER, DNA polymerase β (Pol β) fills in the single-nucleotide gap by extending from the 3'-OH terminus. Pol β also possesses lyase activity that removes the 5'-dRP intermediate. The nick is then sealed by DNA ligase I or ligase IIIα/XRCC1 (35, 38). In long-patch BER, the replicative polymerases δ/ Ɛ or Pol λ take over from

Pol β (35, 36, 38). Because a longer repair patch is synthesized, the damage-containing strand is displaced and is removed by the flap endonuclease FEN1. The nick is sealed by ligase I (35, 36, 38).

Because a number of steps in BER result in SSBs as intermediates, it is possible to measure the repair of oxidative damage using the alkaline CometChip (18, 24, 25). In addition to SSB intermediates, AP sites left behind by monofunctional glycosylases are alkali-labile and can be converted to nicks in the alkaline CometChip assay (pH >13) (39). We exposed cells to γ-radiation (γIR) and H_2O_2 to induce oxidative damage. Using the alkaline CometChip assay, we measured the levels of SBs immediately after treatment as well as after different periods of repair in order to study the kinetics.

To study γIR-induced damage, we irradiated TK6 cells embedded in CometChip with γIR doses between 1 and 14 Gy while keeping the cells on ice to prevent repair activity. Cells were immediately lysed and analyzed for SBs. As shown in Fig. 4-2A, TK6 cells display a linear dose-response to γIR ($R^2 = 0.95$) with the highest dose inducing about five times more SBs than the basal level. To study repair kinetics, cells embedded in CometChip were submerged in warm media following irradiation to enable DNA repair. SB levels were analyzed at multiple repair time points to yield a repair kinetic curve. Our results show that both TK6 and PHA-stimulated T-lymphocytes are able to rapidly rejoin SBs induced by 8 Gy with similar kinetics (Fig. 4-2B), where more than 70% of initial SBs are rejoined after 15 minutes of repair.

Furthermore, we also studied the repair of oxidative damage induced by H_2O_2. Stimulated lymphocytes embedded in CometChip were challenged with a range of H_2O_2 doses (between 10 and 100 μM) via a short incubation at 4°C to prevent repair activity. SB levels analyzed immediately after the challenge show a linear dose-response to H_2O_2 (Fig. 4-2C). Half of the exposed cells were incubated in warm media for two hours to allow DNA repair. Analysis of their SB levels reveals a complete clearance of H_2O_2-induced SBs for all H_2O_2 doses (Fig. 4-2C). We analyzed SB levels at different repair time points prior to two hours to further explore the kinetics. Both TK6 and PHA-stimulated T-lymphocytes display similar initial levels of SBs after being challenged with 100 μM H_2O_2 and are able to reduce the induced damage to near the basal level after two hours of repair (Fig. 4-2D). However, the rate of repair appears to

be faster in TK6 cells. For example, ~60% of the initial damage is corrected after 30 minutes in TK6 cells whereas the stimulated T-lymphocytes retain ~70% of the initial damage at this time. This observation further supports that it is necessary to examine multiple time points in order to study variation in repair.

Alkylation damage repair

MMS

Alkylating agents are one of the major classes of chemotherapeutics (40). Their reactions with nucleobases form a range of alkylating lesions, some of which are highly cytotoxic and mutagenic (41). Methyl methanesulfonate (MMS) is an S_N2 alkylating agent, whose targets are primarily the ring nitrogen (N) atoms on the nucleobases (42). Among the lesions induced by MMS, 7-methylguanine (7meG) is the most abundant (~80%), followed by 3-methyladenine (3meA), which accounts for ~10% of the total lesions (41-43). 7meG appears to be innocuous, being neither mutagenic nor cytotoxic. However, 7meG can rapidly hydrolyze to form abasic sites, which are both cytotoxic and able to mispair during replication (41). On the other hand, 3meA blocks replication and is highly cytotoxic. The alkyladenine glycosylase (AAG) is the primary mammalian glycosylase that recognizes and excises alkylated bases as part of BER.

We used the alkaline CometChip (18) to study the levels of SBs induced by MMS. TK6 and PHA-stimulated T-lymphocytes were exposed to a range of MMS doses. Both cell types exhibit strong linear dose-responses to MMS between 0.5 to 2 mM (Fig. 4-2E). When challenged with 2 mM MMS, the levels of SBs for both cell types reach ~77% DNA in tail, which is ~seven times higher than the background level. 4 mM MMS does not appear to induce further SBs likely because ~77% is the saturation limit for the comet assay. When cells were allowed to repair in warm media following MMS exposure up to 1 mM, both TK6 and the stimulated lymphocytes were able to partially reduce their SB levels after four hours. Beyond 1 mM, the DNA became highly fragmented, resulting in comets with a small fraction of normal DNA fluorescence that could no longer be accurately scored. It is likely that the level of DNA damage induced

at high MMS doses (2 and 4 mM) is sufficient to trigger cell death, resulting in extreme DNA fragmentation (39).

Because four hours of repair appears to be insufficient for complete clearance of MMS-induced damage, we extended the total repair time for both TK6 and the stimulated lymphocytes to 24 hours and analyzed SB levels at multiple earlier time points. While oxidative damage is rapidly repaired by both cell types (Fig. 4-2B and D), alkylation damage induced by MMS requires an extended repair duration. Specifically, ~55% of the initial damage induced by 0.5 mM MMS remains after four hours of repair, and ~30% of the induced damage persists after 24 hours in both cell types (Fig. 4-2F).

Cyclobutane pyrimidine dimer repair by NER

Nucleotide excision repair (NER) is the most versatile pathway that can recognize and repair a diverse set of structurally unrelated DNA lesions (44). Good NER substrates disrupt base pairing, distort the double helix, and are generally bulky in size (45). Deficiency in NER proteins are associated with debilitating disorders (46). Genetic defects in XP proteins cause xeroderma pigmentosum (XP), an autosomal recessive disorder characterized by hypersensitivity to UV radiation, accompanied by a ~2,000-fold increased risk of skin cancer. In addition to cancer induced by sunlight exposure, XP patients are also at risk for cancers at sites that are not exposed to UV light (46-48). There is a ~12-fold increase in frequency of internal neoplasms in all sites not exposed to sunlight for XP patients under 20. Notably, cancers of the brain and oral cavity are disproportionately increased (47). In addition, about ~25% of XP patients develop neurological abnormalities caused by progressive neurological degeneration. Mutations in some NER genes, such as *XPB* and *XPD*, also underlie trichothiodystrophy (TTD). TTD patients exhibit developmental abnormalities but do not show heightened risk of sunlight-induced skin cancer. Patients with defects in CSA or CSB exhibit yet another disorder, Cockyane syndrome (CS), which manifests as photosensitivity and severe developmental defects. CS, however, is not associated with a higher risk of sunlight-induced skin cancer. In addition, several mutations in *XPB*, *XPD*, and *XPG* genes lead to a severe disorder with combined symptoms of both XP and CS patients.

We aimed to measure NER variation in human lymphocytes using UV radiation to induce cyclobutane pyrimidine dimers (CPDs), which account for the majority of UV-induced lesions and are efficiently repaired by NER (49). Using the alkaline CometChip (18), we incorporated the use of T4 endonuclease V (32), a bacterial enzyme that possesses both glycosylase and endonuclease activity specific to CPDs (50). Cells embedded in CometChip were irradiated with UV-C and allowed to repair in warm media for up to 24 hours. After repair, cells were lysed overnight following the alkaline CometChip procedure to expose nuclear DNA, which was then incubated with T4 endonuclease V. The enzyme excises the dimers and creates a nick in the sugar phosphate backbone, contributing to the comet tail formation under electrophoresis.

In order to verify that the UV-lesions recognized by T4 endonuclease V are specifically repaired by NER, we compared a cell line deficient in the 3' endonuclease XPG (*XPG*$^{-/-}$) (28) and a version of the same cell line with a stable expression of the wildtype *XPG* (*XPG/WT*) (29). XPG is essential for the complete assembly of the NER preincision complex (44), and the *XPG*$^{-/-}$ cells have been shown to be deficient in NER activity (28). Without incubation with T4 endonuclease V, both *XPG/WT* and *XPG*$^{-/-}$ display minimal SBs upon UV irradiation and during repair (Fig. 4-3A). On the other hand, incubation with the T4 enzyme results in high levels of SBs (~four times higher than the background level) in both cell lines immediately after UV exposure. While the *XPG/WT* cells are able to repair ~20% of the initial CPDs by four hours and most of the lesions by 24 hours, *XPG*$^{-/-}$ show no reduction in CPDs at any time point (Fig. 4-3B). These results support that T4 endonuclease V can be used in CometChip to study NER kinetics.

We demonstrated in this work that incubation with T4 endonuclease V can be applied to PHA-stimulated T-lymphocytes in order to study NER variation among people. In a preliminary study, we exposed PHA-stimulated T-lymphocytes and TK6 cells to UV-C doses ranging from 0.11 to 3.2 J/m^2 and analyzed their CPD levels immediately after irradiation or after 24 hours of repair (Fig. 4-3C). The CPD levels in both cell types increase linearly with the UV-C doses and reach a plateau at 0.8 J/m^2, where the comet assay reaches the saturation level of ~77% DNA in tail. After 24 hours, TK6 cells show complete

repair for UV doses lower than 0.8 J/m^2 and about 50% of repair for 0.8 J/m^2 and higher (Fig. 4-3C). On the other hand, the stimulated lymphocytes display complete repair for most UV doses except for the highest dose, where DNA becomes too fragmented for the comets to be quantifiable.

NER kinetics of CPDs were further investigated for both TK6 cells and the stimulated lymphocytes. Following 0.2 J/m^2 UV irradiation, CPD levels at multiple time points prior to 24 hours were analyzed by incubation with T4 endonuclease V (Fig. 4-3D). Consistent with prior results (Fig. 4-3C), both cell types are able to repair the majority of CPDs by 24 hours. The repair kinetic curves for both cell types are also similar. In contrast with the slow repair rate of the *XPG/WT* cells, both TK6 and the stimulated lymphocytes are able to repair ~50% of CPDs after four hours.

DSB repair

Double-strand breaks (DSBs) are the most deleterious type of DNA damage, capable of triggering cell death and large genomic alterations (51, 52). Mammalian cells use two main mechanisms to repair DSBs, non-homologous end joining (NHEJ) and homologous recombination (HR). NHEJ is a low-fidelity DSB repair pathway, where broken DNA ends are rejoined to restore the chromosome structure, often at the cost of sequence changes at the junction (53). NHEJ is highly flexible, capable of processing diverse DNA end structures at DSBs (53), and is involved in the repair of most DSBs, including those generated by V(D)J recombination and class-switch recombination (54). HR is another major DSB repair pathway, and unlike NHEJ, HR is highly accurate. HR is involved in repair of both DSBs and interstrand crosslinks where maintenance of genomic integrity is critical, such as collapsed replication forks, incomplete telomeres, and crossovers during meiosis (55). Deficiency in one of these pathways results in hypersensitivity to γIR (56-58).

The neutral comet assay is a commonly used method for detection of DSBs (20), and a neutral CometChip version has been developed (17). In this work, we applied the neutral CometChip to measure the repair of DSBs in PHA-stimulated T-lymphocytes. TK6 cells and stimulated lymphocytes were

irradiated with 75 Gy and analyzed with the neutral CometChip assay (Fig. 4-3E). Both cell types display DSB levels about three times the background level immediately after irradiation and able to rejoin the majority of DSBs after four hours of repair. On the other hand, analysis of earlier time points reveal a slight difference in the repair rates between the two cell types. While two hours is sufficient for a complete repair in TK6, about 20% of the induced DSBs persist in the stimulated lymphocytes (Fig. 4-3E).

Application of H_2O_2 repair assays on PBMCs from healthy volunteers

In a pilot study, we applied the alkaline CometChip procedure to measure and analyze oxidative damage repair kinetics of PBMCs isolated from blood draws from a small population of healthy volunteers. Blood draws were obtained from 56 healthy volunteers, including 29 females and 27 males who were between 21 and 66 years old. Lifestyle information, such as weight, height, medication history, dietary and exercise habits, was also obtained via an optional survey.

Isolated PBMCs from each blood sample were cryopreserved in four separate vials and stored in liquid nitrogen until use. For each experiment, cells from one vial were thawed, and T-lymphocytes were stimulated with PHA-L for three days before treatment with H_2O_2 and analysis with the alkaline CometChip assay. Three independent experiments, corresponding to three vials of PBMCs, were conducted for each blood sample.

Repair kinetics of internal controls

We included TK6 cells as an internal control for the CometChip assay. To control for PBMC processing procedures (e.g. thawing, PHA-stimulation), we also included PBMCs from one individual (code name: #00) in all of the experiments. In preparation for the study, TK6 cells were cultured, cryopreserved in multiple vials, and stored in liquid nitrogen. 440 mL of whole blood from #00 was purchased and processed for PBMC isolation. The isolated PBMCs were also cryopreserved in multiple vials and stored in liquid nitrogen until use. For all experiments with PBMCs isolated from the 56 volunteers, one vial of TK6 cells and one vial of #00 PBMCs were thawed and analyzed in parallel.

As shown in Fig. 4-S1A, both TK6 cells and PHA-stimulated lymphocytes from #00 rapidly repair H_2O_2-induced damage within the first 30 minutes. Afterward, the repair activity appears to continue at a slower rate. To approximate the repair rate, we performed non-linear regression and fitted a biphasic exponential decay model to the data. We then used the resulting equations to calculate the repair half-times for both cell types. Notably, TK6's half-time is ~24 minutes, which is >1.5 times faster than #00's (Fig. 4-S1B).

Multiple-visit study revels lower intra-individual variation compared to inter-individual variation

Before investigating inter-individual variation in repair capacity, we first studied the variability within individuals in comparison to the variability among people. Ten volunteers from our pilot study (code names: #01, #02, #05, #06, #09, #11, #12, #18, #19, and #23) had their blood drawn in multiple visits on different days. PBMCs were isolated from the serial blood draws, stimulated with PHA-L, and analyzed with the alkaline CometChip assay as described above. The PHA-stimulated lymphocytes were embedded in CometChip, exposed to 100 μM H_2O_2, and analyzed for SBs immediately after treatment or after different repair time points up to two hours.

Different visits of #01, #02, #05, #06, #09, #11, #12, #18, #19, and #23 display a range of repair kinetic curves (Fig. 4-4A). The variability (%CV) between visits for each individual is less than 15% across all time points including background (Fig. 4-4B). Notably, we observe a larger variability across the individuals than within the individuals (Fig. 4-4B). Statistically significant differences ($p<0.05$, one-way ANOVA) are observed for the baseline damage level as well as all repair time points except for 0 minute (Fig. 4-4C). We performed post-hoc analysis (Tukey's honest significant test) to compare each pair of the individuals. Only one person (#23) displays no difference from anyone else. Interestingly, only one pair of individuals (#05 and #09) show significant difference at the baseline damage level whereas six pairs differ significantly at the latest repair time point.

Furthermore, we investigated the rate of repair for each individual. Similar to TK6 and #00, the repair kinetics data for all ten individuals follow biphasic exponential decay equations (Fig. 4-4D), enabling calculations of the repair half-times. The average time is ~40 minutes, and there is a difference of ~24 minutes between the fastest and the slowest individuals. Notably, stimulated lymphocytes from all of the ten individuals appear to be slower at repair than TK6 cells. The slowest (#19) takes ~56 minutes to repair half of the damage (Fig. 4-4D), which is more than twice the time by TK6 cells (Fig. 4-S1B).

Oxidative damage repair kinetics from single-visit individuals

While serial blood draws yield valuable information about intra-individual variability, a single blood draw would significantly simplify the sample collection procedure and enable larger studies. To investigate whether one visit per person is sufficient to discern differences between individuals, we obtained one single blood draw for the remaining 46 volunteers in our pilot study. Isolated PBMCs were again stimulated with PHA-L, treated with 100 μM H_2O_2, and analyzed with the alkaline CometChip assay.

Similar to the multi-visit study, a wide range of curve shapes for H_2O_2-induced damage repair kinetics is observed for the single-visit 46 volunteers (Fig. 4-5). The repair kinetic curve for each individual is an average of three independent experiments using three separate portions of PBMCs isolated from one single blood sample. The variability (%CV) between experiments ranges between 20% and 27%. Despite the relatively high level of experimental noise, a larger variability across people is observed for all time points except for the baseline and initial damage levels (Fig. 4-S2A). However, only the differences at the 30-minute and 60-minute time points show statistical significance ($p < 0.05$, one-way ANOVA) (Table 4-S1) (Fig. 4-S2B). In addition, when the damage level at each time point is corrected for background by subtracting the baseline, the differences at 30-minute and 6-minute time points are no longer statistically significant ($p \geq 0.05$, one-way ANOVA) (Table 4-S1).

On the other hand, the variation in the shapes of the kinetic curves suggests that the repair rate may vary among people and can be used as a measure of repair capacity. For example, #03, #04, and #38 rapidly

repair most of the initial damage within the first 30 minutes, but there appears to be no further reduction of SBs after 30 minutes. On the other hand, #24 and #26 display a gradual reduction in SBs over the entire 120 minutes of repair. To quantify the repair rates, we parameterized the kinetic curves by fitting the data to a biphasic exponential decay model. The time it takes to repair 50% of the initial damage (repair half-time) is calculated from the resulting equation as a measure of the repair rate. Results from the 46 volunteers show a broad range of repair half-times with more than seven-fold difference between the fastest (16 minutes) and the slowest (114 minutes) (Fig. 4-5B).

The repair half-times can be divided into quartiles, representing individuals with "very fast", "fast", "medium", and "slow" repair (Fig. 4-5B). Interestingly, #03, #04, and #38 all belong to the "very fast" group. A closer examination of the other members of the group reveals a common trend where most of the initial DNA damage is rapidly reduced during the first 30 minutes (rapid phase) while any further reduction of SBs afterward appears to be much slower (slow phase) (Fig. 4-5C). In contrast, the transition from the rapid phase to the slow phase for the "fast" group appears to be at 60 minutes instead of 30 (Fig. 4-5D). Furthermore, both the "medium" and the "slow" groups appear to have a relatively consistent rate for SB reduction over the entire 120 minutes (Fig. 4-5E and F). Notably, both #24 and #26 belong to the "slow repair" group with #24 being the slowest of the 46 people. Fig. 4-5G shows representatives from different groups to further illustrate the variation in the kinetic curves. A comparison between #24 and #43 highlights the difference between the "medium" and the "slow repair" groups. While both samples have comparable SB levels for most of the repair time points (30 minutes and later), #43 has ~1.5 times higher initial damage level compared to #24, resulting in a steeper repair slope for #43 and a repair rate ~twice as fast (60 minutes vs 114 minutes half-time).

4.5. DISCUSSION

DNA damage has broad academic, drug safety, drug discovery, and diagnostic relevance. There remains a significant gap in clinical applications of DNA repair capacity variation. More extensive evidence supporting a causal relationship between DNA repair capacity and health outcomes is needed. There is a major lack of studies that take into account the complex interactions between different repair pathways, mainly stemming from the lack of available technologies for rapid assessment of multiple pathways in parallel. In this work, we demonstrated the use of CometChip to measure DNA repair kinetics of multiple types of damage as integrated outcomes of some of the major repair pathways in primary human lymphocytes. Further, pilot studies with a small population of healthy volunteers highlight the sensitivity of the CometChip platform and provide important insights into the variation in oxidative damage repair kinetics in the population.

The use of the same sample of stimulated lymphocytes enables a comparison of repair activities across multiple types of DNA damage. A key observation is that the stimulated lymphocytes are capable of repairing most damage, including oxidative, alkylation, CPDs, and DSBs. However, the rates of repair for damage induced by different agents vary widely. For example, most of the oxidative damage induced by H_2O_2 repairs within ~30-60 minutes while CPDs require up to 24 hours. Significantly, the repair rates of different types of damage induced by the same agent also vary. For example, most of SSBs induced by γIR is repaired within 15 minutes while it takes ~2-4 hours for most of γIR-induced DSB removal. Taken together, these results highlight the significance of studying multiple repair processes in parallel for a complete understanding of DNA repair capacity.

Elevated oxidative damage has been shown to correlate with higher cancer risk and the pathology for conditions associated with oxidative stress, such as post-ischemic brain and heart damage (59). Therefore, the oxidative damage repair capacity may provide a sensitive predictor of disease outcomes. This study demonstrated that the CometChip assay can be used to discern small differences in oxidative damage repair between people, evidenced in the lower variability in PBMCs isolated from serial blood draws compared to PBMCs from different individuals.

A key advantage of kinetics analysis is that it allows for estimates of repair rates, which exhibit different degrees of variation depending on the types of DNA damage (5, 60). Reduced repair rates have been show to correlate with elevated cancer risk (60, 61) and treatment outcomes (62, 63). In PBMCs isolated from 46 healthy volunteers, we observed a sevenfold variation in repair half-times of H_2O_2-induced damage, which is in the same order as shown in other studies (5, 60). Interestingly, there are subtle but noticeable differences in the shapes of the average repair kinetics curves for different quartiles. Larger studies are needed to confirm the range of repair rates and the different curve shapes characteristic of the quartiles.

There are a few challenges that need to be addressed going forward. First, the experimental variability in PBMCs isolated from the same blood sample is relatively high, which potentially masks the differences between individuals and reduces the sensitivity of the assay. Because intraindividual variation is relatively low, future studies should consider using serial blood draws to improve reproducibility. In addition, a significant trend toward higher DNA damage levels over time (batch effect) is observed during the course of the study in both TK6 cells and PBMCs from #00 (data not shown), indicating systematic variation that may contribution to some of the differences observed in PBMCs isolated from the volunteers. Further analyses are warranted to examine potential correlations between the batch effect and other experimental factors, such as time of day and culture conditions. Trend correction may be necessary, which will require a thorough re-analysis of the data.

In conclusion, the ability of CometChip to examine the repair of multiple types of DNA damage in parallel presents an exciting opportunity to further shed light on the relationship between DNA repair capacity and human health. Initial studies with human primary lymphocytes reveal significant differences between individuals and provide an important basis to ask specific questions about health outcomes in relation to repair kinetics. The repertoire of DNA damage detection can be further expanded to include specific types of base lesions and interstrand crosslinks, facilitating a more comprehensive understanding of how an individual responds to potential genotoxic agents.

4.6. REFERENCES

1. Wu X, Zhao H, Suk R, Christiani DC. Genetic susceptibility to tobacco-related cancer. Oncogene. 2004;23(38):6500-23. doi: 10.1038/sj.onc.1207811. PubMed PMID: 15322521.
2. Cox JD, Stetz J, Pajak TF. Toxicity criteria of the Radiation Therapy Oncology Group (RTOG) and the European Organization for Research and Treatment of Cancer (EORTC). Int J Radiat Oncol Biol Phys. 1995;31(5):1341-6. doi: 10.1016/0360-3016(95)00060-C. PubMed PMID: 7713792.
3. Jalal S, Earley JN, Turchi JJ. DNA repair: from genome maintenance to biomarker and therapeutic target. Clin Cancer Res. 2011;17(22):6973-84. doi: 10.1158/1078-0432.CCR-11-0761. PubMed PMID: 21908578; PMCID: PMC3218201.
4. Li C, Wang LE, Wei Q. DNA repair phenotype and cancer susceptibility--a mini review. Int J Cancer. 2009;124(5):999-1007. doi: 10.1002/ijc.24126. PubMed PMID: 19065660; PMCID: PMC4349428.
5. Gaivao I, Piasek A, Brevik A, Shaposhnikov S, Collins AR. Comet assay-based methods for measuring DNA repair in vitro; estimates of inter- and intra-individual variation. Cell biology and toxicology. 2009;25(1):45-52. doi: 10.1007/s10565-007-9047-5. PubMed PMID: 18058031.
6. El-Zein RA, Monroy CM, Cortes A, Spitz MR, Greisinger A, Etzel CJ. Rapid method for determination of DNA repair capacity in human peripheral blood lymphocytes amongst smokers. BMC cancer. 2010;10:439. doi: 10.1186/1471-2407-10-439. PubMed PMID: 20718982; PMCID: PMC2933626.
7. Cheng L, Eicher SA, Guo Z, Hong WK, Spitz MR, Wei Q. Reduced DNA repair capacity in head and neck cancer patients. Cancer Epidemiol Biomarkers Prev. 1998;7(6):465-8. PubMed PMID: 9641488.
8. Shi Q, Wang LE, Bondy ML, Brewster A, Singletary SE, Wei Q. Reduced DNA repair of benzo[a]pyrene diol epoxide-induced adducts and common XPD polymorphisms in breast cancer patients. Carcinogenesis. 2004;25(9):1695-700. doi: 10.1093/carcin/bgh167. PubMed PMID: 15090466.
9. Ellis CN, SpringerLink (Online service). Obtaining and Using Genetic Information. 2011. In: Inherited cancer syndromes [Internet]. New York ; London: Springer,. 2nd. [p1-21]. Available from: SpringerLink http://dx.doi.org/10.1007/978-1-4419-6821-0 MIT Access Only.
10. Alter BP. Diagnostic evaludation of FA. In: Eiler ME, Frohnmayer D, Larsen K, Owen J, editors. Fanconi Anemia: Guidelines for Diagnosis and Management. 3rd ed: Fanconi Anemia Reserach Fund, Inc.; 2008.
11. Bernstam VA. CRC Handbook of Gene Level Diagnostics in Clinical Practice. Boca Raton, FL: CRC Press; 1992.

12. Olaussen KA, Mountzios G, Soria JC. ERCC1 as a risk stratifier in platinum-based chemotherapy for nonsmall-cell lung cancer. Curr Opin Pulm Med. 2007;13(4):284-9. doi: 10.1097/MCP.0b013e32816b5c63. PubMed PMID: 17534174.
13. Rouleau M, Patel A, Hendzel MJ, Kaufmann SH, Poirier GG. PARP inhibition: PARP1 and beyond. Nat Rev Cancer. 2010;10(4):293-301. doi: 10.1038/nrc2812. PubMed PMID: 20200537; PMCID: PMC2910902.
14. Nagel ZD, Chaim IA, Samson LD. Inter-individual variation in DNA repair capacity: a need for multi-pathway functional assays to promote translational DNA repair research. DNA Repair (Amst). 2014;19:199-213. doi: 10.1016/j.dnarep.2014.03.009. PubMed PMID: 24780560; PMCID: PMC4071454.
15. Nagel ZD, Margulies CM, Chaim IA, McRee SK, Mazzucato P, Ahmad A, Abo RP, Butty VL, Forget AL, Samson LD. Multiplexed DNA repair assays for multiple lesions and multiple doses via transcription inhibition and transcriptional mutagenesis. Proc Natl Acad Sci U S A. 2014;111(18):E1823-32. doi: 10.1073/pnas.1401182111. PubMed PMID: 24757057; PMCID: PMC4020053.
16. Chaim IA, Nagel ZD, Jordan JJ, Mazzucato P, Ngo LP, Samson LD. In vivo measurements of interindividual differences in DNA glycosylases and APE1 activities. Proc Natl Acad Sci U S A. 2017;114(48):E10379-E88. doi: 10.1073/pnas.1712032114. PubMed PMID: 29122935.
17. Weingeist DM, Ge J, Wood DK, Mutamba JT, Huang Q, Rowland EA, Yaffe MB, Floyd S, Engelward BP. Single-cell microarray enables high-throughput evaluation of DNA double-strand breaks and DNA repair inhibitors. Cell Cycle. 2013;12(6):907-15. doi: 10.4161/cc.23880. PubMed PMID: 23422001; PMCID: PMC3637349.
18. Wood DK, Weingeist DM, Bhatia SN, Engelward BP. Single cell trapping and DNA damage analysis using microwell arrays. Proc Natl Acad Sci U S A. 2010;107(22):10008-13. doi: 10.1073/pnas.1004056107. PubMed PMID: 20534572; PMCID: PMC2890454.
19. Ostling O, Johanson KJ. Microelectrophoretic study of radiation-induced DNA damages in individual mammalian cells. Biochem Biophys Res Commun. 1984;123(1):291-8. PubMed PMID: 6477583.
20. Olive PL, Banath JP. The comet assay: a method to measure DNA damage in individual cells. Nat Protoc. 2006;1(1):23-9. doi: 10.1038/nprot.2006.5. PubMed PMID: 17406208.
21. Hartmann A, Agurell E, Beevers C, Brendler-Schwaab S, Burlinson B, Clay P, Collins A, Smith A, Speit G, Thybaud V, Tice RR. Recommendations for conducting the in vivo alkaline Comet assay. 4th International Comet Assay Workshop. Mutagenesis. 2003;18(1):45-51. PubMed PMID: 12473734.

22. Ceuppens JL, Baroja ML, Lorre K, Van Damme J, Billiau A. Human T cell activation with phytohemagglutinin. The function of IL-6 as an accessory signal. J Immunol. 1988;141(11):3868-74. PubMed PMID: 3263438.
23. Cheng L, Wang LE, Spitz MR, Wei Q. Cryopreserving whole blood for functional assays using viable lymphocytes in molecular epidemiology studies. Cancer Lett. 2001;166(2):155-63. PubMed PMID: 11311488.
24. Ge J, Chow DN, Fessler JL, Weingeist DM, Wood DK, Engelward BP. Micropatterned comet assay enables high throughput and sensitive DNA damage quantification. Mutagenesis. 2015;30(1):11-9. doi: 10.1093/mutage/geu063. PubMed PMID: 25527723; PMCID: PMC4272061.
25. Ge J, Wood DK, Weingeist DM, Prasongtanakij S, Navasumrit P, Ruchirawat M, Engelward BP. Standard fluorescent imaging of live cells is highly genotoxic. Cytometry A. 2013;83(6):552-60. doi: 10.1002/cyto.a.22291. PubMed PMID: 23650257; PMCID: PMC3677558.
26. Liber HL, Thilly WG. Mutation assay at the thymidine kinase locus in diploid human lymphoblasts. Mutat Res. 1982;94(2):467-85. PubMed PMID: 6810168.
27. Skopek TR, Liber HL, Penman BW, Thilly WG. Isolation of a human lymphoblastoid line heterozygous at the thymidine kinase locus: possibility for a rapid human cell mutation assay. Biochem Biophys Res Commun. 1978;84(2):411-6. PubMed PMID: 214074.
28. Ellison AR, Nouspikel T, Jaspers NG, Clarkson SG, Gruenert DC. Complementation of transformed fibroblasts from patients with combined xeroderma pigmentosum-Cockayne syndrome. Exp Cell Res. 1998;243(1):22-8. doi: 10.1006/excr.1998.4147. PubMed PMID: 9716445.
29. Staresincic L, Fagbemi AF, Enzlin JH, Gourdin AM, Wijgers N, Dunand-Sauthier I, Giglia-Mari G, Clarkson SG, Vermeulen W, Scharer OD. Coordination of dual incision and repair synthesis in human nucleotide excision repair. EMBO J. 2009;28(8):1111-20. doi: 10.1038/emboj.2009.49. PubMed PMID: 19279666; PMCID: PMC2683701.
30. Boyum A. Separation of leukocytes from blood and bone marrow. Introduction. Scand J Clin Lab Invest Suppl. 1968;97:7. PubMed PMID: 5707208.
31. Boyum A. Isolation of mononuclear cells and granulocytes from human blood. Isolation of monuclear cells by one centrifugation, and of granulocytes by combining centrifugation and sedimentation at 1 g. Scand J Clin Lab Invest Suppl. 1968;97:77-89. PubMed PMID: 4179068.
32. Collins AR, Mitchell DL, Zunino A, de Wit J, Busch D. UV-sensitive rodent mutant cell lines of complementation groups 6 and 8 differ phenotypically from their human counterparts. Environ Mol Mutagen. 1997;29(2):152-60. PubMed PMID: 9118967.

33. Evans MD, Dizdaroglu M, Cooke MS. Oxidative DNA damage and disease: induction, repair and significance. Mutat Res. 2004;567(1):1-61. doi: 10.1016/j.mrrev.2003.11.001. PubMed PMID: 15341901.
34. Caldecott KW. Single-strand break repair and genetic disease. Nat Rev Genet. 2008;9(8):619-31. doi: 10.1038/nrg2380. PubMed PMID: 18626472.
35. Krokan HE, Bjoras M. Base excision repair. Cold Spring Harb Perspect Biol. 2013;5(4):a012583. doi: 10.1101/cshperspect.a012583. PubMed PMID: 23545420; PMCID: PMC3683898.
36. Wallace SS. Base excision repair: a critical player in many games. DNA Repair (Amst). 2014;19:14-26. doi: 10.1016/j.dnarep.2014.03.030. PubMed PMID: 24780558; PMCID: PMC4100245.
37. Wong D, Demple B. Modulation of the 5'-deoxyribose-5-phosphate lyase and DNA synthesis activities of mammalian DNA polymerase beta by apurinic/apyrimidinic endonuclease 1. J Biol Chem. 2004;279(24):25268-75. doi: 10.1074/jbc.M400804200. PubMed PMID: 15078879.
38. Meira LB, Burgis NE, Samson LD. Base Excision Repair. In: Nigg EA, editor. Genome instability in cancer development. New York: Springer; 2005. p. 125-73.
39. Collins AR. The comet assay for DNA damage and repair: principles, applications, and limitations. Mol Biotechnol. 2004;26(3):249-61. doi: 10.1385/MB:26:3:249. PubMed PMID: 15004294.
40. Kondo N, Takahashi A, Ono K, Ohnishi T. DNA damage induced by alkylating agents and repair pathways. J Nucleic Acids. 2010;2010:543531. doi: 10.4061/2010/543531. PubMed PMID: 21113301; PMCID: PMC2989456.
41. Fu D, Calvo JA, Samson LD. Balancing repair and tolerance of DNA damage caused by alkylating agents. Nat Rev Cancer. 2012;12(2):104-20. doi: 10.1038/nrc3185. PubMed PMID: 22237395; PMCID: PMC3586545.
42. Beranek DT. Distribution of methyl and ethyl adducts following alkylation with monofunctional alkylating agents. Mutat Res. 1990;231(1):11-30. PubMed PMID: 2195323.
43. Jones GD, Le Pla RC, Farmer PB. Phosphotriester adducts (PTEs): DNA's overlooked lesion. Mutagenesis. 2010;25(1):3-16. doi: 10.1093/mutage/gep038. PubMed PMID: 19920061.
44. Marteijn JA, Lans H, Vermeulen W, Hoeijmakers JH. Understanding nucleotide excision repair and its roles in cancer and ageing. Nat Rev Mol Cell Biol. 2014;15(7):465-81. doi: 10.1038/nrm3822. PubMed PMID: 24954209.
45. Scharer OD. Nucleotide excision repair in eukaryotes. Cold Spring Harb Perspect Biol. 2013;5(10):a012609. doi: 10.1101/cshperspect.a012609. PubMed PMID: 24086042; PMCID: PMC3783044.

46. DiGiovanna JJ, Kraemer KH. Shining a light on xeroderma pigmentosum. J Invest Dermatol. 2012;132(3 Pt 2):785-96. doi: 10.1038/jid.2011.426. PubMed PMID: 22217736; PMCID: PMC3279615.
47. Kraemer KH, Lee MM, Scotto J. DNA repair protects against cutaneous and internal neoplasia: evidence from xeroderma pigmentosum. Carcinogenesis. 1984;5(4):511-4. PubMed PMID: 6705149.
48. Kraemer KH, Lee MM, Andrews AD, Lambert WC. The role of sunlight and DNA repair in melanoma and nonmelanoma skin cancer. The xeroderma pigmentosum paradigm. Arch Dermatol. 1994;130(8):1018-21. PubMed PMID: 8053698.
49. Gillet LC, Scharer OD. Molecular mechanisms of mammalian global genome nucleotide excision repair. Chem Rev. 2006;106(2):253-76. doi: 10.1021/cr040483f. PubMed PMID: 16464005.
50. Gallagher PE, Duker NJ. Detection of UV purine photoproducts in a defined sequence of human DNA. Mol Cell Biol. 1986;6(2):707-9. PubMed PMID: 3785156; PMCID: PMC367562.
51. Khanna KK, Jackson SP. DNA double-strand breaks: signaling, repair and the cancer connection. Nat Genet. 2001;27(3):247-54. doi: 10.1038/85798. PubMed PMID: 11242102.
52. Hoeijmakers JH. DNA damage, aging, and cancer. N Engl J Med. 2009;361(15):1475-85. doi: 10.1056/NEJMra0804615. PubMed PMID: 19812404.
53. Lieber MR. The mechanism of double-strand DNA break repair by the nonhomologous DNA end-joining pathway. Annu Rev Biochem. 2010;79:181-211. doi: 10.1146/annurev.biochem.052308.093131. PubMed PMID: 20192759; PMCID: PMC3079308.
54. Woodbine L, Gennery AR, Jeggo PA. The clinical impact of deficiency in DNA non-homologous end-joining. DNA Repair (Amst). 2014;16:84-96. doi: 10.1016/j.dnarep.2014.02.011. PubMed PMID: 24629483.
55. San Filippo J, Sung P, Klein H. Mechanism of eukaryotic homologous recombination. Annu Rev Biochem. 2008;77:229-57. doi: 10.1146/annurev.biochem.77.061306.125255. PubMed PMID: 18275380.
56. Chang HHY, Pannunzio NR, Adachi N, Lieber MR. Non-homologous DNA end joining and alternative pathways to double-strand break repair. Nat Rev Mol Cell Biol. 2017;18(8):495-506. doi: 10.1038/nrm.2017.48. PubMed PMID: 28512351.
57. Samouelian V, Maugard CM, Jolicoeur M, Bertrand R, Arcand SL, Tonin PN, Provencher DM, Mes-Masson AM. Chemosensitivity and radiosensitivity profiles of four new human epithelial ovarian cancer cell lines exhibiting genetic alterations in BRCA2, TGFbeta-RII, KRAS2, TP53 and/or CDNK2A. Cancer Chemother Pharmacol. 2004;54(6):497-504. doi: 10.1007/s00280-004-0843-9. PubMed PMID: 15258697.

58. Foray N, Randrianarison V, Marot D, Perricaudet M, Lenoir G, Feunteun J. Gamma-rays-induced death of human cells carrying mutations of BRCA1 or BRCA2. Oncogene. 1999;18(51):7334-42. doi: 10.1038/sj.onc.1203165. PubMed PMID: 10602489.

59. Kryston TB, Georgiev AB, Pissis P, Georgakilas AG. Role of oxidative stress and DNA damage in human carcinogenesis. Mutat Res. 2011;711(1-2):193-201. doi: 10.1016/j.mrfmmm.2010.12.016. PubMed PMID: 21216256.

60. Palyvoda O, Polanska J, Wygoda A, Rzeszowska-Wolny J. DNA damage and repair in lymphocytes of normal individuals and cancer patients: studies by the comet assay and micronucleus tests. Acta Biochim Pol. 2003;50(1):181-90. doi: 035001181. PubMed PMID: 12673358.

61. Schmezer P, Rajaee-Behbahani N, Risch A, Thiel S, Rittgen W, Drings P, Dienemann H, Kayser KW, Schulz V, Bartsch H. Rapid screening assay for mutagen sensitivity and DNA repair capacity in human peripheral blood lymphocytes. Mutagenesis. 2001;16(1):25-30. PubMed PMID: 11139596.

62. Alapetite C, Thirion P, de la Rochefordiere A, Cosset JM, Moustacchi E. Analysis by alkaline comet assay of cancer patients with severe reactions to radiotherapy: defective rejoining of radioinduced DNA strand breaks in lymphocytes of breast cancer patients. Int J Cancer. 1999;83(1):83-90. PubMed PMID: 10449613.

63. Nadin SB, Vargas-Roig LM, Drago G, Ibarra J, Ciocca DR. DNA damage and repair in peripheral blood lymphocytes from healthy individuals and cancer patients: a pilot study on the implications in the clinical response to chemotherapy. Cancer Lett. 2006;239(1):84-97. doi: 10.1016/j.canlet.2005.07.025. PubMed PMID: 16143448.

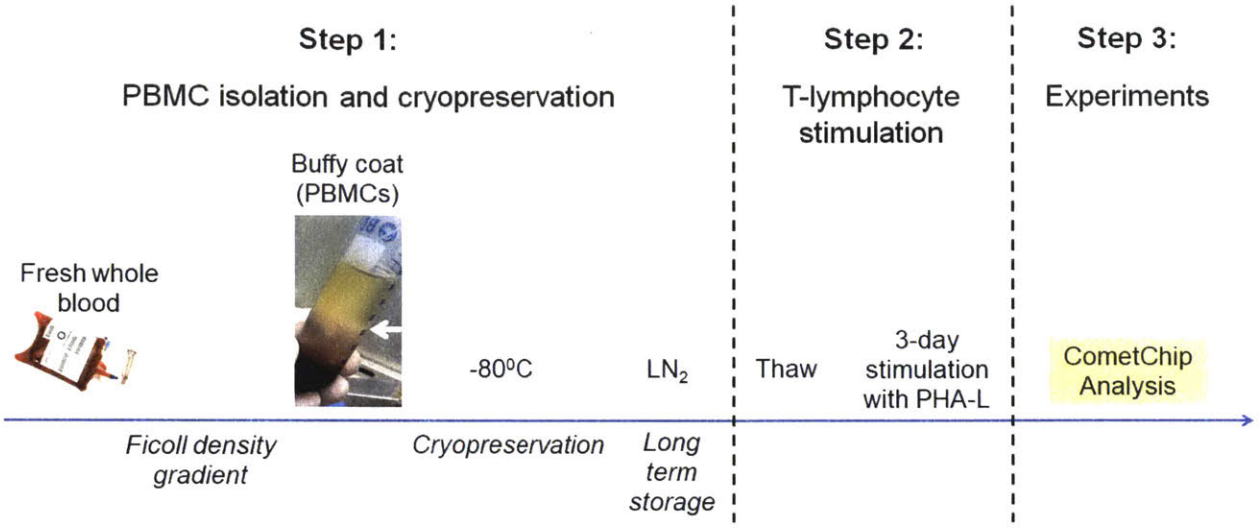

Figure 4-1. Schematic for CometChip analysis of human lymphocytes. Step 1. Fresh whole blood is centrifuged with a density gradient solution, Ficoll-Paque PLUS, to separate red blood cells and granulocytes from the peripheral blood mononuclear cells (PBMCs). PBMCs form a white band above the Ficoll layer after centrifugation (see arrow) and can be extracted. Isolated PBMCs are cryopreserved by slow freezing (about -1°C/minute) to -80°C and then transferred to a liquid nitrogen (LN_2) Dewar. **Step 2.** Cryopreserved PBMCs are rapidly thawed at 37°C to recover viable cells. Resting T-lymphocytes are stimulated to proliferate by incubation with 5 μg/mL PHA-L for three days. **Step 3.** PHA-stimulated T-lymphocytes are collected from culture, exposed to DNA damaging agents, and analyzed for DNA damage levels with CometChip. Cells are analyzed at multiple time points following exposure for DNA repair kinetic studies.

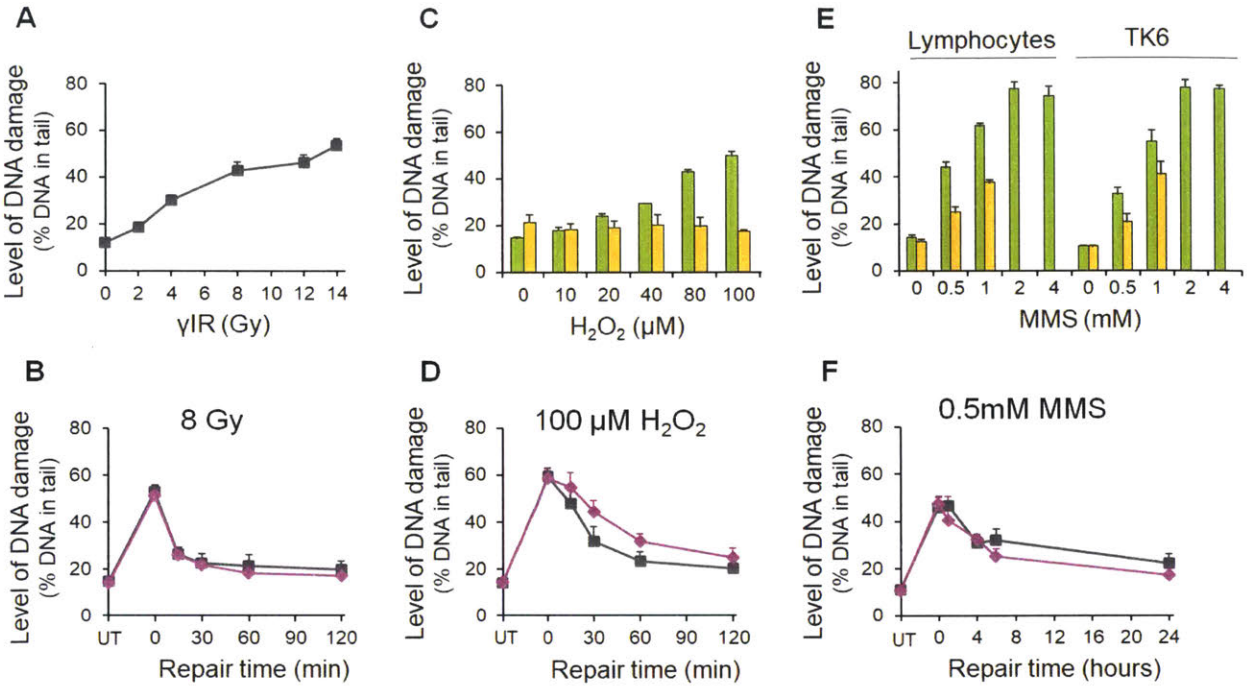

Figure 4-2. Analysis of oxidative damage and alkylation damage by alkaline CometChip. A. Dose-response of TK6 cells to γIR. TK6 cells are irradiated with γIR and immediately analyzed for DNA strand breaks. **B.** Repair kinetics of 8 Gy-induced damage by TK6 (gray) and PHA-stimulated T-lymphocytes (pink). **C.** Repair of H_2O_2-induced damage by PHA-stimulated T-lymphocytes. Green bars represent cells analyzed immediately after exposure. Yellow bars show cells after two hours of repair following H_2O_2 treatment. **D.** Repair kinetics of DNA damage induced by 100 μM H_2O_2. **E.** Repair of MMS-induced damage by PHA-stimulated T-lymphocytes and TK6. Green bars denote DNA damage levels immediately after challenge, and yellow bars represent cells after four hours of repair. **F.** Repair kinetics of DNA damage induced by 0.5 mM MMS. Error bars represent standard errors of the means (SEMs) of independent experiments (biological replicates) or technical triplicates. **A**, **B**, and **D**. Biological triplicates. **F**. Biological duplicates. **C** and **E**. Technical triplicates. Background DNA damage levels are represented as untreated cells (UT). *Gray lines:* TK6. *Pink lines:* PHA-stimulated T-lymphocytes.

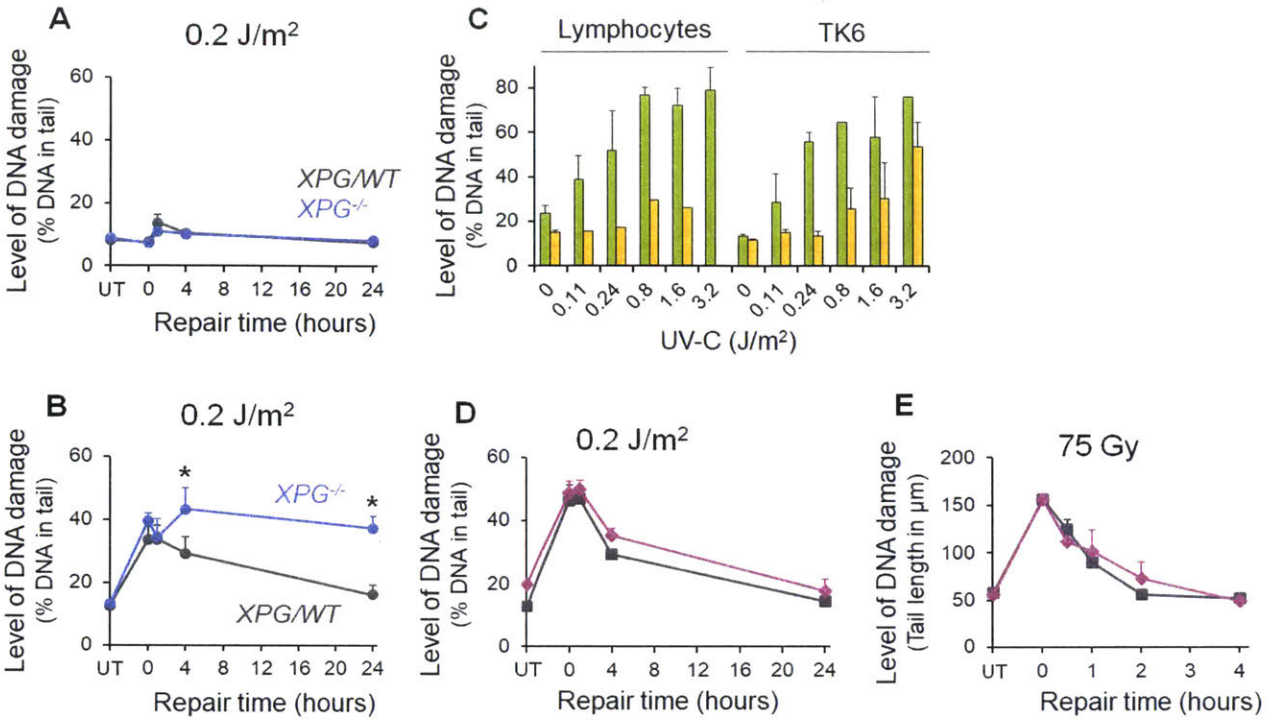

Figure 4-3. A and **B.** Repair kinetics of cyclobutane pyrimidine dimers (CPDs) induced by UV radiation in human skin fibroblast cell lines, *XPG*$^{-/-}$ and *XPG/WT* (see Methods for more details). Cells are irradiated with 0.2 J/m2 254 nm UV light (UVC) to induce CPDs. Cells are lysed overnight, and exposed nuclear DNA is incubated in a T4 endonuclease V reaction buffer without the enzyme (A) or with the enzyme (B) to create DNA nicks specific to CPD sites. SBs are then analyzed following the alkaline CometChip procedure. **C** and **D.** Repair of CPDs in TK6 and PHA-stimulated T-lymphocytes. UV-irradiated cells are lysed and incubated with T4 endonuclease V enzyme and analyzed with the alkaline CometChip assay. **C.** Green bars represent CPD levels immediately after UVC exposure. Yellow bars show CPD levels after 24 hours of repair. **D.** Repair kinetics of CPDs induced by 0.2 J/m^2 UVC. **E.** Repair of DNA double-strand breaks induced by 75 Gy γIR and measured by the neutral CometChip assay. Error bars represent standard errors of the means (SEMs) of independent experiments (biological replicates) or technical triplicates. **A**, **B**, and **D**. Biological triplicates. **E**. Biological duplicates. **C**. Technical triplicates. Background DNA damage levels are represented as untreated cells (UT). *Gray lines:* TK6. *Pink lines:* PHA-stimulated T-lymphocytes.

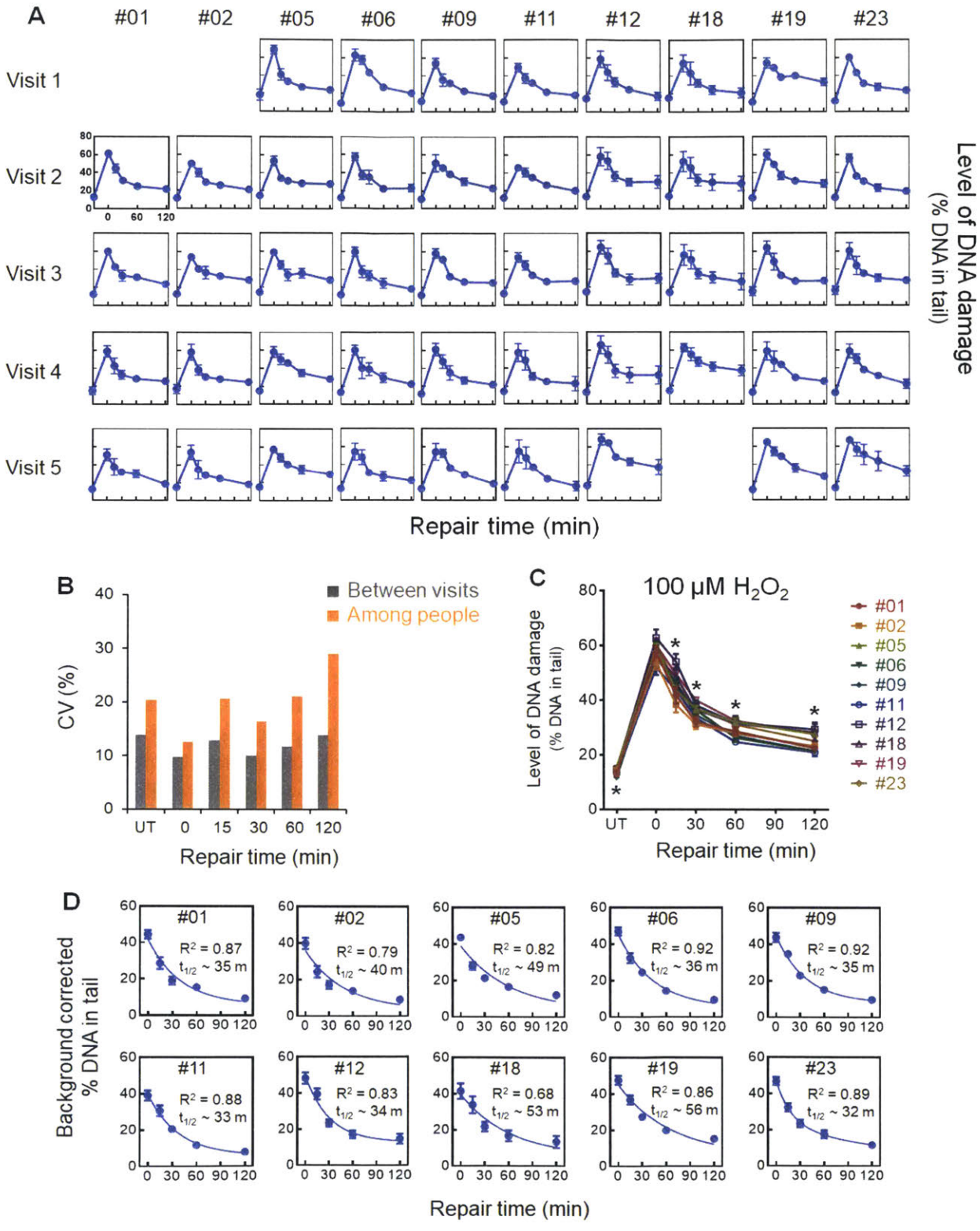

Figure 4-4. Oxidative damage repair of lymphocytes isolated from serial blood draws measured by alkaline CometChip. #01, #02, #05, #06, #09, #11, #12, #18, #19, and #23 represent ten healthy volunteers having blood draws on multiple visits. PBMCs isolated from each visit are cultured and stimulated with 5

μg/mL PHA-L for three days to activate T-lymphocyte proliferation. The stimulated T-lymphocytes are exposed to 100 μM H_2O_2 and analyzed for SBs immediately or after different periods of repair. **A.** Repair kinetics from cells obtained from different visits for each individual. The axis labels for "Visit 2" of #01 are applied to all the other plots. The first data point from the left represents DNA damage level from untreated cells (background damage). Error bars are SEMs from three independent experiments performed with three separate portions of PBMCs isolated from the same blood sample. **B.** Coefficient of variation (%CV) between visits for each person (intra-individual; gray bars) and among the ten volunteers (inter-individual; orange bars). **C.** Comparison of repair kinetics between the ten volunteers. Error bars are SEMs of all the visits from each individual. *$p<0.05$, one-way ANOVA. **D.** The DNA damage levels for all repair time points are corrected for background damage and fitted to a biphasic exponential decay model. Goodness-of-fit is represented by R^2 values. Repair half-times ($t_{1/2}$) are approximated from the model equations (see Methods for more details). Error bars are SEMs of all the visits from each individual.

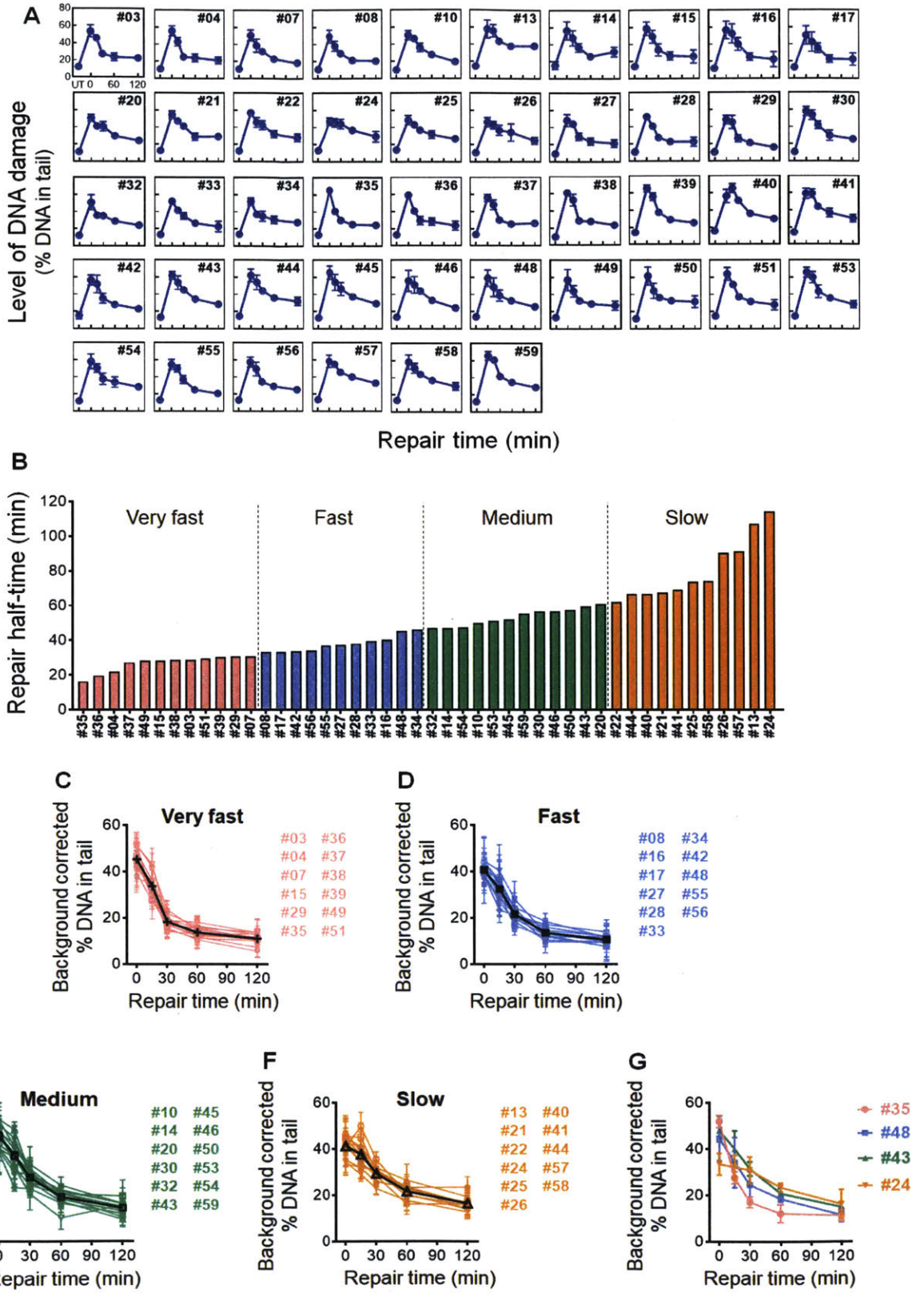

Figure 4-5. Oxidative damage repair of lymphocytes isolated from single blood draws measured by alkaline CometChip. 46 healthy volunteers each had one single blood draw. PBMCs isolated from each

blood sample are cultured and stimulated with 5 μg/mL PHA-L for three days to activate T-lymphocyte proliferation. The stimulated T-lymphocytes are exposed to 100 μM H_2O_2 and analyzed for SBs immediately or after different periods of repair. **A.** Repair kinetics from cells obtained from 46 volunteers who are identified by "#" followed by a unique combination of two digits. The axis labels for #03 are applied to all the other plots. **B.** Rank-ordered repair half-times for the 46 volunteers. See Methods for more details on the calculation of repair half-times. The half-times are divided into quartiles, where the first quartile corresponds to the fastest repair rates of the population ("Very fast") and the fourth is comprised of the slowest rates ("Slow"). **C**, **D**, **E**, and **F**. Background-corrected DNA repair kinetic curves for individuals belonging to each quartile. Black lines represent the average of each quartile. **G.** Representative background-corrected DNA repair kinetic curves from different quartiles. #35 is the fastest of the population, and #24 is the slowest. Error bars are SEMs from three independent experiments performed with three separate portions of PBMCs isolated from the same blood sample.

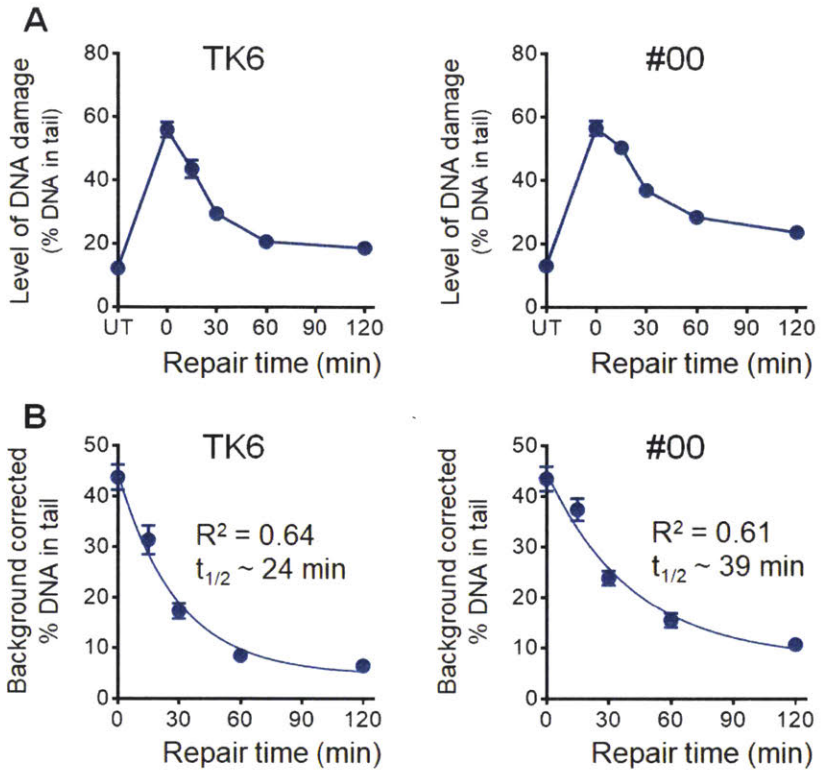

Figure 4-S1. Oxidative damage repair of internal control cells (TK6 and PHA-stimulated T-lymphocytes from #00). Samples of TK6 and PBMCs from #00 are processed in the same way as PBMCs isolated from the 56 volunteers except that TK6 cells are not stimulated with PHA-L during culture. A. Repair kinetics of oxidative damage repair. TK6 and lymphocytes from #00 are treated with 100 µM H_2O_2 and analyzed for SBs immediately or after different periods of repair using alkaline CometChip. B. Background-corrected repair kinetics are fitted to a biphasic exponential decay model. R2 values reflect goodness-of-fit. Half-times ($t_{1/2}$) are calculated from the model equations (see Methods for more details). Error bars are SEMs of 29 independent experiments for TK6 and 30 for #00.

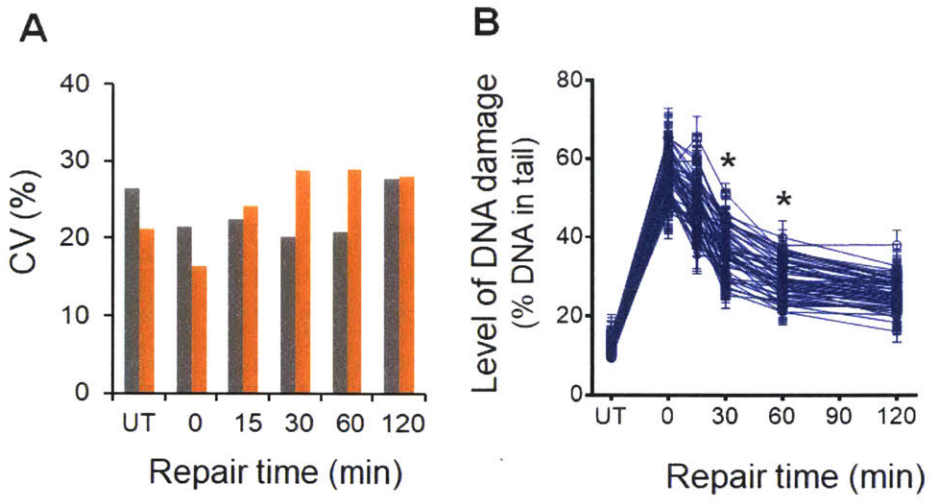

Figure 4-S2. Statistical analysis of results from Figure 4-5A. A. Coefficient of variation (%CV) between triplicate experiments for each volunteer (gray bars) and among the 46 volunteers (orange bars). **C.** Comparison of repair kinetics among the 46 volunteers. Error bars are SEMs of triplicate experiments performed with three separate aliquots of PBMCs isolated from the same blood sample. *$p<0.05$, one-way ANOVA.

Table 4-S1. One-way ANOVA for H_2O_2 repair kinetics of 46 single-visit individuals (Figure 4-5A)

A

		Raw %DNA in tail		Background corrected %DNA in tail	
		F-statistic	*p-value*	*F-statistic*	*p-value*
	Untreated	0.64	0.95		
Repair time	0 min	0.58	0.98	0.64	0.95
	15 min	1.15	0.28	1.08	0.36
	30 min	2.03	< 0.05	1.44	0.07
	60 min	1.92	< 0.05	1.30	0.15
	120 min	1.03	0.44	0.92	0.62

B

Sources	Degree of freedom
Between people	45
Between repeat experiments	92
Total	137

Chapter 5

Conclusions and Future Work

5.1. GENOTOXICITY TESTING

One of the blind spots in cell-based genotoxicity testing is the lack of a sensitive and rapid method to detect bulky DNA lesions, many of which are induced by metabolic activation of environmental carcinogens. One of the most commonly used methods for DNA damage detection is the comet assay, which is based on electrophoretic migration of nuclear DNA in the presence of DNA strand-breaks (SBs) (1). CometChip is a recently developed platform for comet assays, increasing throughput by 10^3 to 10^4 fold as well as improving assay reproducibility.

Bulky DNA lesions are corrected primarily by nucleotide excision repair (NER), which generates a number of DNA SBs as repair intermediates. Based on this observation, we adopt the use of the DNA repair synthesis inhibitors hydroxyurea (HU) and 1-β-D-arabinofuranosyl cytosine (ara-C) to induce accumulation of SBs and analyzed with CometChip for rapid SB detection. To provide physiologically relevant metabolisms, HepaRG™, a human hepatocyte cell line with high levels of liver-specific functions, is incorporated into the assay. The result is a platform tailored to the rapid assessment of bulky DNA adducts induced by chemical agents and/or their bioactivated metabolites. An additional advantage of the platform is that HU/ara-C also inhibits the repair of oxidative and alkylation damage, two of the most common types of DNA damage, enabling an overall improvement in assay sensitivity toward DNA damage detection. Importantly, significant improvement in sensitivity for genotoxic agents is observed in a small chemical screen.

Some questions still need to be addressed for the assessment of the platform as an *in vitro* genotoxicity testing method. Most important is the question of specificity. With the constantly expanding chemical libraries, false positives can be very costly by creating large number of unnecessary follow-up

animal studies (2, 3). Therefore, a validation study needs to be conducted to assess both the false negative and the false positive rates of the assay. Another question pertains to the certainty of a positive genotoxic result. Dose studies were conducted for the small chemical screen, and only the highest doses of many agents induce significant DNA damage. A three-day repeated dosing regimen has been implemented by our collaborators at Integrated Laboratory Systems, Inc. to enhance the effect of metabolic activation. Potentially, we can adapt this approach to confirm our findings.

Future works can capitalize on the advantages of the platform to expand the capacity for different types of DNA damage as well as include conditions that elucidate the test compound's molecular mechanism. Specifically, the use of site-specific endonucleases should be simple to incorporate into the assay. In cases where no significant increase in SBs is observed even at cytotoxic doses, the presence of interstrand crosslinks (ICLs) should be checked by irradiation with γ-rays to induce direct breaks and follow-up analysis for evidence of DNA migration inhibition by ICLs. Small molecule inhibitors can be used to probe for the role of specific molecular processes in response to a DNA damaging challenge. In addition, the advent of CRISPR/Cas systems, a versatile genome editing toolkit (4), suggest the possibility of generating libraries of genetically altered HepaRG™ cell lines to study the role of different pathways in the formation and repair of certain DNA damage.

5.2. CELL SURVIVAL QUANTIFICATION

One of the most critical decisions for proliferating cells under stresses is to divide, senesce, or die. Therefore, cell survival quantification is essential in many branches of biology and is particularly pertinent in chemical safety assessment. The colony formation assay developed more than 60 years ago (5, 6) still remains the gold standard because it is the only method that directly measures the ability of a cell to divide. The long incubation time and large culture dishes render the gold standard incapable of meeting the current challenge of toxicity testing where the massive libraries of existing chemicals are constantly expanded with thousands of new ones every year. To overcome these limitations, we adopt the agarose microarray developed in CometChip to grow microcolonies in a grid and quantify microcolony sizes by DNA

fluorescent staining and automated image analysis. The resulting platform is a miniaturized colony formation assay that [MicroColonyChip (μCC)] is compatible with high-throughput (HT) screening equipment and requires only ~20% of the original incubation time.

Results from validation studies shown in this work highlight key advantages of μCC. Most importantly, μCC is capable of a multi-log dynamic range of measurement and similar sensitivity to the colony formation assay. Direct comparisons with two of the most popular cell viability assays, a tetrazolium salt-based (XTT) and an ATP-based (CellTiter-Glo®) assay, reveal superior performance of the μCC in sensitivity and reproducibility, respectively. Lastly, the incorporation of MCL-5, a metabolically competent cell line, creates a platform suitable for primary screens for toxicity.

Further optimization and development of μCC is necessary to address several concerns. A current limitation of providing collagen type 1 in μCC is that not all cells stay confined to the microwells, as they appear to elongate and spread during microcolony formation. To optimize the assay, it is ideal for the microcolonies to be compact so that there is not significant microcolony overlap. To overcome this limitation, we propose to modify the growth conditions to foster growth within the microwell, rather than growth by attachment to the ligands in the upper layer. Additionally, we will explore varied microwell diameters and inter-colony distances to accommodate different cell types. For example, for larger cells, a microwell with a larger diameter may be desireable, and for cells that migrate away from the microcolony, an increase in the inter-microwell distance may be advantageous. In addition, for adherent cells that can form colonies with collagen 1 (e.g. HepG2 and HeLa), experiments need to carry out to test the sensitivity and robustness of μCC in measuring toxicity in these cell types.

Another possibility for future work is optimization for multiplexing capacity. The goal is to gain mechanistic insights into the cell survival or cell death response. Information about cell death mechanisms, for example, can inform candidate drug design and may also aid in the drug discovery process. Preliminary results show the feasibility of fluorescent staining for a number of biomarkers, such as membrane permeability, apoptosis, and intracellular esterase activity. The versatility of the staining capability on μCC

should be explored. Importantly, computational routines should be developed to enable quantification and interpretation of multiple endpoints.

Finally, a robust and efficient method for single-cell loading should be established. A chief advantage would be a much closer imitation of the colony formation assay, which may potentially further improve assay sensitivity as well as make it easier for new users to be willing to adopt. Colonies from single-cell microwells will be significantly smaller compared to colonies that start with multiple cells in one microwell. The benefit would be significant reduction in required growth area, enabling the use of a new microarray with much smaller distances between the microwells. To facilitate single-cell loading, the microwell dimensions should be such that one cell can fit comfortably but there will be no room for two or more. In addition, if the distance between two microwells is sufficiently small, then the number of off-grid excess cells can be significantly reduced. Potentially, the washing step can then be eliminated, reducing a major source of experimental noise.

5.3. INTERINDIVIDUAL VARIATION IN DNA REPAIR KINETICS

In order to fully assess the impact of DNA damaging agents on human health, how an individual responds also needs to be accounted for. Although there is substantial evidence linking variation in DNA repair capacity to cancer risk and response to treatment, most studies lack a comprehensive survey across multiple major repair pathways, potentially missing valuable information. In addition, there are practical challenges of large population studies that many current assays are either too slow or too noisy to meet. With the capacity to process up to 96 samples in one chip and its scalability using HT screening equipment, CometChip has the potential to overcome these limitations.

In this work, we showed optimal conditions for CometChip to measure repair kinetics of five different types of DNA damage in human primary lymphocytes. The rates of repair vary considerably depending on the types of damage, reflecting the dissimilarities between multiple repair pathways. We investigated the assay's reproducibility and sensitivity using lymphocytes isolated from blood samples from

56 healthy volunteers and showed that there are relatively small but significant differences in oxidative damage repair kinetics among people. Based upon the observation of a sevenfold variation in repair rates, the population is tentatively divided into groups with "very fast", "fast", "medium", or "slow" repair.

A key limitation of this study is the high variability between experiments using PBMCs isolated from the same blood sample. A significant trend toward higher DNA damage during the course of the study is observed in both TK6 and #00 and may contribute to the high experimental noise. Closer examination of the trend and changes in experimental conditions (e.g. time of day, new culture media) may yield insights into the potential cause of this batch effect. In addition, each experiment requires the recovery of cryopreserved PBMCs via thawing and the activation of T-lymphocytes via mitogen stimulation, both of which are highly noisy processes.

Future works to expand the capacity of CometChip for DNA repair measurement should incorporate the use of more site-specific enzymes and whenever possible include a genetic cell model carrying a defect in a major repair pathway in order to assess the contribution of the pathway. Potential correlations between the results in the current population study and the demographic as well as lifestyle information from each volunteer (e.g. age, weight, diet and exercise habits) should be explored. Collaborators in this project also used stimulated T-lymphocytes from the same cultures to analyze for the repair of plasmid reporters carrying ten different types of repair substrates using the FM-HCR assay. Comparisons of oxidative damage repair kinetics and repair capacity profile may potentially shed light into the role of each pathway in the repair of oxidative damage. In the next population study, the repair of all five types of DNA damage should be measured in parallel to provide a more complete understanding of DNA repair capacity.

5.4. REFERENCES

1. Singh NP, McCoy MT, Tice RR, Schneider EL. A simple technique for quantitation of low levels of DNA damage in individual cells. Exp Cell Res. 1988;175(1):184-91. PubMed PMID: 3345800.
2. Kirkland D, Kasper P, Martus HJ, Muller L, van Benthem J, Madia F, Corvi R. Updated recommended lists of genotoxic and non-genotoxic chemicals for assessment of the performance of new or improved genotoxicity tests. Mutat Res Genet Toxicol Environ Mutagen. 2016;795:7-30. doi: 10.1016/j.mrgentox.2015.10.006. PubMed PMID: 26774663.
3. Kirkland D, Kasper P, Muller L, Corvi R, Speit G. Recommended lists of genotoxic and non-genotoxic chemicals for assessment of the performance of new or improved genotoxicity tests: a follow-up to an ECVAM workshop. Mutat Res. 2008;653(1-2):99-108. doi: 10.1016/j.mrgentox.2008.03.008. PubMed PMID: 18539078.
4. Cong L, Ran FA, Cox D, Lin S, Barretto R, Habib N, Hsu PD, Wu X, Jiang W, Marraffini LA, Zhang F. Multiplex genome engineering using CRISPR/Cas systems. Science. 2013;339(6121):819-23. doi: 10.1126/science.1231143. PubMed PMID: 23287718; PMCID: PMC3795411.
5. Puck TT, Marcus PI. A Rapid Method for Viable Cell Titration and Clone Production with Hela Cells in Tissue Culture: The Use of X-Irradiated Cells to Supply Conditioning Factors. Proc Natl Acad Sci U S A. 1955;41(7):432-7. PubMed PMID: 16589695; PMCID: 528114.
6. Puck TT, Marcus PI. Action of x-rays on mammalian cells. J Exp Med. 1956;103:653-66.